TRAPPED SINGLE ATOMS AND ATOMIC ENSEMBLES:

QUANTUM COMPUTATION, COHERENT MANIPULATION,

AND INTERFEROMETRY

Vom Fachbereich Physik der Universität Hannover
zur Erlangung des Grades
Doktor der Naturwissenschaften
Dr. rer. nat.
genehmigte Dissertation
von

Dipl.-Phys. Kai Eckert
geboren am 30. November 1975 in Großburgwedel in Niedersachsen

TRAPPED SINGLE ATOMS AND ATOMIC ENSEMBLES:

QUANTUM COMPUTATION, COHERENT MANIPULATION,

AND INTERFEROMETRY

Vom Fachbereich Physik der Universität Hannover
zur Erlangung des Grades
Doktor der Naturwissenschaften
Dr. rer. nat.
genehmigte Dissertation
von

Dipl.-Phys. Kai Eckert
geboren am 30. November 1975 in Großburgwedel in Niedersachsen

2005

Referent: Prof. Dr. Maciej Lewenstein
Korreferent: Prof. Dr. Gerhard Birkl

Tag der Promotion: 28.01.2005

ABSTRACT

The relatively weak coupling of neutral atoms to the environment makes them interesting candidates for various applications of fundamental concepts of quantum mechanics, for example in quantum computation or in precision interferometry. In a number of recent experiments it has been shown that in the laboratory a high degree of control can be obtained over neutral atoms which are trapped in optical or magnetic potentials.

The mayor part of this work considers the manipulation of individually accessible neutral atoms in optical potentials, for example in optical microtraps or optical lattices. Two concepts to encode quantum bits into spatial degrees of freedom of the atoms are described, and in both cases proposals are given for the implementation of gates for a single, as well as for two quantum bits. In the first approach, it is proposed to encode the quantum bit into motional states of an atom, *i.e.*, in the two lowest vibrational states of the trap. For two quantum bits, approaching the two traps allows to perform quantum gates through an interplay of tunneling and collisional interactions. The capability to realize a *square root of swap* gate is demonstrated, and the suppression of double occupation and of excitations to other unwanted states is discussed. The fidelities of the gate operations are evaluated for Rb atoms in state-of-the-art optical microtraps, with gate durations on the order of milliseconds. Finally, a detailed analysis of the evolution of quantum correlations is provided for such a gate operation, taking into account the indistinguishability of the atoms.

In the second proposal, *spatially delocalized qubits* are presented as an approach with the states of the computational basis defined *via* the presence of a single atom in the ground state of one out of two trapping potentials. Single quantum bit gates and a two quantum bit phase gate are discussed in detail. For Rb atoms in optical microtraps experimental imperfections are explicitly taken into account. It is furthermore demonstrated that spatially delocalized qubits can be used to realize a quantum walk in one dimension, an analogue of the random walk of a classical particle. The dependence of such a quantum walk on temperature and experimental imperfections as shaking in the trap positions is studied. By combining a spatially delocalized quantum bit and a quantum bit implemented into atomic hyperfine states, a scheme to realize a quantum walk on a two-dimensional square lattice is proposed.

In the third part, simple, efficient, and robust methods are presented to coherently manipulate the spatial degrees of freedom of single trapped atoms, for example to move atoms between traps for the initialization of well defined initial states for quantum computation or to create spatial superpositions for applications in interferometry. These techniques, labeled *three level atom optics* techniques, are spatial analogues of the stimulated Raman adiabatic passage, coherent population trapping, and electromagnetically induced transparency

techniques from quantum optics, which are realized here through the tunneling interaction among three trapped states.

The final part of this thesis focuses on a different regime of the manipulation of neutral atoms, namely on the use of ensembles containing a large number of atoms for the purpose of atom interferometry. More precisely, *differential interferometers* are studied, where the quantity of interest is encoded in the difference of two phases obtained by two independent atomic ensembles. Methods using separately or jointly squeezed states of the two atomic ensembles are discussed, which allow to surpass the standard quantum limit to the resolution of the interferometer. It is shown that non-local squeezing gives an optimal method, provided that certain conditions on the preparation and read-out of the atomic ensembles are met. Under realistic conditions the performance of both schemes can be further improved by reading out the phase difference via a quantum non-demolition measurement.

ZUSAMMENFASSUNG

Aufgrund der vergleichsweise schwachen Kopplung an die Umgebung stellen neutrale Atome interessante Kandidaten da für eine Vielzahl von Anwendungen fundamentaler quantenmechanischer Konzepte, zum Beispiel in der Quanteninformationstheorie oder in der Präzisionsinterferometerie. Viele aktuelle Experimente haben gezeigt, dass im Falle von neutralen Atomen in optischen oder magnetischen Potentialen eine sehr gute Kontrolle der experimentellen Parameter möglich ist.

Der Hauptteil dieser Arbeit behandelt die Manipulation von individuell adressierbaren neutralen Atomen in optischen Potentialen. Beispiele für solche Potentiale sind durch optische Mikrofallen oder durch optische Gitter gegeben. In dieser Arbeit werden zwei Konzepte beschrieben, um Quantenbits in räumlichen Freiheitsgraden von Atomen zu kodieren, wobei in beiden Fällen auch Methoden zur Implementierung von Quantengattern sowohl für einzelne als auch für zwei Quantenbits vorgeschlagen werden. Der erste Vorschlag beinhaltet die Kodierung der beiden orthogonalen Zustände des Quantenbits in den tiefsten Vibrationszuständen der optischen Falle. Der Mechanismus für die Implementierung eines Gatters für zwei Quantenbits basiert auf einer Kombination von Tunnelprozessen zwischen den Fallen und einer Kontaktwechselwirkung zwischen den Atomen. Auf diese Weise wird die Realisierung eines *square root of swap*-Gatters erklärt, wobei insbesondere auf die Vermeidung der Besetzung von Zuständen mit mehr als einem Atom pro Falle eingegangen wird. Die Güte der Operationen wird am Beispiel von Rubidiumatomen in optischen Mikrofallen diskutiert. In diesem Fall liegt die Zeit, die zur Realisierung eines Gatter benötigt wird, in der Größenordnung von einigen Millisekunden. Schließlich wird auch die zeitliche Entwicklung quantenmechanischer Korrelationen während einer solchen Operation analisiert. Dabei wird insbesondere auf die Ununterscheidbarkeit der Atome eingegangen.

Der zweite Vorschlag befasst sich mit der Realisierung von so genannten *Spatially Delocalized Qubits*, für die die Basiszustände durch die Position eines Atoms im Grundzustand von einem von zwei Fallenpotentialen dargestellt werden. Auch in diesem Fall werden Gatter für ein und für zwei Quantenbits ausführlich diskutiert. Als eine mögliche Anwendung werden *Quantum Walks* diskutiert. Für diese Analogien zu klassischen *Random Walks* wird insbesondere auf die Abhängigkeit von der Temperatur der Atome in den Mikrofallen sowie von experimentellen Ungenauigkeiten eingegangen. Außerdem wird die Kombination eines *Spatially Delocalized Qubit* mit einem in internen atomaren Zuständen realisierten Quantenbit zur Realisierung von *Quantum Walks* auf einem zwei-dimensionalen Gitter diskutiert.

Im dritten Teil werden effiziente und robuste Methoden zur kohärenten Manipulation der räumlichen atomaren Freiheitsgrade vorgestellt. Diese Methoden können zum Beispiel zum

Verschieben eines Atoms zwischen Fallenpotentialen oder zur Herstellung räumlicher Superpositionszustände verwendet werden. Es handelt sich bei diesen *Three-level atom optics*-Techniken um Analogien zu in der Quantenoptik angewandten Methoden zur Manipulation interner atomare Zustände, die im hier vorgestellten Fall auf der Kontrolle der Tunnelwechselwirkung zwischen den Grundzuständen dreier Fallenpotentiale basieren.

Der letzte Teil dieser Arbeit behandelt schließlich die Manipulation von Atomwolken, also von einer großen Zahl von neutralen Atomen, zum Zwecke der Atominterferometrie. Insbesondere werden so genannte *differenzielle Interferometer* untersucht, bei denen die zu messende Größe in der Differenz der Phasenverschiebungen kodiert ist, die von zwei unabhängigen Atomwolken aufgesammelt werden. In Hinsicht auf diese Anwendung werden Methoden diskutiert, die separat oder gemeinsam gequetschte Zustände der Atomwolken zur Erhöhung der Sensitivität des Interferometers über das so genannte Quantenlimit hinaus zum Ziel haben. Es wird insbesondere gezeigt, dass das Quetschen einer nicht-lokalen Observablen eine optimale Methode darstellt, solange gewisse Anforderungen sowohl an die Herstellung als auch an die Messung der atomaren Zustände erfüllt werden. Zudem kann die Auflösung unter realistischen Bedingungen durch so genannte Quantum-Nondemolition-Messungen zum Auslesen der Phase des Interferometers weiter verbessert werden.

Schlagwörter: Quanteninformation, Verschränkung, Quantengatter, kalte Atome, Atominterferometrie

CONTENTS

Introduction

The fundamental building blocks of classical computation are *bits* as the units of information, and *gates*, a set of operations acting on these bits. Considered from a mathematical point of view, these are abstract concepts, which subsequently form the basic building blocks for theories and models of computation, as well as for the construction of algorithms. But ultimately, these mathematical notions of bits and gates have to be connected to the concrete properties of a specific physical system, for example through the identification of the abstract bit with, say, electrons traveling in electronic circuits. This step was crucial for the practical application of the theoretical notion of bits and gates, as it made the concept of computation interesting to a general audience. A similar step is faced nowadays in *quantum information processing*.

Quantum information processing, or quantum computation, was suggested for the first time by Feynman in 1982 [1]. It is in a similar way built on the concepts of *quantum bits*, or *qubits* in short, as the basic units of information, and on *quantum gates* as a set of operations acting on quantum bits. Contrary to the classical case, the description of these concepts is intrinsically physical, as it is based on the fundamentals of quantum mechanics and draws its power from the strikingly different features of quantum as compared to classical systems. Still, as in the case of classical bits and gates, quantum bits and gates are embedded in a completely formalized theory, which allows to analyze and discuss their properties abstractly and without considering any particular physical system. What distinguishes a single quantum bit from its classical counterpart is the possibility to encode not only the two states of the computational basis, but also arbitrary superpositions of these states. The most intriguing feature of a collection of quantum bits is *quantum entanglement* [2], which refers to statistical correlations for measurements which are much stronger then possible correlations in classical physics [3]. Also, there is a fundamental limitation in reading out the information contained in a quantum register, *i.e.*, in a set of quantum bits. While a register of classical bits can be read out at any time and obtaining the full information, for quantum bits it is not possible to infer their state from just a single measurement, and in general performing a measurement alters the quantum register [4].

For these differences, quantum information processing offers new interesting perspectives, but also poses new challenges, for the development of new tools to answer questions which cannot be answered easily or at all with classical computers. However, taking into account the proceeding miniaturisation of computer processors [5], it is not only interesting, but also unavoidable to be concerned about how the laws of quantum mechanics affect the processing of information, as the development of electronic circuits will ultimately run into

the limit of manipulating single quantum systems. From this point of view, it is inevitable to identify and study concrete physical systems, which allow to implement the abstract notions of quantum bits and gates. To realize a quantum computer in practice is a formidable task, the main challenge being the suppression of unwanted interactions between the environment and the quantum register during a quantum computational process.

Nowadays, there is a large number of candidates for the implementation of tasks of quantum information. In nuclear magnetic resonance (NMR) quantum computers, the quantum bit is implemented into different atoms within the same molecule [6]. A large ensemble of molecules is placed in an external magnetic field and quantum bits can be manipulated through applying electromagnetic fields oscillating at particular frequencies. Certain algorithms for quantum computers for up to five quantum bits have already been demonstrated in such a system. What distinguishes an NMR quantum computer from other architectures is that not an individual quantum system is manipulated, but an ensemble of molecules. This poses difficulties, especially in the initialization of the system. Also, the number of quantum bits which can be manipulated in such a scheme is limited [6].

However, techniques similiar to NMR can also be applied in solid state systems [7], and very generally, a solid state quantum computer seems a natural continuation of the success of classical computers based on semi-conductors. Several other architectures have been identified in this context, e.g., electrons confined in quantum dots [8] and superconducting junctions [9]. The ability to implement single quantum bits has already been demonstrated for many of these proposals, but at present general problems are the reduced control over the system parameters in solid state devices, decoherence, and the read out of the quantum register.

A much higher degree of control can be achieved for cold atoms, either ions or neutral atoms, which are trapped in electrical, magnetic, or optical potentials. These systems, surprisingly, can exhibit features very close to those of solid state physics and are for this reasons in particular envisaged as tools to test predictions and models from condensed matter physics. Concerning quantum information, in ion-trap quantum computers the manipulation of individual as well as of two quantum bits has been realized [10–12], and concepts to make the system scalable to a large number of quantum bits are currently being implemented.

On the other hand, cold neutral atoms are promising candidates for quantum information, because of their weak coupling to the environment. Methods for cooling neutral trapped atoms are very well established, but still it is a very difficult and demanding task to manipulate individual atoms, although a high degree of control has already been demonstrated in experiments to engineer and manipulate the quantum state of cold atomic samples. Techniques for trapping neutral atoms use either magnetic fields coupled to the permanent atomic dipole moment [13] or optical potentials. For the latter case, trapping atoms by the dipole force using standing waves from pairs of counter propagating laser beams, so-called *optical lattices* [14], are promising candidates for the purpose of quantum computation, and important steps, as the trapping of a single atom at each site, have been realized already by Bloch *et al.* [15]. For such a system, the standard proposal is to encode the quantum bit into internal atomic states [16–21], which can be manipulated *via* external lasers. Gates between two quantum bits can be realized using either electric dipole interactions between atoms, which

can be switched on temporarily *via* exciting the atoms to a state with large electric dipole moment [21], or collisional interactions [16, 17]. In the latter case, advantage is taken of the fact that optical lattices potentials can be engineered differently for different internal states [22], as has been demonstrated experimentally [23].

Optical lattices offer many advantages, e.g., for the loading of single atoms or through the high degree of controllability of many parameters [15, 23]. Also, the application of a quantum gate between two atoms using collisional interactions has been demonstrated already [24], though only for all the atoms in the lattice simultaneously. This allows to create interesting types of quantum states, so-called *cluster states* [25], but ultimately quantum computation demands control over individual quantum bits for manipulation and read out, which is not given in most present optical lattice implementations due to the small spacing between the traps. Methods which allow for quantum computation without being able to manipulate individual sites have been studied by Calarco *et al.* [26].

Next to optical lattices, systems of optical microtraps have been proposed, where atoms are trapped in the foci of a laser which passes through an array of microlenses [27]. In such a setup, sites can be accessed individually due to their larger distance, and also the control over each site, e.g., over its displacement, is in general larger. The individual read out and manipulation of atoms in a register of up to 80 sites has been demonstrated [28, 29], as well as the ability to load single atoms into such traps [30–32]. As potentials depending on the internal state can be realized as well in optical microtraps, the same types of quantum bits and gates can be implemented as in the case of optical lattices.

In **Chapters 2** and **3**, as an alternative to using internal states, two concepts are presented to encode the the quantum bit into external, *i.e.*, spatial degrees of freedom of neutral atoms in optical potentials. In the first approach presented in **Chapter 2**, it is proposed to represent the two states of the computational basis through the motional states of a single trapped atom. Operations on single quantum bits can in this case be done *via* external lasers, gates for two quantum bits are shown to be possible through an interplay of tunneling processes and the collisional interaction between the atoms. With the correct timing of the manipulation of the trapping potentials, for an implementation in optical microtraps, error rates below 0.1% can be reached for gate times on the order of a few milliseconds. Taking into account experimental imperfections and decoherence mechanisms, error rates on the percent level are calculated.

For the second proposal, instead of the shape of the atomic wavefunctions its position in space is used to represent the quantum bit by trapping the atom in either of two traps. This concept, labeled *spatially delocalized quantum bit*, is discussed in detail in **Chapter 3**, showing that in this case quantum gates for one and two quantum bits can be done only through a spatial-temporal variation of the trapping potential, without any external lasers or the need for state dependent potentials. Based on the collisional interaction between two atoms, the implementation of a two quantum bit quantum phase gate is presented. Through explicit calculations for parameters from optical microtraps, gate times are evaluated which are again on the order of milliseconds, and experimental imperfection are discussed explicitly.

In Chapter 4, the concept of spatially delocalized quantum bits is used to present an implementation of a *quantum walk*. Such a quantum walk, constructed as an analogue of the

random walk of a classical particle, has been proposed as a possible basis for the development of new types of algorithms for quantum computation, but the purpose of Chapter 4 is rather to study how a quantum walk is modified through certain properties of the underlying experimental system. For a quantum walk in one dimension, the influence of experimental imperfections is studied in-depth, and furthermore the, to the best of my knowledge, first proposal for the implementation of a quantum walk in two dimensions is presented.

For a quantum computer based on neutral atoms in optical traps, also methods to coherently move atoms between traps are of interest, e.g., as tools to initialize a well defined array of traps before the quantum computation or to shuttle around quantum bits. Based on techniques which in optics are very well established and successful for the manipulation of *internal* electronic degrees of freedom of atoms, so-called three-level-optics techniques, in **Chapter 5** tools are proposed, which allow the coherent manipulation of *spatial* degrees of freedom of trapped neutral atoms, e.g., to move atoms between traps or to create superposition states useful for interferometry. These concepts are robust as the fidelity of certain operations does *not* depend on an exact adjustment of experimental parameters.

Up to this point, the focus has been on the manipulation of individually accessible atoms. But also ensembles containing a large number of atoms, between 10^6 and 10^{12}, which cannot be manipulated individually have promising applications, e.g., in interferometry. Usually interferometers are operated with light beams manipulated *via* beam splitters, however replacing the light beams by atomic ensembles which can be manipulated *via* laser beams promises to improve the resolution due to the much smaller (de Broglie) wavelength of atoms as compared to visible light. Also here, quantum properties of the atoms can be exploited: through an interaction of an atomic ensemble with a laser beam, a so-called *squeezed* state of the ensemble can be created [33], which on the microscopic level corresponds to a relatively robust state of entangled atoms [34]. Such a squeezed state in principle allows to further improve the resolution in interferometers [35, 36]. Furthermore, for two separated atomic ensembles, also entanglement of macroscopic degrees of freedom can be generated, with applications as, e.g., quantum memories for entangled states of light [37, 38].

Section 6 provides an analysis of the application of microscopic as well as of macroscopic entanglement between two atomic ensembles for improving the resolution of special interferometers, where the quantity of interest is encoded into the difference of phase shifts obtained by two independent atomic ensembles. As a particular example for such a *differential interferometric setup*, a *Sagnac interferometer* used to measure rotational velocities is considered, and especially conditions for the quality of preparing and measuring the atomic ensembles are extracted. It is shown that, provided these conditions are met, introducing non-local quantum correlations between both ensembles allows for a reduction of the noise in the interferometer by a factor of two.

Furthermore, in **Appendix A**, several concepts to measure quantum correlations in systems of indistinguishable particles are reviewed and analyzed in a general framework. Finally, **Appendix B** contains a short summary of the method used in Chapters 2 to 5 to solve the time-dependent Schrödinger equation.

ELEMENTS OF QUANTUM INFORMATION AND ARCHITECTURES FOR
QUANTUM COMPUTATION

In this chapter, an elementary overview on quantum information theory will be given. The emphasis will be on the concepts which are needed in the following chapters: we will discuss elementary properties of states of one or two quantum bits as well as different types of quantum gates. For a more in-depth discussion of all these concepts, see, e.g., [39, 40], and references therein. In the second part, Section 1.2, requirements on a physical system to be suitable as an architecture for quantum information will be discussed in general, before we will especially consider basic features of setups based on the trapping of neutral atoms in optical potentials.

1.1 Elements of quantum information processing: quantum bits and gates

1.1.1 Quantum bits

A classical bit of information can have two distinct values, most frequently denoted as 0 or 1. Equally a quantum bit (qubit) can have two corresponding states $|0\rangle$ and $|1\rangle$, but contrary to the classical case also all linear superpositions $a_0|0\rangle + a_1|1\rangle$ are possible. More formally, a quantum bit $|\psi\rangle$ is a unit vector in a two-dimensional Hilbert space, $|\psi\rangle \in \mathcal{H}_1 = \mathbb{C}^2$, with $|0\rangle$ and $|1\rangle$ being two orthogonal and normalized vectors in this space, *i.e.*, $\langle 0|1\rangle = 0$ and $\langle 0|0\rangle = 1 = \langle 1|1\rangle$; and $|a_0|^2 + |a_1|^2 = 1$. Then $|a_0|^2$ $(|a_1|^2)$ gives the probability to get the outcome 0 (1) when measuring the qubit in the basis $\{|0\rangle, |1\rangle\}$ (the so-called *computational basis*).

Each possible superposition of $|0\rangle$ and $|1\rangle$ can be represented using three angles δ, θ and ϕ as follows:

$$|\psi\rangle = e^{i\delta}\left(\cos\frac{\theta}{2}|0\rangle + e^{i\phi}\sin\frac{\theta}{2}|1\rangle\right). \tag{1.1}$$

Here e^{δ} is just an irrelevant phase factor which has no observable effects. consequently ignoring this factor, each state can be uniquely identified with a point on the three-dimensional unit sphere, the so-called *Bloch sphere*, using θ and ϕ as azimuthal and polar angle, respectively.

For two and more qubits, there is no such elegant representation of all possible states. A two-qubit state $|\psi\rangle \in \mathcal{H}_A \otimes \mathcal{H}_B = \mathbb{C}^2 \otimes \mathbb{C}^2$ can be described using four complex parameters via

$$|\psi\rangle = c_{00}|00\rangle + c_{01}|01\rangle + c_{10}|10\rangle + c_{11}|11\rangle, \tag{1.2}$$

where the notation $|ij\rangle \equiv |i\rangle_A|j\rangle_B \equiv |i\rangle_A \otimes |j\rangle_B$ has been used. A and B label the two systems. Thus each state of two qubits corresponds to a unit vector $|\psi\rangle = (c_{00}, c_{01}, c_{10}, c_{11})$ in a four dimensional complex vector space with basis vectors

$$|00\rangle = \begin{pmatrix} 1 \\ 0 \\ 0 \\ 0 \end{pmatrix}, \qquad |01\rangle = \begin{pmatrix} 0 \\ 1 \\ 0 \\ 0 \end{pmatrix}, \qquad |10\rangle = \begin{pmatrix} 0 \\ 0 \\ 1 \\ 0 \end{pmatrix}, \qquad |11\rangle = \begin{pmatrix} 0 \\ 0 \\ 0 \\ 1 \end{pmatrix}. \tag{1.3}$$

When the two qubits are measured locally in the computational basis, then the probabilities for outcome i for the first and j for the second qubit are given by $|c_{ij}|^2$, $i, j \in \{0, 1\}$. For two qubits two fundamentally different types of states can be identified. Consider two independently prepared qubits (labeled A and B, respectively)

$$|\psi_A\rangle = a_0|0\rangle + a_1|1\rangle \qquad \text{and} \qquad |\psi_B\rangle = b_0|0\rangle + b_1|1\rangle. \tag{1.4}$$

Then the joint state reads

$$\begin{aligned} |\psi_{\text{Sep}}\rangle &= |\psi_A\rangle \otimes |\psi_B\rangle & (1.5) \\ &= a_0 b_0|00\rangle + a_0 b_1|01\rangle + a_1 b_0|10\rangle + a_1 b_1|11\rangle. & (1.6) \end{aligned}$$

States which can be written as in Eq. (1.6) (and which thus can be produced by only acting locally on the individual qubits) are called *separable states*. Obviously there are states which cannot be written as in Eq. (1.6), these are the so-called *entangled states* [2]. An example is given by the *Bell state*

$$|\Psi^-\rangle = \frac{1}{\sqrt{2}}(|01\rangle - |10\rangle). \tag{1.7}$$

The special feature of such entangled states is that they exhibit statistical correlations from measurements which are stronger than any correlations which can be obtained from classical physics [3].

A mixed state ρ is separable if and only if it can be written as a convex combination of projectors onto separable states, because in this case ρ can be generated using a source generating only separable states.

In the following we will summarize some important concepts for pure two qubit states:

➤ *Schmidt decomposition* — Let $|\psi\rangle$ be a pure state of two qubits. Then there exists a orthonormal basis $\{|e_i\rangle_A\}$ of $\mathcal{H}_A$ and an orthonormal basis $\{|f_i\rangle_B\}$ of $\mathcal{H}_B$, such that

$$|\psi\rangle = c_0|e_0\rangle_A|f_0\rangle_B + c_1|e_1\rangle_A|f_1\rangle_B, \tag{1.8}$$

with real coefficients $c_0 > 0$ and $c_1 \geq 0$, and $|c_0|^2 + |c_1|^2 = 1$. For a proof see, *e.g.*, [39, 41]. The *Schmidt rank* is the number of non-zero coefficients c_i, and a state is separable if and only if its Schmidt rank is one.

➤ *Reduced density matrix* — If for a given (in general mixed) two qubit state ρ_{AB} we are only interested in one of the qubits alone, say in the first qubit labeled A, then all the information[1] is contained in the *reduced density matrix ρ_A*, which is defined as

$$\rho_A \equiv \mathrm{tr}_B(\rho_{AB}) := \sum_{j=0,1} {}_B\langle f_j|\rho_{AB}|f_j\rangle_B. \tag{1.9}$$

Here $\left\{|f_j\rangle_B\right\}_{j=0,1}$ is some basis for the second qubit and we have used the partial scalar product

$${}_B\langle f_j| \left(|i\rangle_A|k\rangle_B\right) := {}_B\langle f_j|k\rangle_B \; |i\rangle_A. \tag{1.10}$$

Evaluating the partial trace in the basis of the Schmidt decomposition (1.8) of a state $|\psi\rangle$ yields

$$\rho_A \quad \equiv \quad \mathrm{tr}_B(|\psi\rangle\langle\psi|) \tag{1.11}$$

$$= \quad |e_0\rangle_A\langle e_0| \, |c_0|^2 + |e_1\rangle_A\langle e_1| \, |c_1|^2 \tag{1.12}$$

$$= \quad \begin{pmatrix} |c_0|^2 & 0 \\ 0 & |c_1|^2 \end{pmatrix}, \tag{1.13}$$

and from the Schmidt decomposition it immediately follows that $\rho_B = \mathrm{tr}_A(|\psi\rangle\langle\psi|)$ has the same eigenvalues as ρ_A.

➤ *Entropy of entanglement* — For a pure state $|\psi\rangle_{AB}$ of two qubits the entropy of Entanglement $E_e(|\psi\rangle_{AB}\langle\psi|)$ is defined as the *von Neumann entropy S* of the reduced density matrix:

$$E_e(|\psi\rangle_{AB}\langle\psi|) = S(\rho_A) = S(\rho_B), \tag{1.14}$$

where the von Neumann entropy of a density matrix ρ with eigenvalues reads λ_i

$$S(\rho) = -\mathrm{tr}(\rho\log\rho) = -\sum_{i,\,\lambda_i>0} \lambda_i\log\lambda_i. \tag{1.15}$$

From the properties of the reduced density matrix it is immediately clear that $S(\rho_A) = S(\rho_B)$ holds and that for two qubits $0 \le S \le 1$ and thus $0 \le E_e(|\psi\rangle_{AB}\langle\psi|) \le 1$. The maximum value is attained for $c_0 = c_1 = 1/\sqrt{2}$, the minimum for $c_0 = 1$ and $c_1 = 0$ and thus especially $E_e(|\psi\rangle_{AB}\langle\psi|) = 0$ if and only if $|\psi\rangle_{AB}$ is separable.

The entropy of entanglement can not be used to quantify[2] the entanglement of a mixed states as, *e.g.*, $E(\rho) = 1$ also for the maximally mixed state $\rho = \mathbb{1}/4$, which is a separable state. One possible extension to mixed states is given by the *entanglement of formation* [43], defined as

$$E_F(\rho) = \min_{\rho=\sum_i p_i|\psi_i\rangle\langle\psi_i|} \sum_i p_i E_e(|\psi_i\rangle\langle\psi_i|), \tag{1.16}$$

where the minimization is performed over all possible decompositions of ρ into projectors onto pure states.

---

[1]That is to say that the statistics for any measurement only on the first qubit can be inferred from the reduced density matrix.

[2]For a stricter discussion of the properties of entanglement measures and for an analysis of various entanglement measures see, *e.g.*, [42].

1.1.2 Quantum gates

Gates for classical computation

The manipulation of classical bits in an electronic circuit is formalized via gates. All electronic circuits can be built from *single bit gates* and *two bit gates*. The only non-trivial single bit gate is the NOT gate, which takes $0 \rightarrow 1$ and $1 \rightarrow 0$, but there is a variety of two bit gates. Three examples are the AND, the NAND, and the XOR gate. All these gates take two bits as an input and have a single bit as their output, and their truth tables (giving the output bit for each combination of input bits) read:

AND	0	1
0	0	0
1	0	1

NAND	0	1
0	1	1
1	1	0

XOR	0	1
0	0	1
1	1	0

To construct any general boolean expression on a set of bits, only a subset of gates is necessary. Such subsets are called *universal sets of gates*, examples are the sets {NAND} [3] or {NOT, AND} [44]. Implicitly in all the constructions it is always assumed, that the value of a bit can be perfectly copied into any other bit.

Single quantum bit gates

Similar to the classical case, the manipulation of quantum bits can be described via quantum gates acting on one, two, or more quantum bits. As the evolution of the state of the qubits should be governed by an hermitian operator, the operators that describe the action of gates on qubits have to be unitary. For the classical NOT-Gate the corresponding unitary operator is easily identified to have the form

$$\text{NOT} = \sigma_1 = \begin{pmatrix} 0 & 1 \\ 1 & 0 \end{pmatrix} \tag{1.17}$$

(modulo the choice of a phase), as it acts on the computational basis as its classical counterpart (σ_i, $i = 1, 2, 3$, denotes the Pauli operators; subsequently all operators will be defined in the computational basis). However, in the quantum case NOT is not the only possible single qubit gate. Further examples include the remaining two Pauli operators

$$\sigma_2 = \begin{pmatrix} 0 & -i \\ i & 0 \end{pmatrix}, \qquad \sigma_3 = \begin{pmatrix} 1 & 0 \\ 0 & -1 \end{pmatrix}, \tag{1.18}$$

---

[3]*e.g.*, NOT x=x NAND x, x OR y=(x NAND x) NAND (y NAND y) and
x XOR y=(x NAND (x NAND y)) NAND (y NAND (x NAND y)).

as well as the rotation operators

$$R_1(\theta) = e^{-i\sigma_1\theta/2} = \begin{pmatrix} \cos\frac{\theta}{2} & -i\sin\frac{\theta}{2} \\ -i\sin\frac{\theta}{2} & \cos\frac{\theta}{2} \end{pmatrix} \tag{1.19}$$

$$R_2(\theta) = e^{-i\sigma_2\theta/2} = \begin{pmatrix} \cos\frac{\theta}{2} & -\sin\frac{\theta}{2} \\ \sin\frac{\theta}{2} & \cos\frac{\theta}{2} \end{pmatrix} \tag{1.20}$$

$$R_3(\theta) = e^{-i\sigma_1\theta/2} = \begin{pmatrix} e^{-i\theta/2} & 0 \\ 0 & e^{i\theta/2} \end{pmatrix}. \tag{1.21}$$

Important and frequently used single qubit gates are the Hadamard gate H, the phase gate S, and the $\pi/8$ gate T:

$$H = \frac{1}{\sqrt{2}}\begin{pmatrix} 1 & 1 \\ 1 & -1 \end{pmatrix}, \qquad S = \begin{pmatrix} 1 & 0 \\ 0 & i \end{pmatrix}, \qquad T = \begin{pmatrix} 1 & 0 \\ 0 & e^{i\pi/4} \end{pmatrix}. \tag{1.22}$$

Note that $H = e^{i\pi/4}R_x(\pi)\,R_z(\pi/2)$, $T = e^{i\pi/8}R_z(\pi/4)$, and $S = T^2$.

Two quantum bit gates

A quantum equivalent to the classical NOT gate was easy to find, but for two bit gates this is sometimes an impossible task. The AND gate for example is obviously *not invertible*, and it can not be made invertible even by adding a second output bit (such that the number of input and output qubits are equal – this is obviously a basic condition for a gate to be invertible). Every quantum gate on the other hand has to be invertible as it is represented by a unitary operator, such that no quantum gate corresponding to the classical AND exists[4]. The XOR gate in contrast can be made invertible by adding a second output qubit with a carefully chosen value. The corresponding quantum gate normally is referred to as the *controlled-not* gate, or CNOT gate [39]. In the computational basis it acts as

$$|00\rangle \to |00\rangle, \qquad |01\rangle \to |01\rangle, \qquad |10\rangle \to |11\rangle, \qquad |11\rangle \to |10\rangle, \tag{1.23}$$

or, in a more compact notation: $|ij\rangle \to |i\,(i\text{ XOR } j)\rangle$. Thus a NOT operation is applied to the second qubit (the *target qubit*) if the first qubit (the *control qubit*) is in state $|1\rangle$. In the basis of Eq. (1.3), the corresponding unitary operator reads

$$\text{CNOT} = \begin{pmatrix} 1 & 0 & 0 & 0 \\ 0 & 1 & 0 & 0 \\ 0 & 0 & 0 & 1 \\ 0 & 0 & 1 & 0 \end{pmatrix}. \tag{1.24}$$

The CNOT gate, supplied with single qubit gates, is already sufficient to construct any unitary operation on an arbitrary number of qubits, thus {CNOT, Single qubit gates} is a universal set of quantum gates [45], just as {NAND} was for classical computation (we will sometimes also call a quantum gate alone a universal gate if together with single qubit gates it allows to construct any possible quantum gate). In particular CNOT can be used to create an entangled

---

[4]It is possible to construct a quantum gate corresponding on the computational basis to the classical AND gate by adding a third qubit – an auxiliary qubit or *ancilla*.

state from a separable one. *e.g.*, starting from a separable state $|\psi\rangle = |0\rangle|0\rangle$ and applying first a Hadamard gate on the first qubit and secondly a controlled-not operation, the Bell state $|\Psi^+\rangle$ is created:

$$|0\rangle|0\rangle \xrightarrow{\text{H}\otimes\text{ID}} \frac{1}{\sqrt{2}}(|0\rangle + |1\rangle)|0\rangle \xrightarrow{\text{CNOT}} \frac{1}{\sqrt{2}}(|0\rangle|0\rangle + |1\rangle|1\rangle) \equiv |\Psi^+\rangle. \qquad (1.25)$$

There are other two qubit gates, three of which should be mentioned here as they will become important in the following chapters:

➤ PHASE — Another universal gate which is easily derived from CNOT is the PHASE gate. It can be constructed by applying local Hadamard rotations on the target qubit before and after the CNOT:

$$\text{PHASE} = (\text{ID} \otimes \text{H})\, \text{CNOT} \,(\text{ID} \otimes \text{H}) = \begin{pmatrix} 1 & 0 & 0 & 0 \\ 0 & 1 & 0 & 0 \\ 0 & 0 & 1 & 0 \\ 0 & 0 & 0 & -1 \end{pmatrix}. \qquad (1.26)$$

➤ SWAP — As an apparently trivial operation we can construct a gate that exchanges the state of the two qubits. The corresponding unitary operator reads

$$\text{SWAP} = \begin{pmatrix} 1 & 0 & 0 & 0 \\ 0 & 0 & 1 & 0 \\ 0 & 1 & 0 & 0 \\ 0 & 0 & 0 & 1 \end{pmatrix}. \qquad (1.27)$$

Despite its very similar appearance, SWAP can *not* substitute the CNOT gate in a universal set of gates. This is most easy to see from the action on a general separable state:

$$a_0 b_0 |00\rangle + a_0 b_1 |01\rangle + a_1 b_0 |10\rangle + a_1 b_1 |11\rangle$$
$$\xrightarrow{\text{SWAP}} a_0 b_0 |00\rangle + a_1 b_0 |01\rangle + a_0 b_1 |10\rangle + a_1 b_1 |11\rangle, \qquad (1.28)$$

The result is always also a separable state, *i.e.*, SWAP can not generate entanglement from a separable state. Its behavior is rather "classical", and thus not sufficient on its own to perform useful quantum computations.

➤ $\sqrt{\text{SWAP}}$ — The non-trivial part of the SWAP gate just exchanges $|01\rangle \leftrightarrow |10\rangle$. To get a more useful gate we try to construct one which stops "half-way" between the initial and the final states of the two qubits. The most straight-forward choice might be

$$\text{HALF-SWAP} = \frac{1}{\sqrt{2}} \begin{pmatrix} \sqrt{2} & 0 & 0 & 0 \\ 0 & 1 & 1 & 0 \\ 0 & 1 & -1 & 0 \\ 0 & 0 & 0 & \sqrt{2} \end{pmatrix}, \qquad (1.29)$$

but applying this gate two times just leaves the identity: $(\text{HALF-SWAP})^2 = \text{ID}$. We can however find an operator $\sqrt{\text{SWAP}}$ fulfilling $\left(\sqrt{\text{SWAP}}\right)^2 = \text{SWAP}$ by adjusting the phases as follows:

$$\sqrt{\text{SWAP}} = \frac{1}{2} \begin{pmatrix} 2 & 0 & 0 & 0 \\ 0 & 1-i & 1+i & 0 \\ 0 & 1+i & 1-i & 0 \\ 0 & 0 & 0 & 2 \end{pmatrix}. \qquad (1.30)$$

When talking about implementing gate operations later in Chapter 2, it will become clear that this is indeed a very natural choice for the phases. It is easy to see that $\sqrt{\textsc{swap}}$ acts non-trivially as it can produce an entangled state from a separable one, *e.g.*,

$$|00\rangle \xrightarrow{\textsc{not}\otimes\textsc{id}} = |10\rangle \xrightarrow{\sqrt{\textsc{swap}}} |\psi_f\rangle = \frac{1+i}{2}|01\rangle + \frac{1-i}{2}|10\rangle, \qquad (1.31)$$

where the last state is a maximally entangled two qubit state, since $E_e(|\psi_f\rangle\langle\psi_f|) = 1$. Moreover, similar to $\textsc{cnot}$ or $\textsc{phase}$, $\sqrt{\textsc{swap}}$ is a universal gate, which can be shown by constructing a $\textsc{phase}$ gate from $\sqrt{\textsc{swap}}$ and the single qubit operation s from Eq. (1.22) [8, 45, 46]:

$$\textsc{phase} = (\textsc{s}^{-1} \otimes \textsc{s}) \sqrt{\textsc{swap}} (\textsc{s}^2 \otimes \textsc{id}) \sqrt{\textsc{swap}} \qquad (1.32)$$

$$= \begin{pmatrix} 1 & 0 & 0 & 0 \\ 0 & i & 0 & 0 \\ 0 & 0 & -i & 0 \\ 0 & 0 & 0 & 1 \end{pmatrix} \sqrt{\textsc{swap}} \cdot \begin{pmatrix} 1 & 0 & 0 & 0 \\ 0 & 1 & 0 & 0 \\ 0 & 0 & -1 & 0 \\ 0 & 0 & 0 & -1 \end{pmatrix} \sqrt{\textsc{swap}}. \qquad (1.33)$$

There are many more quantum gates, including those acting on more than two qubits, *e.g.*, controlled phase gates and Toffoli gates [39, 47]. However, all of them can be decomposed into single qubit operations and applications of one universal two qubit gate (*e.g.*, $\textsc{cnot}$, $\textsc{phase}$, or $\sqrt{\textsc{swap}}$).

1.2 Architectures for quantum information processing

As qubits and quantum gates can be formulated in terms of matrices acting on complex vectors, a system of qubits can obviously be simulated on a classical computer (for an example of such a simulator see, *e.g.*, [48]). So why do we want to construct special architectures for quantum computation, if we can just use a classical computer? The reason is the exponential growth of the Hilbert space with the number of qubits involved. For a quantum computer of 250 qubits, the Hilbert space is $\mathcal{H} = \mathbb{C}^{2^{250}} \cong \mathbb{R}^{2\cdot 2^{250}}$, such that if a real number is represented by 32 bits in our classical computer, $64 \cdot 2^{250}$ bits are necessary to represent only the state vector in the memory of our computer. However, this number is comparable to the number of atoms in the universe, thus to implement 250 quantum bits in a classical computer is unfeasible. On the other hand, if one qubit is represented by two levels of a single atom, than 250 atoms are already enough to form the quantum register.

Here we will give a review of the conditions that are generally demanded from any architecture for quantum information processing. Subsequently, we will especially review physical settings and proposals using neutral atoms trapped in optical potentials to represent the quantum register. An overview over the status of the implementation of quantum computers in various other physical systems is given the *The quantum information roadmapping project* [49].

1.2.1 DiVincenzo's requirements for quantum computing

In 1996, DiVincenco formulated five requirements which some physical system has to fulfill in order qualify for the implemention quantum information processing [50] (see also [39,

49]). In the following we will review these conditions, together with a further condition concerned with larger systems composed of computational units.

Scalable implemention of well-characterized qubits

Qubits as the basic building blocks for quantum computation should be encoded into (part of) a Hilbert space of a physical system. This does not necessarily have to be a collection, *i.e.*, a direct tensor product, of two level-systems, many other choices are also possible, although it is the most straight-forward and natural choice for many systems to use a multi-particle system to encode qubits.

Also the physical resources may only scale linearly with the number of qubits, not exponentially (notice that the scaling is exponential if we encode the qubits in registers of a classical computer as explained in the remark in the beginning of this section), or, saying the same thing in another way, the size of the Hilbert space has to grow exponentially with the system size. This is naturally fulfilled for a multi-particle system, while the Hilbert space of a single particle always only grows algebraically with the system size. *e.g.*, for a Harmonic oscillator the spread of the n-th excited state is $\Delta x = x_0 \sqrt{n + 1/2}$, with x_0 the spread of the ground state, and thus the dimension of the Hilbert space grows only quadratically with the size Δx of the system: $n = (\Delta x)^2/x_0 - 1/2$.

Initialize the system to a well-defined state

An essential ingredient for performing a computation is the ability to initialize the system, *i.e.*, the qubits, into a well-defined initial state. This does not have to be an arbitrary state, as the requirement for producing an arbitrary state can be cast into the requirement to prepare a *certain* initial state ($|000\ldots0\rangle$ is good enough) and to perform an arbitrary unitary computation.

Expressed in physical terms, the condition to prepare a good initial state often corresponds to *cool* the physical system to a ground state, which however in most architecture envisaged for computation is a formidable task on its own. It would certainly be easier to prepare some thermal state of the system, but successful quantum computing demands an initial state with small entropy (to illustrate this condition, note that the maximally mixed state $\rho = \mathbb{1}/2$ is completely invariant under any unitary evolution and thus useless for quantum computing).

We can thus characterize how well the system can be initialized into a state ρ by two figures of merit: the entropy $S(\rho)$ and the fidelity with which ρ can be produced, *i.e.*, the *distance* of ρ to the state $\widetilde{\rho}$ that has actually been produced. Here most frequently the *Uhlmann fidelity* is used, which defines the distance between ρ and $\widetilde{\rho}$ as

$$F(\rho,\widetilde{\rho}) = \left[\operatorname{tr}\left(\sqrt{\sqrt{\rho}\,\widetilde{\rho}\,\sqrt{\rho}}\right)\right]^2. \tag{1.34}$$

If, as it will be usually the case, we aim at producing a pure state $\rho = |\psi\rangle\langle\psi|$, then Eq. (1.34) reduces to

$$
\begin{aligned}
F(|\psi\rangle\langle\psi|,\widetilde{\rho}) &= \operatorname{tr}(\widetilde{\rho}\,|\psi\rangle\langle\psi|) && (1.35)\\
&= \langle\psi|\widetilde{\rho}|\psi\rangle. && (1.36)
\end{aligned}
$$

Long decoherence times

An important concern against the realization of a large-scale quantum computer is the problem of isolating it from the environment. Interaction between the system and the environment builds up (quantum) correlations, viz entanglement, between them, and as a consequence the state of the system alone, ignoring the degrees of freedom of the environment through tracing them out, evolves into a mixed state. This process is called decoherence, and the time scale on which these processes happen is called decoherence time. for a single qubit decoherence two different decoherence times are distinguished: the T_1 time (or *longitudinal* relaxation time) measures the lifetime of the state with higher energy $|1\rangle$. But the more important time scale is the lifetime T_2 (*transverse* relaxation time) of superposition states (because this is a mere quantum effect).

If after one step of a quantum computation the expected state of the quantum register would have been $|\psi\rangle$, but the actual outcome is $\widetilde{\rho}$ (mixed because the environment has been traced out), then we can again use the fidelity

$$F(|\psi\rangle\langle\psi|, \widetilde{\rho}) = \langle\psi|\widetilde{\rho}|\psi\rangle \tag{1.37}$$

or, alternatively, the error $\varepsilon = 1 - F$ to characterize the strength of decoherence.

It is not completely clear which error can be tolerated in the gate operations, but $\varepsilon = 0$ is *not* necessary, since there exist algorithms to perform *error correction* during and after the computation (by encoding a single logical qubit into more than one real qubit). These algorithms currently need around $\varepsilon \lesssim 10^{-6} \ldots 10^{-5}$, but it is an open question whether this is optimal or whether protocol tolerating larger errors exist.

A universal set of quantum gates

After initializing the system to a well-defined state, the major part of quantum information processing concerns the application of a unitary operation, broken down into a sequence of quantum gates. As described in section 1.1.2, it is enough to be able to perform a certain subsets of gates, *e.g.*, all single-qubit gates plus the CNOT gate. The demand to be able to perform such gates implicitly contains the requirement to address qubits individually, which means that, if the qubits are carried by particles and these particles are addressed optically, then they have to be spaced by more than a wavelength.

It is on the other hand not necessary to be able to have the ability to perform gates between *any pair* of qubits, since from a universal set of gates especially the SWAP gate can be performed, and thus information can be transported through the system. It is however necessary that any two qubits are connected indirectly through other qubits.

The quality of a gate can again be characterized *via* the fidelity. Say the unitary operation U should be realized, but in the system only $\widetilde{U}$ can be done. Then we choose a basis of input states $\mathcal{B}$, and average the fidelity of the correct outcome (from U) with the outcome

of applying $\widetilde{U}$ over all the possible income states:

$$F(U, \widetilde{U}) \;=\; \frac{1}{|\mathcal{B}|} \sum_{|\psi\rangle \in \mathcal{B}} F(U|\psi\rangle\langle\psi|U^\dagger, \widetilde{U}|\psi\rangle\langle\psi|\widetilde{U}^\dagger) \tag{1.38}$$

$$=\; \frac{1}{|\mathcal{B}|} \sum_{|\psi\rangle \in \mathcal{B}} \mathrm{tr}\left(\widetilde{U}|\psi\rangle\langle\psi|\widetilde{U}^\dagger U|\psi\rangle\langle\psi|U^\dagger\right) \tag{1.39}$$

$$=\; \frac{1}{|\mathcal{B}|} \sum_{|\psi\rangle \in \mathcal{B}} \mathrm{tr}\left(\langle\psi|U^\dagger \widetilde{U}|\psi\rangle\langle\psi|\widetilde{U}^\dagger U|\psi\rangle\right) \tag{1.40}$$

$$=\; \frac{1}{|\mathcal{B}|} \sum_{|\psi\rangle \in \mathcal{B}} |\langle\psi|U^\dagger \widetilde{U}|\psi\rangle|^2. \tag{1.41}$$

The error $\varepsilon = 1 - F$ which can be tolerated within a quantum computation (using error correction) is of the same order of magnitude as the error resulting from decoherence.

Not only a small error is important, but also the gate operation should to be fast enough. The relevant time scale is given by the decoherence times of the system, which should be long compared to the time required to perform an elementary operation.

Capability to measure the output result

Finally, a form of measurement of the final state of the registers of the quantum computer is necessary. Obviously this requires access to individual qubits. Furthermore normally a *strong measurement* is required, *i.e.*, a projective measurement that for a single qubit in a state $a_0|0\rangle + a_1|1\rangle$ registers $|0\rangle$ ($|1\rangle$) with a probability $|a_0|^2$ ($|a_1|^2$) and collapses the wavefunction into $|0\rangle$ ($|1\rangle$). For such measurements there has to be a large coupling between the system and some measurement device, which can be switched of during computation as otherwise it acts as a decoherence process. Also quantum computation with *weak measurements* is possible (measurements with a weak and usually continuous coupling between the system and the measurement device), but this usually requires an ensemble of identical quantum computers to achieve a macroscopically observable signal.

Flying qubits

For a large scale quantum computer it would be eligible to be able to move around quantum information between different distant computational units. For such a transport next to *stationary* qubits (the qubits used for computational tasks) a form of *flying* qubits (usually photons are envisaged in this context) is necessary, together with an interface to convert information from stationary to flying qubits and vice versa. Furthermore it has to be possible to faithfully transmit the flying qubits between different locations.

In this thesis we will most of the time deal only with a subset of these conditions, as we will analyze a given physical system. Thus in the main part the focus will be on how to implement the qubit and on how to construct elementary gate operations. We will however always also analyze the other conditions with respect to the concrete implementation.

1.2.2 Quantum computation with neutral atoms

Trapped neutral atoms are natural and promising candidates for quantum information processing tasks for several fundamental reasons:

- The structure of energy-levels for atoms is simple compared to, *e.g.*, molecules. However, there are a number of choices of levels to represent qubits for an atom in a trap. Furthermore, compared to, *e.g.*, condensed matter systems, neutral atoms are very well understood systems.

- As neutral atoms are not charged, they do not couple strongly to the environment. Thus they are comparatively less sensitive to decoherence through interaction with the environment.

- Techniques for laser-cooling and Raman sideband cooling of atoms in traps are very well established [51–54].

- Further advantages include an efficient detection mechanism (*quantum jump technique* [55]) and the scalability of the system.

The architectures for quantum computation using neutral atoms can above all be distinguished by the way atoms are trapped. The most established techniques use coupling of laser fields to the atoms induced dipole moment (quadratic stark effect): an oscillating electrical field $E(r,t) = \frac{1}{2}E_0(r) \exp(i\omega t) + \text{c.c.}$ induces a time-dependent dipole moment $\mu = \alpha E$ in the atom, which interacts with the E field and creates a Stark-shift of the atomic energy: $U_{\text{dipole}} = -\frac{1}{2}\langle \mu E \rangle$. A more careful derivation [56] for a two-level system with energy difference $\hbar\omega_o$ and dipole moment d shows that the lower and upper energy levels are shifted by $+\hbar\widetilde{\Omega}(r)/2$ and $-\hbar\widetilde{\Omega}(r)/2$, where

$$\widetilde{\Omega}(r) = \sqrt{\Omega^2(r) + \delta^2}, \tag{1.42}$$

is the generalized Rabi frequency for Rabi frequency $\Omega(r) = dE_0(r)\hbar$ and detuning $\delta = \omega - \omega_0$ from the transition. If the detuning is large compared to the Rabi frequency, $|\delta| \gg \Omega$, then we can expand $\widetilde{\Omega}$ in Ω/δ to find

$$U_{\text{dipole}} = \frac{1}{2}\hbar\widetilde{\Omega}(r) \approx \frac{1}{2}\hbar\delta + \hbar\frac{\Omega^2(r)}{4\delta}. \tag{1.43}$$

The second term of Eq. (1.43) is position dependent for laser profiles with non-zero intensity gradient, and thus the atoms feel a position-dependent conservative potential (see Fig. 1.1). For an atom in the lower level the resulting force, the *dipole force* reads:

$$F_{\text{dipol}} = -\nabla\hbar\widetilde{\Omega}(r) = -\hbar\frac{\Omega(r)\,\nabla\Omega(2r)}{\delta}. \tag{1.44}$$

For red detuned laser, $\delta < 0$, the dipole force points in the direction of growing intensity. Thus atoms can be trapped inside the intensity maxima of a laser beam. For blue detuning, $\delta > 0$, the dipole force points in the direction of less intensity and trapping thus occurs in the intensity minima.
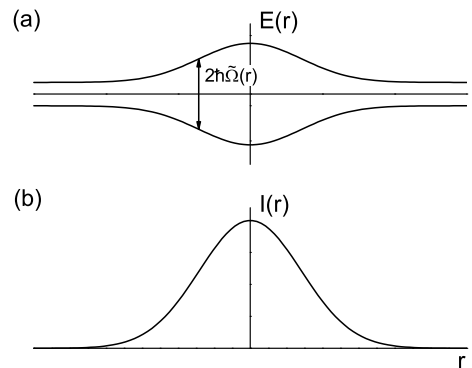
Figure 1.1.   *(a) The energy $E(r)$ of the upper and lower level of a two-level system subjected to a gaussian shaped laser beam with negative detuning with respect to the transition frequency. (b) The Intensity profile of the laser.*

A review of trapping atoms using dipolar forces can be found in [57]; a dipole trap has first been realized experimentally by Chu [58]. For quantum information processing, setups that generate and manipulate a large number of traps at the same time are of special interest. We will consider two configurations, namely *optical lattices* and *optical microtraps* further down, but let us mention before, that trapping of neutral atoms is also possible magnetically via the interaction of a magnetic field with their permanent dipole moment $\boldsymbol{\mu}_{\mathrm{mag}}$. The potential in this case is given by $V(r) = -\boldsymbol{\mu}_{\mathrm{mag}} \, \boldsymbol{B}(r)$, and traps can be created using combinations of static magnetic fields and current-carrying wires [59]. These systems currently are not as "clear" as optical systems, but in principal the integration of the whole setup for trapping atoms on a chip, *atom chips* [59, 60], is more straight-forward.

Optical lattices

In an optical lattice, potential wells are created using the dipole force produced by *standing wave* patterns formed from pairs of counter-propagating laser beams. Depending on the specific configuration of lasers, different geometries can be realized [14]. Two pairs of lasers in the correct configuration create a three-dimensional lattice where the particles are trapped in all three dimensions. Furthermore distance and position of the traps can be manipulated changing polarization and/or intensity of the lasers.

As the most easy case let us consider only a single pair of orthogonally polarized laser beams with wave vector $\boldsymbol{k}$, propagating in $\pm z$ direction (the so-called 1D lin⊥lin configuration) and an atom with an $j = \frac{1}{2}$ ground state (states $|g, m_j = \pm\frac{1}{2}\rangle$) and an $j = \frac{3}{2}$ excited state (states $|e, m_j = \pm\frac{3}{2}\rangle$ and $|e, m_j = \pm\frac{1}{2}\rangle$), cf. Fig. 1.2. Subsequently, we will follow the discussions of [22, 61]. The spatial part of the electric field can be decomposed into two standing waves
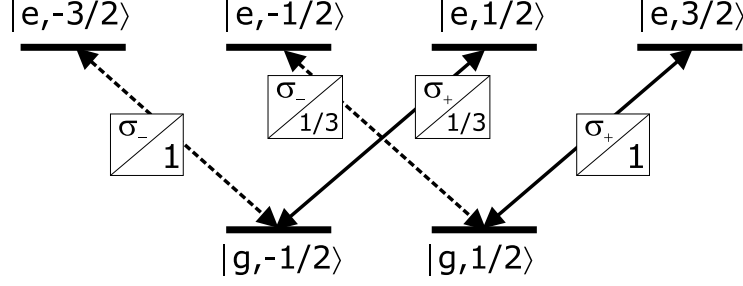
Figure 1.2. *Level scheme used for the lin ⊥ lin optical lattice configuration [22, 61]. The boxes give the polarization that couples the respective levels, and the corresponding Clebsch-Gordan-Coefficients.*

with offset $\pi/(2k) = \lambda/4$ and polarizations σ_+ and σ_-:

$$\boldsymbol{E}_0(\boldsymbol{r}) = -E_0\left[\boldsymbol{x}e^{ikz} + i\boldsymbol{y}e^{-ikz}\right] \tag{1.45}$$

$$= \sqrt{2}E_0\left[\boldsymbol{e}_+\cos(kz) - i\boldsymbol{e}_-\sin(kz)\right]. \tag{1.46}$$

σ_+ light couples only $|g,\frac{1}{2}\rangle \leftrightarrow |e,\frac{3}{2}\rangle$ and $|g,-\frac{1}{2}\rangle \leftrightarrow |e,\frac{1}{2}\rangle$, respectively, σ_- light only $|g,\frac{1}{2}\rangle \leftrightarrow |e,-\frac{1}{2}\rangle$ and $|g,-\frac{1}{2}\rangle \leftrightarrow |e,-\frac{3}{2}\rangle$. If in Eq. (1.46) only the σ_+ part would be present, then from Eq. (1.43) (leaving out the first term which has no spatial dependence) for large detuning δ from the atomic transition, the light shifts for the $|g,\pm\frac{1}{2}\rangle$ states would be

$$U^+_{\frac{1}{2}}(z) = U_0\cos^2(kz) \quad \text{and} \quad U^+_{-\frac{1}{2}}(z) = \frac{1}{3}U_0\cos^2(kz), \tag{1.47a}$$

and in the case that only the σ_- part would be present,

$$U^-_{\frac{1}{2}}(z) = \frac{1}{3}U_0\sin^2(kz) \quad \text{and} \quad U^-_{-\frac{1}{2}}(z) = U_0\sin^2(kz). \tag{1.47b}$$

Here $U_0 = \hbar\Omega^2/(4\delta)$, and the factors $\frac{1}{3}$ are due to the different Clebsch-Gordan coefficients for the transitions, cf., Fig. 1.2. Because the $|g,\pm\frac{1}{2}\rangle$ states are neither coupled directly nor connected to the same excited state, the potentials generated from σ_+ and σ_- light can simply be added for low laser intensity, such that we obtain different trapping potentials for the two states $|g,\pm\frac{1}{2}\rangle$:

$$U_{\frac{1}{2}}(z) = U_0\cos^2(kz) + \frac{1}{3}U_0\sin^2(kz) = \frac{2}{3}U_0\cos^2(kz) + \frac{1}{3}U_0, \tag{1.48a}$$

$$U_{-\frac{1}{2}}(z) = U_0\sin^2(kz) + \frac{1}{3}U_0\cos^2(kz) = \frac{2}{3}U_0\sin^2(kz) + \frac{1}{3}U_0. \tag{1.48b}$$

Such a configuration of one pair of counter-propagating lasers provides confinement only in one dimension. Confinement in all three dimensions can be obtained using two further orthogonal standing waves. Also more complicated configurations are possible [14]. The distance of traps (for the same internal state) is given by $\lambda/2$.

In Eq. (1.48) the minima of $U_{\frac{1}{2}}$ coincide with the maxima of $U_{-\frac{1}{2}}$ and vice versa. Minima and maxima can be moved on top of each other by changing the angle between the two linearly polarized lasers. If Eq. (1.45) is replaced by

$$\boldsymbol{E}_0(\boldsymbol{r}) = -E_0 \left[\boldsymbol{x} e^{ikz} + i(\boldsymbol{x} \sin\theta + \boldsymbol{y} \cos\theta) e^{-ikz} \right], \qquad (1.49)$$

then from decomposing this into $\sigma_{\pm}$ polarizations we find the potentials

$$U_{\frac{1}{2}}(z) \;=\; U_0 \cos^2\left(kz - \frac{\theta}{2}\right) + \frac{1}{3} U_0 \sin^2\left(kz + \frac{\theta}{2}\right) \qquad (1.50a)$$

$$U_{-\frac{1}{2}}(z) \;=\; U_0 \sin^2\left(kz + \frac{\theta}{2}\right) + \frac{1}{3} U_0 \cos^2\left(kz - \frac{\theta}{2}\right). \qquad (1.50b)$$

Changing θ from $\theta = 0$ to $\theta = \pi/2$ moves the potentials on top of each other. Such a state-dependent manipulation of an optical lattice has been demonstrated experimentally [23] for ^{87}Rb atoms trapped in a three dimensional lattice using lasers of wavelength $\lambda = 820$ nm. If the two computational basis states of the qubits are identified with the $|g, \pm\frac{1}{2}\rangle$ states, this is most interesting for quantum information as to some extend it allows to individually manipulate $|0\rangle$ and $|1\rangle$.

Superimposing two pairs of counter propagating laser beams with different frequencies and the same linear polarization e offers another way to manipulate the trapping potentials [62]. Rewriting the space-depending part of Eq. (1.43) by replacing $\delta = \omega - \omega_0$ as

$$U_{\text{dipol}} = \hbar \widetilde{\Omega}(\boldsymbol{r}) = \frac{\hbar}{4} \frac{\Omega^2(\boldsymbol{r})}{\omega - \omega_0} = -\hbar \frac{\Omega^2(\boldsymbol{r})}{4\omega_0} \frac{1}{1 - \frac{\omega}{\omega_0}}, \qquad (1.51)$$

it becomes clear, that for the laser frequency ω being much smaller than the transition frequency ω_0, the potential is frequency independent [63, 64]. The electric field for two pairs of counterpropagating lasers with frequencies ω_1 and ω_2 reads

$$\boldsymbol{E} = \Re \left[e \left(E_1 e^{ik_1 z - i\omega_1 t} + E_2 e^{ik_2 z - i\omega_2 t} \right) \right], \quad k_i = \frac{c}{\omega_i}, \qquad (1.52)$$

and the corresponding optical potential along the z-axis reads, after averaging out the parts oscillating at frequencies $\omega_1 - \omega_2$ and $\omega_1 + \omega_2$,

$$U(z) = U_1 \cos^2(k_1 z) + U_2 \cos(k_2 z) \quad \text{with} \quad U_i \approx \hbar \frac{\Omega_i^2}{4\omega_0} \propto I_i = E_i^2. \qquad (1.53)$$

Trapping in the other two directions can again be achieved using additional pairs of lasers. If especially ω_1 and ω_2 correspond to the first and second harmonic of a laser, *i.e.*, $\omega_2 = 2\omega_1$, then setting $I_2 = 0$ produces a lattice with periodicity $\lambda = 2\pi/(k_1)$. Increasing I_2 then serves to lower each second barrier between sites, cf., Fig. 1.3. Changing the phase of the laser of frequency ω_1 by $\pi/2$ allows to also lower the other set of potential wells. A possible candidate for such an optical lattice are ground state ^{87}Rb atoms trapped by a CO_2 laser. The first and second harmonic in this case have wavelength $\lambda_1 = 10.6$ μm and $\lambda_2 = 5.2$ μm. The D1 line of ^{87}Rb on the other hand has $\lambda_0 = 795$ nm, such that in this case the light shift potential are to a good approximation independent of the wavelength of the lasers [62–64].
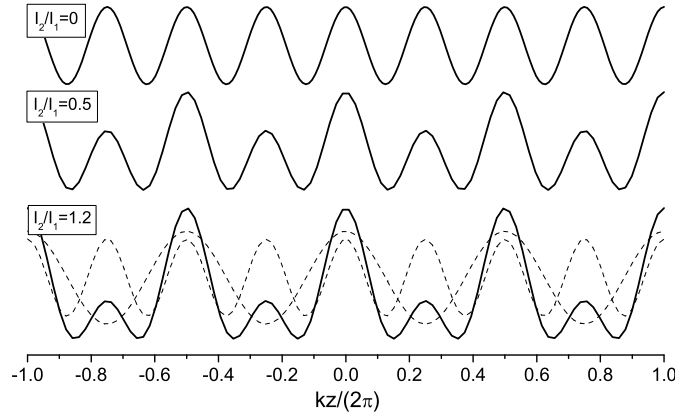
Figure 1.3. *The light potentials for two pairs of counter propagating lasers with frequencies corresponding to the first and second harmonic, cf., Eq. (1.53) with $\omega_2 = 2\omega_1$. From top to bottom I_2 is increased, such that every second potential barrier is lowered. Dashed lines in the bottom picture show the individual potentials of the two lasers.*

Optical microtraps

An alternative way to generate trap arrays, namely using *microfabricated optical elements*, has been proposed and demonstrated in [27–29]: arrays of spherical, diffractive microlenses are implemented into fused silica substrates. The lenses have typical diameters and separations of ~ 100 μm. Illuminating the substrate with a red detuned laser beam produces an array of foci, *i.e.*, points of maximal intensity of light, and thus by the dipole force an array of traps with confinement in all three dimensions is generated, cf. Fig. 1.4 (a). The separation of traps in this case is the same as the spacing between the lenses, and thus it is much larger as in the case of optical lattices, such that individual traps can be accessed. Two dimensional arrays of around 80 traps have been demonstrated [29]. The technique of microfabricated optical elements is in principle also much more flexible than an optical lattice, at it allows to realize a large variety of other trapping geometries, as, *e.g.*, different patterns of traps, or waveguides with complex spatial variation [28, 65].

The shape of the potentials is determined by the spatial dependence of the laser intensity in the foci, *i.e.*, the potentials are gaussian-shaped in all the three spatial dimensions. For spherical lenses they have a cylindrical symmetry, and usually trapping is less tight in the direction of propagation of the laser beam, thus in this case the typical potential of one trap has the form

$$U\left(\boldsymbol{r} = (x,y,z)\right) = U_0 \exp\left(-\frac{1}{2}\frac{m\omega_\perp^2}{U_0}\left[x^2 + y^2\right] - \frac{1}{2}\frac{m\omega_\parallel^2}{U_0}z^2\right). \tag{1.54}$$

For large potential depth U_0 the traps can be approximated by a harmonic potential with
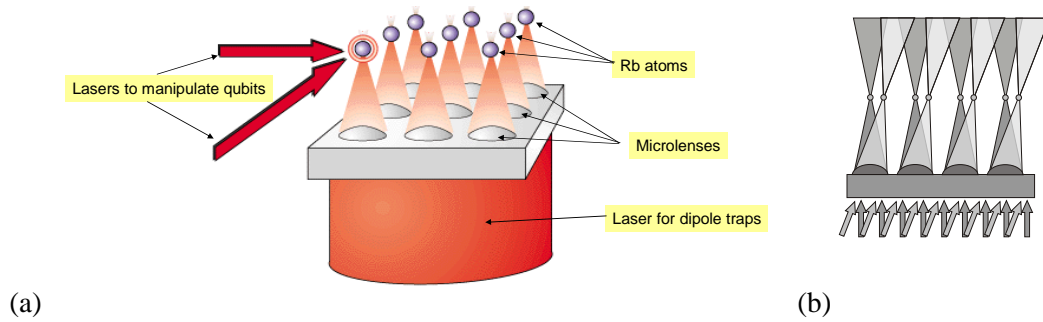
Figure 1.4.   *(a) Schematic illustration of the realization of a two dimensional array of optical microtraps obtained by focusing a red detuned laser with an array of microlenses as discussed in [29]. (b) Changing the distance between two sets of traps by illuminating the lenses by two laser beams tilted with respect to each other. Figure (b) from [29].*

frequency $\omega_\perp$ in x and y, and $\omega_\parallel$ in z direction, with typical trapping frequencies being $\omega_\perp = 2 \times 10^6$ s^{-1} and $\omega_\parallel = 2 \times 10^5$ s^{-1} [27].

Various manipulations of the trapping potential necessary for quantum information processing are possible. As in optical lattices, state dependent potentials can be generated playing with the level structure of the atoms and the polarizations of the lasers. Various methods to achieve a variation of the spatial potential, *i.e.*, approaching and separating traps, seem possible or have already been realized experimentally: (i) Tilting the laser with respect to the substrate allows to move the traps in space, such that using two lasers inclined with respect to each other generates two sets of traps which can be approached and separated, as demonstrated in [29], cf., Fig. 1.4 (b). (ii) Two parallel laser beams can be used, which are focused in such a way that the trapping potentials are longitudinally shifted along the common laser beam direction.

An alternative way to generate an array of manipulable small microtraps is to use holographic techniques [30]. Here a computer designed diffractive optical element is used as a diffraction grating to split a single beam into several ones, which are then focused again to form a set of traps. As the hologram can be computer-calculated and especially changed in real-time, in principle each site can be moved and switched on and of individually. In such a scheme, recently the realization of up to four traps has been demonstrated experimentally.

Quantum computation with optical lattices and optical microtraps

Let us apply the criteria of Divincenzo from section 1.2.1 to optical lattices as well as for optical microtraps, see also [49, 66]

➤ *Well-characterized qubits* —   For both systems motional as well as internal states provide choices for the implementation of qubits. Using motional states has been proposed in [46, 62] and will be further discussed in Chapter 2. Using internal states [16–21] is especially interesting, because in this case state dependent potentials are possible. Further

definitions of a qubit using neither internal nor motional states are possible. An example will be discussed in Chapter 3.

➤ *Initialization of a well-defined state* — To achieve a well-defined initial state, each trap has to be loaded with exactly one atom. For optical lattices this can be achieved *via* loading from a laser-cooled sample in a magneto-optical trap (MOT) and using a transition to a Mott insulator [67], a state with a well-defined number of atoms per lattice site, as has already been demonstrated experimentally [15]. For optical microtraps it has been demonstrated [30–32] that it is possible to load a single atom in such a trap with sub-poissonian statistics. The idea is to strongly reduce the trapping volume, such that only one atom can be loaded at a time. However, the process is statistical, such that loading a large number of traps to initialize a large register of qubits is challenging. In this case also further cooling of the atoms to the motional ground state will be required. This is possible using techniques of laser and Raman sideband cooling [29, 51–54], where ground-state populations larger than 95% have been achieved [51]. Preparation of internal state is possible with very high fidelities $F > 0.9999$ *via* optical-pumping techniques [49].

➤ *Long decoherence times* — Scattering of photons from the trapping lasers provides the main source of decoherence. The rate of such scattering events is on the order of $1 \ldots 100$ per second [32, 68] for Rubidium atoms and a wavelength of the trapping laser of $\lambda = 820 \, \text{nm}$ (which is far off resonance from the Rubidium D1 and D2 line (795 nm and 780 nm, respectively). This leads to decoherence times on the order of $10 \, \text{ms} \ldots 1 \, \text{s}$. A further source of decoherence are fluctuations of the intensity of the lasers (changing the trapping depth and frequency) and, in the case of optical lattices, also fluctuations of the polarization (displacing the traps). The decoherence times for these sources in current experiments are expected to be of the same order of magnitude [32]. Shaking of the trapping potentials will also be induced by mechanical vibrations of the experimental setup.

➤ *A universal set of quantum gates* — Depending on how the qubit is implemented and how the trapping potentials can be manipulated there are many possible techniques to implement quantum gates. In most cases the manipulation of individual qubits *via* methods from laser spectroscopy is straight-forward. However, as in optical lattices the distance of the atoms is only half the wavelength of the trapping lasers, addressing single sites, and thus individual qubits, is a problem in certain configurations. Especially designed lattices (where the atoms are separated by more than one wavelength [69]), loading atoms only in a part of the lattice [69], using lasers with long wavelengths (*e.g.*, CO_2 lasers, where individual addressing of Rb atoms has been demonstrated [70]), or using gradient fields to distinguish atoms in neighboring traps allow to avoid this problem, which, due to the large separation of traps is avoided for implementations of optical microtraps [29]. Also it has been proposed to circumvent the problem of addressing individual sites through marker qubits [26].

For two qubits gates the use of either collisional or of electric dipole interactions has been proposed. In the former case, state-dependent potentials together with a qubit encoded in internal states [16, 17] or tunneling dependent on motional states allow for conditional dynamics [46, 62]. A proposal using motional states will be presented in detail in Chapter 2. In the case of dipole interactions especially the excitation of a Rydberg state with large electrical dipole moment [21] is of interest, as contrary to other proposals here atoms do not have to be moved, allowing fast gate operation times only limited by the interaction

strength. If atoms have to be moved during the gate process, as it is the case for all proposals using collisional interaction, operation times are limited by the trap frequency (which is in the range of $10^4 \ldots 10^6 \, \text{s}^{-1}$). Additionally, also a two-qubit gate using purely geometric evolution has been proposed [71].

In optical lattices, a two qubit gate based on the collisional interaction has been demonstrated experimentally [24] using state dependent lattice potentials. With this method however it is impossible to perform gate operations between a selected pair of neighboring qubits, but it only allows gate operations between all pairs of neighbors simultaneously, as only the complete lattice can be shifted at once.

➤ *Capability to measure the output result* — Detection of the atomic state using the *quantum-jump* technique [55] is a well-established method in quantum optics, but again the read-out of specific sites is a problem in standard optical lattices.

1.3   Conclusion

In this section, basic elements of quantum information processing have been discussed, concentrating especially on properties of quantum bits and on their manipulation via gate operations. Subsequently, the list of the so-called DiVincenzo criteria has been presented. This list gives a number of conditions which have to be met by any physical system in order to be able to perform full quantum computation. For neutral atoms trapped in optical potentials, a system which will be of special importance in the next Chapters, the realization of the trapping potentials has been discussed together with methods to manipulate these potentials, and the criteria for quantum computation have been evaluated for this particular setup.

CHAPTER 2

QUANTUM INFORMATION PROCESSING WITH MOTIONAL STATES OF
TRAPPED NEUTRAL ATOMS

2.1 Overview

Many proposed implementations of quantum computing with trapped neutral atom use internal states to represent the qubit and realize gate operations by applying state dependent operations to the atoms, *e.g.*, state-dependent excitation to a level with large dipole-moment or state-dependent potentials. In this chapter we address the realization of a two-qubit gate for neutral atoms trapped in optical potentials with the qubit implemented *in the motional states* of the atoms. In this case, gates can be realized without state-dependent operations through an interplay of tunneling and interactions between the atoms.

More precisely, the computational basis states $|0\rangle$ and $|1\rangle$ are represented by the atom being in the ground or the first vibrational state of the trap, respectively. For such a system we will show how to implement the universal $\sqrt{\text{SWAP}}$ gate, based on an interplay of tunneling between traps and collisional atomic interactions. Note that, as for the ion-trap case, the observation of neutral atoms cooled down to the ground and first vibrational state as well as superpositions of these states have been observed in experiments [72].

For performing quantum computation in such a system, we will assume traps occupied with single laser-cooled Rb atoms, which initially are well separated, such that neither tunneling nor collisional interactions are important. Both these mechanisms are switched on continuously by adiabatically approaching two traps to a close distance. After a specified time the traps are separated again, and as we will show, the strong dependence of the dynamics on the vibrational states of the trapped atoms can be used to control the interaction such that finally each trap again holds exactly a single atom and furthermore the desired gate operation is realized. The results we present in the following apply to ^{85}Rb as well as to ^{87}Rb, although they have negative and positive scattering length, respectively. The process of approaching and separating two adjacent traps is possible in optical lattices using pairs of counter-propagating lasers with two different frequencies, as well as in optical microtraps using, *e.g.*, two lasers illuminating the lenses, cf., section 1.2.2. For trap frequencies of 1×10^4 s^{-1}, a parameter realistic for optical microtraps, the gate duration is less then 20 ms for a fidelity $F \gtrsim 1 - 10^{-3}$.

In the following, in Section 2.2 we will first discuss in detail the model we use to describe the system of the two traps, which then in Section 2.3 will be employed for a detailed analysis of the operation of a $\sqrt{\text{SWAP}}$ gate. Thereafter, in Section 2.4 we will discuss the evolution of quantum correlations during the gate operation. As for the process two indistinguishable atoms have to be brought to a close distance, the quantum statistical nature of the particles (bosonic in the case of ^{85}Rb and ^{87}Rb) has to be taken into account. Finally, Section 2.5 will be devoted to aspects of implementing such a quantum gate, where especially an implementation for RB atoms in arrays of optical microtraps will be considered.

2.1.1   Related work

An implementation of a $\sqrt{\text{SWAP}}$ gate for two qubits has been proposed by Schliemann *et al.* in [73] for two electrons confined in two coupled quantum dots. In this case, the qubit is implemented in the electronic spin, and the interaction mechanism is given by the repulsive Coulomb interaction between the two electrons.

Charron *et al.* propose to implement a phase gate between two ^{87}Rb atoms in an optical lattice potential [62]. In this case the qubits are also implemented in the motional states, and a scheme relying on the destructive interference between different pathways leading to the same state is used in order to suppress double occupation.

2.2   Model: Hamiltonian and states

2.2.1   The Hamiltonian

The Hamiltonian which describes the dynamics of two indistinguishable atoms in a time-varying single-particle potential $V(\boldsymbol{r}, t)$ in the presence of a two-particle interaction $U(\boldsymbol{r}_i, \boldsymbol{r}_j) = U(\boldsymbol{r}_i - \boldsymbol{r}_j)$ is written as

$$H = \sum_{i=1,2} \left[\frac{1}{2m} \boldsymbol{p}_i^2 + V(\boldsymbol{r}_i, t) \right] + U(\boldsymbol{r}_1 - \boldsymbol{r}_2), \tag{2.1}$$

where m is the atomic mass, and $\boldsymbol{r}_i$, $\boldsymbol{p}_i$ are the (three-dimensional) position and momentum operator for atom i. To simplify the problem let the single-particle potential V be of the form

$$V(\boldsymbol{r}, t) = v(x, t) + v_p(y) + v_p(z), \tag{2.2}$$

i.e., the three spatial directions are not coupled and the potentials in y and z directions are are time-independent and identical. We will assume that the particles are cooled down to the y and z ground state, and we will assume a much stronger confinement in y and z directions, such that in these two directions the atoms remain all the time in the vibrational ground state.

For cold bosonic atoms, the interaction term is dominated by s-wave scattering [17, 74]. Such a scattering can be described by a contact potential of the form

$$U(\boldsymbol{r}_1 - \boldsymbol{r}_2) = \frac{4\pi a_t \hbar^2}{m} \, \delta^3(\boldsymbol{r}_1 - \boldsymbol{r}_2). \tag{2.3}$$

Here a_t is the *s*-wave scattering length of the Rb atoms, which in the spin triplet has the values $a_t = -369a_0 = -19.53$ nm for ^{85}Rb and $a_t = 106a_0 = 5.61$ nm for ^{87}Rb. Thus interaction for ^{85}Rb is attractive, while it is repulsive for ^{87}Rb. a_0 is the *Bohr radius*. As the single-particle potential does not couple the *x* degree of freedom with the orthogonal directions and as we assume the atom to be in the *y* and *z* vibrational ground state all the time, it is possible to integrate out the *y* and *z* directions to get an effective one-dimensional Hamiltonian [17]. To do this consider the Hamiltonian in second quantized notation

$$
\begin{aligned}
\hat{H} &= \int d^3r\, \hat{\Psi}^\dagger(\boldsymbol{r}) \left[-\frac{\hbar^2}{2m} \boldsymbol{p}^2 + V(\boldsymbol{r}, t) \right] \hat{\Psi}(\boldsymbol{r}) + \\
&\quad + \frac{1}{2} \int d^3r \int d^3r'\, \hat{\Psi}^\dagger(\boldsymbol{r}) \hat{\Psi}^\dagger(\boldsymbol{r}') U(\boldsymbol{r} - \boldsymbol{r}') \hat{\Psi}(\boldsymbol{r}) \hat{\Psi}(\boldsymbol{r}'),
\end{aligned}
\tag{2.4}
$$

where $\hat{\Psi}^\dagger(\boldsymbol{r})$ is a field operator for an atom (we will consider a single internal state only). Assuming to know the ground state wave function $\psi_p(x)$ of a particle in the potential v_p, the integral over two of the three dimensions can be performed and an effective one-dimensional Hamiltonian remains:

$$
\begin{aligned}
\hat{H}_{1D} &= \int dx\, \hat{\Psi}^\dagger(x) \left[-\frac{\hbar^2}{2m} p_x^2 + v(x, t) \right] \hat{\Psi}(x) + \\
&\quad + \frac{1}{2} \int dx \int dx'\, \hat{\Psi}^\dagger(x) \hat{\Psi}^\dagger(x) u(x - x') \hat{\Psi}(x) \hat{\Psi}(x).
\end{aligned}
\tag{2.5}
$$

The one-dimensional contact interaction potential $u(x - x')$ which has been introduced here can be evaluated as

$$
u(x - x') = \int dy\, dz \int dy'\, dz'\, U(\boldsymbol{r} - \boldsymbol{r}') |\psi_p(y)\psi_p(y')\psi_p(z)\psi_p(z')|^2
\tag{2.6}
$$

$$
= \frac{4\pi a_t \hbar^2}{m} \delta(x - x') \left[\int dy\, |\psi_p(y)|^4 \right]^2,
\tag{2.7}
$$

where $\psi_p(y)$ is the spatial wavefunction of the ground state in *y* and *z* direction. Assuming the potential v_p to have harmonic shape with frequency ω_p, *i.e.*, $v_p(y) = \frac{1}{2} m \omega_p^2 y^2$, then the ground state reads

$$
\psi_p(y) = \frac{\sqrt{\alpha_p}}{\sqrt[4]{\pi}} e^{-\frac{\alpha_p^2}{2}x^2}, \qquad \alpha_p = \sqrt{\frac{m\omega_p}{\hbar}},
\tag{2.8}
$$

where α_p is the inverse of the size of the ground state. In this case

$$
u(x - x') = \frac{2a_t \hbar^2 \alpha_p^2}{m} \delta(x - x') = 2a_t \hbar \omega_p\, \delta(x - x')
\tag{2.9}
$$

is the effective one-dimensional potential modeling the two-particle interaction. The complete effective one-dimensional Hamiltonian which we will subsequently use intensively reads

$$
H = \frac{1}{2m} p_x^2 + v(x, t) + 2a_t \hbar \omega_p\, \delta(x_1 - x_2).
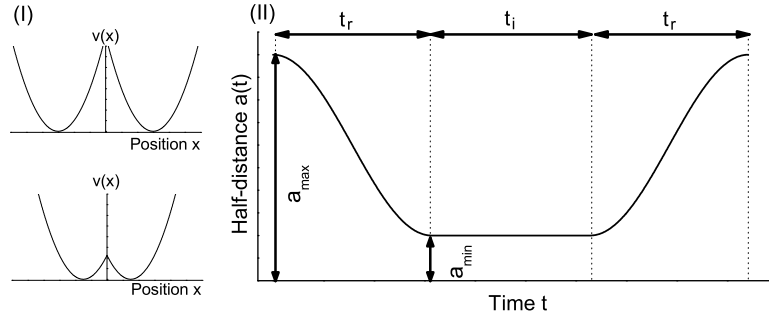\tag{2.10}
$$

Figure 2.1.   *(I) Model potentials composed of two concatenated harmonic potentials used for the simulation of the gates. (II) Temporal variation of the separation of the traps. $a(t)$ is half the distance between them. The approaching process from the maximal distance a_{max} to a distance a_{min} is modeled as the first half of a cosine, taking a time t_r. During a time t_i the traps are kept at the minimal distance, before they are separated again.*

Throughout this chapter we approximate the potentials from Eqns. (1.53) or (1.54) by a simplified potential consisting of two harmonic traps of frequency ω_x, centered at $x = \pm a(t)$ and concatenated at $x = 0$ (see Fig. (2.1,I)):

$$v(x, t) = \frac{m}{2}\omega_x^2 \left\{ [x + a(t)]^2 \, \Theta(-x) + [x - a(t)]^2 \, \Theta(x) \right\}. \tag{2.11}$$

Here $\Theta(x)$ is the step-function. The temporal variation of the half-distance of the traps is modeled as

$$a(t) = \begin{cases} (a_{\max} - a_{\min})\frac{1+\cos(\pi t/t_r)}{2} + a_{\min} & 0 < t < t_r \\ a_{\min} & t_r < t < t_r + t_i \\ (a_{\max} - a_{\min})\frac{1+\cos(\pi(t-t_r-t_i)/t_r)}{2} + a_{\min} & t_r + t_i < t < 2t_r + t_i \end{cases}, \tag{2.12}$$

see Fig. (2.1,II). Initially the traps are separated by $a(t) = 2a_{\max}$. They are approached to a separation $a(t) = 2a_{\max}$ in a time t_r (*ramping time*), thereby continuously turning on tunneling and interaction. After waiting a time t_i (*interaction time*[1]), the traps are separated in a process symmetric to the approaching, taking again a time t_r. We will always demand that the process of approaching and separating the traps is adiabatic, such that the population of eigenstates remains unchanged throughout the process. Thus if the traps are moved with velocity v, we demand $v < \sqrt{2\Delta E/m}$, where ΔE is the typical spacing between the levels. Inserting $\Delta E = \Delta E_0 \equiv \hbar\omega_x$, this directly allows to estimate the time t necessary to move the traps by $\Delta x = \alpha^{-1}$, where $\alpha^{-1} = \sqrt{\hbar/(m\omega)}$ is the size of the ground state of a single potential, as $t > 1/(\sqrt{2}\omega_x)$. The times t_r will be bigger than this estimation by about an order of magnitude as $\Delta E < \Delta E_0$ during the process of approaching the traps.

---

[1]The true interaction time is larger than t_i as tunneling and interaction are present also for $a > a_{\min}$.

2.2.2 Single-particle states

We will implement the qubits into the ground and first excited vibrational states of each trap, *i.e.*, we will use the motional states of the atoms. When the two traps are far apart, *i.e.*, for the trap distance a it holds $a\alpha \gg 1$, then these states are the energy eigenstates of two one-dimensional harmonic oscillators displaced by $\pm a$:

$$\langle x|0\rangle_{L,R} = \frac{\sqrt{\alpha}}{\sqrt[4]{\pi}} e^{-\frac{1}{2}\alpha^2(x\pm a)^2}, \tag{2.13a}$$

$$\langle x|1\rangle_{L,R} = \frac{\sqrt{2\alpha}}{\sqrt[4]{\pi}} e^{-\frac{1}{2}\alpha^2(x\pm a)^2} \alpha(x \pm a), \tag{2.13b}$$

with L and R labeling the left and right trap, respectively. As the two traps are approached, these single-particle states start to overlap and are no longer orthogonal. To numerically integrate the Schrödinger equation and to compute entanglement throughout the gate process, we construct an orthonormal single-particle basis for arbitrary distances of the two traps by applying the *Gram-Schmidt method* [75]. The goal is to construct a new basis of single-particle states denoted by $|\bar{i}\rangle_s$ with $i = 0, 1, 2, 3...$ and $s = L, R$, such that (i) it holds $_s\langle \bar{i}|\bar{j}\rangle_t = \delta_{ij}\delta_{st}$, (ii) for $a \to \infty$ we have that $|\bar{i}\rangle_s \to |i\rangle_s$, and (iii) for parity transformations $x \mapsto -x$ we want the following symmetry property to hold always: $|\bar{i}\rangle_{L,R} \mapsto (-1)^i |\bar{i}\rangle_{R,L}$. This is a property that obviously holds for the $|i\rangle_{L,R}$. The four states that fulfill these properties and that for large distances correspond to the two lowest states of each trap read

$$\langle x|\bar{0}\rangle_{L,R} = \langle x|0\rangle_{L,R}\frac{\xi_0^+ + \xi_0^-}{2} + \langle x|0\rangle_{R,L}\frac{\xi_0^+ - \xi_0^-}{2} \tag{2.14a}$$

$$\langle x|\bar{1}\rangle_{L,R} = (\langle x|1\rangle_{L,R} - \frac{xe^{-a^2\alpha^2}}{\pi^{1/4}\alpha^{3/2}}\langle x|0\rangle_{R,L})\frac{\xi_1^+ + \xi_1^-}{2}$$

$$+ (\langle x|1\rangle_{R,L} - \frac{xe^{-a^2\alpha^2}}{\pi^{1/4}\alpha^{3/2}}\langle x|0\rangle_{L,R})\frac{\xi_1^- - \xi_1^+}{2} \tag{2.14b}$$

where $\xi_0^\pm(a)$ and $\xi_1^\pm(a)$ will be given later in Eq. (2.21). For large separation of the traps, *i.e.* $a\alpha \gg 1$, we have $\xi_i^+ = \xi_i^-$ for all i and $e^{-a^2\alpha^2} \to 0$, and thus the $|\bar{i}\rangle_{L,R}$ become the eigenstates of a single harmonic trap centered at $\mp a$.

In general the states $|\bar{i}\rangle_{L,R}$ are constructed as follows: we start by defining (non-normalized) states involving one state of each trap:

$$|i\rangle^\pm \equiv \frac{1}{\sqrt{2}}\left[|i\rangle_L \pm (-1)^i|i\rangle_R\right] \qquad i = 0, 1, 2, 3, \dots \tag{2.15}$$

where the superscript $+$ $(-)$ indicates positive (negative) parity with respect to the middle between the two traps. We then group these states according to their parity into two sets $S^\pm = \{|0\rangle^\pm, |1\rangle^\pm, \dots\}$. States from different sets are orthogonal. We focus first on the positive parity set S^+. This set contains states that are neither orthogonal nor normalized. To perform the orthonormalization, we use the Gram-Schmidt (GM) method starting by normalizing $\langle x|0\rangle^+$:

$$\phi_0^+(x, a) \equiv \frac{\langle x|0\rangle^+}{\int dx\, |\langle x|0\rangle^+|^2}. \tag{2.16}$$

Then the first linearly independent function ϕ_1^+ is defined as:

$$\phi_1^+(x,a) = \frac{\langle x|1\rangle^+ + a_{10}\phi_0^+(x,a)}{\int dx\,|\langle x|1\rangle^+ + a_{10}\phi_0^+(x,a)|^2}. \tag{2.17}$$

where $a_{10} = -\int dx\,\left(\phi_0^+(x,a)\right)^* \langle x|1\rangle^+$, which guaranties that $\langle\phi_0^+|\phi_1^+\rangle = 0$. This procedure can be repeated to recursively define all the states with positive parity $\phi_n^+(x,a)$ as follows:

$$\phi_n^+(x,a) = \frac{\langle x|n\rangle^+ + \sum_{m<n} a_{nm}\phi_m^+(x,a)}{\int dx\,\left|\langle x|n\rangle^+ + \sum_{m<n} a_{mn}\phi_m^+(x,a)\right|^2 dx}, \tag{2.18}$$

where

$$a_{nm} = -\int dx\,\left(\phi_n^+(x,a)\right)^* \langle x|m\rangle^+. \tag{2.19}$$

In an analogous way, the set of linearly independent functions $\left\{\phi_0^-, \phi_1^-, \phi_2^-, \phi_3^-, ...\right\}$ is determined from S^-. States $|\phi_n^+\rangle$ are constructed exclusively from states of the set of positive parity states S^+, and thus also have positive parity. For the same reason, states $|\phi_n^-\rangle$ always have negative parity. Therefore, the whole set of states $\left\{\phi_0^\pm, \phi_1^\pm, \phi_2^\pm, \phi_3^\pm, ...\right\}$ is a set of orthonormalized states. Explicitly, the first four orthonormalized functions read

$$\phi_0^\pm(x,a) = \xi_0^\pm(a)\langle x\,|0\rangle^\pm \qquad \text{and} \tag{2.20a}$$

$$\phi_1^\pm(x,a) = \xi_1^\pm(a)\left(\langle x\,|1\rangle^\pm \pm \frac{x\alpha^{3/2}}{\sqrt[4]{4\pi}}e^{-a^2\alpha^2}\langle x\,|0\rangle^\mp\right), \tag{2.20b}$$

where

$$\xi_0^\pm(a) = \frac{1}{\sqrt{1 \pm e^{-a^2\alpha^2}}}, \tag{2.21a}$$

$$\xi_1^\pm(a) = \frac{e^{a^2\alpha^2}}{\sqrt{\left(e^{a^2\alpha^2} \pm 1\right)\left(e^{a^2\alpha^2} - e^{-a^2\alpha^2} \pm 2a^2\alpha^2\right)}}. \tag{2.21b}$$

Once the orthonormal set $\{\phi_n^\pm\}$ has been obtained, it is straightforward to write down the single-particle basis that we will use:

$$\langle x|\bar{n}\rangle_L = \frac{1}{\sqrt{2}}\left(\phi_n^+ + \phi_n^-\right) \tag{2.22a}$$

$$\langle x|\bar{n}\rangle_R = (-1)^n \frac{1}{\sqrt{2}}\left(\phi_n^+ - \phi_n^-\right), \tag{2.22b}$$

These states are (i) orthonormal due to the orthonormality of the $\phi_n^\pm$ and (ii) in the limit $a\alpha \gg 1$ we have that $a_{nm} \to 0$ for $n \neq m$, such that $\langle x|\bar{n}\rangle_{L,R}$ become the corresponding harmonic oscillator energy eigenstates for each trap. (iii) These new orthonormal states in general do not have a well defined parity with respect to the center of the corresponding trap, but it is straightforward to check from Eqs. (2.22) that they satisfy the following property under parity transformation $P: x \mapsto -x$ with respect to the midpoint between the two traps, $x = 0$:

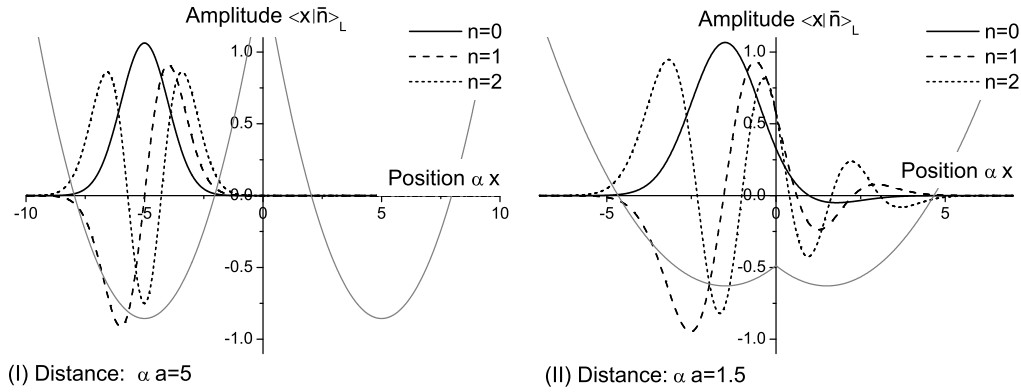$$\langle x|\bar{n}\rangle_{L,R} \xrightarrow{P} (-1)^n \langle x|\bar{n}\rangle_{R,L}. \tag{2.23}$$

Figure 2.2. *The states $\langle x|\overline{n}\rangle_L$ constructed via the Gram-Schmidt method for two different distances of the traps.*

In the simulations that are presented in the following we have included states $\langle x|\overline{n}\rangle_{L,R}$ up to $n = 3$. The states up to $n = 2$ are depicted in Fig. 2.2 for two different distances of traps. Let us note explicitly that the basis we use consists of states which in the limit of large separation are localized in one of the traps. It is however *not* a basis of eigenstates of the single-particle Hamiltonian.

2.2.3 A basis of two-particle states

In order to describe the dynamics of the two qubit operations, we shall now construct a basis of states of two particles. Also this basis should fulfill certain properties to simplify the analysis of the gate: (i) we analyze bosonic atoms here, so the basis should fulfill bosonic statistics, *i.e.*, it should be symmetric under the permutation of particles. Then for a n-dimensional single-particle basis, there are $n(n + 1)/2$ two-particle basis states to be constructed. (ii) As the Hamiltonian from Eq. (2.10) is symmetric with respect to parity transformation, *i.e.*, $H(x) = H(-x)$, it does not couple states of opposite parity. For this reason we want the basis we introduce to have well defined positive or negative parity. (iii) In the limit of large separation of the traps, $\alpha a \gg 1$, there are states which have contributions of two states being in the same trap. As these types of states are not favorable as final states for the quantum gate operation, also the basis should be divided into those states which contain only singly occupied traps and those which only contain double-occupation (always in the limit of large separation of the traps).

We will subsequently abbreviate notation by setting $|\overline{m}(1)\rangle_s \otimes |\overline{n}(2)\rangle_t \equiv |\overline{m}\rangle_s|\overline{n}\rangle_t$, where 1, 2 label the particles and $s,t \in \{L,R\}$ labels the traps. Furthermore we will indicate states with positive or negative parity writing $|\ldots\rangle^+$ or $|\ldots\rangle^-$, respectively. States which represent double occupation will carry a subscript D. Limiting ourselves for this description to the four single particle states with lowest energy, then the ten-dimensional basis we use for the

bosonic two particle sector reads

$$|00\rangle^+ \;=\; \frac{1}{\sqrt{2}}\left(|\bar{0}\rangle_L|\bar{0}\rangle_R + |\bar{0}\rangle_R|\bar{0}\rangle_L\right), \tag{2.24a}$$

$$|01\rangle^+ \;=\; \frac{1}{2}\left(|\bar{0}\rangle_L|\bar{1}\rangle_R + |\bar{1}\rangle_R|\bar{0}\rangle_L - |\bar{0}\rangle_R|\bar{1}\rangle_L - |\bar{1}\rangle_L|\bar{0}\rangle_R\right), \tag{2.24b}$$

$$|11\rangle^+ \;=\; \frac{1}{\sqrt{2}}\left(|\bar{1}\rangle_L|\bar{1}\rangle_R + |\bar{1}\rangle_R|\bar{1}\rangle_L\right), \tag{2.24c}$$

$$|00\rangle_D^+ \;=\; \frac{1}{\sqrt{2}}\left(|\bar{0}\rangle_L|\bar{0}\rangle_L + |\bar{0}\rangle_R|\bar{0}\rangle_R\right), \tag{2.24d}$$

$$|01\rangle_D^+ \;=\; \frac{1}{2}\left(|\bar{0}\rangle_L|\bar{1}\rangle_L + |\bar{1}\rangle_L|\bar{0}\rangle_L - |\bar{0}\rangle_R|\bar{1}\rangle_R - |\bar{1}\rangle_R|\bar{0}\rangle_R\right), \tag{2.24e}$$

$$|11\rangle_D^+ \;=\; \frac{1}{\sqrt{2}}(|\bar{1}\rangle_L|\bar{1}\rangle_L + |\bar{1}\rangle_R|\bar{1}\rangle_R), \tag{2.24f}$$

for the states with positive parity and

$$|01\rangle^- \;=\; \frac{1}{2}\left(|\bar{0}\rangle_L|\bar{1}\rangle_R + |\bar{1}\rangle_R|\bar{0}\rangle_L + |\bar{0}\rangle_R|\bar{1}\rangle_L + |\bar{1}\rangle_L|\bar{0}\rangle_R\right), \tag{2.25a}$$

$$|00\rangle_D^- \;=\; \frac{1}{\sqrt{2}}\left(|\bar{0}\rangle_L|\bar{0}\rangle_L - |\bar{0}\rangle_R|\bar{0}\rangle_R\right), \tag{2.25b}$$

$$|01\rangle_D^- \;=\; \frac{1}{2}\left(|\bar{0}\rangle_L|\bar{1}\rangle_L + |\bar{1}\rangle_L|\bar{0}\rangle_L + |\bar{0}\rangle_R|\bar{1}\rangle_R + |\bar{1}\rangle_R|\bar{0}\rangle_R\right), \tag{2.25c}$$

$$|11\rangle_D^- \;=\; \frac{1}{\sqrt{2}}\left(|\bar{1}\rangle_L|\bar{1}\rangle_L - |\bar{1}\rangle_R|\bar{1}\rangle_R\right) \tag{2.25d}$$

for the states with negative parity. Using the parity property of states $|\bar{n}\rangle_{L,R}$ from Eq. (2.23) the parity property (ii) demanded for the two particle states is easily checked. In the simulations we present in the following up to eight single-particle states will be considered, which gives rise to a bosonic two-particle Hilbert space of 36 states (20 states having positive parity from which 10 correspond to double occupancy; and 16 states having negative parity with 10 accounting for double occupancy).

Finally note that the fact that we are able to expand the wavefunction into this finite number of two-particle orthogonal states has also an important advantage with respect to the time needed for the simulation of a gate operation. We have checked the accuracy of the restriction of the simulation to this subspace by comparing the results of the simulations to a direct numerical integration of the Schrödinger equation for the two-particle spatial wavefunction which is about four orders of magnitude slower. In these numerical simulations, the contact interaction potential $u(x - x') \propto \delta(x)$ has been approximated *via* a gaussian potential with properly adjusted width and height.

2.3 Gate operation

2.3.1 Single qubit gates

With the traps well separated, single qubit operations, *e.g.*, a Hadamard or a NOT gate, can be realized by using two laser pulses in a Raman configuration focused solely on one of the

traps. Transfer of atoms between vibrational levels using Raman pulses tuned to the blue sideband has been observed experimentally [76].

2.3.2 Two qubit operations: a $\sqrt{\text{SWAP}}$ gate

For the two qubit operations we start from the two traps being far apart, each containing one atom. In this situation we can neglect the bosonic nature of the particles and for all practical purposes forget about the symmetrization [4]. Only then it is possible to speak about well-defined qubits and we choose to introduce labels A and B for them by labeling the atom found in the left trap as A and the atom in the right trap as B. Approaching the two traps, the wavefunctions of atoms in the left and in the right trap start to overlap, and the indistinguishability of the atoms has to be taken into account. In this case there is no precise definition of the qubits. Only if the process of approaching and separating the traps is done such that after the operation there is again one atom in each of the well separated traps, then we can finally attribute (new) labels A and B to each of the atoms; and only then some gate operation has been performed successfully

These considerations suggest the following mapping of the states of the computational basis into the two-particle basis states of Eq. (2.24) and Eq. (2.25)):

$$|0\rangle_A|0\rangle_B \quad \rightarrow \quad |00\rangle^+ \tag{2.26a}$$

$$|0\rangle_A|1\rangle_B \quad \rightarrow \quad |01\rangle \equiv \frac{1}{\sqrt{2}}\left(|01\rangle^+ + |01\rangle^-\right) \tag{2.26b}$$

$$|1\rangle_A|0\rangle_B \quad \rightarrow \quad |10\rangle \equiv \frac{1}{\sqrt{2}}\left(|01\rangle^+ - |01\rangle^-\right) \tag{2.26c}$$

$$|1\rangle_A|1\rangle_B \quad \rightarrow \quad |11\rangle^+. \tag{2.26d}$$

Note that the two particle states at the r.h.s of Eqs. (2.26) for $\alpha a \gg 1$ have a trivial evolution at the trapping frequency or at multiples of it that can be removed by including these phases into the definition of the single particle states.

Identification of resonant couplings

Assuming the two atoms initially to be in a superposition of the states from Eqs. (2.26), then after realizing the gate operation, we want to finish in another superposition of the same states. Taking the evolution to be completely in the adiabatic regime as discussed in Section 2.2.1, then transitions are only allowed between states that (i) are initially degenerate in energy and at short distances (ii) become coupled via tunneling and/or cold collisions. Therefore, in order to find the most suitable gate to be implemented in this system, we have to identify these resonant couplings.

Let us discuss first the case for which there is no interaction between the atoms, *i.e.*, the case where $a_t = 0$ in Eq. (2.10). In this case tunneling is the only mechanism present in the system, and the resonant couplings are easily identified as

$$|00\rangle^+ \quad \leftrightarrow \quad |00\rangle^+, \tag{2.27a}$$

$$|01\rangle \quad \leftrightarrow \quad |01\rangle_D \leftrightarrow |10\rangle \leftrightarrow |10\rangle_D \leftrightarrow |01\rangle, \tag{2.27b}$$

$$\text{and} \quad |11\rangle^+ \quad \leftrightarrow \quad |11\rangle^+, \tag{2.27c}$$
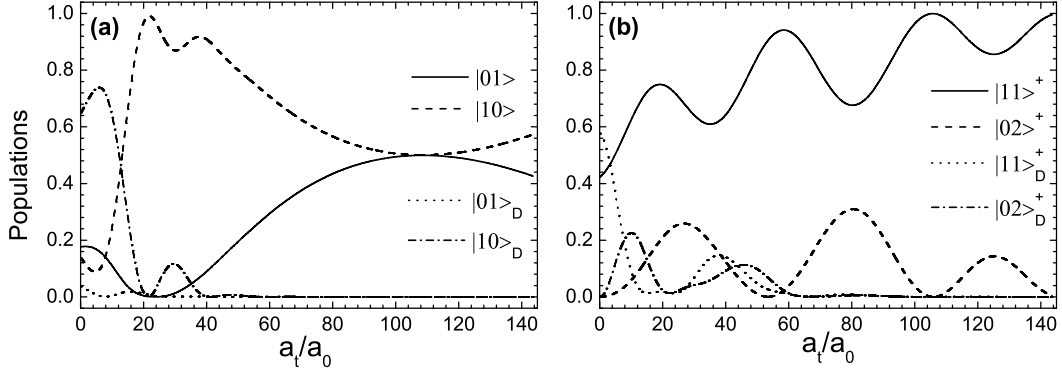
Figure 2.3. *Populations of the final state of the system after adiabatically approaching and separating the traps as a function of the scattering length. The initial states are (a) $|01\rangle$ and (b) $|11\rangle^+$. The parameter setting is: $\omega_x = 1.25 \times 10^4 \ s^{-1}$, $\omega_p = 7.9 \times 10^6 \ s^{-1}$, $1/\alpha = 241 \ nm$, $a_{max}\alpha = 5$, $a_{min}\alpha = 1.99$, $\omega_x t_r = 70$, and $\omega_x t_i = 69$.*

where $|01\rangle_D \equiv (|01\rangle_D^+ + |01\rangle_D^-)/\sqrt{2}$ and $|10\rangle_D \equiv (|01\rangle_D^+ - |01\rangle_D^-)/\sqrt{2}$. Therefore, in general there is a non-negligible probability (even if the traps are moved adiabatically) to have both atoms in the same trap after the gate operation. Note that the kinetic and trapping terms of the Hamiltonian do not directly couple $|01\rangle$ with $|10\rangle$ since they are single particle Hamiltonians and, therefore, they do not allow for the simultaneous change of the motional states of both atoms. The coupling between $|01\rangle$ and $|10\rangle$ is mediated through the double occupancy states $|01\rangle_D$ and $|10\rangle_D$. As the ratio of the tunneling strength of the ground and the first excited state can be controlled by the distance of the trap, it is possible to realize a SWAP gate. However, this is not a universal gate as explained in section 1.1.2. On the other hand a $\sqrt{\text{SWAP}}$ gate is impossible to produce, as doing only 'half' the SWAP operation leaves a state with double-occupancy of the traps.

Producing a two qubit gate necessarily needs a two particle interaction term in the Hamiltonian, *i.e.*, in the case of Eq. (2.10) it needs $a_t \neq 0$. Fig. 2.3 shows, for a particular parameter set, the final state of the system after the whole process of approaching and separating the traps as a function of the scattering length a_t. In (I) the initial state is $|01\rangle$ and in (II) it is $|11\rangle^+$. In the plot the scattering length is used as a free parameter to illustrate the problem of double-occupancy. But notice that in the experiment in principal it is possible to tune the value of the scattering length via *Feshbach resonances* [77]. Also, the effective one dimensional scattering properties can be tuned by changing the ω_p, *i.e.*, the confinement in the orthogonal directions, as can be seen from Eq. (2.9).

From Fig. 2.3 it is clear that for $a_t = 0$ double-occupancy is indeed present in the final state of the system. This problem is naturally suppressed when taking into account the interaction between the atoms. In the case of positive scattering length, for $\alpha a \gg 1$ a state with double occupancy always has larger energy than the respective state which has one atom in each trap, *i.e.*, $^{\pm}\langle nm|H|nm\rangle^{\pm} \leq {}_D^{\pm}\langle nm|H|nm\rangle_D^{\pm}$, such that in the presence of interaction for the four

states from Eqs. (2.26) only the following resonant couplings are present:

$$|01\rangle \quad \leftrightarrow \quad |10\rangle \tag{2.28a}$$

$$|11\rangle^+ \quad \leftrightarrow \quad |02\rangle^+, \tag{2.28b}$$

where

$$|02\rangle^+ = \frac{1}{2}\left(|\bar{0}\rangle_L|\bar{2}\rangle_R + |\bar{2}\rangle_R|\bar{0}\rangle_L + |\bar{0}\rangle_R|\bar{2}\rangle_L + |\bar{2}\rangle_L|\bar{0}\rangle_R\right). \tag{2.29}$$

Notice that now the collisional interaction term Eq. (2.9) allows for the simultaneous change of the motional states of both atoms without populating states with double occupation intermediately.

These considerations concerning how the interaction influences the couplings are clearly confirmed in Fig. 2.3. If the initial state is $|01\rangle$, then the double-occupancy population decreases as the scattering length is increased. If the scattering length is large enough and the approaching sufficiently slow such that the evolution is adiabatic, then the population of double-occupied states vanishes completely, cf., Fig. 2.3(a). The same happens for $|11\rangle^+$, Fig. 2.3(b), but in this case a coupling to $|02\rangle^+$ becomes important. Clearly this state should not be populated during the operation, as it lies outside the computational basis, so for any gate the coupling from Eq. (2.28b) has to be suppressed or controlled. Suppressing the coupling is possible through breaking the degeneracy between $|11\rangle^+$ and $|02\rangle^+$, for instance, by using an anharmonic trapping potential such that the vibrational frequencies are no longer equally spaced. Then the population of $|02\rangle^+$ is only determined by the non-adiabaticity of the process. In the following, for the model potential of Eq. (2.11) where the levels are equally spaced for distant traps, we will instead adjust the parameters of the setup and the interaction time in such a way that at the end of the gate operation $|02\rangle^+$ is not populated.

Gate operation

For the scattering length $a_t = 106a_0$, corresponding to ^{87}Rb atoms in the spin triplet and indicated by an arrow in Fig. 2.3, the temporal evolution of the populations of the important states is plotted in Fig. 2.4. The figure has been obtained by expanding the two-particle wavefunction in the basis explained above and numerically integrating the time-dependent Schrödinger equation. The parameters are as in Fig. 2.3, and the initial states are (a) $|00\rangle^+$, (b) $|01\rangle$, and (c) $|11\rangle^+$. Obviously states representing double occupation are present during the interaction, but in all cases they vanish as the two traps are eventually separated. Due to the specific choice of parameters also the population of $|02\rangle^+$ vanishes in the final state, cf., Fig. 2.3(c). Furthermore, as can be seen from Fig. 2.3(b), $|01\rangle$ evolves to an equal superposition of $|01\rangle$ and $|10\rangle$. Further inspection of the phases shows that, after absorbing part of the phases into the single basis states and neglecting a global phase,

$$|01\rangle \rightarrow \frac{1+i}{2}|01\rangle + \frac{1-i}{2}|10\rangle. \tag{2.30}$$

As also $|00\rangle^+ \rightarrow |00\rangle^+$ and $|11\rangle^+ \rightarrow |11\rangle^+$, for these parameters a $\sqrt{\text{SWAP}}$ gate operation is realized.

For ^{85}Rb atoms with negative scattering length $a_t = -369\,a_0$, the search for parameters to construct a $\sqrt{\text{SWAP}}$ operation is slightly more involved. Due to the attractive character of the
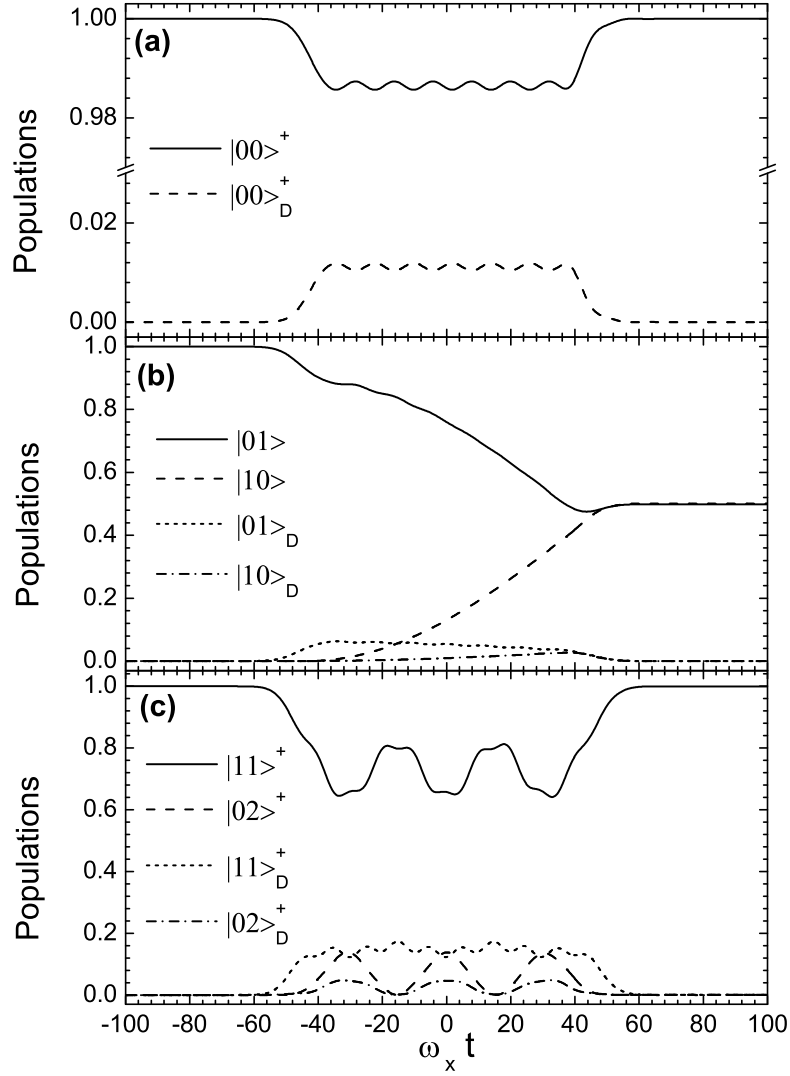
Figure 2.4.   *Simulated* $\sqrt{\text{SWAP}}$ *gate operation for* ^{87}Rb *with positive scattering length* $a_t = 106\,a_0$, *i.e., for repulsive interaction. The rest of the parameters is as in Fig. 2.3. The initial state of the two atoms is (a)* $|00\rangle^+$, *(b)* $|01\rangle$ *(c)* $|11\rangle^+$. *In the case of (b) the final relative phases of* $|01\rangle$ *and* $|10\rangle$ *are as in Eq.* (1.30).

interaction states with two particles in the same trap can more easily become resonant to states from the computational basis, *e.g.*, $|01\rangle_D^+$ can become resonant with $|00\rangle^+$, and the parameters have to be chosen to avoid such a degeneracy. Fig. 2.5 shows a gate simulation for ^{85}Rb for parameters allowing to correctly reproduce the $\sqrt{\text{SWAP}}$. Unlike for ^{87}Rb, Fig. 2.5 shows that starting from the $|00\rangle^+$ state, $|01\rangle_D^+$ is populated during the gate operation.

On the other hand, it is important to notice that the results obtained for ^{87}Rb (Fig. 2.4) can be also directly implemented in ^{85}Rb by making use of the strong variation of the scattering length in the vicinity of a magnetic field induced Feshbach resonance [77].

To check the accuracy of the previous simulations in which the two particle wavefunction was expanded in a finite set of states, we also have numerically integrated the Schrödinger equation for the two particle spatial wavefunction by using an operator split method and an FFT routine on a two dimensional grid. Fig. 2.6 shows the results of this integration for the same parameter values as in Fig. 2.5. The snapshots give the joint-probability distributions for the two particles for three different initial states: (a) $|00\rangle^+$, (b) $|01\rangle$ and (c) $|11\rangle^+$. The bosonic nature of the atoms manifests in the symmetry of the joint-probability distribution along the diagonal $x_1 = x_2$, and integrating the distributions in the direction of one of the axes, x_1 and x_2, gives the spatial single-particle distributions for particle 2 and particle 1, respectively. In (a) and (c) the final state coincides with the initial one, in (b) $|01\rangle$ evolves towards the maximally entangled state $[(1 + i)|01\rangle + (1 - i)|10\rangle]/2$ whose joint-probability distribution corresponds to the donut-like shape of the last frame.

Fidelity

Finally the accuracy of the simulated gate operation U with respect to the perfect gate operation $\sqrt{\text{SWAP}}$ is evaluated through the averaged fidelity $F\left(\sqrt{\text{SWAP}}, U\right)$, see Eq. (1.41). Fig. 2.7(a) shows the averaged fidelity for ^{87}Rb and the parameters from Fig. 2.5 with the approaching time t_r and the minimal distance of $a_{\min}$ of the traps as parameters. Clearly, the fidelity is very sensitive to the minimum distance due to the exponential dependence of tunneling at short distances. Note that the fidelity of the gate operation corresponding to the parameters of Fig. 2.5 is $F > 0.9997$ with a gate duration of $2t_r + t_i \sim 17\,\text{ms}$ for $\omega_x = 1.25 \times 10^4\,\text{s}^{-1}$. An important issue is how much the gate duration can be decreased while maintaining a high fidelity. In Fig. 2.7 the gate duration is reduced by a factor of two which increases the error by around one order of magnitude. In fact, as soon as the rising time t_r is decreased, non-adiabatic effects occur which in turn result in the population of several unwanted states, *e.g.* double-occupation, in the final state of the system. However, it could be possible to use the techniques developed in [78] to optimize the speed of the gate operation, while suppressing excitations to these unwanted states.

2.4 Quantum correlations during the gate operation

The $\sqrt{\text{SWAP}}$ gate evolves the separable state $|01\rangle$ to a maximally entangled state of the two qubits. The aim of this section is to analyze the dynamics of entanglement during the gate operation. For this purpose let us first discuss appropriate methods to measure the entanglement in such a system. The initial and, as long as double occupancy is suppressed, also
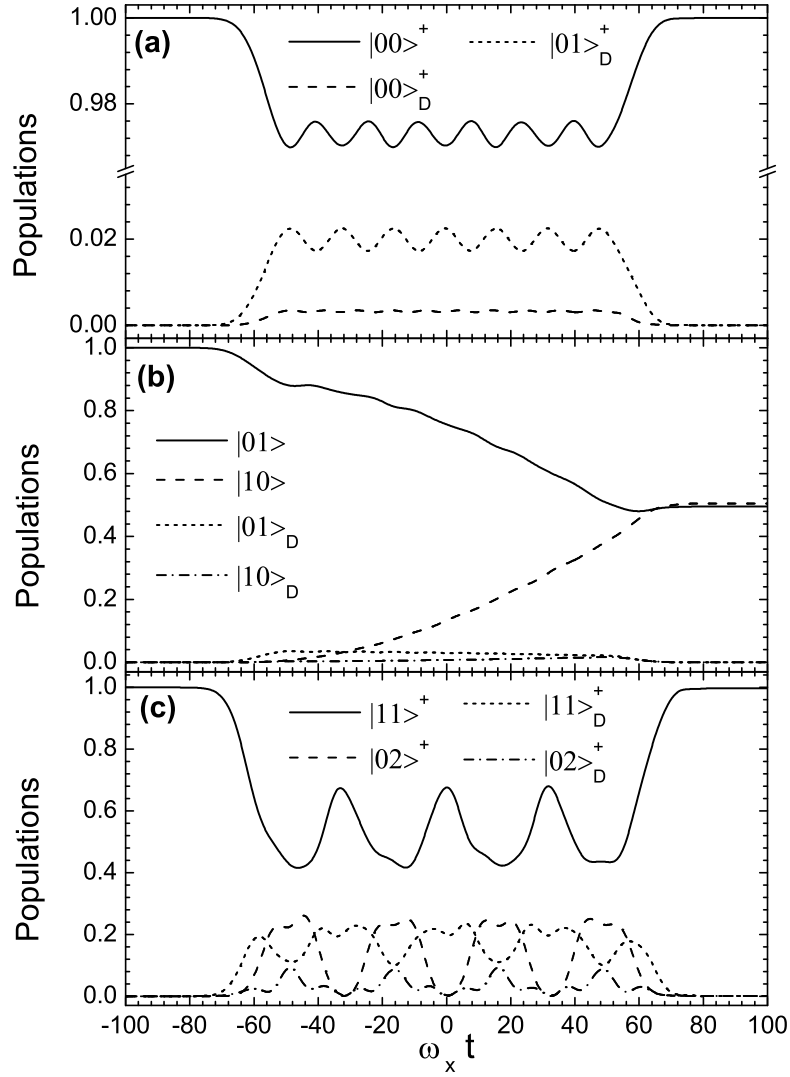
Figure 2.5.   *Simulated* $\sqrt{\text{SWAP}}$ *gate operation for* ^{87}Rb *with negative scattering length* $a_t = -369\ a_0$ *corresponding to attractive interaction for the following parameters:* $\omega_x = 1.25 \times 10^4\ s^{-1}$, $\omega_p = 1.6 \times 10^6\ s^{-1}$, $1/\alpha = 244\ nm$, $a_{\max}\alpha = 5$, $a_{\min}\alpha = 1.956$, $\omega_x t_r = 77$, $\omega_x t_i = 97.2$, and $a_t = -369\ a_0$. *The initial state of the two atoms is (a)* $|00\rangle^+$, *(b)* $|01\rangle$ *(c)* $|11\rangle^+$.
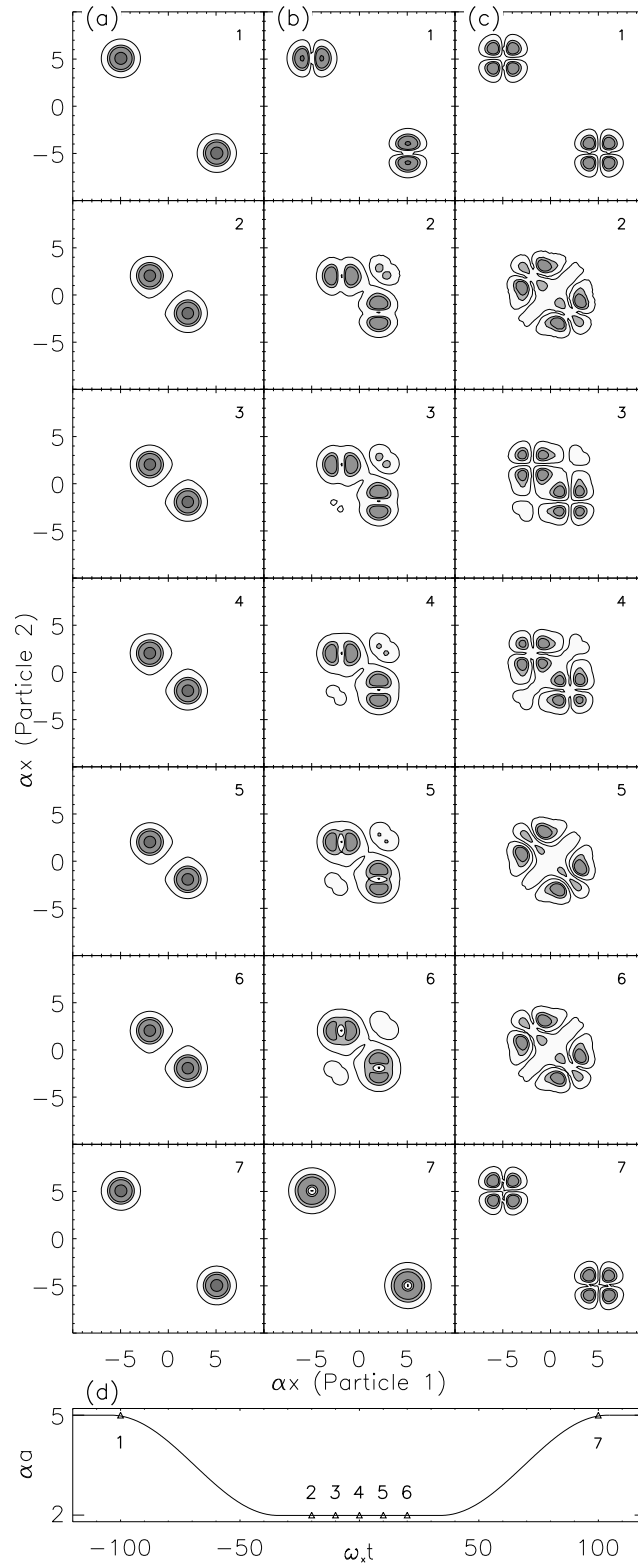
Figure 2.6. *Snapshots of the spatial two-particle wavefunction $|\psi(x_1, x_2)|^2$ for ^{87}Rb and the parameters from Fig. 2.4 for the three initial states (a) $|00\rangle^+$, (b) $|01\rangle$, and (c) $|11\rangle^+$. In (b) the final state corresponds to $[(1 + i)|01\rangle + (1 - i)|10\rangle]/2$.*
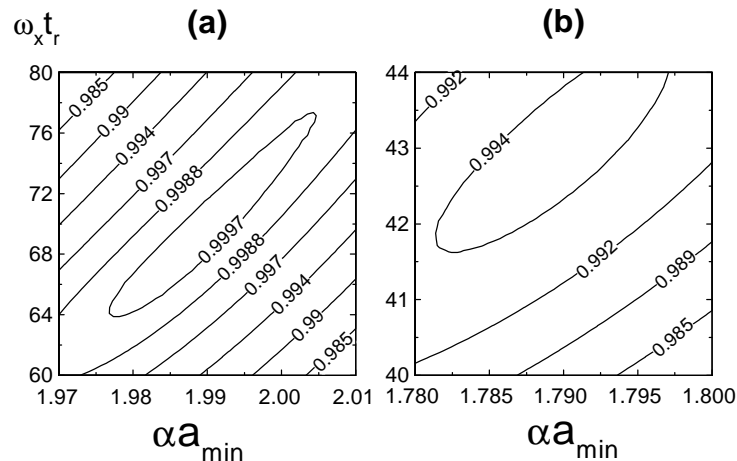
Figure 2.7.   *Averaged fidelity* $F(\sqrt{\textsc{swap}}, U)$ *of the gate operation* U *in the parameter plane* t_r *versus* a_{min} *corresponding to the operation of a* $\sqrt{\textsc{swap}}$ *gate for* ^{87}Rb *with positive scattering length* $a_t = 106\, a_0$. *In (a) the interaction time is* $\omega_x t_i = 69$, *in (b) it has been reduced to* $\omega_x t_i = 20$. *This increases the error rate by a factor of* 10.

the final state consist of well separated and thus for practical purposes [4] distinguishable particles. In this context usual entanglement measures apply, *e.g.*, the entropy of entanglement from Section 1.1.1, as only pure states are considered here. During the gate operation there is a significant overlap of the wavefunctions of states of the different traps, and the indistinguishable nature of the bosonic atoms has to be taken into account. The usual entanglement measures can no longer be applied, as they rely on the tensor product structure of the underlying Hilbert space, while bosons (or fermions) live in the symmetric (or anti-symmetric) subspace of a tensor product. Or, to state the problem in a different way, it is necessary to distinguish between two types of correlations: the statistical correlations arising from symmetrization and quantum correlations, *i.e.*, further correlations useful in the context of quantum information. Various solutions for this problem have been discussed in [73, 79–85], and we give a systematic approach to this problem and compare the various methods in Appendix A.

Entanglement, or, to be more precise, quantum correlations, have been analyzed in [73] for a gate operation between two fermions using a special correlation measure, the *fermionic concurrence*. Here we will undertake a similar analysis for a system of two bosons and, as a little more general approach, we will study the applicability of the various methods in the context of the $\sqrt{\textsc{swap}}$ gate operation described before.

To connect to the notation of Section A.2, bosonic creation and annihilation operators $b_{i,s}^\dagger$ and $b_{i,s}$ are introduced for the single particle states from Eqs. (2.22), where $s \in \{L, R\}$, such that $b_{i,s}^\dagger|\Omega\rangle = |\bar{i}\rangle_s$. From our simulations of the gate operation by expanding the wavefunction in the restricted set of two-particle states from Eqs. (2.24,2.25) (including states up to $i = 3$), we can then for every time t construct the matrix $v(t)$ which is given by the expansion
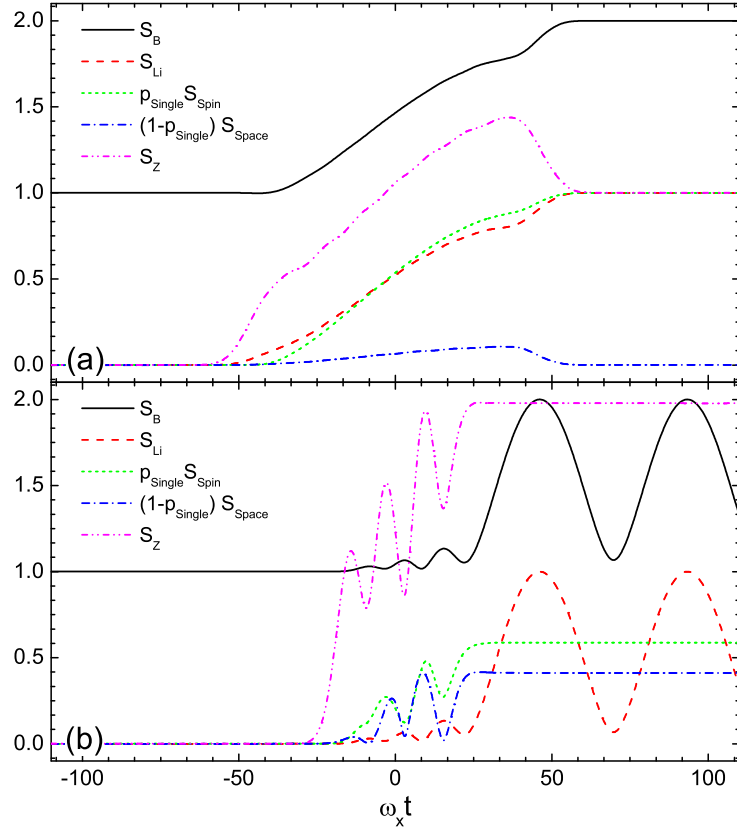
Figure 2.8. *(a) Quantum correlations for the parameters of Fig. 2.4, i.e., for the $\sqrt{\text{SWAP}}$ gate, applied to $|01\rangle$. Quantum correlations are measured in terms of the bosonic entropy S_B, Li's bosonic entropy S_{Li}, Zanardi's entroy S_Z measuring correlations in the occupation number representation, and the pure spin or spatial correlations S_{spin} and $S_{spatial}$ obtained after projecting on the respective subspaces. For a more detailed discussion see text and Appendix A. (b) Quantum correlations for the following set of parameters: $a_t = 10a_0$, $\omega_x t_r = 52.7$, $\omega_x t_i = 20.4$. The rest of the parameters is as in Fig. 2.4.*

of $|\psi(t)\rangle$ in term of the modes $b_{i,s}$:

$$|\psi(t)\rangle = \sum_{i,j=1//s,r=L,R}^{N} v_{(is)(jr)}(t) b_{i,s}^{\dagger} b_{j,r}^{\dagger} |\Omega\rangle. \qquad (2.31)$$

In Fig. 2.8 (a), the time evolution of four different measures of correlations is shown: (i) the bosonic von Neumann entropy S_B from Paškauskas *et al.* [81], see Eq. (A.42), (ii) the bosonic von Neumann entropy S_{Li} from Li *et al.* [82], see Eq. (A.44), (iii) Zanardi's entropy S_Z [79], see Eq. (A.25) (iv) the probabalistic spin entanglement[2] p_{Single}spin obtained after projecting onto the subspace spanned by the set $\{|00\rangle^+, |01\rangle^+, |01\rangle^-, |11\rangle^+\}$, *i.e.*, the subspace of the two atoms being in states centered in different traps, (v) the probabilistic spatial entanglement $(1 - p_{Single})S_{space}$ found after projecting onto the subspace with both particles in the same trap. For (iv) and (v), the entropies are calculated from the renormalized state after projecting, but they are weighted by the probabilities p_{Single} and $1 - p_{Single}$ to find the state in the respective space. For this particular gate realization, neither the initial nor the final state contain contributions from double occupation, such that in these cases $p_{single} = 1$. The quantity $p_{single}S_{spin}$ thus here coincides before and after the gate operation with the usual notion of the entropy of entanglement of distinguishable particles and we should expect that all the quantities which measure quantum correlations of indistinguishable particles, have the same initial and final value as S_{spin}: initially $S_{spin} = 0$ and finally $S_{spin} = 1$.

It strikes out that S_B does not fulfill this condition as it has the value $S_B = 1$ already before the gate operation and $S_B=2$ after it. The reason for this can be seen from the Slater decomposition, see Section A.3.5, of $|01\rangle = b_{0,L}^{\dagger} b_{1,R}^{\dagger} |\Omega\rangle$, which reads

$$|01\rangle = \frac{1}{4} \left[\left(-ib_{0,L}^{\dagger} + b_{1,R}^{\dagger} \right) \left(-ib_{0,L}^{\dagger} + b_{1,R}^{\dagger} \right) + \left(b_{0,L}^{\dagger} - ib_{1,R}^{\dagger} \right) \left(b_{0,L}^{\dagger} - ib_{1,R}^{\dagger} \right) \right] |\Omega\rangle. \qquad (2.32)$$

$|01\rangle$ thus has initially Slater rank 2, *i.e.*, it does not have the minimal Slater rank, although it can be written as the product of two modes. According to the definition of Li *et al.* [82], such a state is considered as separable, and consistently $S_{Li} = 0$ initially. This problem is an example for the difficulties encountered discussing quantum correlations of indistinguishable particles, as discussed in more detail in Appendix A: assuming modes $b_{0,L}^{\dagger}$ and $b_{1,R}^{\dagger}$ to belong to different parties, $|01\rangle$ is obviously a separable state, while it constitutes a perfectly spatially entangled state of two particles if $(b_1')^{\dagger} = (-ib_{0,L}^{\dagger} + b_{1,R}^{\dagger})/\sqrt{2}$ belongs to one party and $(b_2')^{\dagger} = (b_{0,L}^{\dagger} - ib_{1,R}^{\dagger})/\sqrt{2}$ to the other[3]. Apart from the difference of 1 between S_B and S_{Li}, their evolution during the gate operation is nearly identical.

Zanardi's entropy S_Z, based on writing $|\psi(t)\rangle$ in the occupation number representation and calculating the von Neumann entropy in this representation (using a fixed partition of the single particle states between the two parties, here a partition between the states centered in the left and the right trap), correctly reproduces the initial and final values of $S_{spatial}$. Most interestingly, it takes a maximal value of $S_Z \approx 1.4$ during the gate operation. This can be related to the presence of a mixture of spatial and spin entanglement, as discussed in

---

[2]We will term this type of entanglement spin entanglement in general, although in this case we consider pseudo-spins composed from the two lowest vibrational levels of the traps.

[3]In this case the the state reads $(|n_1 = 2, n_2 = 0\rangle + |n_1 = 0, n_2 = 2\rangle)/\sqrt{2}$ in the occupation number representation, cf., Section A.3.4, where n_i are the occupation numbers of modes b_i'.

Section A.3.2 (see also [84]). It is however in this context, where the qubits are explicitly implemented in the vibrational levels and it is assumed to have one atom per trap, not clear how this larger entanglement can be exploited.

To illustrate further the properties of the different quantum correlation measures, let us consider a different set of parameters. We choose a smaller $a_t = 10a_0$, such that double occupation is no longer negligible, and fix the rest of the parameters such that the final state reads

$$
\begin{aligned}
|\psi_{\text{final}}\rangle \;=\; 2\Big[& v_{(0L)(1R)} b_{0,L}^{\dagger} b_{1,R}^{\dagger} + v_{(1L)(0R)} b_{1,L}^{\dagger} b_{0,R}^{\dagger} + \\
& + v_{(0L)(1L)} b_{0,L}^{\dagger} b_{1,L}^{\dagger} + v_{(0R)(1R)} b_{0,R}^{\dagger} b_{1,R}^{\dagger} \Big] |\Omega\rangle
\end{aligned}
\tag{2.33}
$$

with $4|v_{(0L)(1R)}|^2 = 4|v_{(1L)(0R)}|^2 \approx 0.3$ and $4|v_{(0L)(1L)}|^2 = 4|v_{(0R)(1R)}|^2 \approx 0.2$. This is a combination of a spin correlated and a spatially correlated state. Projecting onto the subspace of a single particle in each trap only leaves the first two terms and thus an entangled state with respect to the definition of the qubit through the vibrational levels of the traps, while the projection onto double-occupation gives a superposition of two particles in the left trap and two particles in the right trap. As $|\psi_{\text{final}}\rangle$ in the occupation number basis $|n_{0L}\, n_{1L}\rangle|n_{0R}\, n_{1R}\rangle$ reads

$$
|\psi_{\text{final}}\rangle = 2\left[v_{(0L)(1R)}|10\rangle|01\rangle + v_{(1L)(0R)}|01\rangle|10\rangle + v_{(0L)(1L)}|11\rangle|00\rangle + v_{(0R)(1R)}|00\rangle|11\rangle \right],
\tag{2.34}
$$

we have $S_Z \approx 1.97$, as S_Z is just the entropy calculated in this basis with respect to the split left – right. This suggests that such a state should be (nearly) as useful as, *e.g.*, two singlets shared between the two parties, but it is not clear immediately how to access this resources. Gittings *et al.* discuss a protocol to achieve this for a very similar state of photons [84], which however possesses some drawbacks, see the discussion in Section A.3.4.

The entropies S_{B} and S_{Li} again evolve very similar, see Fig. 2.8 (b),but with a difference of 1. It is astonishing, that both oscillate for times $\omega_x t \gtrsim 50$, where the traps are already eventually separated. Especially, S_{Li} takes values between $S_{\text{Li}} = 0$ and $S_{\text{Li}} = 1$. These oscillations are due to the presence of collisional interactions present also after the gate operation in the case of two atoms occupying the same trap. This produces a collisional phase shift which alters the Slater decomposition. As the entropies S_B and S_{Li} are defined *via* the Slater decomposition or similar concepts, they also change in time although the interaction is purely local with respect to the division between the traps. This underlines that all concepts based on the Slater decomposition are problematic in cases where a locality condition is automatically implied in the definition of the system.

In summary, this discussion showed that for indistinguishable particles interacting at short distances, different types of quantum correlations appear that go beyond the particle correlations explored in the context of the $\sqrt{\text{SWAP}}$ gate. Even for pure fidelities for the gate operations, strong quantum correlations might be present. What remains is to demonstrate their usefulness and also to develop a framework that allows to quantify these correlations depending on the implementation of the qubits, on the notion of locality, and on the class of allowed operations. A step towards the latter problem is undertaken in Appendix A.

2.5   Aspects of the implementation in optical microtraps

Scalable systems of optical microtraps allowing for the implementation of the motional state qubit and for the realisation of the trap displacement necessary to implement the $\sqrt{\textsc{swap}}$ gate, can be realized as described in Section 1.2.2. With laser powers of $1-10$ mW per trap, for ^{87}Rb atoms the trap frequencies in the direction of the laser beams are typically $\omega_x \sim 10^4 - 10^5$ s^{-1}, while the transverse trap frequencies can be one or two orders of magnitude larger [27]. In the case of, *e.g.*, using two tilted lasers to generate the two sets of traps which can be displaced against each other, this means that the potential is steeper in the direction of moving the traps. To achieve the condition of stronger confinement in the directions perpendicular to the direction of displacement, which has been used throughout the calculations, a further laser could be used to generate an additional two-dimensional confining potential [27]. For the parameters we used in the gate simulations, the minimum distance of $\alpha a_{\min} \sim 2$ corresponds to a separation of the traps of 1 μm which is achievable in the present optical microtraps [29].

In the optical microtrap experiments, the trapping potential is Gaussian shaped with typical depth of $1-10$ mK $\times k_B$ [27]. For a single trap it is thus a good approximation to assume a harmonic potential for the low-lying states. For two traps being close together, the actual potentials will deviate from the form assumed in Eq. (2.11). Nevertheless, it is possible to generalize the methods applied here to these particular potentials, see for example Section 3.5.

Let us discuss how the error rate of $\lesssim 1\%$ arising from non-adiabatic effects as discussed in section IIIA modifies for this particular implementation. The lifetime of the atoms in the traps is about $100-1000$ ms. In this case coherence is mostly limited by spontaneous scattering of photons. Such scattering processes occur in ~ 10 ms but as shown in photon echo experiments with strongly confining trapping potentials [68] one atom scatters approximately 50 photons during the coherence time, as with motional states not every scattering process implies a loss of decoherence (Lamb-Dicke effect [86]), as it is the case for internal states. For the parameters from Fig. Fig. 2.4 this gives rise to a qubit error rate of another 2% such that the total error rate is approximately 3%. If furthermore single site addressing is desired before and after the operation, then typical initial and final distances between the traps have to be about 5-20 μm which for Rb means $\alpha a_{max} = 10 - 40$ instead of $\alpha a_{max} = 5$ which we used in our previous calculations. It is straightforward to estimate that the time needed for the complete process in this case ranges between 18 and 40 ms with an error rate due to non-adiabatic couplings to other vibrational states of $4-8\%$. Taking into account the contributions from the spontaneous scattering the cumulated qubit error rate can finally be estimated to lie between 5 and 12%, which should be enough for proof-of-principle experiments.

To generate the traps for implementing the motional state qubits it could also be envisaged to use optical lattices formed from two pairs of counter propagating lasers with different frequency. As described in Section 1.2.2, this setup also allows to generate two sets of traps with a potential barrier of variable height between them. Finally, the concept could also be used for neutral atoms trapped in magnetic potentials [60].

2.6   Conclusion

In this chapter we have discussed how quantum computation with neutral atoms in optical potentials can be performed for qubits implemented in the vibrational states of the trapping potentials. The interaction between two different qubits in mediated via tunneling an cold controlled collisions, which can be switched on and off via changing the distance, *i.e.*, the potential barrier, between two adjacent traps. Such a setup can be realized in optical microtraps or optical lattices as well as in magnetic microtraps.

For the purpose of identifying a gate natural to implement in such as system and to simulate the gate operation, an orthogonal time-dependent two-particle basis has been introduced. The simulations based on the expansion of the wavefunction into a finite number of states have also been verified using a direct numerical integration of the Schrödinger equation for the two-particle wavefunction. We have discussed the couplings in the presence and absence of interaction between the particles and have shown how an interplay of tunneling and collisional processes allows for a simultaneous change of the motional states of the two atoms, which gives rise to the implementation of a high-fidelity $\sqrt{\textsc{swap}}$ gate. In this context, the dependence of the fidelity on experimental parameters has been discussed.

Based on expressing the state in the basis of two-particle states, we have used this particular $\sqrt{\textsc{swap}}$ operation as an example to study in detail quantum correlations between particles with bosonic statistical nature, taking into account their indistinguishability as the two traps are close to each other. The evolution of various measures quantifying quantum correlations from different point of views has been computed during the gate operation, the different measures have been compared, and also their usefulness an applicability has been discussed.

We finally gave some practical considerations with respect to the implementation of this proposal especially in a system of optical microtraps and analyzed the gate fidelity in the presence of decoherence mechanisms as the scattering of photons. Due to the rather slow gate time, which is in the order of the inverse trapping frequency, decoherence increases the error rates up to the percent level.

CHAPTER 3

QUANTUM INFORMATION PROCESSING WITH SPATIALLY DELOCALIZED QUBITS

3.1 Overview

Several concepts to implement a qubit using neutral atoms in a set of optical traps have been addressed already: for many proposals internal states of the atoms are used, in this case the spatial atomic wavefunction is independent of the state of the qubit[1]. In the preceding chapter we have proposed to use the two lowest motional states of the atom in the trapping potential to represent the qubit. In this case, the internal atomic state is not changed during the computation, but the spatial wavefunction depends on the state of the qubit, although it is centered around the same position in space. In this chapter, as a further approach, we will consider encoding the qubit into the spatial position of the atom. To be more precise, a qubit is constructed from two separated traps and from a single atom, which can be in a superposition of the ground states of these two traps. The atom being in the left or the right trap will be identified with the qubit being in states $|0\rangle$ or $|1\rangle$, respectively. We will refer to this representation as the *spatially delocalized qubit* (SDQ) since $|\langle 0|\boldsymbol{r}|0\rangle - \langle 1|\boldsymbol{r}|1\rangle| \neq 0$.

As we will show, implementing the qubit in this way allows to perform single qubit as well as two qubit gates without the need for manipulating the atoms with external lasers. All the operations are realized via temporal manipulations of the trapping potentials only; also state dependent potentials are not necessary. Single qubit gates are realized via tunneling between the two traps forming the qubit, and we suggest to construct a two qubit gate by again exploiting cold collisional interactions between two atoms.

We will subsequently describe in detail in Sections 3.2 and 3.3 how single qubit gates and a two qubit phase gate can be performed. In Section 3.4 a setup allowing for the generation of a maximally entangled state of two spatially delocalized qubits in a single step will be analyzed. Finally, in Section 3.5, the proposal will be especially applied to the scenario of atoms in optical microtraps, including an analysis of possible imperfections and decoherence and the deduction of error rates and gate times for realistic parameters of this system.

---

[1]During the operation of a two qubit gate this does not necessarily have to be true, see, *e.g.*, the realization of gates for qubits implemented in internal states via state-dependent optical potentials.
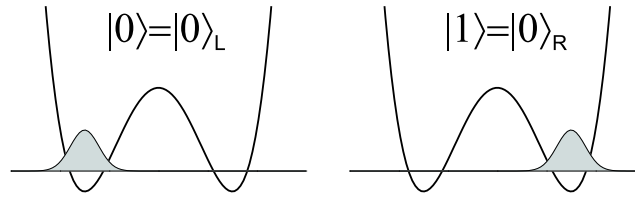
Figure 3.1.   *Definition of the* spatially delocalized qubit*: the atom in the ground state of the left or the right trapping potential defines the states* $|0\rangle$ *or* $|1\rangle$ *of the computational basis, respectively.*

3.1.1   Related work

Similar setups have been proposed to implement quantum gates for electrons confined in semiconductor quantum dots, with the qubit encoded in two tunnel-split ground states, the so-called *charge qubit*, and the qubit operations realized via tunneling and the Coulomb interaction between the electrons [87, 88].

Recently an implementation of quantum gates based on a concept similiar to the spatially delocalized qubit has been suggested in *photonic crystals* [89]. Photonic crystals, also known as photonic band gap materials, are ordered inhomogeneous dielectric media with a spatially periodic dielectric constant, which allow for the propagation of photons in the same way as semiconductors allow for the propagation of electrons. Structures can be designed to confine photons to a plane, to a waveguide-like structure, or to localize them in a cavity-like structure [90]. Angelakis *et al.* proposed to define a qubit via a single photon travelling in two waveguides [89]. Single qubit gates can be perfomed via approaching the two waveguides, and a two qubit phase gate is shown to be realizeable through a strong non-linearity produced by a doping the waveguide with suitably chosen three level atoms.

Based on the proposal of spatially delocalized qubits, Simon *et al.* considered the application of qubits and gates in magnetic microtraps [91]. They showed how to increase the robustness of certain important single qubit gates *via adiabatic passage techniques*.

3.2   Quantum bits and single qubit gates

Let us state the definition of the spatially delocalized qubit more precisely: each qubit consists of two traps separated by a distance $2a$ and a single atom. The computational basis states $|0\rangle$ and $|1\rangle$ will be implemented by the atom being in the ground state of one of the two traps: $|0\rangle = |0\rangle_L$ and $|1\rangle = |0\rangle_R$, where $|0\rangle_{L/R}$ denote the vibrational ground states of the left and the right trap, respectively (see Fig. 3.1). The whole register of qubits is then constructed from a single line of traps, each two of which form one qubit. Having many lines of traps in parallel, as it is, *e.g.*, naturally the case for an optical lattice or for optical microtraps, allows to parallelize the operation of the quantum computer. Our definition of the quantum register assumes to be able to store deterministically zero or one atom in each trap and to cool it to the vibrational ground state in all three spatial dimensions. The traps

will be modeled as in Chapter 2 by a piecewise harmonic potential, and single as well as two qubit operations will be realized by approaching and separating these traps as shown in Fig. 2.1, *i.e.*, these operations will be described *via* the maximal an minimal distances a_{max} and a_{min}, the time t_r used to approach the traps, and *via* the time t_i for which the traps are kept at the minimal distance, see Fig. 2.1. We will eventually in Section 3.5 consider an implementation using two gaussian shaped potentials, which is a realistic scenario for optical microtrap experiments. For the numerical simulations we perform, we again assume the confinement to be stronger in directions perpendicular to the direction of approaching the traps, such that excitations in this perpendicular direction can be neglected and the system is effectively one-dimensional.

Single qubit operation, *e.g.*, a Hadamard gate, can be performed by adiabatically approaching the two traps and thus allowing tunneling to take place. In order to illustrate this operation, it is convenient to consider the two lowest energy eigenstates of the double well potential for an arbitrary distance $2a$. These two states are symmetric and antisymmetric, denoted by $|S\rangle$ and $|A\rangle$ respectively. In terms of these states, the qubit basis reads: $|0\rangle = \frac{1}{\sqrt{2}}(|S\rangle + |A\rangle)$, and $|1\rangle = \frac{1}{\sqrt{2}}(|S\rangle + |A\rangle)$. Neglecting higher vibrational states, the Hamilton operator of the system has the form

$$H = \begin{pmatrix} E(a) & -\hbar\Omega(a)/2 \\ -\hbar\Omega(a)/2 & E(a) \end{pmatrix}, \tag{3.1}$$

where the off-diagonal term $\hbar\Omega(a)/2$ describes the coupling between the levels. The eigenenergies are $E_{S,A}(a) = E(a) \mp \frac{1}{2}\hbar\Omega(a)$. Let us assume that the atom is initially in the left trap, i.e, $|\psi(t=0)\rangle = |0\rangle$. In this case it is straightforward to check that if the trap distance is varied as $a = a(t)$, then its time evolution will be given by

$$|\psi(t)\rangle = e^{-\frac{i}{\hbar}\int dt\, E(a(t))}\left[\cos(\chi_{\mathrm{total}})|0\rangle + i\sin(\chi_{\mathrm{total}})|1\rangle\right]\ , \quad \chi_{\mathrm{total}} = \frac{1}{2}\int dt\,\hbar\Omega(a(t)). \tag{3.2}$$

Thus, the atomic wavefunction oscillates in a Rabi-type fashion between the left and right trap; for a fixed, the flopping frequency is given by $\frac{1}{2}\Omega(a)$. Obviously, for large trap separations states $|S\rangle$ and $|A\rangle$ become degenerate in energy, i.e., $\Omega(a) = 0$ for $a \to \infty$, and then up to a trivial phase the atom does not evolve in time. Therefore, it is possible to realize single-qubit operations via tunneling by experimentally controlling the Rabi frequency through the temporal variation of the trap distance, *i.e.*, through the parameters a_{min}, t_r, and t_i.

To illustrate the single-qubit operations, Fig. 3.2 shows the result of numerically integrating the one dimensional Schrödinger equation in the parameter plane t_r versus t_i for fixed maximal and minimal distances $\alpha a_{\mathrm{max}} = 5$ and $\alpha a_{\mathrm{min}} = 1.8$. Initially, the atom is in the left trap, *i.e.*, $|\psi(t=t_{\mathrm{init}})\rangle = |0\rangle$. Fig. 3.2 (a) shows $\rho_1 = |\langle\psi(t=t_{\mathrm{final}})|1\rangle|^2$, the population of state $|1\rangle$ after the eventual separation of the traps. Obviously, for fixed $\omega_x t_r$ the population oscillates between the two traps, therein resembling the interaction of a laser with a two-level system. For this reason we have added in Fig. 1 dashed lines indicating the $\frac{\pi}{2}, \pi$, and $\frac{3\pi}{2}$ laser pulse notation conventionally used in quantum optics[2]. In Fig. 3.2 (b) the adiabaticity condition is analyzed: the plot shows the total population of the ground states of the two

---

[2]A $\frac{\pi}{2}$ pulse corresponds to the Hadamard gate ʜ with an additional phase factor i, see Eq. (3.2), a π pulse to a ɴᴏᴛ operation, etc.
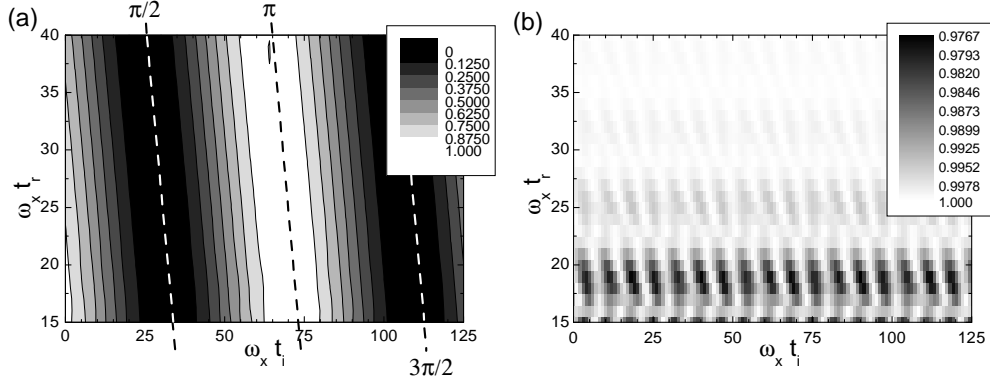
Figure 3.2. *Single qubit operations for $\alpha a_{max} = 5$, $\alpha a_{min} = 1.8$ and the atom initially in the left trap: (a) Population ρ_1 of the right trap, the dashed lines indicate the $\frac{1}{2}\pi$, π, and $\frac{3}{2}\pi$ pulses; (b) The sum of the ground state populations of the left and the right trap, $\rho_0 + \rho_1$. $\alpha^{-1} = \sqrt{\hbar/m\omega_x}$ is the position spread of the ground state with m the mass of the neutral atom and ω_x the trapping frequency.*

traps, *i.e.*, $\rho_0 + \rho_1$, where $\rho_0 = |\langle\psi(t = t_{\text{final}})|0\rangle|^2$. For small values of t_r, corresponding to a fast approaching and separation of the traps, excited vibrational states are populated and thus $\rho_0 + \rho_1 < 1$. In the following considerations we will focus on the adiabatic regime, though excitations are still included into the numerical simulations.

3.3   A two qubit phase gate

For the two-qubit gate operations we will assume that the two qubits are arranged in a 1D configuration, i.e., the four traps form a line, as illustrated in Fig. 3.3 (a,i). It is also possible to arrange the qubits side-by-side in a 2D configuration, *i.e.*, the traps form a square as in Fig. 2(a,ii). This however puts greater demand on the ability to move single traps as will be commented later. The traps involved are, as in the figure, labeled A_0, A_1 for the first qubit and B_0, B_1 for the second, and the respective ground states are denoted $|0\rangle_A$, $|1\rangle_A$ and $|0\rangle_B$, $|1\rangle_B$. The mechanism exploited to realize the two qubit gate operation is again, as in the case of qubits implemented in the motional states from Chapter 2, the collisional interaction between cold bosonic neutral atoms. For ^{87}Rb atoms the collisional interaction can be described by a contact potential of the form $U(\boldsymbol{r}_1, \boldsymbol{r}_2) = 4\pi a_t \hbar^2 m^{-1} \delta^{(3)}(\boldsymbol{r}_1 - \boldsymbol{r}_2)$, where $a_t = 106\,a_0 = 5.61$ nm is the *s*-wave scattering length in the spin triplet, as described in Section 2.2.1.

Because states $|0\rangle$ and $|1\rangle$ are localized in different spatial positions, it is enough to perform a suitable spatiotemporal variation of the potentials in order to pick up a collisional phase shift if and only if both qubits are in state $|1\rangle$. This suggests that the phase gate is the most natural universal two qubit gate which can be realized in this system. As explained in Eq. (1.26), a phase gate transforms product states $|i\rangle_A|j\rangle_B$, $i, j \in \{0, 1\}$ into $\exp(i\,\delta_{i1}\delta_{j1}\pi)|i\rangle_A|j\rangle_B$.
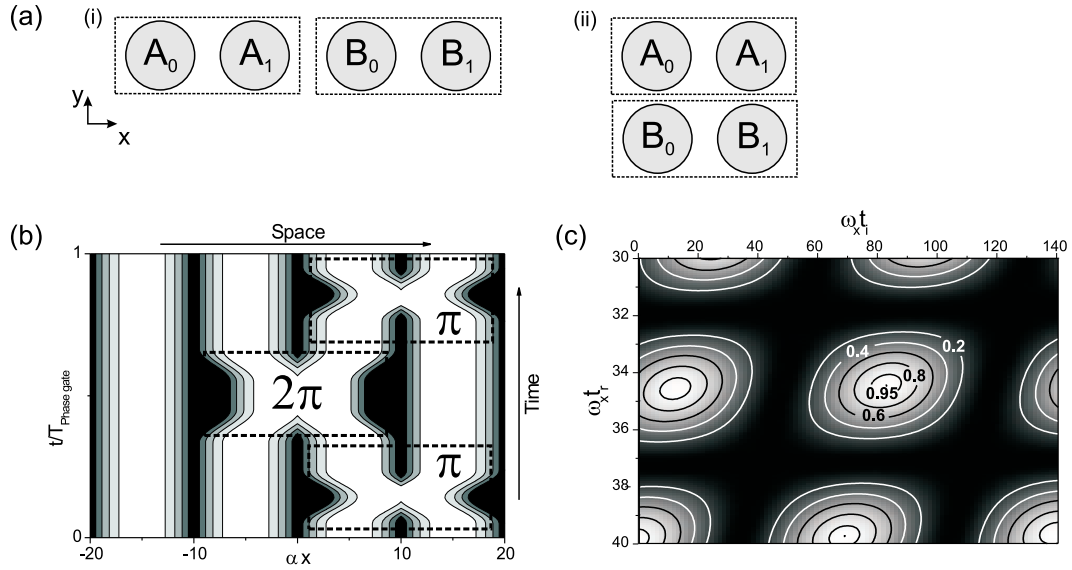
Figure 3.3. *Two-qubit phase gate operation. (a) Arrangements of the qubits: (i) in-line, and (ii) side-by-side; (b) Contourplot of the spatio-temporal variation of the trapping potential for arrangement (i). The centers of the four traps are white, dark gray corresponds to larger potential energy, the dashed boxes indicate the applications of π and 2π pulses; (c) Fidelity $F = \rho \cdot (\cos(\phi_C - \pi) + 1)/2$. Parameters as in Fig. 1 with $a_t = 106\,a_0$, $\omega_x = \omega_y = 2 \cdot 10^5\,s^{-1}$, and $\omega_z = 1.1 \cdot 10^6\,s^{-1}$.*

For the in-line arrangement, the temporal variation of the potential necessary to implement a phase gate is shown in Fig. 2(b), where horizontal and vertical axes denote space and time, respectively. The procedure consists of three steps:

➤ *π pulse* — As the first step a π pulse is applied on the second qubit, exchanging $|0\rangle_B$ and $|1\rangle_B$. During this step only single-particle phases arise which can be included into the definition of the single-particle states. If the initial state was $|0\rangle_A|0\rangle_B$, then after the π pulse, traps A_1 and B_0 would contain no atom. For initial states $|1\rangle_A|0\rangle_B$ or $|0\rangle_A|1\rangle_B$, exactly one atom would be either in A_1 or in B_0. Starting from $|1\rangle_A|1\rangle_B$ both middle traps would be occupied.

➤ *Collisional phase* — Now the two traps in the center, A_1 and B_0, are approached and eventually separated with the parameters chosen such that in case of only one atom being in either one of these traps, a $2\pi n$ pulse is applied with n integer. Then initial and final state coincide, except for a single particle phase ϕ_S which again can be included into the definition of $|1\rangle_A$ or $|0\rangle_B$. Starting from $|1\rangle_A|1\rangle_B$, after the first pulse A_1 and B_0 would both be occupied, and during the $2\pi n$ pulse the two atoms would collide. For an adiabatic evolution we can neglect not only the probability to populate excited vibrational states, but also to find two atoms in the same trap. Due to the collisional interaction, for suitable chosen parameters these states are not degenerated with states where each atom occupies a different trap, see the discussion in Section 2.3.2. Thus for $a_t \neq 0$ initial and final state are the same

except for a phase ϕ and, in order to realize the desired phase gate operation, we need its collisional part $\phi_C = \phi - 2\phi_S$ to be an odd multiple of π. The fidelity of this operation can be expressed as

$$F = \rho \cdot (\cos(\phi_C - \pi) + 1)/2, \tag{3.3}$$

which is plotted for the adiabatic regime[3] in Fig. 2(c). Here ρ is the final probability to find the atom in the same state as it was before the $2\pi n$ pulse, neglecting the collisional phase. To calculate the collisional phase ϕ_C, we have integrated the two-particle 1D Schrödinger equation replacing $U(\boldsymbol{r}_1, \boldsymbol{r}_2)$ by an effective one-dimensional interaction potential under the assumption that no transverse excitations occur, see Eq. (2.9).

➤ π *pulse* — Finally, to complete the phase gate operation another π pulse is applied to the second qubit.

In the case of 2D arrays of microtraps, as they are typically realized in the experiment [29], the easiest operation is to move complete columns of microtraps. Thus for the linear configuration of qubits as in Fig. 3.3, it is enough to be able to move selectively some columns, with the additional benefit that the operation is applied to many pairs of qubits in parallel which might allow for an easy implementation of error correcting codes. Note that even if *no* local approaching of traps is possible, but only the odd subset of traps can be shifted towards the even subset[4], still interesting operations are feasible. For instance, a linear *cluster state* [25, 92] can be created by initially and finally approaching traps within a qubit for a $\pi/2$ pulse (indentically for all the qubits), and in between performing the collisional phase operation as above (between all pairs of neighboring qubits). For just two qubits starting from $|0\rangle_A|0\rangle_B$ this produces (neglecting an overall phase)

$$|0\rangle_A|0\rangle_B \xrightarrow{\pi/2} \frac{1}{2}(|0\rangle_A + |1\rangle_A)(|0\rangle_B + |1\rangle_B) \xrightarrow{\text{collisional phase}}$$
$$\frac{1}{2}(|0\rangle_A|0\rangle_B + |0\rangle_A|1\rangle_B - |1\rangle_A|0\rangle_B + |1\rangle_A|1\rangle_B) \xrightarrow{\pi/2}$$
$$\frac{1}{2}[|0\rangle_A(|0\rangle_B - |1\rangle_B) + |1\rangle_A(|0\rangle_B + |1\rangle_B)]. \tag{3.4}$$

This is, up to a local operation on the second qubit, the two qubit cluster state. In general, *i.e.*, for more qubits, cluster states are highly and robustly entangled states of many particles. To realize the phase gate in the side-by-side arrangement, the initial and final π pulse can be omitted and only the 2π pulse between traps A_1 and B_1 is necessary. Although conceptually much more easier, the implementation in this arrangement demands the ability to move single traps instead of columns which makes it experimentally more involved. On the other hand such a freedom in moving the traps might be achievable for example for microtraps created using holographic techniques as described in [30]. In the following section, starting from such an side-by-side arrangement of four traps, we will assume to be able to symmetrically approach all the traps to the center and show, that this allows to generate a maximally entangled state of the two qubits in a single step.

---

[3]The fidelities are still obtained from a full numerical simulation of the (one- or two-particle) Schrödinger equation, but t_r is chosen large enough to supress excitations to higher vibrational states nearly completely.

[4]This is true also for an implementation in optical lattices, using a configuration of counterpropagating lasers of different frequency (Section 1.2.2)
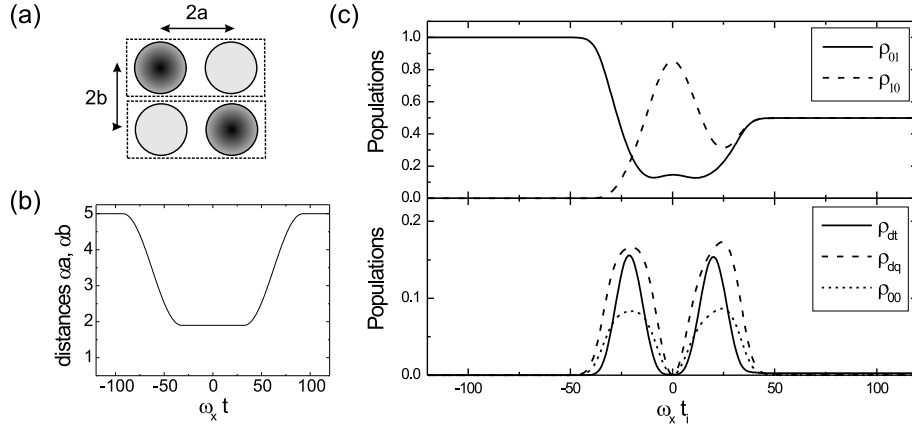
Figure 3.4. *Creation of a maximally entangled two-qubit state with two ^{87}Rb atoms in a single step: (a) The initial state is $|0\rangle_A|1\rangle_B$, with 2a and 2b being the separation of the traps in x and y direction, respectively; (b) the four traps are approached towards the center of the square adiabatically and simultaneously, i.e., $a(t) = b(t)$; (c) Above: Population of states $|0\rangle_A|1\rangle_B$ and $|1\rangle_A|0\rangle_B$; Below: Population of the state $|0\rangle_A|0\rangle_B$ (equal to the population of $|1\rangle_A|1\rangle_B$), double qubit population ρ_{dq}, and double trap population ρ_{dt}. The parameters are: $\alpha a_{max} = \alpha b_{max} = 5$, $\alpha a_{min} = \alpha b_{min} = 1.9$, $\omega_x t_r = 80$, $\omega_x t_i = 58$, $a_t = 106 a_0$, $\omega_x = \omega_y = 2 \cdot 10^5 \, s^{-1}$, and $\omega_z = 1.1 \times 10^6 \, s^{-1}$.*

3.4 Generating entanglement in one step

Assume the four traps of the two qubits arranged in a side-by-side arrangement, Fig. 3.4 (a), with the two atoms located in the upper left and lower right traps, respectively, corresponding to the initial state $|0\rangle_A|1\rangle_B$. When the traps are approached towards the center by changing the distance $2a$ of traps within a qubit and the distance $2b$ between the qubits simultaneously, then the general two particle state will read

$$|\psi(t)\rangle = \sum_{i,j=0,1} c_{ij}|i_A\rangle|j_B\rangle + \sum_{\alpha=A,B} c_\alpha|0_\alpha\rangle|1_\alpha\rangle + \sum_{i=0,1}\sum_{\alpha=A,B} c_{i\alpha}|i_\alpha\rangle|i_\alpha\rangle. \qquad (3.5)$$

Thus the state of the two qubits includes the four states of the computational basis (the first sum from Eq. (3.5)), but also a contribution from both atoms being 'within' one qubit, but in different traps, and from double trap occupation. Here the states $|i_\alpha\rangle$ can be constructed via the Gram-Schmidt method as in chapter 2. For the traps being close, they contain contributions from more than one trap. The double qubit and the double trap occupation will be denoted by ρ_{dq} and ρ_{dt}, respectively, defined as

$$\rho_{dq} = \sum_{\alpha=A,B} c_\alpha c_\alpha^* \quad \text{and} \quad \rho_{dt} = \sum_{i=0,1}\sum_{\alpha=A,B} c_{i\alpha}c_{i\alpha}^*. \qquad (3.6)$$

In order to create a maximally entangled state, we will assume again an adiabatic process, such that finally the population of higher vibrational states and of states representing double
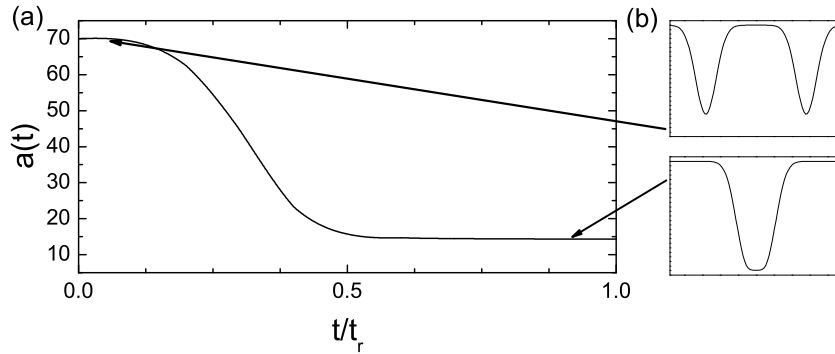
Figure 3.5.   *(a) The optimized variation of the approaching process a(t).
The optimization has been done with respect to the two lowest symmetric
vibrational states. The parameters are $U_0 = 200\hbar\omega_x$, $\alpha a_{max} = 70$, and
$\alpha a_{min} = 14.35$. (b) shows the trapping potentials for the maximal (top) and
minimal (bottom) distance.*

occupation of a trap are negligible (the latter only for $a_t \neq 0$). If furthermore the ap-
proaching of the traps is chosen to be symmetric, *i.e.*, $a(t) = b(t)$ (see Fig. 3.4 (b)), then
$\rho_{00}(t) = \rho_{11}(t) = \rho_{dq}(t)/2$, and, thus, in particular, these populations oscillate at the same
frequency. If finally all these populations are zero, then the state of a system is a combina-
tion of $|0\rangle_A|1\rangle_B$ and $|1\rangle_A|0\rangle_B$ only. For appropriately chosen parameters it is then possible to
obtain a maximally entangled state at the end of the process. For such a set of parameters,
the time evolution of the populations is shown in Fig. 3.4 (c).

3.5   Practical considerations

3.5.1   Gaussian-shaped potentials

So far, the proposal for quantum computation using spatially delocalized qubits has been
presented rather generally using a simplified trapping potential. Now we will specialize
to the case of atoms trapped in optical microtrap arrays. We will present calculations for
the gaussian trapping potentials present in this case and we will analyze reductions of the
fidelity due to experimental imperfections as shaking of the traps. Eventually, we will
discuss methods to improve the demands on the controllability of the system and present an
estimation of the influence of decoherence.

The optical potentials for atoms trapped by optical mictrotraps are described by the gaussian
shaped potentials from Eq. (1.54). An analysis of the energy eigenvalues and eigenstates
of the sum of two such potentials as a function of the separation between the traps shows
that the cosine function previously used to adiabatically approach the traps in the case of the
simple harmonic potentials leads to values of the approaching time t_r larger by two top three
orders of magnitude. For this reason, we have applied the techniques described in reference
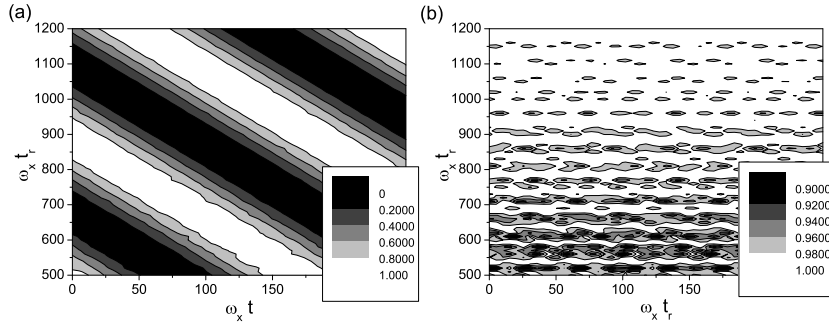[78] in order to optimize the temporal variation of the trap separation while suppressing the

Figure 3.6.   *Single qubit gates for Gaussian shaped trapping potentials for the following parameters: $\omega_x = 6 \times 10^5$ s^{-1}, $\alpha^{-1} = 35.4$ nm, $U_0 = 200\hbar\omega_x = 0.9$ mK$\times k_B$, $\alpha a_{max} = 70$, and $\alpha a_{min} = 14.35$. (a) Population $\rho_1 = |\langle 1|\psi(t)\rangle|^2$ of the right trap in the parameter plane $\omega_x t_i$ versus $\omega_x t_r$, showing Rabi-type oscillations. The atom was in the left trap initially. (b) Sum of the populations of the left and the right trap, $\rho_0 + \rho_1$. For $\omega_x t_r > 1100$, the fidelity can be made larger than $\rho_0 + \rho_1 > 0.99$.*

population of excited vibrational states. A typical trap depth is $U_0 = 200\hbar\omega_x$, and for this parameter Fig. 3.5 shows the result of optimizing the change of the distance of the traps from $\alpha a_{max} = 70$ to $\alpha a_{min} = 14.35$. The optimization is done with respect to the transition form the symmetric ground to the first symmetric excited vibrational state. For the distance $2a_{min}$, there is only single flat potential well, as can be seen in the Fig. 3.5. Fig. 3.6 shows ρ_1, the population of the right trap under the variation of t_i and t_r. The error rate due to the excitation of other vibrational states can be made smaller than 1% for $\omega t_r > 1100$, which is a reduction by one order of magnitude compared to the non-optimized $a(t)$.

3.5.2   Experimental imperfections

The error rate will be enhanced through further experimental imperfections. An important imperfection encountered in the experiment will be shaking of the trapping potentials due to mechanical vibrations of the setup. Parametric excitations to higher vibrational states can only occur if the shaking frequency is close to the trapping frequency. Typical shaking frequencies present in the experiment range from 1 s^{-1} to 5×10^3 s^{-1} and are thus well below the trapping frequencies ω_x and $\omega_\perp$, which are on the order of $10^5 s^{-1}$ or larger. Thus excitations through mechanical vibrations should be strongly suppressed. But shaking in the trap position also increases the error rate because it alters the (optimized) path $a(t)$, and can thus cause non-adiabatic transitions while the traps are approached or separated. The effects of a periodic variation $\Delta a(t) = \Delta a \sin(\omega_s t)$ of the trap separation during the gate operation for various amplitudes Δa and shaking frequencies ω_s are analyzed in Fig. 3.7 and Fig. 3.8, respectively. For fixed ω_s, the shaking amplitude has been set to $\Delta a = ca_{min}$, and clearly an amplitude with a magnitude of around one percent of the minimal distance, $c \lesssim 0.01$, allows for fidelities $F > 0.99$ (Fig. 3.7 (i)). Changing the shaking frequency ω_s for fixed (small) $\Delta a = 0.003a_{min}$ does not affect the fidelity significantly, see Fig. 3.8 (i).

On the other hand introducing shaking does change the frequency Ω of the Rabi oscillations between the ground states of the two traps as can be seen from Fig. 3.7 (ii) and Fig. 3.8 (ii).

Intensity fluctuations of the trapping lasers affect the depth of the trapping potentials, and the implications for the gate operation should be similar to shaking. We have analyzed how periodic variations of the trap depth U_0 lead to non-adiabatic transitions while approaching or separating the traps. These fluctuations can be assumed to be correlated from trap to trap if the same red-detuned laser is used to generate all traps. In this case fluctuations of U_0 on the order of 5% do not reduce the fidelity below $F = 0.999$, Fig. 3.9 (i), but again the frequency of the Rabi oscillations is affected. Finally, fluctuations in the phase of the lasers could be a source of errors. In optical lattices, with the optical potential formed through the interference of two counter-propagating lasers, such fluctuations lead to displacement of the trapping potentials, an effect similar to shaking due to mechanical vibrations. Phase fluctuations do not affect optical microtraps, because the atoms are trapped in the foci of the laser beams and traps are not generate through interference effects. Thus the trapping potentials are not changed even if the phase of the lasers cannot be controlled very well.

The reason for the change of the Rabi oscillation frequency Ω of the oscillations between the ground states is the strong exponential dependence of the tunneling rate on the distance of the traps. Although moderate shaking amplitudes still allow for large fidelities in the sense that no transitions to other vibrational states occur, they modify the unitary operation on the qubit itself, and, for this reason, a very precise control is demanded to enable quantum computation in this scenario. In Chapter 4 we will study the role of experimental imperfections again in a slightly relaxed scenario, namely for quantum walks.

3.5.3 Adiabatic passage techniques

In [91] *adiabatic passage techniques* have been studied in the context of applying the concept of spatially delocalized qubits in magnetic microtrap potentials. The aim of these technique is to increase the robustness of certain types of gates. The idea of adiabatic passage as applied to the single qubit gates discussed before is to introduce a detuning Δ between the two trapping potentials, and change it during the gate operation: $\Delta = \Delta(t)$. Then, in the basis of the two ground states, the Hamilton operator from Eq. (3.1) has to be replaced by the following operator, written in the basis $|0\rangle = |0\rangle_L$ and $|1\rangle = |0\rangle_R$:

$$H = \begin{pmatrix} E_0(t) - \Delta(t) & -\hbar\Omega(t)/2 \\ -\hbar\Omega(t)/2 & E_0(t) + \Delta(t) \end{pmatrix}. \tag{3.7}$$

We will assume $E_0(t) \equiv E_0$ to be constant during the process. The eigen-energies of this Hamiltonian read

$$E_\pm = \pm \sqrt{\hbar^2\Omega^2(t)/4 + \Delta(t)^2} + E_0. \tag{3.8}$$

If thus the traps are approached and separated as before, but initially $\Delta(t) > 0$ and finally $\Delta(t) < 0$, and if the evolution of the system is adiabatically, then the two traps will exchange population during the process, independent of the timing. In [91] it has been shown, that this technique allows for a NOT operation (or a π pulse in the quantum optics language used above) to reduce the population of higher vibrational states during the gate operation by a
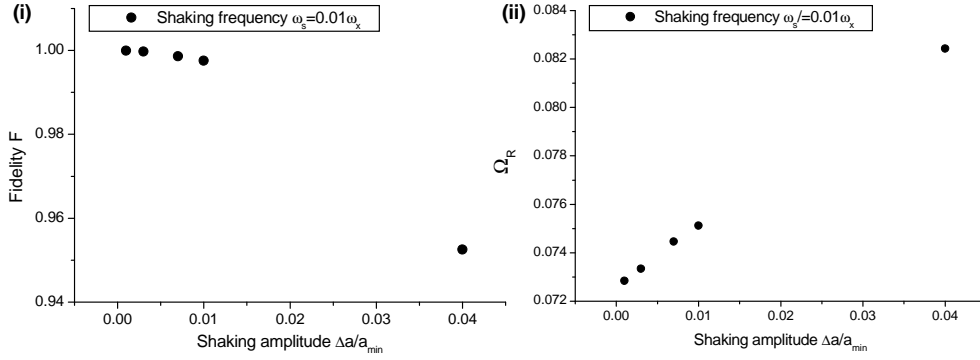
Figure 3.7. *(a) Fidelity F (sum of the population of the two ground states) and (b) frequency of Rabi-type oscillations between the traps for a sinusoidal variation $\Delta a(t) = \Delta a \sin \omega_s t$ of the distance of the traps with fixed frequency $\omega_s = 0.01\,\omega_x$ as a function of the amplitude Δa. Δa given in terms of $a_{\min}$.*
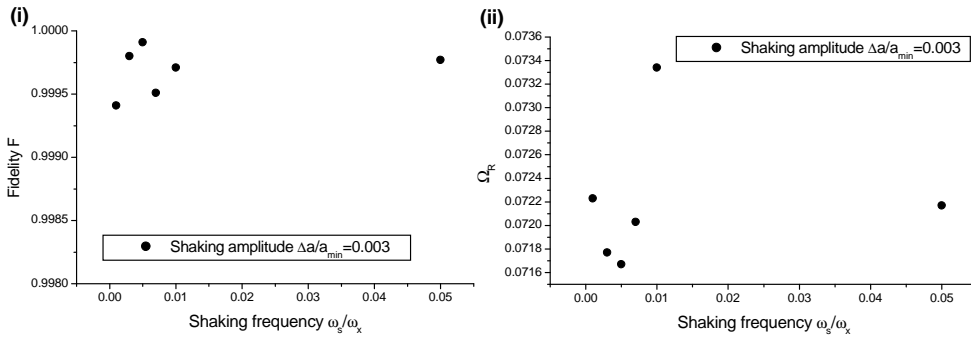

Figure 3.8. *Like Fig. 3.7, but varying ω_s for fixed amplitude $\Delta a = 0.003 a_{\min}$.*
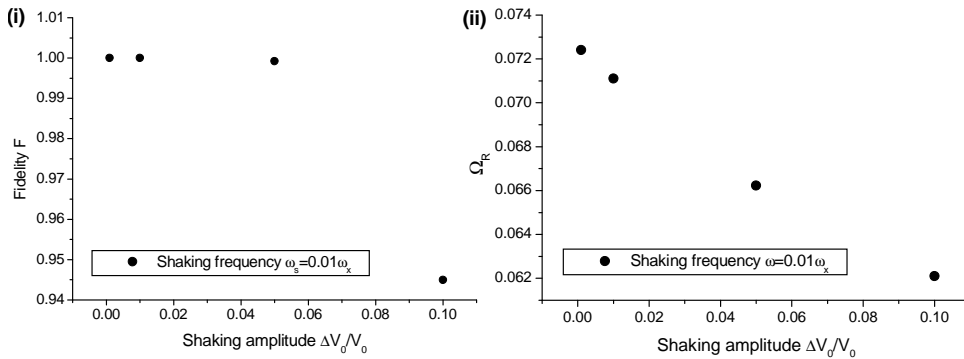

Figure 3.9. *Like Fig. 3.7, but as a function of the amplitude for a sinusoidal variation $\Delta U = \Delta U_0 \sin \omega_s t$ of the depth of the trapping potentials.*

factor of two while keeping the gate time constant. It is also shown that a similar technique can be used to implement a Hadamard gate ʜ in a comparable robust way[5].

This adiabatic passage technique still is sensitive (although less) to parameters as the minimal distance of traps or to timing issues. In Chapter 5 we will propose methods for the robust implementation of a certain restricted set of operations on the external degrees of freedom of trapped atoms, as, *e.g.*, to move an atom from one trap to another or to engineer a superposition. These techniques are designed such, that in a certain region they are completely insensitive to the change of a complete set of parameters as, *e.g.*, the minimal distance between the traps or the timing of operations.

3.5.4   Gate time and decoherence

Typical trapping frequencies for state-of-the-art 2D arrays of optical microtraps for ^{87}Rb atoms are 10^5-10^6 s^{-1} in the transverse directions and 10^4-10^5 s^{-1} along the laser beam direction [27, 29]. In order not to populate excited vibrational states and neglect double trap occupation, the trap displacement has to be adiabatic with respect to the lowest relevant trapping frequency. This adiabaticity condition yields realization times for single and two-qubit operations on the order of 10 ms or below. This value should be compared with the typical lifetime of the atoms in the microtraps of $\sim$ 1 s, and the rate of spontaneous scattering of photons from the trapping lases. For the parameters used here, one scattering process occurs in around $0.1 - 1$ s, which corresponds to a rate of 1-10 s^{-1}. This can be further reduced by increasing the laser detuning.

On the other hand, the proposal demands cooling the motional degree of freedom to the ground state. Sideband cooling to a temperature $T \lesssim 1\,\mu$K with a ground state population of 98.4% has been achieved in optical lattices with parameters very similar to the ones used for the optical microtraps [51], and heating rates below $1\,\mu$K/s corresponding to 1/80 and 1/16 vibrational quanta per second in the directions of strong and weak trapping, respectively, have been estimated [53]. Summing up effects of fluctuations of the trap positions, photon scattering, and heating, we can estimate an overall error rate of approximately 0.02 for a single qubit operation for gaussian traps with $\omega_x t_r = 1100$, corresponding to a total gate time of 4 ms.

3.6   Conclusion

In conclusion, a novel implementation of quantum bits and gates for neutral atoms trapped in optical potentials, *e.g.*, optical or magnetic microtraps or optical lattices has been proposed and analyzed . Based on the representation of the quantum bit through the presence of an atom in one out of two trapping potentials, the implementation of single qubit gates as well as of a two qubit phase gate has been considered. We analyzed the performance,

---

[5]If Rabi oscillations are used for the gate operation, then a Hadamard gate is more sensitive to changes in timing or in the distance of the traps than a ɴᴏᴛ gate, as in the further case the operation is taking place on the flank of a Rabi oscillation (*i.e.*, the populations are sensitive to linear order on small variations of the timing), and not, as in the latter case, on an extremum (where the sensitivity is only quadratic).

error rates, and influences of decoherence in a realistic experimental scenario using parameters relevant for experiments with ^{87}Rb atoms trapped in arrays of optical microtraps. We showed that gate times on the order of a few microseconds are possible. Also, an implementation has been shown to be possible in magnetic microtrap potentials [91].

Clearly, the achievable error rates show that the SDQ configuration with neutral atoms in optical microtraps does *not* outperform the proposals making use of internal states [16–20] or vibrational states [46, 62] taking into account realistic experimental imperfections. But it offers some important practical advantages, which especially lie in the relative simplicity and closeness to experimental implementations: (i) Spontaneous emission leads to decoherence only in a much reduced fashion. As long as the microtraps are moved adiabatically, atoms remain in the ground state of both the internal and external degrees of freedom for typical gate times. (ii) There is no momentum transfer in single or two-qubit operations as, in general, it is the case when these operations are realized via laser pulses. This momentum transfer could heat the atoms and, eventually, take them out of the microtrap. (iii) In the SDQ configuration one has that $|\langle 0|r|0\rangle - \langle 1|r|1\rangle| \neq 0$. Therefore all interactions are space dependent, which can be used to realize the gate operations without the need for state dependent potentials. Finally, this means that (iv) single and two-qubit gates are realized by the same kind of operation, i.e., by approaching the microtraps, which implies a simplification in the experimental set-up.

Finally, we note that most of the concepts developed here can be also applied to quantum dots with the qubit introduced in two tunnel-split ground states [87, 88]; and to Josephson-junctions based on the charge degree of freedom with the Cooper-pairs tunneling coherently through the superconducting junction [9].

CHAPTER 4

IMPLEMENTATIONS OF QUANTUM WALKS IN OPTICAL MICROTRAPS

4.1 Overview

In classical computation, random walks are powerful tools to address a large number of problems in many areas of science, as, for example, graph-connectivity or satisfiability problems [93]. It is this success of random walks that motivated to come up with quantum analogues and to study their properties in order to explore whether they help to might extend the (currently rather small) set of quantum algorithms. Two distinct types of quantum walks[1] have been identified: for the *continuous time quantum walk* a time-independent Hamiltonian governs a continuous evolution of a single particle in a Hilbert space spanned by the vertices of a graph [94], while the *discrete time quantum walk* requires a *quantum coin* as an additional degree of freedom in order to allow for a discrete time unitary evolution in the space of the nodes of a graph. The connection between both types of quantum walks is not clear up to now [95], but in both cases different topologies of the underlying graph have been studied, *e.g.*, discrete time quantum walks on circles [96], on an infinite line [97], on more-dimensional regular grids [98], and on hypercubes [99]. The field has recently been reviewed by Kempe [95].

A few algorithms based on quantum walks have been proposed [100–103]. When implementing such algorithms in a physical system, to be useful for a computational problem it ultimately has to be broken down into a series of gates acting on a register of qubits [95]. From the more fundamental point of view however more straight-forward implementations are interesting, *i.e.*, direct implementations of a quantum walker (a particle, a photon, etc.) moving, *e.g.*, in position or momentum space. Such an implementation is also the scope of this chapter. We propose an implementation of discrete time quantum walks for a single neutral atom in an array of optical microtraps or an optical lattice. The particle is walking in position space, but in contrast to the proposal in [104] also the quantum coin is represented by a spatial degree of freedom, as it is implemented as the spatially delocalized qubit (Chapter 3), *i.e.*, by the presence of the atom in the ground state of one out of two trapping potentials. The particle is manipulated *only* by varying the trapping potentials, which

---

[1]In the literature also the name *quantum random walk* is used, but here we choose to leave out the word random, as the time evolution of the system during the quantum walk, in contrast to the classical random walk, is described as a completely deterministic process.

induces tunneling between traps, and no state dependent potentials are necessary. Such a concept can be applied to neutral atoms trapped in optical lattices, in magnetic potentials, as well as in arrays of microtraps; here we will especially analyze the latter case.

In Section 4.2 we will give a more detailed overview about the concept of discrete time quantum walks, before presenting in Section 4.3 two different concepts to realize such a walk in one dimension using the spatially delocalized qubit. In the main part, Section 4.4, we will discuss the influence of non-adiabatic processes and of shaking of the trap positions for the one dimensional walk, and we will estimate the effect of decoherence. We will also consider dependencies of the quantum walk on the vibrational trapping state and from this deduce the temperature–dependence, and show that, within a range of parameters accessible in experiments, a transition from the quantum walk to the classical random walk can be studied. This is not only interesting from a fundamental point of view, but also allows to assess the degree of control that can be reached in the experiment.

Finally, in Section 4.5, it will be shown how a combination of a spatially delocalized qubit and a hyperfine qubit together with state dependent potentials allows to implement a quantum walk on a two-dimensional square lattice . Quantum walks in higher dimensions offer a very rich structure of dynamics, much richer than for the one dimensional case [95, 98], and recently a search algorithm using a modified quantum walk on a two-dimensional grid has been proposed [103].

It has been noted [105, 106], that essentially only interference is necessary for a quantum walk, such that it can be implemented with classical fields. Nevertheless considering setups with neutral atoms is justified by a strong interest in these systems as tools for quantum computation, as well as by the possibility to include further effects as, *e.g.*, quantum walks with two or more particles. A generalization of the quantum walk to two indistinguishable (fermionic or bosonic) atoms has recently be performed in [107].

4.1.1 Related work

So far some setups for one-dimensional realizations of a discrete time quantum walk have been proposed in a variety of physical systems: (i) a quantum walk in momentum space for a system of trapped ions [108], (ii) a walk in position space for a single neutral atom in an optical lattices with state dependent potentials and the coin being implemented in an internal degree of freedom [104], (iii) single-photon sources together with linear optical elements [109], and also (iv) with optical cavities[2] [105, 112, 113].

4.2 Quantum walks

4.2.1 One dimensional walk

The most simple version of a classical random walk (CRW) is to let a particle move on a one-dimensional infinite line, such that it can only hop between sites $x = k \cdot a$ labeled by

---

[2]Indeed, an experiment closely related to quantum walks has been performed already: Bouwmeester *et al.* implemented a quantum Galton's Board (or quantum quincunx, [110]) using a light beam propagating through a grid of Landau-Zener crossings [111].

the discrete index $k \in \{\ldots, -2, -1, 0, 1, 2, \ldots\}$, with a being the distance between sites. At each discrete time step, the particle moves with equal probability to either of the adjacent sites. For such a balanced CRW, the probability to have taken n steps out of N total steps to the right is given by

$$P_N(n) = \frac{1}{2^N} \frac{N!}{n!(N-n)!},\qquad(4.1)$$

and thus the probability to be at a certain site for a large number of steps approaches a gaussian function centered around its initial position x_0, with the variance $\sigma^2 = \langle (x - x_0)^2 \rangle$ growing linearly with the number of steps N.

To define a quantum analogue to this CRW, attach a state $|k\rangle$ to each site $x = k \cdot a$, *i.e.*, the particle is walking in $\mathcal{H}_W = \text{span}\{|k\rangle, k = \ldots, -2, -1, 0, 1, 2, \ldots\}$. It seems to be a natural generalization to replace the random move by walking to the left and to the right in superposition, but this turns out to be non-unitary [114]. For this reason a *quantum coin* is introduced as an additional degree of freedom. In the simplest case of the quantum walk (QW) on a line, the coin space $\mathcal{H}_C$ is two-dimensional. In this case we will denote the states spanning $\mathcal{H}_C$ by $|+\rangle$ and $|-\rangle$, and the total Hilbert space is $\mathcal{H}_W \otimes \mathcal{H}_C$. Each step of the quantum walk is then composed from two operations: (i) applying a unitary operation H to the coin (simultaneously at all sites), *e.g.*, a Hadamard operation:

$$\forall k: \quad (\mathbb{1} \otimes \textsc{h})|k, \pm\rangle = \frac{1}{\sqrt{2}}(|k, +\rangle \pm |k, -\rangle),\qquad(4.2)$$

followed by (ii) applying a displacement operation O_{1D} which moves the particle left or right depending on the coin:

$$\forall k: \quad O_{1D}|k, \pm\rangle = |k \pm 1, \pm\rangle,\qquad(4.3)$$

where we have not explicitly written the tensor product: $|k\rangle \otimes |\pm\rangle \equiv |k, \pm\rangle$ etc. The probability distribution arising from the iterated application of $W = O_{1D}(\mathbb{1} \otimes \textsc{h})$ is, except for the first three steps, significantly different from the distribution of the classical walk: if the coin initially is in a suitable superposition of $|-\rangle$ and $|+\rangle$ it has two maxima symmetrically displaced from the starting point. In general the exact form of the distribution, especially the relative height of the maxima, depends on the initial coin state. Compared to the classical random walk, its quantum counterpart propagates faster along the line: its variance grows quadratically with the number of steps N, $\sigma^2 \propto N^2$, compared to $\sigma^2 \propto N$ for the classical random walk. Fig. 4.2.1 shows a comparison of a classical random walk and a quantum walk. Note that for the QW after an odd (even) number of steps all the even (odd) site are empty as long as the displacement operation is perfect.

4.2.2 Two-dimensional quantum walks

For the walk on a line, the Hadamard gate $\textsc{h}$ is, up to phases which can be absorbed also completely into the initial state, the only unbiased coin operator [115]. For a two-dimensional regular square lattice a much richer structure of coin operators and possible probability distributions arises. As has been observed by Mackay *et al.* [98] and by Tregenna *et al.* [115] in this case different unbiased coin operators and initial states can be chosen that produce significantly different dynamics, ranging from a very localized distribution with a sharp centered spike to distributions having the shape of a ring.
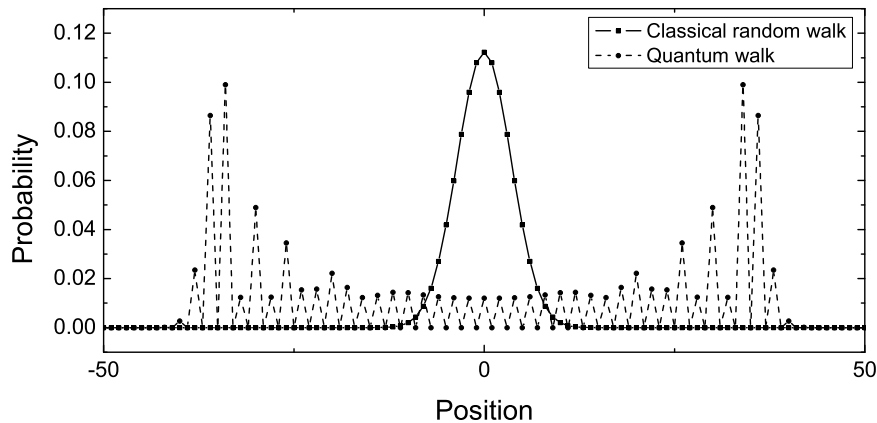
Figure 4.1.   *Comparison of the probability distributions after N = 50 steps for the balanced classical random walk (squares) and a quantum walk using a Hadamard coin operator and the initial state $|\psi\rangle = |0\rangle \otimes (|+\rangle + i|-\rangle)/\sqrt{2}$. In the latter case the probability distribution is shown after tracing out the coin degree of freedom .*

4.2.3   Quantum walks and decoherence

Quantum walks as such are, as they correspond to strongly delocalized states of a quantum particle, very sensitive to the effects of decoherence. Kendon *et al.* studied quantum walks under the influence of decoherence analytically and numerically in [116–118] and find an increasing sensitivity to effects of decoherence as the particle is spread out over more and more sites. Under the presence of decoherence, the distribution ultimately collapses, in the limit of a large number of steps, to the classical distribution of a random walk[3]. The figure of merit determining the shape of the distribution is the product Np, where N is the number of steps of the quantum walk and p is the decoherence rate per step. Kendon et al. identify an interesting property of the quantum walk: for a particular region of values for Np and for decoherence affecting the position of the particle only or the position as well as the coin, the quantum walk on the line for example exhibits a very uniform, *i.e.*, flat, distribution. In this way decoherence might help to increase a possible quantum speed-up reached through quantum walks. Similar improvements have been found for hitting times [95] on the hypercube and mixing times [95] on the circle, two figures of merit describing how fast quantum walks explore the position space in various geometries.

---

[3]In this sense it is justified to talk about the quantum walk as a quantum version of the classical walk, despite the fact that the evolution in the classical case is random while the quantum version evolves completely deterministically.

4.3 Implementations of a one dimensional walk

To implement the coin at each site, we will follow the idea of spatially delocalized qubits introduced in Chapter 3, *i.e.*, the basis states will be represented by a single atom occupying the ground state of one of two adjacent traps. Unitary operations (here we only need single qubit operations as described in Section 3.2) are performed by approaching the two traps forming the coin, allowing the atom to tunnel between them. In the following we will use quantum optics notation to describe the effect of tunneling between traps, *e.g.*, an operation exchanging the population of two traps will be termed π pulse, a Hadamard operation will be termed $\pi/2$ pulse.

We propose two closely related configurations, both leading to a quantum walk. For the first configuration two rows of traps are necessary. Each coin is defined by one trap from each row. By moving both rows in opposite directions with appropriately chosen distance and velocity, the coin operations are performed when the traps pass each other at close distance. The displacement is implicit through a redefinition of the coin each time two traps have passed. Fig. 4.2 shows the probability distributions resulting from an integration of the two dimensional Schrödinger equation. In order to demonstrate the idea here, the simulation is done for the simplified piecewise harmonic potentials from Section 2.2.1 (see figure caption for details). Fig. 4.2 (I–III) show the coin operation, (III-IV) the redefinition of the coins and (V) gives the probability distribution after the sixth displacement operation. The onset of the quantum walk character of the distribution is clearly visible as two maxima symmetrically displaced from the origin appear. Due to the redefinition of the coins there are no empty sites, as it is the case for the quantum walk defined above. Realizing this setup using optical microtraps generated directly by microlenses is quite challenging as the traps have two be formed from two sets of lenses, which have to be displaced against each other in a continuous way. To reduce the possibly necessary mechanical movement, setups using holographic techniques [30] might be useful.

In what follows we will concentrate on the coin being implemented *parallel* to the direction of displacement, such that only a single line of traps is necessary, see Fig. 4.3. Labeling the traps of the kth qubit by $2k$ and $2k + 1$, for coin operations the traps $2k$ and $2k + 1$ are approached, while for the steps in the walk a π-pulse between traps in adjacent qubits, *i.e.*, between traps $2k + 1$ and $2(k + 1)$, moves the atom one step to the left or to the right, respectively. Contrary to the displacement operator from Eq. (4.3), this procedure flips the coin operator at each move, *i.e.*, we have $O_{1D}|k, \pm\rangle = |k \pm 1, \mp\rangle$[4]. Clearly the experimental requirement is to be able to move all odd (or all even) traps as a whole to both directions, thus approaching each second trap to its left or right neighbor. This can be realized in optical lattices and in optical microtraps as described in Section 1.2.2, and also in magnetic microtraps [60].

The simulations for illustrating the basic operations in Fig. 4.3 are performed again for piecewise harmonic potentials. All the following simulations however are for realistic gaussian trapping potentials with a potential depth of $U_0 = 200 \ \hbar\omega_x$, an initial separa-tion[5] of $2\alpha a_{max} = 60$ and a minimal distance of $2\alpha a_{min} = 28.8$. The latter distance is for

---

[4]Such a walk is termed termed *flip-flop walk* in [103].
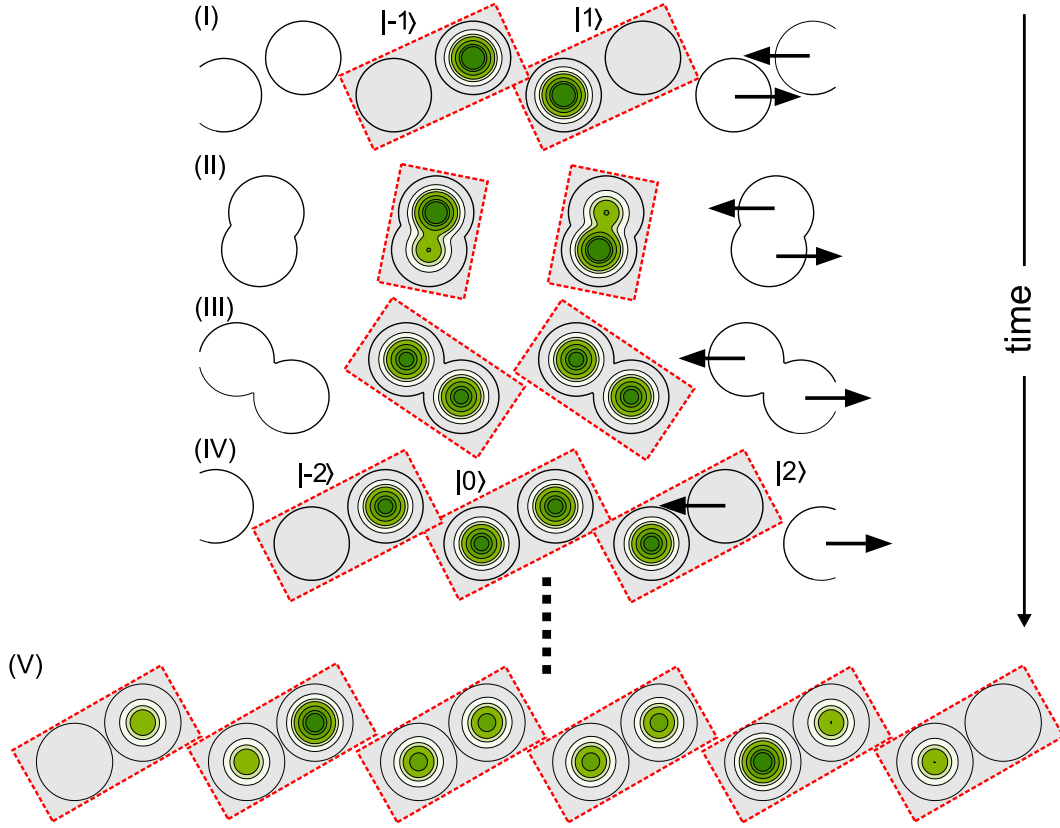[5]As compared to Chapter 3 here the initial separation is chosen smaller.

Figure 4.2. *Quantum walk configuration with two rows of traps, the qubit is implemented perpendicular to the rows (dashed rectangles show which two traps form each qubit). The upper (lower) row moves left (right) with constant velocity. (I) After the first step $|\psi\rangle = 1/\sqrt{2}(|-1, -\rangle + i|+1, +\rangle)$; (II)-(III) the coin operation, in this case a Hadamard gate, is performed as the traps pass each other; (IV) the shift O_{1D} is implicit through a redefinition of the qubits. After an even (odd) number of shift operations only the even (odd) qubits (compared to the standard quantum walk definition) are defined; (V) the probability distribution after the sixth displacement operation. For the numerical simulation we used a potential which, along the line connecting the centers of two traps, reads $V(x) = \alpha^2 \hbar \omega_x \min\left\{(x-a)^2, (x+a)^2\right\}$, while it is simply harmonic in the direction perpendicular to this line. The velocity is chosen such that during the passing of two traps a Hadamard operation is performed. The initial state is $|\psi_{init}\rangle = \frac{1}{\sqrt{2}}(|0, -\rangle + |0, +\rangle)$.*
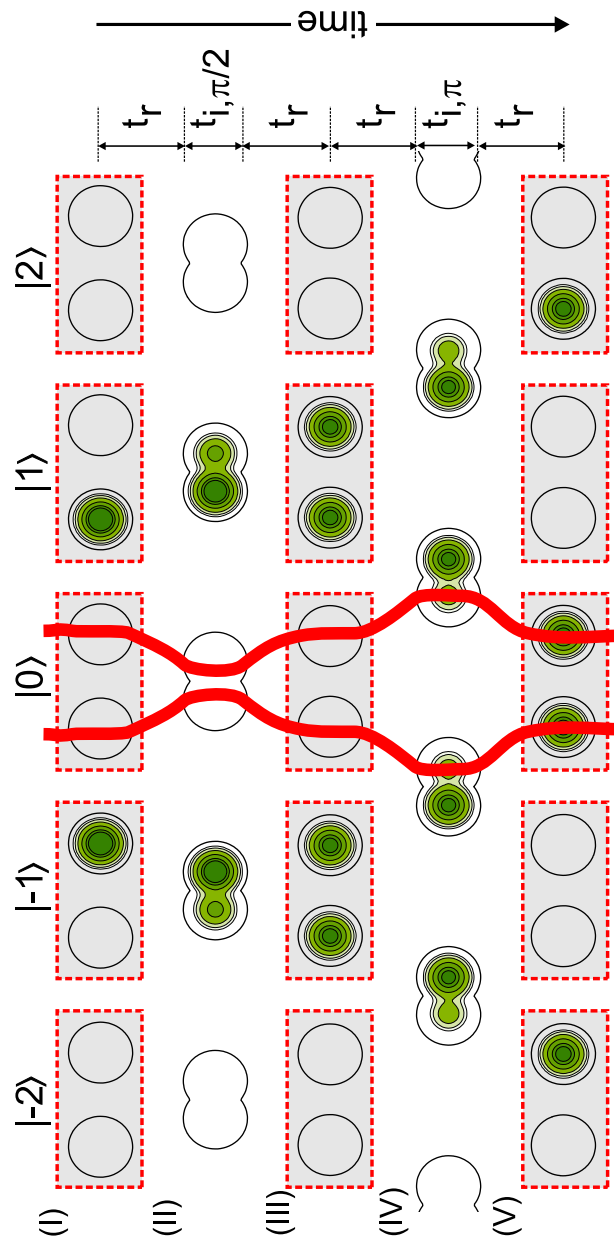
Figure 4.3. *Configuration with one row of traps, the qubit is implemented parallel to the rows (grey boxes). (I) After the first step: $|\psi\rangle = |-1,+\rangle + |+1,-\rangle)/\sqrt{2}$; (II) traps inside each qubit are approached to give the coin operation; (IV) the shift O_{1D} is realized through approaching traps of adjacent qubits.*
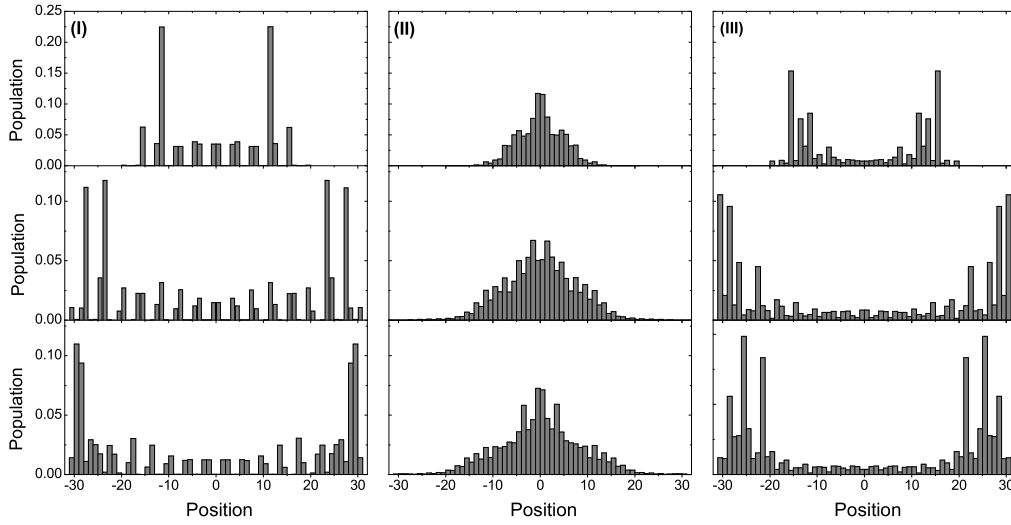
Figure 4.4.   *The probability distribution to find the atom at a specific trap site,*
with (I) the ground state and (II) the first excited state as the initial vibrational
state, for a one-dimensional quantum walk on a finite line of 62 traps; from top
to bottom distributions after n = 10, 20, and 30 steps are shown. Parameters:
$V_0 = 200\hbar\omega_x$, $\alpha a_{max} = 60$, $\alpha a_{min} = 28.8$, and $\omega_x t_r = 100$; $\omega_x t_{i,\pi} = 20.25$
for the π pulse and $\omega_x t_{i,\pi/2} = 112$ for the $\pi/2$ pulse (For simplicity we fixed
a_{min} and then searched for the smallest t_i that produces the desired operation.
As tunneling already happens for $a > a_{min}$, $t_i = 0$ does not give the identity
operation, and for this reason $t_{i,\pi/2} > t_{i,\pi}$). (III) like (II), but with $\omega_x t_r = 200$,
such that non-adiabatic excitations are suppressed.

the given trapping parameters close enough for tunneling to take place. For these parame-
ters, optimizing the path $a(t)$ between a_{max} and a_{min} allows to reduce the time necessary to
adiabatically approach – or separate – the traps to $\omega_x t_r = 100$ or below while maintaining a
fidelity larger than $F = 0.999$. The time t_i for which the traps are kept at the distance a_{min}
is chosen such that alternately a π pulse and a $\pi/2$ pulse are applied.

Initially the atom is prepared in an equal superposition of the two ground states of the central
qubit, *i.e.*, of the two central traps, such that $|\psi_{init}\rangle = \frac{1}{\sqrt{2}}(|0,+\rangle + |0,-\rangle)$. In this case, Fig. 4.4
(a) shows the probability distribution obtained from a quantum walk after $n = 10$, 20 and
25 steps (starting from a displacement step), showing the typical shape of the distributions.
In the next section, we will analyze, how the probability distributions change of different
vibrational states are involved or experimental imperfections are present.

4.4   Temperature, experimental imperfections, and decoherence

4.4.1   Excited vibrational states: the influence of temperature

Tunneling as well as adiabaticity do crucially depend on the timing of the change of the trap
separation. For all simulations, the time t_r needed to move the traps together or apart, and

t_i, the time for which the trap separation is kept constant, are chosen to apply the correct operations for the vibrational *ground state*. If the atom starts in an excited vibrational state, then the tunneling rate is larger and thus in general the coin operator H as well as the displacement operator O_{1D} will change. The former will be distinct from the Hadamard operator and generally biased,

$$H^{\text{general}}|k, \pm\rangle = \sqrt{p}|k, +\rangle \pm \sqrt{1-p}\, e^{i\Delta_H}|k, -\rangle, \qquad (4.4)$$

(the standard unbiased Hadamard operator has $p = \frac{1}{2}$ and $\Delta_H = 0$), the latter will take a general form

$$O_{1D}^{\text{general}}|k, \pm\rangle = \sqrt{c}|k \pm 1, \mp\rangle \pm \sqrt{1-c}\, e^{i\Delta_O}|k, \pm\rangle. \qquad (4.5)$$

($c = 1$ and $\Delta_O = 0$ for the standard displacement operator). For an atom in a fixed vibrational level, p, Δ_H, c and Δ_O, and thus the operators H and O_{1D} are constant, because the movement of traps is assumed to be unchanged throughout the process. In such a case the qualitative shape of the probability distribution is not modified significantly, it still shows the characteristic symmetrically displaced peaks. However, a simulation for an atom initially in the first excited vibrational state, cf. Fig. 4.4 (ii), shows a distribution which essentially has a central peak and long symmetric tails. The difference to the expected result can be attributed to the fact that the approaching and separation processes were optimized to suppress non-adiabatic excitations *from the ground state*. For higher vibrational states such excitations are non-negligible, causing coin as well as displacement operator to induce transitions between different trapping states. Then effectively the dimension of the coin space increases. A quantum walk distribution should be re-obtained when restricting the quantum walk to some fixed vibrational state by suppressing non-adiabatic transitions. This can be done by increasing the time t_r used to approach the traps. Then, as can be seen from Fig. 4.4 (iii), a quantum walk-like probability distribution reappears, although this distributions is different from the one for the ground state due to different coin and displacement operators.

A more realistic assumption than starting from a pure state with the atom being in a specific vibrational level is to consider a thermal Boltzmann distribution of the vibrational modes, described by a mixed state [119],

$$\rho = \frac{1}{z} \sum_{j=0}^{\infty} e^{-\beta E_j}|j\rangle\langle j|, \qquad z = \sum_{j}^{\infty} e^{-\beta E_j}, \qquad \beta = \frac{1}{k_B T}, \qquad (4.6)$$

where E_j is the energy of the jth vibrational mode. In this case, the experimentally accessible data are the classically averaged probability distributions for the individual levels, weighted with factors $\exp(-\beta E_J)/z$. Probability distributions after $n = 20$ steps are shown in Fig. 4.5 for initial ground state populations between 99% and 25%, corresponding to a mean number of vibrational quanta between $\langle v \rangle = 0.01$ and $\langle v \rangle = 3$, or to temperatures between $T = 0.2\ \mu\text{K}$ and $T = 2.7\ \mu\text{K}$ (for Rb atoms and trap frequency $\omega_x = 10^5\ \text{s}^{-1}$), respectively. The characteristics of the quantum walk remain visible even at $\langle v \rangle = 3$. In optical lattices with parameters similar to what we consider here, ground state populations of above 98% have been achieved [51]. Thus we can expect that the range of temperatures necessary to observe the quantum distribution is well within the reach of experiments.
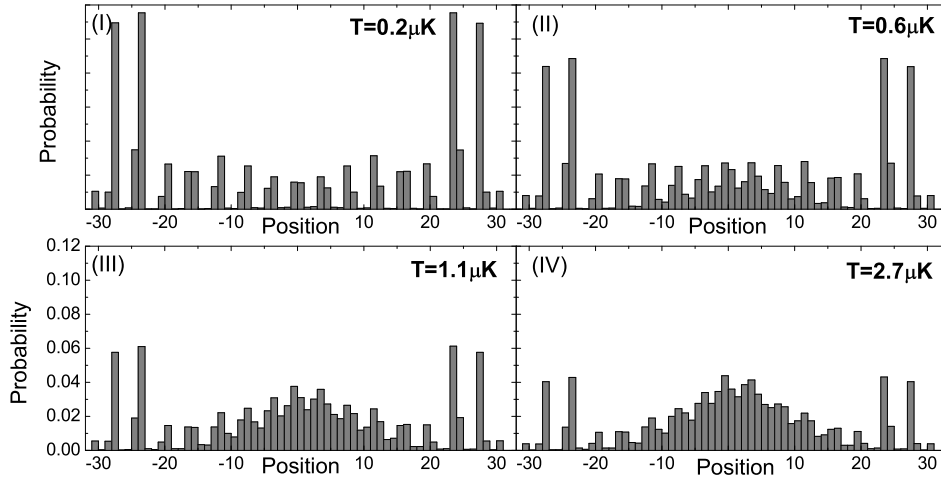
Figure 4.5.   *Probability distributions after n = 20 steps for thermal Boltz-mann distributions of vibrational modes, initial ground state population (I) 99% (corresponding to ⟨v⟩ = 0.1 and, for trap frequency $\omega_x = 10^5 \ s^{-1}$, to T = 0.2 μK), (II) 75% (⟨v⟩ = 1/3, T = 0.6 μK), (III) 50% (⟨v⟩ = 1, T = 1.1 μK), and (IV) 25% (⟨v⟩ = 3, T = 2.7 μK). All other parameters as in Fig. 4.4.*

4.4.2   Experimental imperfections

As discussed in Section 3.5.2, a lack of control of the trap positions presents an important experimental imperfection. For this reason, we will consider again shaking of the traps in order to evaluate how strongly the generated transitions to other vibrational states and the changes in the Rabi frequencies during the tunneling process influence the probability distribution of the quantum walk. The latter error will change coin and displacement operator, and these will even be different from step to step as the shaking and the displacement of the traps for the gate operations are not correlated. On the other hand, we assume the movement of traps in even or odd sets (traps $2k$ or $2k + 1$, respectively) to be correlated. This is justified for an implementation with optical microtraps, where each set of traps can be generated from the same laser beam, Section 1.2.2, and also for optical lattices with tunneling controlled by changing the intensity of one out of two counterpropagating laser beams. The consequences of this random variation should be similar to the effects observed in the presence of decoherence: the quantum walk probability distribution collapses to the distribution of a classical random walk.

In Fig. 4.6 probability distributions for a sinusoidal variation of the trap distances around the desired value with frequency $\omega_{\text{Shake}} = 0.01 \ \omega_x$ are shown for different amplitudes $\alpha\Delta a$. The transition from the quantum to a classical distribution takes place for amplitudes on the order of a percent of the minimal distance, the intermediate flat distribution is clearly visible at $\alpha\Delta a \approx 0.09$. For larger amplitudes of shaking the non-adiabatic transitions are dominant, Fig. 4.7 (a). At the same time, the variance decreases strongly, Fig. 4.7 (b). For smaller amplitudes however the variance initially *increases* with increasing amplitude of shaking. To quantify the flatness of the distribution we also calculate the total variational distance
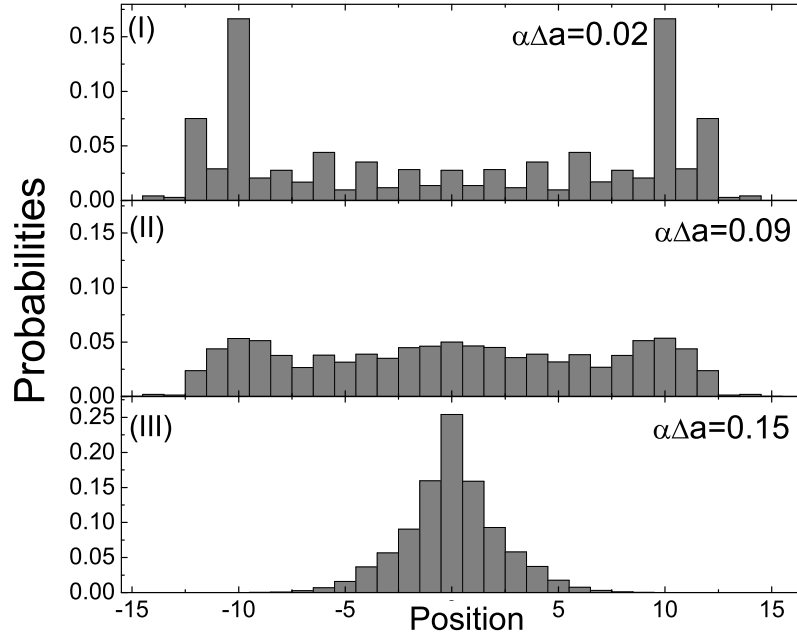
Figure 4.6.   *The effect of shaking of the trap position on the quantum walk. Shaking is modelled by a sinusoidal variation of the trap distances around the perfect value, with frequency $\omega_{Shake} = 0.01\omega_x$ and amplitude $\alpha\Delta a$ (all the other parameters are as in Fig. 4.4). (I-III) show the probability distributions for various values of $\alpha\Delta a$ (after tracing over the coin degree of freedom).*

$v(t) = \sum_n |P(n,t) - P_u(t)|$ to the uniform distribution $P_u(t)$ of width $t/\sqrt{2}$ [116]. Here $P(n,t)$ is the probability to find the particle in the traps belonging to the nth qubit after t steps. As Fig. 4.7 (c) shows, the total variational distance decreases initially, before it increases again as the probability distribution approaches a gaussian. This means, that small amplitudes Δa help to increase the variance but at the same time make the distribution more flat.

4.4.3   Estimation of decoherence effects

The influence of other decoherence mechanisms present in the experiment is determined by the duration of the operations necessary for the quantum walk. As described before, for processes relying on tunneling, the duration of a single operation is on the order of the inverse trapping frequency, which here is assumed to be $\omega_x = 10^5$ s^{-1}. For the parameters used here a single application of O_{1D} $(1 \otimes H)$ takes around 5 ms. From scattering of photons from the trapping laser, with scattering rates on the order of $0.1 \ldots 1$ s^{-1} [27, 29], the probability for a decoherence event to occur within a single step is $p = 0.0005 \ldots 0.005$ and for $n = 17$ applications of O_{1D} H we have $np = 0.0085 \ldots 0.085$. For optical lattices the same decoherence mechanism is present, but also decoherence through fluctuations in the phase of the lasers producing the lattice, giving rise to fluctuations in the trapping potentials should be taken into account. On the other hand, operations can be an order of magnitude faster, as the initial separation of the atoms can be made shorter, such that decoherence rates
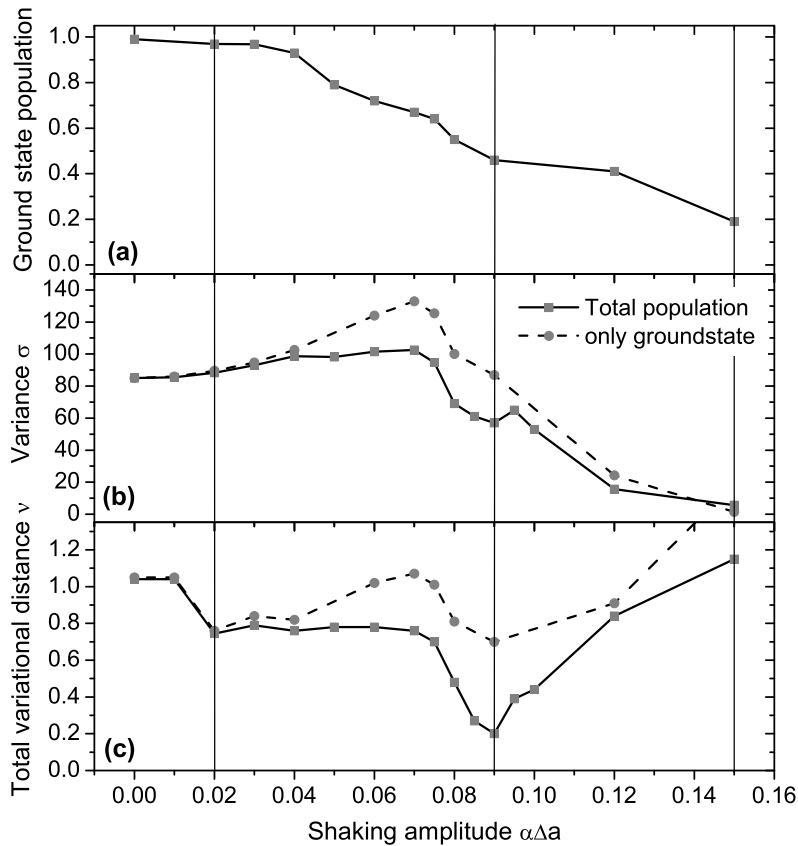
Figure 4.7.   *The effect of shaking of the trap position on the quantum walk for the same parameters as in Fig. 4.7. (a) Ground state population, (b) variance, and (c) variational distance v from the uniform distribution after 17 steps. In (b) and (c) full lines and squares give the respective values for the full population, dotted lines and circles for the ground state only.*

similar to the case of optical microtraps can be expected. Notice, that here the adiabatic passage techniques as discussed in [91] and Section 3.5.3 can be applied to increase the speed of the gate operation.

In both cases these decoherence mechanisms affect the coin degree of freedom as well as the position, and for this case the crossover from the quantum to the classical distribution has been numerically estimated in [116] to take place at $tp \approx 2.6$. For this reason it should be possible to observe the quantum walk in such systems and to analyze changes caused by temperature and shaking without being limited by decoherence from the scattering of photons.

The observed dependence on temperature and on non-adiabatic transitions of the quantum walk with delocalized qubits might thus be interesting as a tool to analyze to which extent the ground state population, the shaping of the trapping potentials, and tunneling processes can be controlled for a particular experimental setup. In addition, quantum walks in this

particular physical system could be used to investigate how decoherence acts with respect to the spatial degree of freedom.

4.5 A quantum walk in two dimensions

For a two-dimensional walk on a regular square lattice, *i.e.*, for a position Hilbert space

$$\mathcal{H}_W = \text{span}\{|(k,l)\rangle, \ k \text{ and } l \in \{\dots, -2, -1, 0, 1, 2, \dots\}\}, \tag{4.7}$$

the number of next neighbors to any site is four, such that a four dimensional coin degree of freedom is necessary to control the displacement of the particle in the different directions: $\mathcal{H}_c = \mathbb{C}^4$. Here we propose to implement such a coin by a suitable combination of a spatially delocalized qubit (SDQ) and a hyperfine qubit (HFQ) combined with spin-dependent transport (Section 1.2.2), *i.e.*, $\mathcal{H}_C$ is a tensor product of the Hilbert space formed from the vibrational ground states of two adjacent traps and from two hyperfine states of the atom: $\mathcal{H}_C = \mathcal{H}_{SDQ} \otimes \mathcal{H}_{HFQ}$. Labeling the two hyperfine states as $|\pm\rangle_{HFQ}$, $\mathcal{H}_C$ is defined as follows:

$$\mathcal{H}_C = \text{span}\{|+\rangle_{SDQ} \otimes |+\rangle_{HFQ} \equiv |++\rangle, |-+\rangle, |--\rangle, |+-\rangle\}. \tag{4.8}$$

4.5.1 Separable quantum walk

There is no unique extension of the Hadamard operator H to $\mathcal{H}_C$, because in two-dimensions there are different classes of unbiased coin operators [115]. The most obvious and simple generalization is to take a Hadamard coin independently for both directions. Here, this can be realized by first approaching the traps to perform a $\pi/2$ pulse for the delocalized qubit as above, and then putting the atom in a superposition of the two hyperfine levels by a $\pi/2$ two-photon [120] or microwave [104] pulse, which realizes $H_{2D} = H_{SDQ} \otimes H_{HFQ}$ (cf. Fig. 4.8 (a-c) for the case of $|++\rangle$ as initial state). For the coin-dependent displacement assume that at every vertex of the two-dimensional grid, each two traps forming a coin are aligned horizontally. Then in this direction first the walking operator O_{1D} can be applied, *i.e.*, within each row traps of neighboring qubits are approached as described above to give a π pulse, followed by translating the lattice potential in opposite vertical directions for each spin state, as proposed in [104] for one dimensional quantum walks (see Fig. 4.8 (d)). In total, the action of the walking operator O_{2D} in $\mathcal{H}_W \otimes \mathcal{H}_C$ is given by

$$O_{2D}|(k,l), \pm\pm\rangle = |(k \pm 1, l \pm 1), \mp\pm\rangle. \tag{4.9}$$

Fig. 4.9 (I–III) shows probability distributions arising from an iterated application of $O_{2D}(\mathbb{1} \otimes H_{2D})$ to the initial state $|\psi_{\text{init}}\rangle = |(0,0), ++\rangle$. From its construction it is easy to see that the coin operator H_{2D} does not mix the horizontal and vertical direction. For this reason one obtains the one-dimensional quantum walk distribution when projecting the distributions along the x or y directions to obtain the single-particle probabilities (due to the choice of the initial conditions it is not symmetric in this case). H_{2D} is thus called a separable Hadamard walk in the classification of [98].
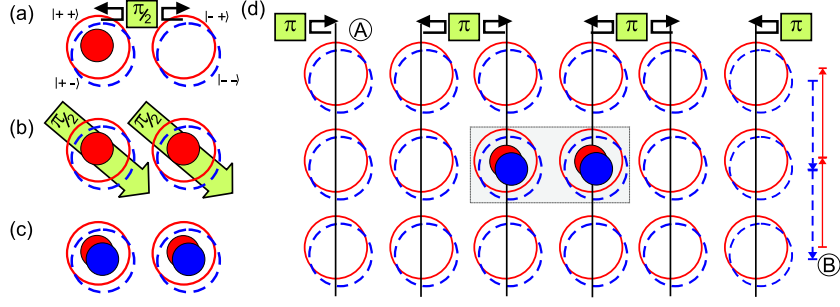
Figure 4.8. *Implementation of the coin and the coin operator $H_{2D} = H_{SDQ} \otimes H_{HFQ}$ for the two-dimensional walk: (a) The four levels are formed as a tensor product of a delocalized qubit (left and right traps) and a hyperfine qubit (dark and greyfilled circles symbolize the $|+\rangle$ and $|-\rangle$ hyperfine states, full and dashed lines denote the respective trapping potentials). The initial state is $|++\rangle$. (a) $\to$ (b) For H_{SDQ} the traps are approached for both hyperfine states. (b) $\to$ (c) For H_{HFQ} a $\pi/2$ pulse between the two hyperfine levels is applied to all traps simultaneously. (d) shows the implementation of the two-dimensional walking operator O_{2D} through a combination of tunneling and spin dependent transport: (A) Traps in horizontally adjacent traps are approached to give a π-pulse as in the one-dimensional walk. (B) The lattice is displaced in opposite vertical directions for the two hyperfine states.*

4.5.2 Entangled quantum walk

More complicated coin operators are also possible, and we will show how to implement one which entangles the two directions. A method to implement such a coin operator is to change the trapping potentials for both hyperfine states independently, for example applying a $\pi/2$ pulse on delocalized qubit for the $|+\rangle$ hyperfine state and a $\pi/2$ pulse followed by a π pulse on the delocalized qubit for the $|-\rangle$ hyperfine state:

$$H_{\text{SD}}^- = \frac{1}{\sqrt{2}}\begin{pmatrix} 1 & 1 \\ 1 & -1 \end{pmatrix} \qquad \text{and} \qquad H_{\text{SD}}^+ = \frac{1}{\sqrt{2}}\begin{pmatrix} 1 & -1 \\ 1 & 1 \end{pmatrix}. \tag{4.10}$$

Subsequently a $\pi/2$ pulse on the hyperfine state identically in both traps is applied as before[6]. The full coin operator reads

$$H_{2D}^{\text{Ent}} = (\mathbb{1} \otimes H_{\text{HF}}) \cdot \left(H_{\text{SD}}^+ \otimes |+\rangle\langle+| + H_{\text{SD}}^- \otimes |-\rangle\langle-| \right) \tag{4.11a}$$

$$= \frac{1}{2}\begin{pmatrix} 1 & 1 & 1 & -1 \\ 1 & -1 & 1 & 1 \\ 1 & 1 & -1 & 1 \\ 1 & -1 & -1 & -1 \end{pmatrix}. \tag{4.11b}$$

---

[6]As an alternative, different laser pulses could be applied to the two traps forming the spatially delocalized qubit, followed by applying the same operation on the delocalized qubit for both hyperfine states; but this requires local addressability of traps.
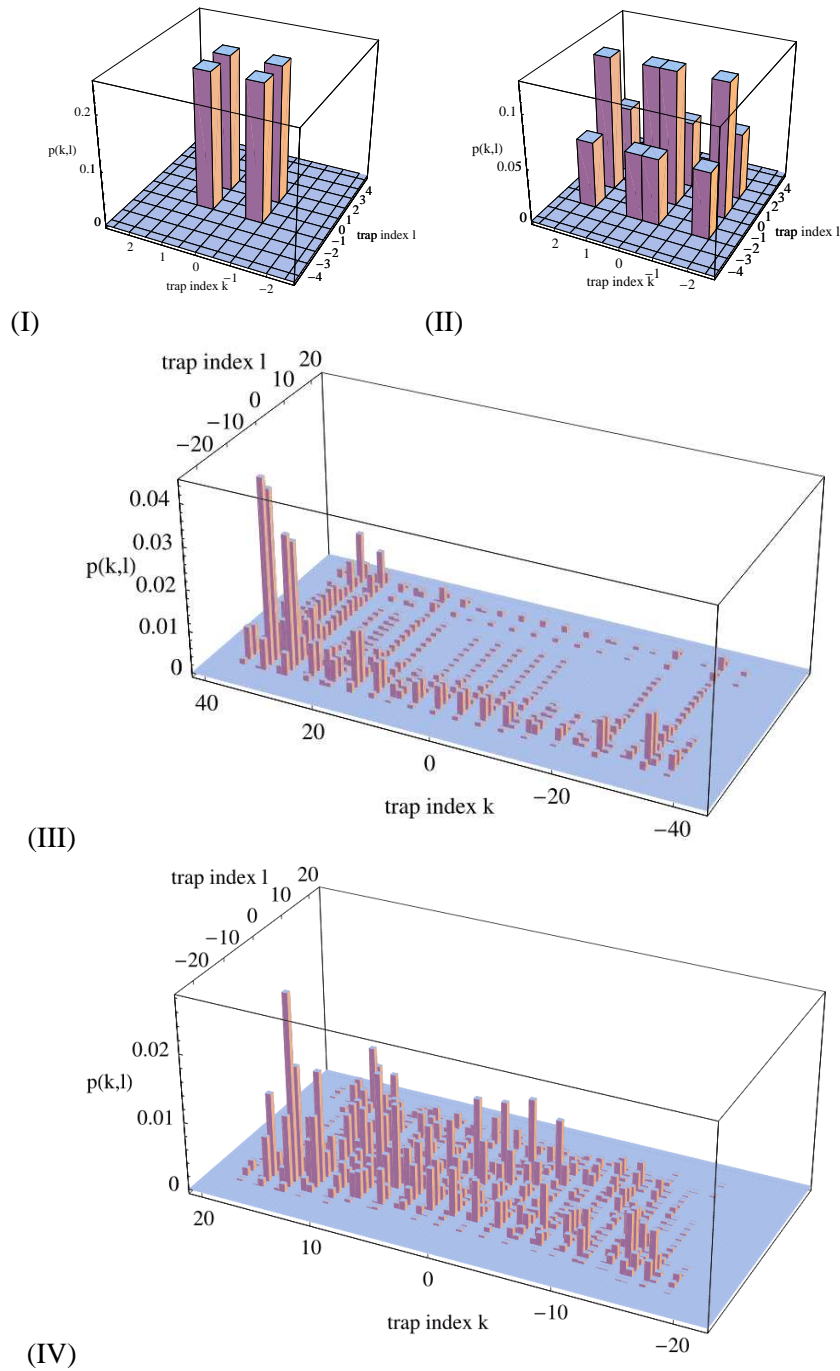
(I)

(II)

(III)

(IV)

Figure 4.9. *(I–III) Probability distributions for the two-dimensional quantum walk obtained from alternatingly applying H_{2D} and O_{2D} after (I) $n = 1$, (II) $n = 2$, and (III) $n = 25$ steps. (IV) Probability distributions for the coin operator H_{2D}^{Ent} after $n = 25$ steps. In both cases the initial state is $|\psi_{init}\rangle = |(0, 0), ++\rangle$. The coordinates on x and y axes label the the traps, thus in x direction each two traps form one site; note that the total population of each trap is shown (sum of probabilities for both hyperfine states).*

It is non-separable as it mixes different directions [98, 115]. The result for the initial state $|\psi_{\text{init}}\rangle = |(0,0), ++\rangle$ is shown in Fig. 4.9 (IV). Similar sequences of operations can be used to generate different coin operators. As has been noted in [115], even for a fixed entangling coin operator very different probability distributions can be obtained through varying the initial state. At least for a system of optical microtraps it should be possible to engineer the initial state carefully enough, because due to the large separation of traps, single sites can easily be addressed. In this way these systems can be an interesting testbed to explore the rich structure of probability distributions of two dimensional quantum walks.

4.6 Conclusion

In summary, here we have discussed the implementation of quantum walks with a neutral atom trapped in the ground state of optical potentials by using the concept of spatially delocalized qubits, *i.e.*, a coin defined by the presence of the atom in one out of two trapping potentials. We have shown that in this case a quantum walk on a line can be performed in a simple way only through a variation of the trapping potentials, without the need for additional lasers to address internal states of the atom. Our simulations were performed with realistic parameters for present optical microtrap systems, but the concept is as well applicable to optical lattices or to magnetic microtraps. We have studied the influences of various experimental imperfections on the probability distribution and have found a strong change if the atom is initially not in the ground state of the trap, leading to a strong dependence of the quantum walk on temperature. This can be attributed to non-adiabatic excitations to other vibrational states during the movement of the traps. We have also studied the influence of shaking and found a transition from quantum to classical probability distributions, taking place for shaking amplitudes on the order of 1% of the tunneling distance. As an intermediate step, this transition exhibits a very flat distribution. An estimation of other decoherence effects such as scattering of photons from the trapping lasers suggests that quantum walks should be observable in the experiment and the effects of temperature and shaking should be accessible to experimental investigation. In this way, implementing the quantum walk with spatially delocalized coins could give information on the extend to which the ground state population and the movement of the traps can be controlled.

Finally, we have combined the concept of the spatially delocalized qubit with a hyperfine qubit and state dependent potentials to obtain a scheme to implement a quantum walk on a two-dimensional regular lattice. Within this scheme, which again is close to what is realizable with state-of-the-art technology in optical microtraps as well as in optical lattices, different coin operators (separable as well as non-separable) are possible, such that in this setup the variety of different distributions in two-dimensional quantum walks can be explored.

TOOLS FOR THE MANIPULATION OF EXTERNAL DEGREES OF
FREEDOM OF NEUTRAL ATOMS: THREE LEVEL ATOM OPTICS

5.1 Overview

Introducing a coherent coupling between two orthogonal states of some quantum system
gives rise to oscillations of the probability amplitudes for finding the system in one of these
states. In Chapter 3 such a coupling between the ground-states of two traps has been used for
the implementation of quantum gates for spatially delocalized qubits. Much more promi-
nent, however, is the example of Rabi oscillations induced by coupling two *internal* states
of an atom *via* a laser mode.

When three instead of two states are considered, the interaction between them gives rise to
a much richer phenomenology. Again the most prominent example is the electric-dipole
interaction between a three level atom and two laser modes. In this scenario, a large num-
ber of techniques have been proposed and reported. Such methods include the stimulated
Raman adiabatic passage (STIRAP) method used to produce a complete population transfer
between two internal quantum states of an atom or molecule [121], the modification of the
optical properties of a medium by means of coherent population trapping (CPT) [120], and
the electromagnetically induced transparency (EIT) [122, 123] phenomena. All these *three
level optics* techniques have been studied intensively, and applications ranging from the
quantum control of atoms and molecules [124], laser cooling [125–127], and slowing down
light to a few meters per second [128] to non-linear optics with few photons [129] have been
identified and studied theoretically as well as experimentally. Three level systems have also
been analyzed in other contexts, including classical mechanics [130, 131].

As noticed in Chapter 3, coherently moving atoms between two traps by Rabi-type oscil-
lations induced by the tunneling interaction is not robust under a variation of the system
parameters and requires precise control of distance and timing. The aim of this chapter is to
introduce methods reminiscent of the three level optics techniques for the efficient, robust,
and coherent manipulation of the *external* degrees of freedom of a trapped neutral atom.
The basic elements of this proposal will be a single atom and three traps, and the atomic
wavefunction will be controlled through a temporal variation of the distance of the traps. As
these methods aim at controlling the spatial wavefunction of the atom instead of its internal
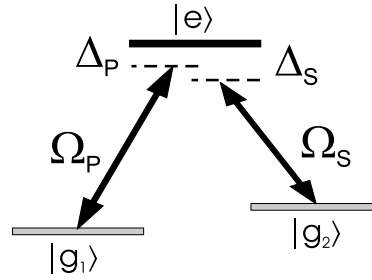
Figure 5.1. *A three level Λ system. The two pairs of states $|g_1\rangle$, $|e\rangle$ and $|e\rangle$, $|g_2\rangle$ are each coupled via one laser mode (pump laser and stokes laser, respectively) with Rabi frequencies Ω_P and Ω_S and detunings Δ_P and Δ_S from the respective transition frequencies.*

degree of freedom, we will choose to subsequently refer to them collectively as *three level atom optics* (TLAO) techniques, since the interference of (single) atom matter waves is at the core of all these techniques.

Subsequently, in Section 5.2, the effects observed in three level atoms and exploited for many applications will be reviewed, before in Section 5.3 these ideas will be transfered to the system of an atom and three traps. An in-depth analysis of the robustness of the various methods with respect to variations of parameters and to experimental imperfections will be performed. In Section 5.4 some further effects, *e.g.*, for excited vibrational states, will be studied and an outlook for further applications of these tools will be given. Finally we will conclude in Section 5.5.

5.1.1 Related work

Improving population transfer in a two-level system has been shown to be possible in optic *via* the method of adiabatic passage [132]. This method has been applied in [91] to improve the performance of the gates for spatially delocalized qubits, as has also been discussed in Section 3.5.2. Very recently, a method similiar to the STIRAP-like process presented here has been proposed by Greentree *et al.* [133] to achieve robust population transfer in a system of three coupled quantum dots.

5.2 Effects in three level optics

To study new effects arising in optics when going from two to three internal atomic states, consider the Λ scheme depicted in Fig. 5.1, *i.e.*, three levels $|g_1\rangle$, $|e\rangle$ and $|g_2\rangle$ and couplings induced *via* two laser modes between two pairs of levels: the *Pump laser* couples level $|g_1\rangle$ to $|e\rangle$ with a (time-dependent) Rabi frequency $\Omega_P(t)$ and a detuning Δ_P, the *Stokes laser* couples $|g_2\rangle$ and $|e\rangle$ with corresponding Rabi frequency $\Omega_S(t)$ and detuning Δ_S. In the rotating wave approximation [134], *i.e.*, neglecting terms which are oscillating fast at the

sum of laser and transition frequency, the Hamiltonian of the system reads [121]

$$
\begin{aligned}
H_{\Lambda-\text{System}} \quad = \quad & 2\Delta_P|e\rangle\langle e| + 2(\Delta_P - \Delta_S)|g_2\rangle\langle g_2| \\
& + \Omega_P(t)(|g_1\rangle\langle e| + |e\rangle\langle g_1|) + \Omega_S(t)(|e\rangle\langle g_2| + |g_2\rangle\langle e|).
\end{aligned} \tag{5.1}
$$

The time-dependent eigenstates of this Hamiltonian[1] under the assumption of one and two photon resonance, $\Delta_P = \Delta_S = 0$, read

$$
|+\rangle \quad = \quad \frac{1}{\sqrt{2}}[\,\sin\Theta|g_1\rangle + |e\rangle + \cos\Theta|g_2\rangle], \tag{5.2a}
$$

$$
|D\rangle \quad = \quad \cos\Theta|g_1\rangle - \sin\Theta|g_2\rangle, \tag{5.2b}
$$

$$
|-\rangle \quad = \quad \frac{1}{\sqrt{2}}[\,\sin\Theta|g_1\rangle - |e\rangle + \cos\Theta|g_2\rangle]. \tag{5.2c}
$$

Here the time-dependence (or, more precisely, the dependence on the Rabi frequencies) is in the *mixing angle* $\Theta = \Theta(t)$, which fulfills

$$
\tan\Theta(t) = \frac{\Omega_P(t)}{\Omega_S(t)}. \tag{5.3}
$$

The eigenvalues corresponding to the eigenstates from Eqs. (5.2) are given by

$$
\lambda_D = 0 \qquad \text{and} \qquad \lambda_{\pm} = \pm\sqrt{\Omega_P^2 + \Omega_S^2}. \tag{5.4}
$$

Assume all the population initially to be in $|g_1\rangle$. If only the Rabi frequency of the Stokes laser coupling levels $|e\rangle$ and $|g_2\rangle$ is non-zero, then the mixing angle $\Theta = 0$ and thus $|D\rangle = |g_1\rangle$. Thus the initial state of the system corresponds to the so-called dark state $|D\rangle$. The idea behind all the effects of three level optics is (i) to let the state vector follow the vector of the dark state adiabatically, and (ii) to choose the final ration of Ω_P and Ω_S such that the dark state corresponds to the desired final state of the system[2]. The advantage of this procedure is that the only requirements are the adiabaticity of the process and the correct adjustment of the final ratio Ω_P/Ω_S. There is no further dependence on the pulse shapes or areas. Another important benefit with respect to the manipulation of internal atomic states is that level $|e\rangle$ is never populated during the (ideally completely adiabatic) process, such that spontaneous emission from this level is of no importance.

The three most prominent effects of three level optics are (compare Fig. 5.2):

➤ *STIRAP (Stimulated Rapid Adiabatic Passage)* — If the mixing angle is evolved from $\Theta = 0$ to $\Theta = \frac{\pi}{2}$, then finally the dark state corresponds to $|g_2\rangle$, and thus the population is transferred from $|g_1\rangle$ to $|g_2\rangle$, without intermediate population of $|e\rangle$. For the Rabi frequencies this corresponds to the 'counter-intuitive' sequence of first turning on the Stokes laser and ultimately turning off the pump laser. The STIRAP effect has been used for quantum control of atoms and molecules in many context, *e.g.*, for atomic interferometry [124, 136], for

---

[1]When the number of photons in the two laser modes are taken into account, these states are referred to as *dressed states*.

[2]When the detunings Δ_P and Δ_S are non-zero, then more complicated scenarios are possible through employing a sequence of adiabatic and diabatic crossings [135].
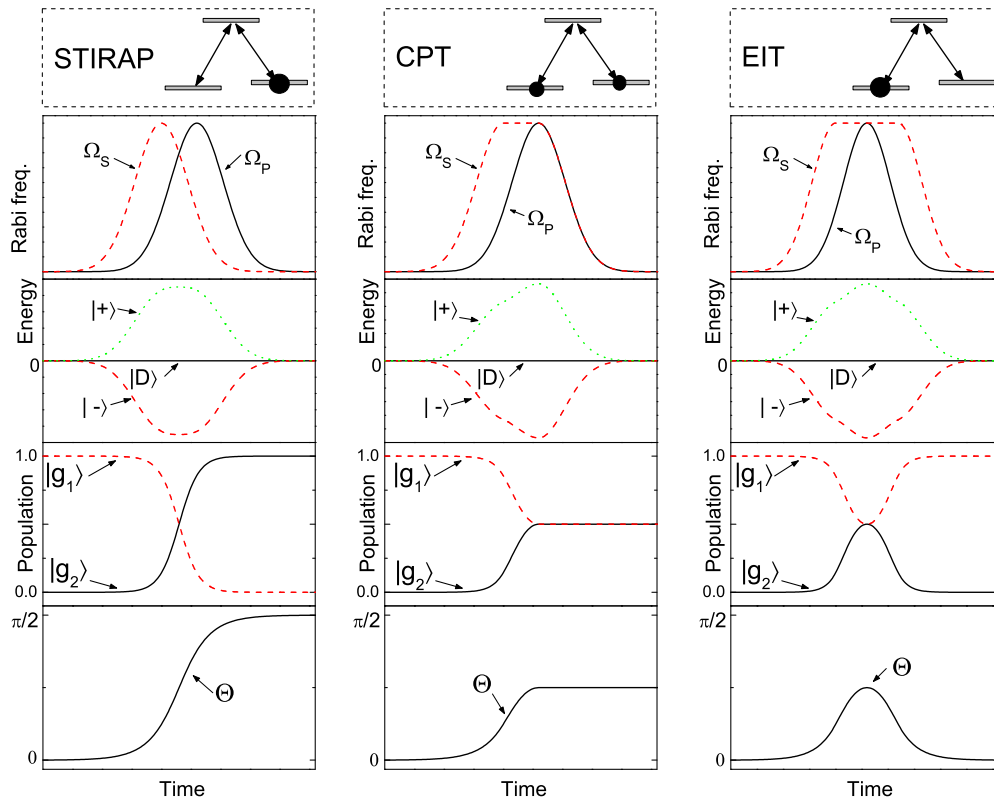
Figure 5.2.   *Effects of three level optics: stimulated Raman adiabatic passage (STIRAP), coherent population trapping (CPT), and electromagnetically induced transparency (EIT). From top to bottom the Rabi frequencies $\Omega_S(t)$ and $\Omega_P(t)$, the eigenvalues $\lambda_\pm(t)$ and $\lambda_D(t)$, the populations of the states $|g_{1/2}\rangle$ (for a completely adiabatic transfer), and the mixing angle $\Theta(t)$ are shown as a function of time.*
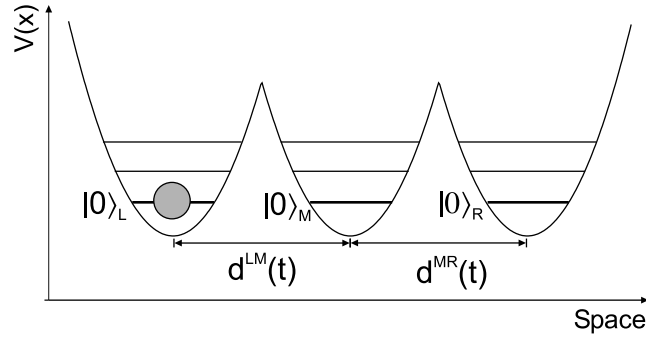
Figure 5.3. *Three trap potential; d^{LM} (d^{MR}) is the separation between left and middle (middle and right) traps. In the limit of a large separation $|n\rangle_L$, $|n\rangle_M$, $|n\rangle_R$ are the nth vibrational energy eigenstates of the corresponding single trap potentials.*

generation of single photons on demand [137], or for converting an atomic condensate to a molecular condensate with large efficiency [138].

➤ *CPT (Coherent Population Trapping)* — Instead of transferring the complete population, it is possible to generate an equally weighted superposition of the states $|g_1\rangle$ and $|g_2\rangle$ by adjusting Θ to a final value of $\pi/4$, such that $|D\rangle = \frac{1}{\sqrt{2}}[|g_1\rangle - |g_2\rangle]$. This requires a precise control of the ratio of the Rabi frequencies in order to achieve $\Omega_P/\Omega_S \xrightarrow{t\to\infty} 1$, as for this aim both Rabi frequencies have to be brought to zero simultaneously. This is more demanding then $\Omega_P/\Omega_S \xrightarrow{t\to\infty} \infty$ in the case of STIRAP. Possible applications range from the construction of beamsplitters for the splitting of matter waves [136] to laser cooling [125].

➤ *EIT (Electromagnetically Induced Transparency)* — Finally the transition to $|g_2\rangle$ can be inhibited completely despite the presence of the pump laser by strongly coupling $|e\rangle$ and $|g_2\rangle$ at all times where $\Omega_P \neq 0$, corresponding to evolve θ from zero to some non-zero value and finally back to zero. The EIT process can turn an initially opaque medium into nearly completely transparent [123]. Also the refractive properties of the medium can be changed drastically and media with very unusual optical properties can be created [123, 139]. This can be employed, *e.g.*, to strongly reduce the velocity of light propagating in the medium [128], to construct a quantum memory for photons [140], and also for laser cooling [126, 127].

5.3 Manipulation of external atomic degrees of freedom

5.3.1 Setup

The preceding section showed that three level optics to manipulate electronic degrees of freedom of atoms and molecules has a big number of applications in very different areas of physics. As these concepts can be formulated more generally, they can be extend in

completely different scenarios, and can especially also be applied for the manipulation of external degrees of freedom of trapped atoms as will be shown now.

We will subsequently consider three dipole traps arranged linearly, as shown in Fig. 5.3, and assume them to be modeled via three piece-wise harmonic potentials of frequency ω_x. A three level system can be formed, in the limit of a large distance between the traps, from the three ground states, labeled $|0\rangle_L$, $|0\rangle_M$, and $|0\rangle_R$. The initial configuration is given by a single atom in the ground-state of the leftmost traps and the other two traps empty.

The three states are coupled through tunneling which can be controlled *via* changing the distance between the traps. The temporal variation of the distance is modeled through a truncated cosine function, *i.e.*, to approach left and middle (middle and right) traps takes a time t_r^{LM} (t_r^{MR}, here usually we will have $t_r^{LM} = t_r^{MR} \equiv t_r$), while t_i^{LM} (t_i^{MR}) is the time the traps remain at the minimum distance, see Fig. 2.1. Furthermore, a delay time t_{Delay} describes the sequence of approaching processes. The strength of the coupling between the vibrational ground states of each pair of neighboring traps is given, in the absence of the third trap, by the following 'tunneling Rabi frequency' (corresponding to the splitting energy between the lowest symmetric and anti-symmetric ground state) as a function of the distance αd between the traps:

$$\frac{\Omega(\alpha d)}{\omega_x} = \frac{-1 + e^{(\alpha d)^2} \left[1 + \alpha d \left(1 - \text{erf}(\alpha d)\right)\right]}{\sqrt{\pi} \left(e^{2(\alpha d)^2} - 1\right)} \, 2\alpha d, \tag{5.5}$$

where $\text{erf}(x) = \frac{2}{\sqrt{\pi}} \int_0^x dt \, \exp(-t^2)$ is the *error function* and as before $\alpha^{-1} = \sqrt{\hbar/m\omega_x}$ is the size of the atomic ground state, with m being the atomic mass.

Although Eq. (5.5) is useful to explore the analogies to three level optics, a more appropriate treatment accounting for coupling to the excited vibrational states and direct coupling from the left to the right trap requires the integration of the Schrödinger equation. For the simulations shown here, a strong confinement in the z-direction, i.e., $\omega_z \gg \omega_x$, has been assumed, such that corresponding excitations can be neglected. In what follows we will numerically integrate the 1D Schrödinger equation to simulate the dynamics of the neutral atom in the three trap potential, but consistency has been checked with the results of an integration of the 2D Schrödinger equation for the case $\omega_x = \omega_y$.

The general experimental requirements in general are similar to the requirements to implement the spatially delocalized qubit, see Chapter 3. We assume, that initially no or one atom can be stored per trap at will, and we require to be able to change the distance between the two pairs of traps independently. For arrays of optical microtraps generated by arrays of microlenses this can be achieved by illuminating each lens with three laser beams whose angles can be changed individually, or by introducing traps formed from a second array of lenses. In the case of traps formed *via* holographic techniques [30], it has already been demonstrated that three traps can be created and manipulated with big freedom. Also, loading of single atoms has already been demonstrated for this setup. Finally, such an individual manipulation of the trap distances is also feasible in magnetic microtraps.
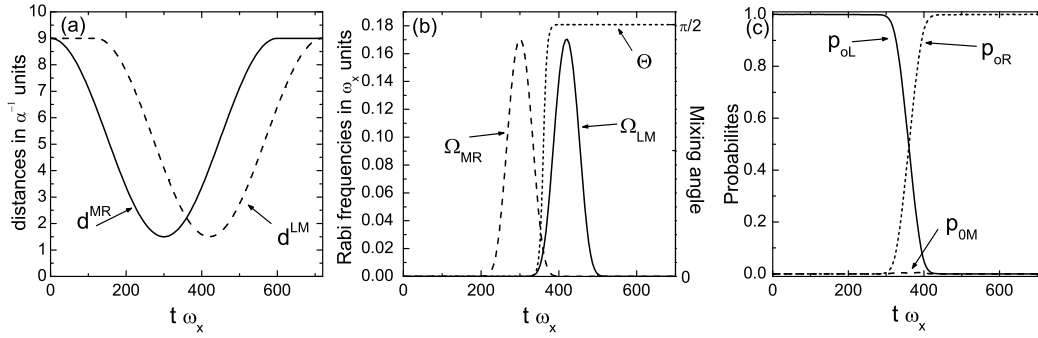
Figure 5.4. *(a) Approaching sequence for a STIRAP-like process, (b) the evolution of the tunneling Rabi frequencies $\Omega_{LM}(t)$ and $\Omega_{MR}(t)$ between the left and the middle and the middle and the right trap, calculated from Eq. (5.5), together with the mixing angle $\Theta(t) = \arctan(\Omega_{LM}(t)/\Omega_{MR}(t))$, and (c) the corresponding ground state populations; The parameters are $d^{LM}_{max}\alpha = d^{MR}_{max}\alpha = 9$, $d^{LM}_{min}\alpha = d^{MR}_{min}\alpha = 1.5$, $t^{LM}_r\omega_x = t^{MR}_r\omega_x = 300$, $t^{LM}_i\omega_x = t^{MR}_i\omega_x = 0$, and $t_{delay}\omega_x = 120$.*

5.3.2 STIRAP process – robust transfer of population

To implement a robust method to move an atom from the leftmost to the rightmost trap, the counter-intuitive STIRAP sequence is applied: first the right and the middle trap are approached and separated, and, with an appropriate delay, the same sequence is used for the left and the middle trap [Fig. 5.4 (a)]. For a correct adjustment of the parameters, this adiabatically changes the mixing angle from $\Theta = 0$ to $\Theta = \pi/2$ [Fig. 5.4 (b)] and thus moves the atom directly from $|0\rangle_L$ to $|0\rangle_R$, with an almost negligible amplitude to be in the middle trap ground state [Fig. 5.4 (c)]. The spatial wavefunctions $\langle x|D\rangle$ of the dark state for various times during the approaching process are plotted in Fig. 5.5.

It is an important advantage of this STIRAP-like process, that, as its optical analogue, it is robust with respect to the variation of many experimental parameters. Employing Rabi-type oscillations between only two traps to move the atom between them suffers from a strong dependence on timing and on the distances of the traps. Also the method of adiabatic passage in a two-level system, although improving the performance of the process, is sensitive to changes of these parameters[3] [91]. As shown in Fig. 5.6 (a), the STIRAP process works for a large range of the time delays t_{Delay} between the two traps and of the minimum distance d_{min}. A similar robustness is present for variations of, *e.g.*, t_r and t_i, the only requirements being the adiabaticity of the process and the order of approaching and separating the traps. Introducing a shaking of the trapping potentials, an important decoherence mechanism already analyzed for a Rabi-type process in Chapter 3, also does not

---

[3]It should be noted, that there is an important advantage of the method of adiabatic passage in a two level system as compared to the STIRAP-like method presented here: STIRAP only helps (with the parameters used here) to move an atom from the left to the right trap, while the opposite process requires a change of the parameters (more precisely a change of the order of approaching the traps). In contrast, moving the atom *via* adiabatic passage in a two level system, allows to move the atom in both directions.
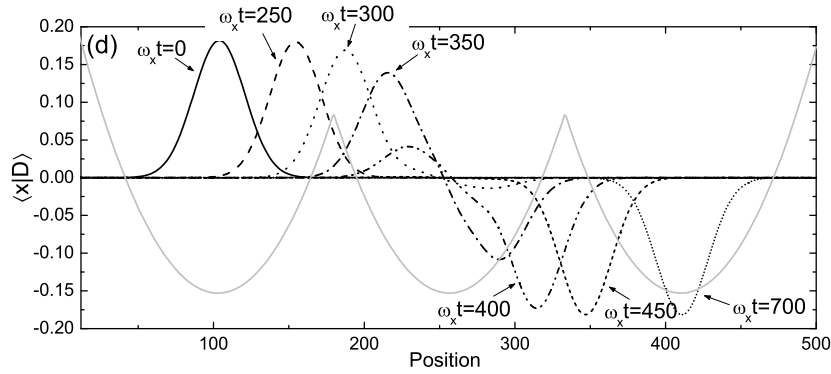
Figure 5.5. *The spatial wavefunction $\langle x|D\rangle$ of the dark state for various times as the traps are approached and separated according to the STIRAP sequence for the same parameters as in Fig. 5.4. Grey line: the potential at $t = 0$.*

degrade the transfer efficiency significantly for a large range of amplitudes a_{Shake} of shaking of the distance between the outer traps. The shaking is again assumed to be well below the trapping frequency, $\omega_{\text{Shake}} = 10^{-2}\omega_x$ in Fig. 5.6 (b), and for a proper approximate choice of the delay time, shaking amplitudes of more than 5% of the minimal distances of the traps can be tolerated.

Another parameter difficult control to high precision is the horizontal alignment of the traps. In case the plane containing the traps is tilted, an additional potential

$$\Delta V_{\text{tilt}}(x) = \gamma\hbar\omega_x\alpha x \tag{5.6}$$

stemming from gravity is added to the dipolar trapping potential $U(x)$. The parameter γ determines the slope of the ramp. For the parameters of our simulations, a value of $\gamma = 10^{-2}$ corresponds to a difference in the potential energy of $3 \cdot 10^{-2}\,\hbar\omega_x$ between the outer traps at the minimal distance. As can be seen from Fig. 5.6 (c), even for $\gamma \lesssim 0.02$ the transfer efficiency remains large as long as the time to approach and separate the traps is chosen large enough. If on the other hand coherent transfer is done by simple Rabi-type oscillations between two traps, then already much smaller values of γ makes the final population going to zero. This is shown in Fig. 5.6 (d), where next to the transfer efficiency for STIRAP for $\omega_x t_r = 300$ two curves for Rabi-type oscillations are shown for a slow ($\omega_x t_r = 300$) and for a fast (but for this configuration still adiabatic, $\omega_x t_r = 32$) approaching process. Surprisingly, the efficiency drops completely to zero, without oscillations, and in the former (slower) case this happens much faster than in the latter case. This is easily explained by the fact, that tilting the potential lifts the degeneray of the ground states of the two traps, and for a completely adiabatic process thus the final state of the system will be equal to the initial state. The population that for small tilts γ still is found in the other trap undergoes a diabatic process, such that in the case of rapidly approaching the traps the transfer process is more efficient. Such an observation has been made by Tiecke *et al.* [141] and by Scharnberg *et al.* [142] in the analysis of a processes for splitting a wavepacket between two traps, and we will come back to this problem when considering an analogue to the CPT process in the next section.
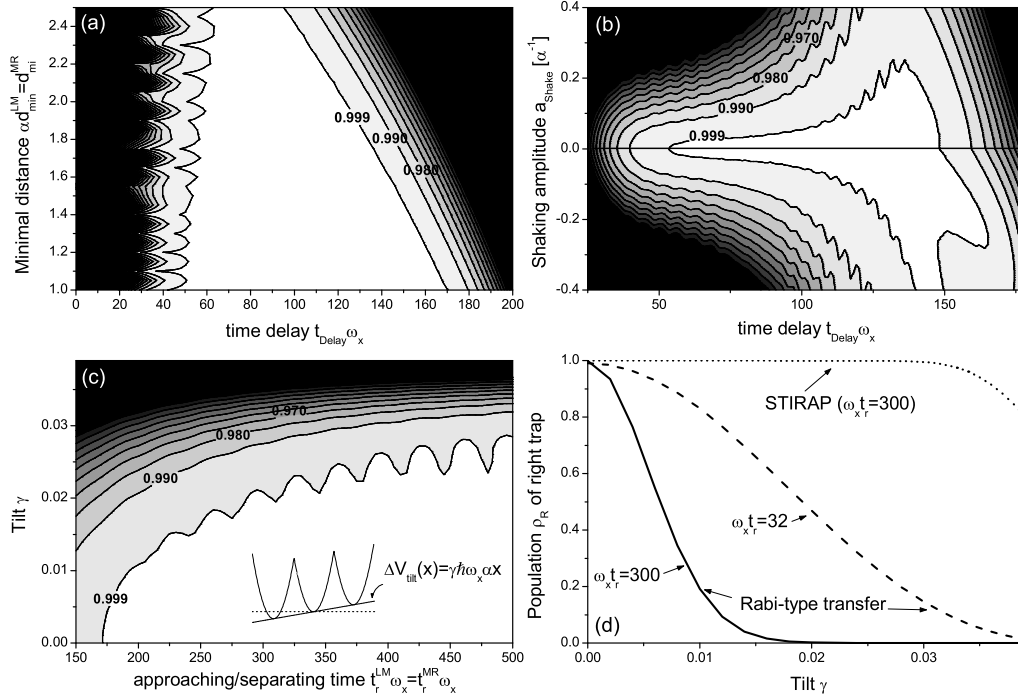
Figure 5.6. *Robustness of the TLAO version of STIRAP. All parameters not varied in the figures are as in Fig. 5.4. (a-c) show the transfer efficiency from $|0\rangle_L$ and $|0\rangle_R$, i.e., the population $\rho_R = |_R\langle 0|\psi(t)\rangle|^2$. In (a) the time delay t_{Delay} between the two approaches (horizontal axis) and the minimal distances of traps (vertical axis) are modified. (b) shows the transfer efficiency as a function of t_{Delay} (horizontal axis) and of the amplitude of a shaking a_{Shake} in the positions of the outer traps (vertical axis) with $\omega_{Shake} = 10^{-2}\omega_x$. For $a_{Shake} > 0$ the shaking of the outer traps is in phase, for $a_{Shake} < 0$ it is out of phase by π. (c) Transfer efficiency for an additional tilted potential $V_{tilt}(x) = \gamma \hbar\omega_x \alpha x$, parametrized by γ as a function of the time t_r needed to approach and separate the traps; in (d) the dependence of the transfer efficiency on the tilt of the potentials is compared for STIRAP for the parameters from (c) with $\omega_x t_r = 300$ and for the transfer via Rabi-type oscillations in two traps for $\omega_x t_r = 300$ ($\omega_x t_i = 12$) and $\omega_x t_r = 32$ ($\omega_x t_i = 25$, in this case the process is still adiabatic) and all the other parameters as in Fig. 3.2.*
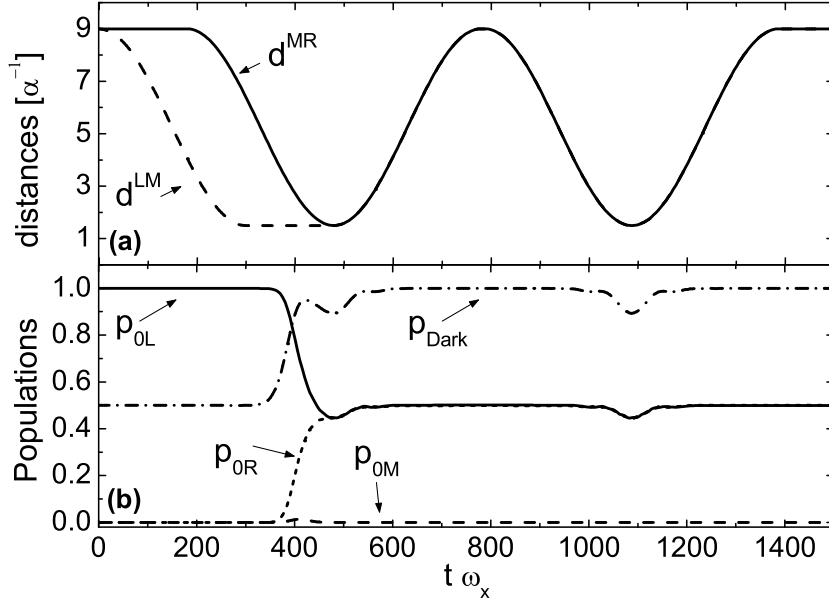
Figure 5.7. *(a) Approaching sequence for a CPT-like process; (b) ground state and dark state populations, $p_{\text{Dark}} = |\langle D(\Theta = \pi/2)|\psi(t)\rangle|^2$; parameters are as in Fig. 5.7, except for $t_i^{LM}\omega_x = 0$, $t_i^{MR}\omega_x = t_{delay}\omega_x = 180$ for $t\omega_x \leq 780$ and $t_i^{MR}\omega_x = 0 = t_{Delay}\omega_x$ for $t\omega_x > 780$. The CPT process to create the dark state takes place between $t\omega_x = 0$ and $t\omega_x = 780$, the remaining part of the sequence is to check that the state is dark, i.e., decoupled from the tunneling interaction.*

5.3.3   CPT process – creation of a dark state

Changing the mixing angle only up to $\Theta = \pi/2$ creates the spatial equivalent to a dark state, *i.e.*, a spatial superposition with maximum atomic coherence having $|c_{0L}c_{0R}^*| = 1/2$, where c_{0L} and c_{0R} are the probability amplitudes of $|0\rangle_L$ and $|0\rangle_R$. To obtain $\lim_{t\to\infty}\Theta = \pi/2$, the traps are approached with an appropriate delay but separated simultaneously and symmetrically as shown in Fig. 5.7 (a) for times up to $\omega_x t = 780$. Fig. 5.7 (b) shows that indeed the dark state $|D(\Theta = \pi/2)\rangle = (|0\rangle_L - |0\rangle_R)/\sqrt{2}$ is created. To prove that this state is really dark, *i.e.*, that it is decoupled from the tunneling interaction, the two outermost traps are approached and separated simultaneously to the middle one as in Fig. 5.7 (a) from $\omega_x t = 780$ till the end. Clearly, the atom after the separation remains in the dark state in spite of the tunneling interaction being present.

The CPT process is robust with respect to the variation of external parameters as distances or timing, as long as the symmetry of the separation of the two traps is maintained. For this reason, a process as shaking of the trapping potentials might strongly influence the efficiency in certain situations. Fig. 5.8 (a) shows the effect of the same type of shaking as discussed before, including a distinction of shaking breaking or not breaking the symmetry. In the further case, if the two extreme traps shake in phase, corresponding to $a_{\text{Shake}} > 0$
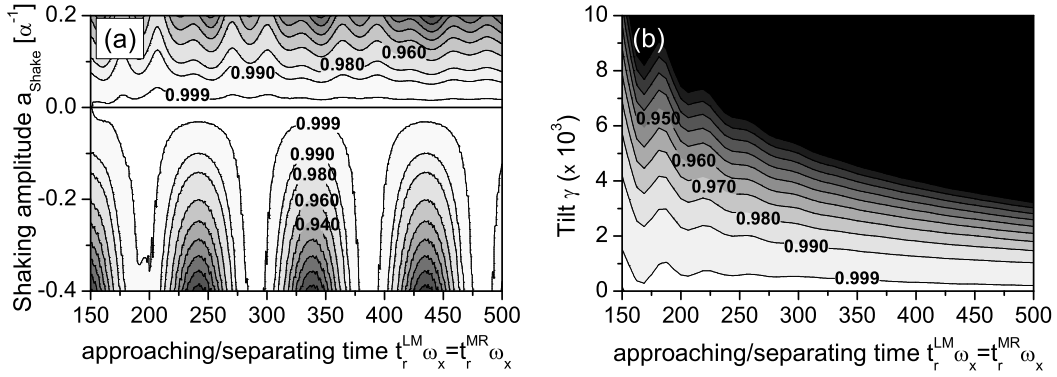
Figure 5.8. *Robustness of the CPT process. All parameters not varied in the figures are as in Fig. 5.7. (a) shows how shaking of the traps alters the efficiency, i.e., the eventual population of the dark state, $\rho_{\text{Dark}} = |\langle D(\Theta = \pi/2)|\psi(t)\rangle|^2$. The horizontal direction shows the dependence on the time t_r used to approach and separate the traps, the delay time between the approaching processes is adapted to t_r as $t_{\text{Delay}} = 0.6t_r$. The vertical axis gives the amplitude a_{max} of shaking, where $a_{\text{Shake}} > 0$ and $a_{\text{Shake}} < 0$ refer to a shaking of the outer traps in phase or out of phase by π, respectively. (b) p_{Split} [see Eq. (5.7)] for an additional tilted potential parametrized by γ [see Eq. (5.6)] as a function of the time t_r needed to approach and separate the traps.*

in the figure, the efficiency is reduced, and although still large amplitudes can be tolerated for a creation of a dark state with high fidelity, such amplitudes are an order of magnitude smaller than in the STIRAP case. If on the other hand the shaking is out of phase by π, i.e., the traps move always in different directions such that the symmetry is not broken (the case $a_{\text{Shake}} < 0$ in the figure), then the transfer efficiency to the dark state is comparable to the STIRAP case.

Tilting the trapping potentials by adding a ramp $V_{\text{tilt}}(x)$ always breaks the symmetry and the expected faster reduction of the efficiency as compared to STIRAP is visible in Fig. 5.8 (b), where the quantity

$$p_{\text{Split}} = \frac{|c_{0L}|}{\sqrt{2}} + \frac{|c_{0R}|}{\sqrt{2}} \tag{5.7}$$

is plotted. p_{Split} is the overlap with an equal superposition of the atom being in the ground state of the left and of the right trap, but ignores the relative phase between the two states. This relative phase is time dependent due to the different energies of the left and the right ground state in the titled potential. Obviously the value of γ that can be tolerated is an order of magnitude smaller than for the STIRAP-like process. Additionally, same effect, which seems counter-intuitive on first sight, already observed in Fig. 5.6 (d) for complete transfer through normal Rabi-type tunneling can be seen here: the efficiency grows for *faster* separation of the traps. Also for the CPT process a very slow and thus very adiabatic process does not evolve $|0\rangle_L$ to $|0\rangle_R$ in the case $\gamma \neq 0$; the observation of population in the right trap then is due to non-adiabatic processes. As the evolution of the eigenvalues is more complicated for three traps than for two, the final state in the case of complete adiabaticity
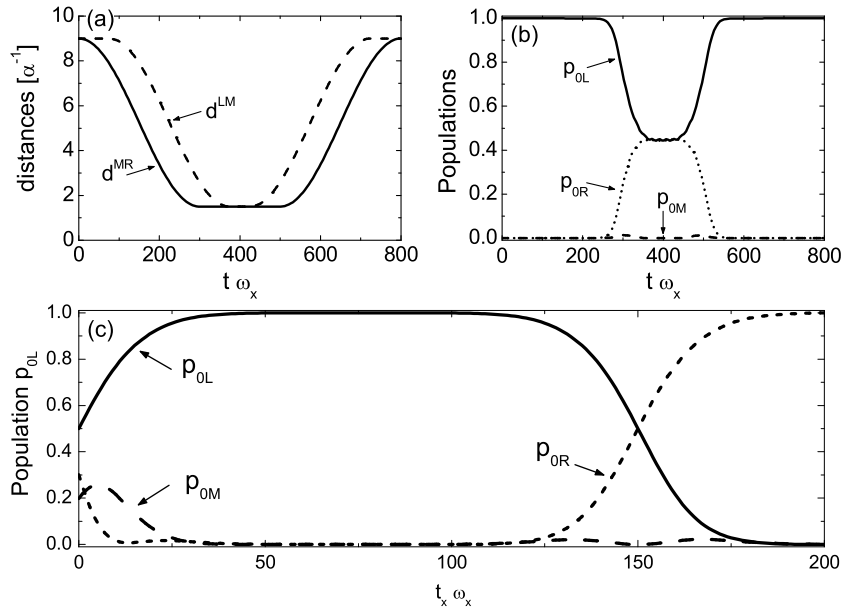
Figure 5.9.   *An EIT-like process: (a) approaching sequence and (b) corresponding ground state populations. Parameters: $d_{max}^{LM}\alpha = d_{max}^{MR}\alpha = 9$, $d_{min}^{LM}\alpha = d_{min}^{MR}\alpha = 1.5$, $t_r^{LM}\omega_x = t_r^{MR}\omega_x = 300$, $t_i^{LM}\omega_x = 50$, $t_i^{MR}\omega_x = 200$, and $t_{Delay}\omega_x = 120$. (c) Ground state populations as a function of the time delay t_r, all the other parameters are as in (b).*

does not necessarily have to be the state with lowest energy. *e.g.*, for the potentials and the parameters used here, the ground state of the left trap does evolve into the ground state of the middle trap for $t_r \rightarrow \infty$.

The robust coherent splitting of the atomic wave function together with the possibility of individual trap manipulation anticipates applications in atomic interferometry. On the other hand, the sensitivity of the superposition dark states to dephasing [120] could be used in dipole trap systems to measure experimental imperfections such as uncorrelated shaking in the trap positions and/or intensity fluctuations of the trapping lasers.

5.3.4   EIT process – Inhibiting tunneling

Finally, similar to EIT in optics, by driving the transition $|0\rangle_M \leftrightarrow |0\rangle_R$ via the tunneling interaction, the transition from $|0\rangle_L$ to $|0\rangle_M$ can be inhibited. Fig. 5.9 (a) and (b) show this inhibition in spite of the proximity between the left and the middle trap. The robustness of the transition cancellation is, similar to the STIRAP case, indicated through the large range of delay times t_{Delay} for which no population is transfered. This atom optics EIT technique can create conditional phase shifts for quantum logic.
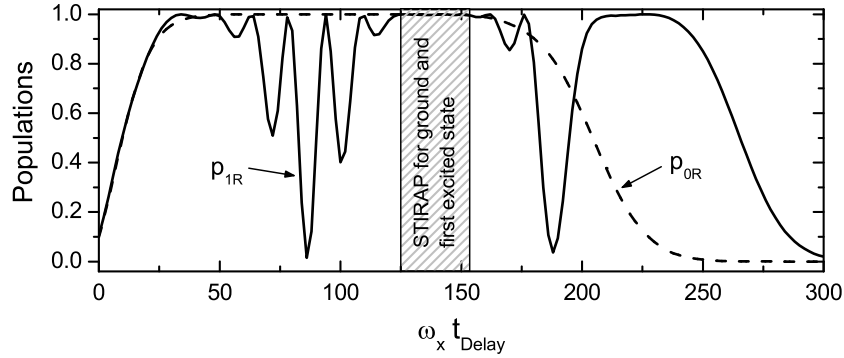
Figure 5.10.   *Three level atom optics for the first excited vibrational state: transfer efficiency for the STIRAP process as a function of the delay time $t_{\text{delay}}\omega_x$ (solid line), the other parameters are $t_r^{LM}\omega_x = t_r^{MR}\omega_x = 300$, $t_i^{LM}\omega_x = t_i^{MR}\omega_x = 0$. The dashed line shows the transfer efficiency for the same parameters but for the vibrational ground state. In the dashed region in both cases robust and efficient transfer is possible.*

5.4 Extensions and outlook

5.4.1 Excited vibrational states

It is worth noting the option to initially put the atom in an excited vibrational state. Usually, depending on the exact shape of the trapping potential, the evolution of the higher vibrational states is more complex, which on on hand offers the possibility to observe new effects which differ from the effects discussed before, but on the other hand renders the processes more complicated and might limit the robustness. Still, *e.g.*, the STIRAP effect can be observed in such a case, as it is shown in Fig. 5.10 for the transfer of an atom starting in the first exited vibrational state of the left trap, $|1\rangle_L$, to the first excited vibrational state of the right trap, $|1\rangle_R$. Obviously, the variation of the transfer efficiency as a function of the delay time t_{Delay} in this case is more complex than for the ground state, but there is a, though smaller, region where t_{Delay} can be varied without changing the eventual population of the right trap. Also, there exist parameters where the process is efficient for both, an atom starting in the ground state $|0\rangle_L$ and in the first excited state $|1\rangle_L$ (the dashed region in the figure). This means that inside this region even mixed states $\rho = p|0\rangle\langle 0| + (1-p)|1\rangle\langle 1|$ can be transported robustly, which relaxes the cooling requirements for the experimental setup.

On the other hand, exploiting the more complex variation of the dressed level structure of the first excited states, effects different from STIRAP, CPT, or EIT can be observed. In Fig. 5.11 it is demonstrated, that the atomic wavefunction can be coherently and equally split between the left and the middle trap, see the plateau around $t\omega_x = 180$. This effect requires a combination of adiabatic and diabatic processes . Finally, the variety of effects observed in TLAO can be increased significantly by including detunings between the vibrational levels of the traps. In the optics case, Fewell *et al.* [135] have extensively analyzed possible configurations of detunings and approaching sequences.
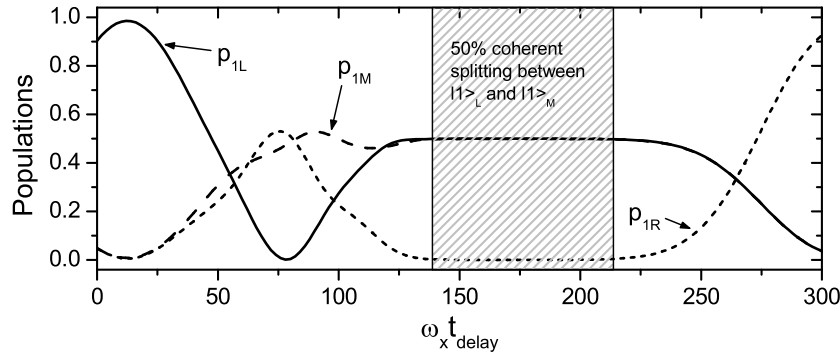
Figure 5.11. *Three level atom optics for the first excited vibrational state: final populations after the complete process as a function of the delay time $t_{delay}\omega_x$ for the parameters $t_r^{LM}\omega_x = 550, t_r^{MR}\omega_x = 400$, $t_i^{LM}\omega_x = 75, t_i^{MR}\omega_x = 400$. In both cases $d_{max}^{LM}\alpha = d_{max}^{MR}\alpha = 9$ and $d_{min}^{LM}\alpha = d_{min}^{MR}\alpha = 1.5$. In the dashed region the population is splitted coherently between $|1\rangle_L$ and $|1\rangle_R$.*

5.4.2 Robust population transfer in systems of n traps

When increasing the number of quantum states from two to three, new and interesting effects arose, such that increasing the number of states further seems promising. Indeed, in quantum optics a number of effects in n-level systems have been identified which, provided the possibility to control the couplings between trapped states with large enough freedom, can be applied also for the manipulation of external degrees of freedom using the mapping to trapped states as proposed here. One possible extension is to apply a STIRAP-like scheme for the robust transfer from the first to the n-th trap in a linear chain of traps. In the optics case, it has been shown that large transfer efficiency can be reached *via* the so-called *straddling scheme* [143], where the pump pulse (between the first and the second level) and the Stokes pulse (between the $n-1$-th and the n level) are applied in the same counter-intuitive order as for STIRAP, and all the intermediated transitions are driven for the whole time where pump and Stokes laser are active, with intensities larger by an order of magnitude. Greentree *et. al* [133] have studied such a scheme for an electron in an array of quantum dots.

To give another example for a possible application of a multi-level scheme, Unanyan *et al.* have developed methods for the creation of arbitrary superpositions in a system where three states are coupled via three lasers to a single fourth level [144]. In such a system, the existence of two degenerates dark states can be exploited to create arbitrary superpositions of states. Unanyan *et al.* also considered such a system as interesting for the measurement of geometric phases [145]. When transferring this four-level scheme to a system of four traps, it seems more demanding to control individually the three couplings, although this seems possible in microtraps generated holographically; the configuration has to be necessarily two-dimensional, which might lead to further interesting effects.

5.4.3 Effects for two atoms

It is another obvious extension to increase the number of atoms present in the traps and to exploit the interplay of tunneling and contact interaction. Mompart *et al.* have analyzed coherent population trapping for two electrons with aligned spins in a three-level system coupled via two laser pulses [146]. In this case, where the interaction is *via* the Coulomb interaction, a dark states exists which can be interpreted as the dark state of *the hole*. A possible application of the scheme is the measurement of some superposition-state matrix elements of the electron-electron correlation, that otherwise are not easily accessible. A similar system could be constructed in atom optics through two (indistinguishable) atoms in a system of three traps.

5.4.4 Three level atom optics in waveguides

The technique of creating trapping potentials through illuminating microlenses with a red-detuned laser beam also allows the generation of structures which confine atoms only in two spatial dimensions. The construction of atomic waveguides from cylindrical lenses has been demonstrated experimentally, as well as a beam splitter for matter waves traveling in such waveguides [27, 65]. In general, these technique allows the construction of complex waveguide geometries, *e.g.*, of curved structures. Atomic waveguides have also been constructed in systems of magnetic microtraps [147].

These structures could potentially be explored for three level atom optics to manipulate matter waves. For this aim, the time dependence of the trap distances has to be translated into a spatial dependence of the distances of three waveguides. Potential applications are the transfer of wavepackets between waveguides, the creation of superpositions which could be used for example for *Sagnac interferometry* (see Section 6.2.2), or the selection of only the population of the ground state (in the direction of confinement) of a matter wave traveling in a waveguide *via* the EIT effect [4].

5.5 Conclusion

In this chapter, three level atom optics techniques have been introduced as a set of robust and efficient techniques for the coherent manipulation of external degrees of freedom of trapped neutral atoms, especially for the transport between traps or for the creation of spatial superpositions. These methods are the natural analogues to largely investigated techniques of three level optics as STIRAP, CPT, and EIT used to manipulate electronic degrees of freedom of atoms or molecules in quantum optics. In the atom optics case, the interaction is mediated via tunneling and controlled by the shaping of the process of varying the separation between the traps. The fact that TLAO uses the tunneling interaction instead of a coupling through modes of an electro-magnetic field, distinguishes it from the quantum

---

[4]In the latter case, the EIT sequence has to be designed such that only the ground state population remains in the same waveguide, while the population of higher vibrational states is partially taken out of this waveguide. If this part is subsequently discarded, then the relative ground state population is increased.

optics case: the process takes place in the millisecond range, there are no dipole selection rules, and the use of excited states is possible.

As has been shown, the STIRAP-like process works without the need for a precise control of timing and distances, it tolerates relatively large shaking amplitudes, and it is even robust with respect to differences in the ground state energies of the traps. All these features make it an interesting method to move atoms among traps in order to create defect-free lattices, *e.g.*, to initialize a register of qubits for quantum computation, or to shuttle around qubits. The spatial analogue of the CPT technique also allows for inaccuracies in the parameters, but requires the separation process to be symmetric. However, under the influence of shaking with amplitudes of about 5% of the minimal trap distance, the dark state can still be populated with an efficiency of larger than 0.99, which is a reasonable value for applications like interferometry. This should be within reach of experiments since mechanical vibrations as the main source of shaking should mainly give rise to a correlated movement of all the traps.

The use of excited vibrational states and including systems with more than a single atom and exploiting either interaction between the them or their statistical properties gives rise to a large variety of additional effects, and also it can be envisaged to control the propagation of atoms in waveguides by similar techniques.

CHAPTER 6

DIFFERENTIAL ATOMIC INTERFEROMETRY BELOW THE STANDARD QUANTUM LIMIT

6.1 Overview

Among the many applications of interferometry, there is a subclass which requires the comparison of the result of two interferometers, *i.e.*, phase shifts are measured in two either identical or different interferometric setups, and the quantity of interest is encoded in the difference of these two phases. Possible applications of such *differential interferometers* are, for example, the comparison of two atomic clocks, measurements of the difference of gravitation at different points in space to test predictions of the violation of Einstein's general relativity [148, 149], or Sagnac interferometers [150, 151], *i.e.*, interferometric setups to measure angular velocities.

The description of particles through matter waves, introduced 1924 by de Broglie, suggests to replace photons by atoms for interferometric applications, as achievable wavelengths lie orders of magnitudes below the wavelength of visible light, promising thus higher resolution. Recently, many experiments based on cold neutral atoms have been performed [152], demonstrating the capability of these setups for high-resolution interferometry.

In atomic interference experiments where classical, *i.e.*, not quantum mechanically correlated ensembles are used as input states, the phase measured in the interferometer has a standard deviation due to quantum projection noise scaling as $\Delta\phi_{\text{SQL}} \sim 1/\sqrt{N}$ with the number of atoms N in the ensemble. This is the so-called *standard quantum limit* which can be surpassed by using non-classical states of the atoms. In this case the standard deviation can at most reach the *Heisenberg limit* $\Delta\phi_{\text{Heisenberg}} \sim 1/N$ [35, 153]. Various methods have been proposed to construct quantum states of atoms to reach this limit. It has been shown [154] that a GHZ-type state [155], which can be constructed by applying cNOT operations between pairs of atoms, allows to saturate the Heisenberg limit. For ensembles of many atoms, the use of spin squeezed states enables to improve the performance of interferometers [33, 35, 36]. Such spin squeezed states can be generated, e.g., by a quantum non-demolition (QND) measurement of the atoms *via* a light beam [156, 157], by absorbing a non-classical state of light in the atomic ensemble [158, 159], or by exploiting a non-linear interaction.

As has been shown [34], atoms in a squeezed atomic ensemble are microscopically entangled with each other. For two atomic ensembles, it is also possible to entangle macroscopic degrees of freedom, either by performing two QND measurements on two commuting, non-local observables [160, 161] or by absorbing two entangled (two-mode squeezed) light beams, one in each atomic ensemble [162].

In this chapter, we will analyze and compare the performance of differential atomic interferometers when the two ensembles passing the interferometer are either microscopically or macroscopically entangled initially. We will compare four cases: (i) classical states of both ensembles, *i.e.*, coherent input states, (ii) individually squeezed ensembles, (iii) squeezing *one* joint component of both ensembles, and (iv) squeezing *two commutating* joint components. In (i-iii) microscopic entanglement is present, *i.e.*, entanglement on the level of individual atoms [34], while in (iv) a macroscopic entangled state is produced.

To be more precise, here we will focus on a Sagnac interferometer with ^{87}Rb atoms [163] and use a QND interaction to perform the spin squeezing. Especially, fluctuations of the number of atoms will be taken into account in both the preparation and the measurement stage, and we will estimate limits on the difference of the number of atoms in the two ensembles, as well as on the detection efficiency in the fluorescence measurements necessary to obtain a scaling at the Heisenberg limit. As we will show, joint squeezing of the observables gives an improvement of the variance by a factor of two as compared to only squeezing the ensembles individually. Under realistic conditions, the performance of all the schemes including squeezing can be improved significantly by reading out the phase difference *via* another QND measurement.

6.1.1 Related work

Recently, Petersen *et al.* proposed [164] to exploit macroscopic entanglement between atomic ensembles for the estimation of several components of a magnetic field. They show that by a continuous measurement of two probe beams performing a QND measurement of two non-local components of the atomic spin, two components of an external magnetic field can simultaneously be measured at the Heisenberg limit.

6.2 Introduction: Mach-Zehnder type interferometers and the Sagnac effect

6.2.1 Mach-Zehnder interferometer for light

The standard example of a *Mach-Zehnder* light interferometer is constructed from two beamsplitters and two perfect mirrors, cf., Fig. 6.1. A light beam incident on the first beamsplitter BS_1 can take two different paths to reach the second beamsplitter BS_2, and the light intensity in both exits is finally measured via two detectors. If both paths are exactly equal, taking into account phase shifts from mirrors and beamsplitters, there is no phase-difference between the two paths for light reaching detector D_1, such that constructive interference occurs. There is a phase-shift of π, and thus destructive interference, for
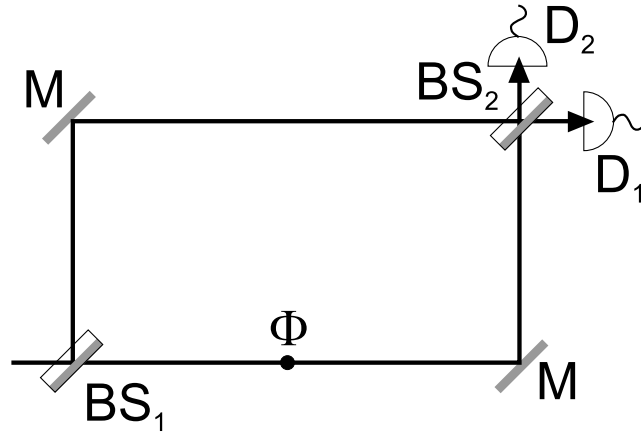
Figure 6.1.   *Illustration of a Mach-Zehnder interferometer consisting of two beamsplitters BS$_{1/2}$, two mirrors M and a detector in each of the two exit ports (D$_{1/2}$)*

light reaching detector D$_2$ [165]. Thus D$_2$ is dark while D$_1$ detects all the light incident onto the interferometer. Introducing an additional phase shift ϕ into one of the arms modulates the signal on detector D$_1$ as $I_1 = I_0 \cos(\phi)$.

6.2.2   The Sagnac effect

Such a Mach-Zehnder setup can, e.g., be used as a Sagnac interferometer, *i.e.*, for the measurement of rotations of the laboratory frame. To simplify the situation slightly, replace the two mirrors by a circular loop of radius R as in Fig. 6.2. If both partial waves travel the same distance in the interferometer, Fig. 6.2 (a), then no phase difference appears. If on the other hand the path-lengths differ for both beams due to a rotation of the laboratory frame as in Fig. 6.2 (b), then a phase difference appears which scales proportional to the differences between the paths. Neglecting corrections of higher relativistic order, the following expression can be derived for the phase difference obtained by a wave of energy E traveling in the two arms of the interferometer [166]:

$$\phi_{\mathrm{rot}} = \frac{\pi E}{hc^2} \boldsymbol{A}\, \boldsymbol{\Omega}. \tag{6.1}$$

Here $\boldsymbol{A} = A\boldsymbol{e}_A$, where A is the area and $\boldsymbol{e}_A$ is the normal vector of the plane enclosed by the arms of the interferometer. $\boldsymbol{\Omega}$ is the angular velocity. For light with wavelength λ, we have $E = hc/\lambda$ and thus

$$\phi_{\mathrm{rot}} = \frac{4\pi}{c\lambda} \boldsymbol{A}\, \boldsymbol{\Omega}. \tag{6.2}$$

To enhance the resolution of the interferometer, *i.e.*, to increase the phase ϕ_{rot} for constant angular velocity $\boldsymbol{\Omega}$, either the area of the interferometer can be made larger, which, e.g., can be done by letting the light revolve around the area many times, or the energy E can be increased. An increase by several orders of magnitude is possible if atoms are fed into the
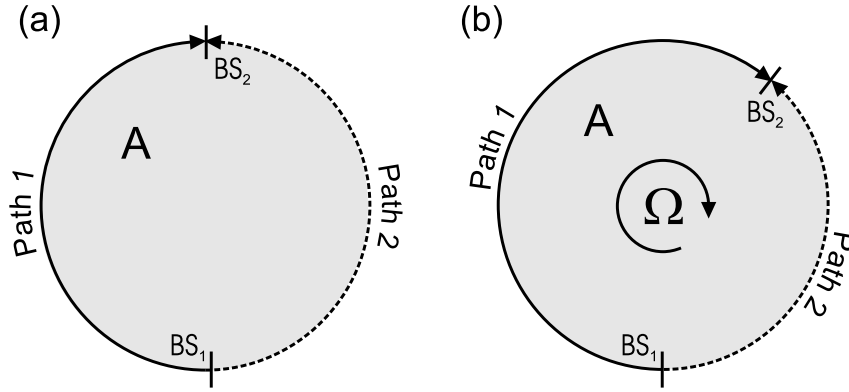
Figure 6.2.   *(a) A Mach Zehnder interferometer in a non-rotating laboratory frame. There is no phase difference between the two paths; (b) the interferometer for a rotating laboratory frame. The different path-lengths for the two waves traveling in opposite direction give rise to a phase difference phi$_{\mathrm{rot}}$ from which the rotational velocity Ω can be obtained.*

interferometer instead of photons, where in the case of slow atoms $E \approx m_{\mathrm{atom}} c^2$, with m_{atom} being the atomic mass. Then the Sagnac phase reads

$$\phi_{\mathrm{rot}} = \frac{4\pi \, m_{\mathrm{atom}}}{h} A \, \Omega. \tag{6.3}$$

For ^{87}Rb with $m_{\mathrm{atom}} = 1.44 \times 10^{-25}$ kg, and $\lambda = 1000$ nm, and for the same enclosed area A, the atom interferometer promises a much larger resolution[1]:

$$\frac{\phi_{\mathrm{rot}}^{\mathrm{atoms}}}{\phi_{\mathrm{rot}}^{\mathrm{light}}} = \frac{m\lambda c}{h} \approx 10^{11}. \tag{6.4}$$

6.2.3   Mach-Zehnder atom interferometer setup

To construct an interferometer for atoms, which we assume to effectively have two levels $|g\rangle$ and $|e\rangle$, beamsplitters and mirrors are replaced by classical laser pulses: two counter-propagating laser beams in a Raman configuration producing a $\pi/2$ pulse or a π pulse on the transition $|g\rangle \leftrightarrow |e\rangle$ are used to split or to deflect the atomic wave packet by the photon recoil momentum exchanged between the photon and the atom. After the second beamsplitter, the population of the two exit ports is detected by fluorescence measurements. The scheme of the Mach-Zehnder atom interferometer is illustrated in Fig. 6.3.

To be more precise, all the atoms enter the interferometer in state $|g, k = 0\rangle$, where k denotes the atomic momentum in the direction of the laser beams. The first $\pi/2$ pulse creates a superposition $(|g, k = 0\rangle + |e, k = 2k_r\rangle)/\sqrt{2}$ of the two internal atomic states. Because the Raman laser beams are counter-propagating, two photon recoil momenta k_r are transfered

---

[1]It has, however, to be taken into account that with light interferometers much larger areas A can be achieved, such that the advantage of using atoms in an interferometer is reduced by some orders of magnitude.
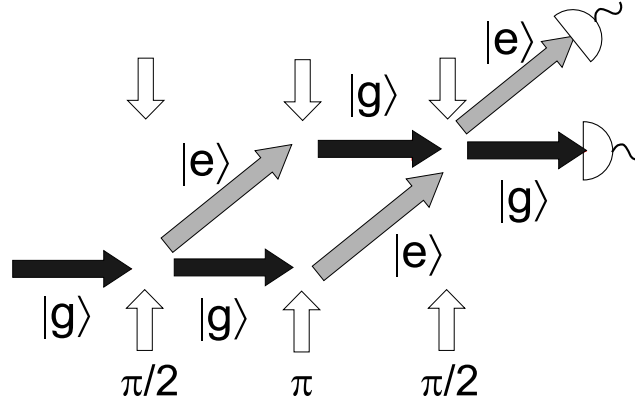
Figure 6.3. *Scheme for the Mach-Zehnder interferometer for atoms. The green arrows represent the pairs of counter-propagating lasers implementing mirrors and beamsplitters. π and $\pi/2$ denote a π pulse or a $\pi/2$ pulse, respectively, on the transition $|g\rangle \leftrightarrow |e\rangle$*

to the atoms in state $|e\rangle$, such that the atomic wave packet is splitted into two parts. This produces a relatively large enclosed area, which is important for a large phase shift, cf., Eq. (6.3). The subsequent π pulse exchanges $|g, k = 0\rangle \leftrightarrow |e, k = 2k_r\rangle$, thus deflecting both partial beams. The final $\pi/2$ pulse closes the interferometer and transforms $|g, k = 0\rangle \to (|g, k = 0\rangle + |e, k = 2k_r\rangle)/\sqrt{2}$ and $|e, k = 0\rangle \to (|e, k = 2k_r\rangle + |g, k = 0\rangle)/\sqrt{2}$. After this last pulse, the two exits can be distinguished by the internal state of the atoms, and thus the populations in both ports can be detected by fluorescence.

The atomic ensemble in the interferometer can be described most conveniently in terms of a *collective spin operator*

$$\boldsymbol{J} = \sum_{i=1}^{N_J} \boldsymbol{\sigma}^i, \tag{6.5}$$

where the sum runs over all the N_J atoms in the ensemble and the $\boldsymbol{\sigma}^i$ are the spin-$\frac{1}{2}$ operators for the two atomic levels $|g\rangle$ and $|e\rangle$ of the i-th atom, defined as

$$\boldsymbol{\sigma}^i = (\sigma_x^i, \sigma_y^i, \sigma_z^i), \qquad \text{with} \qquad \sigma_z^i = \frac{1}{2}[|g\rangle_i\langle g| - |e\rangle_i\langle e|], \tag{6.6}$$

$$\sigma_x^i = \frac{1}{2}[|g\rangle_i\langle e| + |e\rangle_i\langle g|], \qquad \text{and} \qquad \sigma_y^i = \frac{1}{2i}[|g\rangle_i\langle e| - |e\rangle_i\langle g|]. \tag{6.7}$$

Within this representation, a measurement of the difference of populations of the two atomic levels corresponds to measuring J_z, and the initial preparation of $|g\rangle^{\otimes N_J}$ corresponds to the preparation of an eigenstate of J_z with the following expectation value and variance of the collective spin vector:

$$\langle \boldsymbol{J} \rangle = \frac{N_J}{2}\hat{z}, \qquad \left((\Delta J_x)^2, (\Delta J_y)^2, (\Delta J_z)^2\right) = \left(\frac{N_J}{4}, \frac{N_J}{4}, 0\right). \tag{6.8}$$

To illustrate the operations performed in the interferometer, we will represent the spin by a vector in three-dimensional space with a disk on its end illustrating the non-zero variances in the orthogonal directions. The initial state is illustrated in Fig. 6.4.
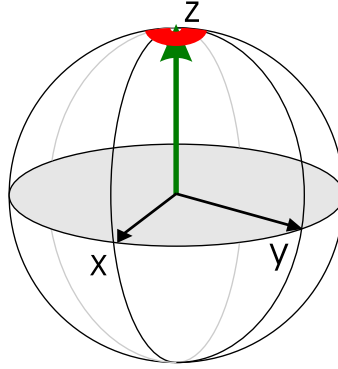
Figure 6.4.   *The representation of spin **J** of the atomic ensemble before the interferometer. All the atoms are prepared in |g⟩, such that the spin is polarized in z direction. The disc on the tip of the vector represents the uncertainties in the x and y directions.*

To simplify the analysis and at the same time to make it applicable to more general interferometric setups, we model the interferometer as follows[2]:

➤ *First Beamsplitter* — The first pair of lasers rotate the collective spin vector by an angle $\pi/2$ around the y axis, such that it is an eigenvector of J_x. This state, which has expectation value

$$\langle \boldsymbol{J}^{\text{in}} \rangle = \frac{N_J}{2}\hat{\boldsymbol{x}} \qquad (6.9)$$

and variance

$$\left((\Delta J_x^{\text{in}})^2, (\Delta J_y^{\text{in}})^2, (\Delta J_z^{\text{in}})^2 \right) = \left(0, \frac{N_J}{4}, \frac{N_J}{4} \right) \qquad (6.10)$$

will subsequently be used as the initial state.

➤ *Interferometric phase* — The interferometer itself, including the pair of lasers producing the π pulse, is described by rotating the spin vector around the z axis by an angle Φ_J. The corresponding matrix describing the evolution of the vector of spin operators (we will use the Heisenberg picture throughout our analysis) reads

$$\mathcal{R}_z(\Phi_J) = \begin{pmatrix} \cos(\Phi_J) & \sin(\Phi_J) & 0 \\ -\sin(\Phi_J) & \cos(\Phi_J) & 0 \\ 0 & 0 & 1 \end{pmatrix}. \qquad (6.11)$$

---
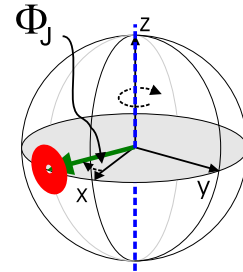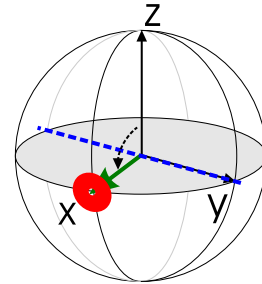
[2]For a more detailed analysis of how the operations in the case of the interferometer from Fig. 6.3 are translated into rotations of the collective spin in the case of the interferometer see, e.g., [152, 163].

➤ *Second beamsplitter* — The final beamsplitter which closes the interferometer is modeled through a rotation around the x axis by an angle $-\pi/2$. The corresponding rotation matrix reads

$$\mathcal{R}_x\left(-\frac{\pi}{2}\right) = \begin{pmatrix} 1 & 0 & 0 \\ 0 & 0 & -1 \\ 0 & 1 & 0 \end{pmatrix}, \qquad (6.12)$$

such that after this operation the angle Φ_J is encoded in the z direction where it is directly accessible by measuring the populations of levels $|g\rangle$ and $|e\rangle$.
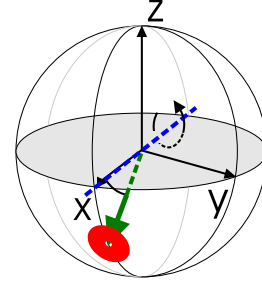
The total interferometer is thus described by $\mathcal{R}_x(-\pi/2)\mathcal{R}_z(\Phi_J)$ and the final state $\boldsymbol{J}_{\mathrm{out}}$ can be calculated as

$$\boldsymbol{J}^{\mathrm{out}} = \mathcal{R}_x(-\pi/2)\mathcal{R}_z(\Phi_J)\boldsymbol{J}^{\mathrm{in}} = \begin{pmatrix} J_x \cos\Phi_J + J_y \sin\Phi_J \\ -J_z \\ J_y \cos\Phi_J - J_x \sin\Phi_J \end{pmatrix}, \qquad (6.13)$$

where notation has been simplified by writing $J_i \equiv J_i^{\mathrm{in}}$. For $\boldsymbol{J}_{\mathrm{in}}$ from Eq. (6.9) we have that

$$\langle J_z^{\mathrm{out}}\rangle = -\frac{N_J}{2}\sin\Phi_J. \qquad (6.14)$$

The final rotation has been performed around the x axis, rather than around the y-axis again, in order to make the interferometer maximally sensitive for small angles Φ_J: for $\Phi_J \ll 1$ it holds $-\frac{N_J}{2}\sin\Phi_J \approx -\frac{N_J}{2}\Phi_J$.

6.3 Coherent ensembles

Such a setup can thus directly be used to measure the phase Φ_J. However, Φ_J does normally not only contain a contribution ϕ_{rot} from the rotation, but also contributions θ_{rest} from other sources, e.g., there is an additional phase shift if the setup is accelerated in the direction of the laser beams[3]. Thus in general $\Phi_J = \phi_{\mathrm{rot}} + \theta_{\mathrm{rest}}$. To extract only the Sagnac phase ϕ_{rot}, a second atomic ensemble, whose spin vector will be denoted by $\boldsymbol{L}$, is sent through the interferometer in the opposite direction, see Fig. 6.5. Reversing the direction of propagation amounts to change $\boldsymbol{A}$ to $-\boldsymbol{A}$ in Eq. (6.3), such that $\phi_{\mathrm{rot}} \rightarrow -\phi_{\mathrm{rot}}$. On the other hand, phase shifts from acceleration etc. remain unchanged, such that $\Phi_L = -\phi_{\mathrm{rot}} + \theta_{\mathrm{rest}}$ and by subtracting the total phases the Sagnac phase shift can be extracted: $\Phi_J - \Phi_L = 2\phi_{\mathrm{rot}}$. We will assume that the two atomic ensembles do not interact while propagating through the interferometer, which is justified through the low atomic density of the two ensembles [167].

Assuming the initial (internal) states of the ensembles to be identical, and letting

$$\boldsymbol{L}^{\mathrm{out}} = \mathcal{R}_x(-\pi/2)\mathcal{R}_z(\Phi_L)\boldsymbol{L}^{\mathrm{in}}, \qquad (6.15)$$

---

[3]There is obviously no additional phase shift if the interferometer is just moving with constant linear velocity v, as the Sagnac phase ϕ_{rot} is a relativistically invariant quantity.
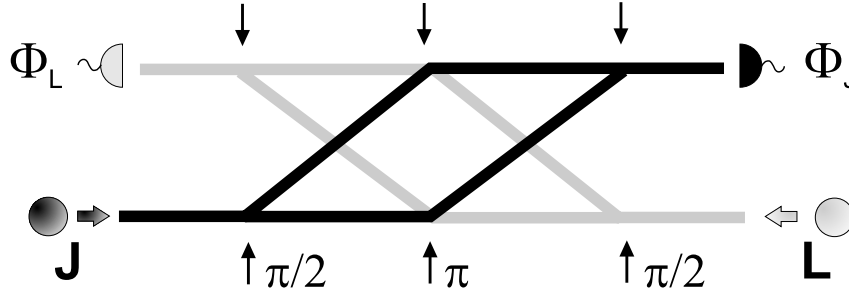
Figure 6.5.   *Scheme of the setup for Sagnac interferometry. Two atomic ensembles, labeled **L** and **J**, enter the interferometer from the opposite sites and are manipulated by the same three pairs of lasers. Finally, phases Φ_J and Φ_L are detected by fluorescence measurements.*

an operator related to the Sagnac phase can directly be defined as

$$\hat{\phi}_{\rm rot} = -\frac{J_z^{\rm out}}{N_J} + \frac{L_z^{\rm out}}{N_L}. \tag{6.16}$$

Evaluating expectation value and variance of $\hat{\phi}_{\rm rot}$ using Eq. (6.9) and the analogous expression for $\boldsymbol{L}^{\rm in}$, we obtain

$$\langle \hat{\phi}_{\rm rot} \rangle = \phi_{\rm rot}, \tag{6.17}$$

$$\left(\Delta \hat{\phi}_{\rm rot} \right)^2 = \frac{1}{4N_J} + \frac{1}{4N_L}. \tag{6.18}$$

The declining of the variance $\Delta \hat{\phi}_{\rm rot}$ proportional to N_J^{-1} corresponds to to the so-called *standard quantum limit*. We will always assume $\phi_{\rm rot}$, $\theta_{\rm rest} \ll 1$, such that higher order terms with respect to the angles can be ignored. However, corrections to the result for $\langle \hat{\phi}_{\rm rot} \rangle$ are only of fifth order in $\phi_{\rm rot}$, $\theta_{\rm rest}$.

6.3.1   Number fluctuations

Let us consider further errors which can lead to an increase of the variance given in Eq. (6.17). Such errors can take place before, during, and after the interferometer step itself. We will now discuss the former and the latter cases, leaving the errors from decoherence and so on to a later discussion in Section 6.6.

The state after the source of the atomic ensembles is best described by a density operator, this is to say, by a mixture of states with different atom numbers. Here we will assume that the number measurements after the interferometer do project both ensembles onto number states with a fixed atom number N_J and N_L, respectively. To describe the source we introduce a parameter γ, which describes the typical difference between the number of atom in the two ensembles: $|N_J - N_L| = \gamma \sqrt{\bar{N}}$, where $\bar{N} = (N_J + N_L)/2$ is the mean number of atoms of both ensembles. To leading order γ does not appear in Eq. (6.17), because $N_J \neq N_L$ has

been taken into account already in the definition of $\hat{\phi}_{\text{rot}}$, and the variance is simply dominated by the ensemble with the smaller number of atoms. It will however become important later in Section 6.5 when non-local (joint) observables are considered.

To take into account noise in the measurement process, for both exits of the interferometer we replace the numbers of atoms in ensembles J and L as follows:

$$N_{X,i} \rightarrow N_{X,i} + \delta N_{X,i}, \qquad X \in \{J, L\}, \ i \in \{g, e\}, \tag{6.19}$$

where now $N_{X,i}$ is the number of atoms that would have been measured with perfect detectors. The new operators $\delta N_{X,i}$ have zero mean but non-vanishing variance:

$$\langle \delta N_{X,i} \rangle = 0, \qquad [\Delta(\delta N_{x,i})]^2 = \alpha N_{X,i}. \tag{6.20}$$

These new number operators lead to

$$J_z^{\text{out}} \rightarrow J_z^{\text{out}} + \frac{\delta N_{J,e} - \delta N_{J,g}}{2} \quad \text{and} \quad N_J \rightarrow N_J + \delta N_{J,e} + \delta N_{J,g}, \tag{6.21}$$

and to similar equations for the second ensemble L. Substituting this into Eq. (6.16) we obtain the leading corrections from imperfect measurements to the expectation value and the variance as[4]

$$\langle \hat{\phi}_{\text{rot}} \rangle = \phi_{\text{rot}} - \alpha \left(\frac{1}{N_J} + \frac{1}{N_L} \right) \tag{6.22}$$

$$(\Delta \hat{\phi}_{\text{rot}})^2 = \frac{1}{4N_J} + \frac{1}{4N_L} + \alpha \left(\frac{1}{N_J} + \frac{1}{N_L} \right) \approx \frac{1}{2\bar{N}} + \frac{2\alpha}{\bar{N}}. \tag{6.23}$$

The shift in the expectation value itself is of second order compared to the leading terms in the standard deviation $\Delta \hat{\phi}_{\text{rot}}$, and can thus be neglected. The importance of the second term in the variance is depending on the order of magnitude of α. The number of atoms in the two exit ports is usually detected by fluorescence measurements sensitive to the internal atomic state. In this case α^{-1} is determined by the number of photons which are scattered on average by one atom and subsequently also registered in the detector. Usually $\alpha \ll 1$ can be expected [168], such that $1/2\bar{N}$ is still the leading term in the variance.

6.4 Individually squeezed ensembles

The standard quantum limit to the resolution of the phase shift in the interferometer stems from the non-vanishing uncertainty of the spins along the direction of rotation of the atomic spin in the interferometer, *i.e.*, along the equator of the Bloch sphere. A standard method in interferometry to surpass this limit is to reduce the uncertainty in the direction of rotation, such that the sensitivity is increased. If the number of atoms N_J in the ensemble J is large and the spin is, as above, polarized into the x direction, then in the commutation relation

---

[4]In the expectation values N_J and N_L always refer to the perfect quantities as defined above on the right hand side of mapping Eq. (6.19).
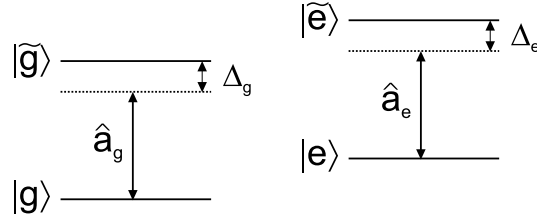
Figure 6.6.   *Level scheme for the QND interaction. The two modes used for the interferometer, |g⟩ and |e⟩, are coupled off-resonantly to two auxiliary levels via two electromagnetic field modes a_g and a_e, respectively.*

$[J_y, J_z] = iJ_x$, the macroscopic J_x can be replaced by its expectation value: $[J_y, J_z] = iN_J/2$. The Heisenberg uncertainty relation which follows from this commutator,

$$\Delta J_y \, \Delta J_z \geq \frac{N_J}{4}, \tag{6.24}$$

is already minimized by the coherent state from Eq. (6.9), such that reducing, say, ΔJ_y below $\sqrt{N_J}/2$ implies to increase ΔJ_z above this value. Such a state, which minimizes the Heisenberg uncertainty relation and has $\Delta J_y < \Delta J_z$ (or vice versa) is called a *spin squeezed state* [33, 36]. Microscopically, such a state state corresponds to an entangled state of individual spins [34]. There has been strong interest into spin squeezed states not only for precision measurements [33, 35, 36], but also for quantum information [160–162].

Basically three different approaches to create spin squeezed states of atoms have been proposed and, in the case of (i) and (iii), also realized experimentally: (i) quantum-state transfer from squeezed light to atoms [158, 159, 162], (ii) the use of systems which exhibit an interaction among the spins, such as Bose-Einstein-Condensates [169] or cold atoms in an optical lattice [170], or (iii) quantum non-demolition (QND) measurements of a spin component *via* Faraday rotation and quantum projective measurements of coherent states of light [156]. Recently also the generation of a non-linear interaction using a coherent light beam has been proposed [171], a proposal which is similar to the QND scheme, but does not need a final projective measurement of the light.

Here we will use the QND interaction approach (iii), and especially we will use the methods presented in [156] to show how the resolution of the measurement of the Sagnac phase can be improved with squeezed states. While in this section we will analyze the straightforward approach of squeezing both ensembles separately, we will subsequently also consider squeezing of joint (*i.e.*, non-local) observables and eventually also address macroscopically entangled ensembles in the interferometer.

6.4.1   Stokes vector description of light and QND interaction

Following [156] assume that two electromagnetic field modes a_g and a_e couple states $|g⟩$ and $|e⟩$ off-resonantly to two states states $|\widetilde{g}⟩$ and $|\widetilde{e}⟩$, cf., Fig. 6.6. These modes might, e.g., be two polarization modes or two modes with different frequency. Using creation and

annihilation operators $\hat{a}^\dagger_{g,e}$ and $\hat{a}_{g,e}$, a light pulse of duration T can be described, analogously to the case of atoms, by a spin vector $\boldsymbol{S} = (S_x, S_y, S_z)$ through

$$S_x = \frac{1}{2} \int_0^T dt \left(\hat{a}^\dagger_g \hat{a}_e + \hat{a}^\dagger_e \hat{a}_g \right), \tag{6.25}$$

$$S_y = \frac{1}{2i} \int_0^T dt \left(\hat{a}^\dagger_g \hat{a}_e - \hat{a}^\dagger_e \hat{a}_g \right), \tag{6.26}$$

$$S_z = \frac{1}{2} \int_0^T dt \left(\hat{a}^\dagger_g \hat{a}_g - \hat{a}^\dagger_e \hat{a}_e \right). \tag{6.27}$$

This defines the so called *Stokes vector* for light. S_z measures the difference of the number of photons in each mode.

For a certain choice of the parameters (as detuning, atomic and photonic density; see the comments in Section 6.6. For a more detailed analysis see [156, 172]), the Hamiltonian describing the interaction between the light and the atoms of the ensemble $\boldsymbol{J}$ can be written as

$$H_{\mathrm{QND}} = \hbar \Omega\, S_z J_z, \tag{6.28}$$

and similarly for $\boldsymbol{L}$. The constant Ω is determined by the parameters of the interaction. H_{QND} induces a rotation of the Stokes vector around the z axis and if $\hat{a}_{e,g}$ represent two field modes with $\sigma_\pm$ circular polarizations, then it corresponds to a rotation of the plane of polarization, an effect known as *paramagnetic Faraday rotation* [172]. Also the atomic spin is rotated around the z axis due to an AC Stark shift from the light field [173].

In more detail, interaction between the light and the atomic ensemble for a time t changes the Stokes and the atomic spin vector in the Heisenberg picture according to

$$\boldsymbol{S} \rightarrow \boldsymbol{S}' = \mathcal{R}(-\chi J_z)\boldsymbol{S} = \begin{pmatrix} \cos(\chi J_z)S_x - \sin(\chi J_z)S_y \\ \sin(\chi J_z)S_x + \cos(\chi J_z)S_y \\ S_z \end{pmatrix} \tag{6.29}$$

and

$$\boldsymbol{J} \rightarrow \boldsymbol{J}' = \mathcal{R}(-\chi S_z)\boldsymbol{J} = \begin{pmatrix} \cos(\chi S_z)J_x - \sin(\chi S_z)J_y \\ \sin(\chi S_z)J_x + \cos(\chi S_z)J_y \\ J_z \end{pmatrix}, \tag{6.30}$$

respectively. To simplify notation, the abbreviation $\Omega t =: \chi$ has been used. If the Stokes vector $\boldsymbol{S}$ is initially polarized in x direction, *i.e.*,

$$\langle \boldsymbol{S}^{\mathrm{in}} \rangle = \frac{n}{2}\hat{\boldsymbol{x}}, \tag{6.31}$$

with $n \gg 1$ the number of photons, then in Eq. (6.29) it is appropriate to replace S_x by its macroscopic expectation value. For the y component we obtain

$$S'_y = \sin(\chi J_z)\frac{n}{2} + \cos(\chi J_z)S_y \approx \frac{n\chi}{2}J_z + S_y. \tag{6.32}$$

In the second step $N_J\chi^2 \ll 1$ has been assumed. Eq. (6.32) shows that measuring S'_y reveals information about the z component of the atomic spin vector, with some added noise given by S_y. It has been shown, e.g., by an analysis in terms of gaussian states [174], that the process of projecting the S_y component induces a squeezing of the atomic spin in z direction. To include the knowledge about J_z into the calculation, we finally replace $J_z^{\text{out}} \rightarrow J_z^{\text{out}} - \frac{2}{n\chi}S'_y$ [156], because $\boldsymbol{J}'$ is fed into the interferometer, but only the difference $J_z^{\text{out}} - J'_z$ is of interest to the phase measurement.

6.4.2   Sagnac interferometer with squeezed states

To exploit the possibility of squeezing, the QND measurement step is included into the interferometer directly after the first beamsplitter, followed by an additional $\pi/2$ pulse around the x axis. This is necessary because large sensitivity, *i.e.*, small uncertainty, is needed in the direction of rotation of the spin in the interferometer, *i.e.*, in the equatorial plane of the Bloch sphere. The classical laser pulse for this rotation must not transfer momentum to the atoms, which can be achieved by shining in both Raman lasers from the same side. All the steps used in the interferometric sequence are shown in Fig. 6.7. The transformation of $\boldsymbol{J}^{\text{in}}$ now includes the QND interaction and the additional rotation:

$$\boldsymbol{J}^{\text{out}} = \mathcal{R}_x\left(-\frac{\pi}{2}\right)\mathcal{R}_z(\Phi_J)\mathcal{R}_x\left(\frac{\pi}{2}\right)\mathcal{R}_z(-\chi_J S_z)\boldsymbol{J}^{\text{in}}. \tag{6.33}$$

$\boldsymbol{L}^{\text{in}}$ transforms similarly, and we will denote by $\boldsymbol{T}$ the corresponding stokes vector. To correctly adjust the definition of $\hat{\phi}_{\text{rot}}$ from Eq. (6.16), now the results from the measurements of S'_y and T'_y have to be included, leading to[5]

$$\hat{\phi}_{\text{rot}} = -\frac{1}{N_J}\left(J_z^{\text{out}} - \frac{2}{n\chi}S'_y\right) + \frac{1}{N_L}\left(L_z^{\text{out}} - \frac{2}{n\chi}T'_y\right). \tag{6.34}$$

From this, mean and variance of $\hat{\phi}_{\text{rot}}$ can be evaluated. Again including the imperfections of the final measurements of the atomic population, we find

$$\langle\hat{\phi}_{\text{rot}}\rangle = \phi_{\text{rot}} - \alpha\left(\frac{1}{N_J} + \frac{1}{N_L}\right) \approx \phi_{\text{rot}} - \frac{2\alpha}{\bar{N}} \tag{6.35}$$

as before. However, the scaling of the variance now reflects the improved resolution through squeezing:

$$(\Delta\hat{\phi}_{\text{rot}})^2 = \frac{1}{n\chi^2}\left(\frac{1}{N_J^2} + \frac{1}{N_L^2}\right) + \alpha\left(\frac{1}{N_J} + \frac{1}{N_L}\right) \approx \frac{2}{n\chi^2\bar{N}^2} + \frac{2\alpha}{\bar{N}}. \tag{6.36}$$

The first term, scaling as the inverse of *the square of the number of atoms* surpasses the N^{-1} scaling in the case of coherent ensembles. An $\bar{N}^{-1}$ scaling corresponds to the so-called

---

[5]We assume that the parameters describing the two light ensembles itself and the interaction are equal for both interactions, e.g., $n_J = n_L$ and $\chi_J = \chi_L$. As long as the deviations from this equality are small compared to the absolute values, especially as long as $\frac{|\chi_J - \chi_L|}{\chi_J + \chi_L} \ll 1$, corrections in the variance are only to higher order.
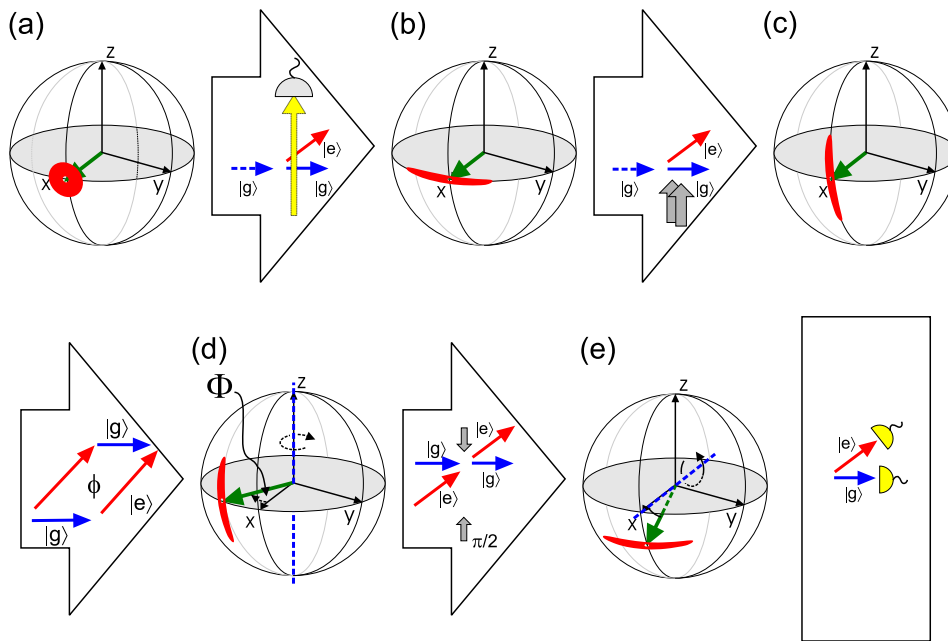
Figure 6.7. *Evolution of the atomic spin vector of a single ensemble for the interferometric scheme including squeezing of the input state. (a) The atomic spin and the Stokes vector are prepared as in Eq. (6.9) and Eq. (6.31), respectively. After projecting the quantum state of the light, (b), a classical laser pulse rotates the atomic spin by $\pi/2$ around the x axis, (c). (d) The interferometric phase Φ is included as a rotation around z. (e) The final beamsplitter pulse performs another rotation around x, such that the phase shift can be obtained via fluorescence measurements.*

Heisenberg limit[6], here however it comes with a factor $1/(n\chi^2) \gg 1$. Thus the Heisenberg limit is not attained, but rather we have a Heisenberg-like scaling. Each $1/(n\chi^2 \bar{N}^2)$-term stems from the quantum projection noise of the measurement on one light ensemble. The second term in $(\Delta\hat{\phi}_{\text{rot}})^2$, proportional to parameter α describing the atomic measurements, retains the scaling $\propto 1/\bar{N}$. This shows, that the resolution can only be improved beyond the standard quantum limit if the number measurements can be performed well enough. In Section 6.6, the constraints on α given by Eq. (6.36) will be evaluated.

Eq. (6.36) is valid only under certain other assumptions. $N\chi^2 \ll 1$ has already been mentioned before, and provided that also

$$n\chi^2 \ll \sqrt{8}\left[\sqrt{\bar{N}}\left(\theta_{\text{rest}}^2 + \phi_{\text{rot}}^2\right)\right]^{-1} \tag{6.37}$$

holds, the Eq. (6.36) gives indeed the terms of leading order in the variance.

6.4.3 QND readout

As an alternative to directly measuring the number of atoms in the exit ports and calculating $\langle J_z \rangle$ and $\langle L_z \rangle$ as their difference, a second QND measurement could be used. Nevertheless, also in this case a measurement of the number of atoms is still necessary, because QND measurements do not reveal the populations of $|g\rangle$ and $|e\rangle$, itself but only their difference. N_J and N_L are however needed to rescale J_z and L_z properly, see Eq. (6.34).

For the QND readout of J_z another ensemble of light is prepared, labeled $\widetilde{S}$ which interacts with the atomic ensemble J after the last beamsplitter and before the final fluorescence detection. From measuring $\widetilde{S}'_y$, the value of $\langle J_z^{\text{out}} \rangle$ can be inferred, and labeling the corresponding Stokes vector for the ensemble L by $\widetilde{T}$, the operator for the phase ϕ_{rot} is defined as

$$\hat{\phi}_{\text{rot}} = -\frac{1}{N_J}\frac{2}{n\chi}\left(\widetilde{S}'_y - S'_y\right) + \frac{1}{N_L}\frac{2}{n\chi}\left(\widetilde{T}'_y - T'_y\right). \tag{6.38}$$

---

[6]The uncertainty $(\Delta\Phi_J)^2$ of the measurement of a rotation in the equatorial plane cannot be improved beyond a scaling N_J^{-1}. This follows from the Heisenberg uncertainty relation

$$\Delta J_y \Delta J_z \geq \frac{1}{2}|\langle[J_y, J_z]\rangle| = \frac{1}{2}|\langle J_x \rangle|$$

for the atomic spin operators by constructing an operator for the phase as $\hat{\Phi}_J = J_y/|\langle J_x \rangle|$ for small $\langle \Phi_J \rangle$. Then $\Delta\Phi_J \Delta J_z \geq \frac{1}{2}$. The uncertainty of J_z itself is limited as J_z itself is bounded: $-N_J/2 \leq J_z \leq N_J/2$. From $\langle J^2 \rangle = \langle J_x^2 \rangle + \langle J_y^2 \rangle + \langle J_z^2 \rangle \leq \frac{N_J}{2}\left(\frac{N_J}{2} + 1\right)$ it follows

$$\Delta J_z \leq \sqrt{\frac{N_J}{2}\left(\frac{N_J}{2} + 1\right) - \langle J_x^2 \rangle - \langle J_y^2 \rangle - \langle J_z \rangle^2} \leq \sqrt{\frac{N_J}{2}\left(\frac{N_J}{2} + 1\right)},$$

and thus approximately $\Delta J_z \leq N_J/2$ for N_J large. From inserting this into the uncertainty relation follows the Heisenberg limit $\Delta\Phi_J \geq N_J^{-1}$.

Then

$$\langle\hat{\phi}_{\text{rot}}\rangle = \phi_{\text{rot}} - \alpha\theta_{\text{rest}}\left(\frac{2}{N_J} + \frac{1}{N_L}\right) \tag{6.39}$$

$$(\Delta\hat{\phi}_{\text{rot}})^2 = \frac{1}{n\chi^2}\left(\frac{1}{N_J^2} + \frac{1}{N_L^2}\right) + \alpha\left(\theta_{\text{rest}}^2 + \phi_{\text{rot}}^2\right)\left(\frac{1}{N_J} + \frac{1}{N_L}\right) \tag{6.40}$$

$$\approx \frac{4}{n\chi^2\bar{N}^2} + \frac{2\alpha}{\bar{N}}\left(\theta_{\text{rest}}^2 + \phi_{\text{rot}}^2\right). \tag{6.41}$$

Thus, the demand on α is less stringent than before, because in the variance the additional factor $\left(\theta_{\text{rest}}^2 + \phi_{\text{rot}}^2\right)$ appears which we assume to be small as we are operating close to the point of maximal resolution where $\theta_{\text{rest}}, \phi_{\text{rot}} \ll 1$.

Another benefit of reading out the result via a QND measurement is that it couples to the atomic ensemble in the same way as the QND measurement for squeezing. Potential asymmetries in the light-atom interaction are thus canceled [175].

On the other hand the contribution from the first term now has a factor of 2 compared to Eq. (6.36). As each contribution of $1/(n\chi^2\bar{N})$ to the total variance is originating from the quantum projection noise from one measurement of a light ensemble, in principle the factor of 2 could be canceled by *not* measuring the light used for squeezing the atomic ensemble, but storing it during the interferometer phase and reusing it for the final QND readout. Then only two projective measurements are necessary (for S and T) instead of four. In this case for the interactions after the last beamsplitter $\chi \rightarrow -\chi$ is necessary in order to get the minus signs in Eq. (6.38). This can be achieved by an additional rotation of the atomic spins by π around the x axis before the last QND measurement. However, such a procedure might be extremely difficult to implement.

6.5 Squeezing a non-local observable

The considerations in the previous section make it obvious that the $1/(n\chi^2\bar{N}^2)$ term in the variance comes with a factor given by the number of QND interactions with *different* ensembles of light. For this reason let us now consider the case where the initial state of the two atomic ensembles is prepared with only a single QND pulse, which consecutively interacts with both atomic ensembles. The first interaction with ensemble J transforms $J^{\text{in}} \rightarrow \mathcal{R}_z(-\chi S_z)J^{\text{in}}$, the second interaction (between S and L) transforms $L^{\text{in}} \rightarrow \mathcal{R}_z(-\chi S_z)L^{\text{in}}$, as S_z remains unchanged during the first QND interaction. S itself transforms as $S^{\text{out}} = \mathcal{R}_z(-\chi L_z)\mathcal{R}_z(-\chi J_z)S^{\text{in}}$, and especially the y component reads

$$S_y^{\text{out}} = \cos(\chi L_z)\left[\cos(\chi J_z)S_y + \sin(\chi J_z)S_x\right] + \sin(\chi L_z)\left[\cos(\chi J_z)S_x - \sin(J_z\chi)S_y\right], \tag{6.42}$$

such that for $N\chi^2 \ll 1$ and S initially prepared as in Eq. (6.31) we have

$$S_y^{\text{out}} \approx \frac{n\chi}{2}(J_z + L_z) + S_y. \tag{6.43}$$

Measuring S_y^{out} thus reveals information about $\langle J_z + L_z \rangle$ and performs a squeezing operation on this joint operator. We now apply the same operations as before to the ensemble J, but

for the ensemble L perform a rotation by π around the x axis before the final measurement, such the Sagnac shift ϕ_{rot} is effectively encoded into the sum of the z components instead of the difference.

Then the operator which extracts ϕ_{rot} can be defined as

$$\hat{\phi}_{\text{rot}} = \frac{1}{N_J} J_z^{\text{out}} + \frac{1}{N_L} L_z^{\text{out}} - \frac{2}{n\chi\bar{N}} S_y^{\text{out}}. \tag{6.44}$$

Note that the operator $2S_y^{\text{out}}/(n\chi\bar{N})$ which we subtract now is *not* exactly the estimation of $J_z^{\text{out}}/N_J + L_z^{\text{out}}/N_L$, as the former does not contain the weights $N_{J/L}^{-1}$. As a consequence, we expect to loose the advantages of squeezing if the numbers of atoms in the two ensembles differ a lot, i.e., if $\gamma \gg 1$, because in this case the operator which is squeezed initially and the operator which is measured finally deviate strongly from each other. We could also choose to finally measure the uncorrected operator $(J_z + L_z)/\bar{N}$, in this case the expectation value $\langle\hat{\phi}_{\text{rot}}\rangle$ would to first order contain a contribution from θ, while in the case of defining $\hat{\phi}_{\text{rot}}$ as in Eq. (6.44) the expectation value remains unchanged:

$$\langle\hat{\phi}_{\text{rot}}\rangle = \phi_{\text{rot}} - \frac{2\alpha}{\bar{N}}. \tag{6.45}$$

The variance becomes

$$(\Delta\hat{\phi}_{\text{rot}})^2 = \frac{2}{n\chi^2\bar{N}^2} + \frac{2\alpha}{\bar{N}} + \frac{\gamma^2}{8\bar{N}^2}, \tag{6.46}$$

where next to the assumptions leading to Eq. (6.36) also

$$\gamma\sqrt{\bar{N}}(n\chi^2)^2(\theta_{\text{rest}}^2 + \phi_{\text{rot}}^2) \ll 1 \tag{6.47}$$

is necessary. The third term, proportional to γ^2, stems from the mismatch between the squeezed and the measured operator and makes obvious the importance of the preparation process, because now $1/(n\chi^2\bar{N})$ is the leading term only if $n\chi^2\gamma^2/8 \ll 1$. As we will see later, for typical parameters this corresponds to $|N_J - N_L| \ll \bar{N}$.

Also in this case a QND measurement could be used after the interferometer to directly read out the joint observable $J_z^{\text{out}} + L_z^{\text{out}}$ by defining

$$\hat{\phi}_{\text{rot}} = \frac{2}{n\chi}\frac{1}{\bar{N}}\left(S_y' - \widetilde{S}_y'\right), \tag{6.48}$$

where again $\widetilde{S}$ labels the Stokes vector used for read-out. Notice that in this way, by using only one QND measurement for the read-out, it is not possible to measure the correctly rescaled observable $J_z^{\text{out}}/N_J + L_z^{\text{out}}/N_L$, and consequently now there is a contribution from the difference of the atom numbers already in the expectation value:

$$\langle\hat{\phi}_{\text{rot}}\rangle = \phi_{\text{rot}} + \frac{\gamma}{\sqrt{\bar{N}}}\frac{\theta}{2} + \frac{\alpha\,\phi}{2\bar{N}}. \tag{6.49}$$

We will discuss in the next paragraph how this contribution can be compensated. The variance improves as before, *i.e.*, $\alpha \to \alpha(\theta_{\text{rest}}^2 + \phi_{\text{rot}}^2)$, and also the leading term in γ improves:

$$(\Delta\hat{\phi}_{\text{rot}})^2 = \frac{2}{n\chi^2\bar{N}^2} + \frac{2\alpha}{\bar{N}}(\theta_{\text{rest}}^2 + \phi_{\text{rot}}^2) + \frac{\gamma^2}{8\bar{N}^2}\alpha(\theta_{\text{rest}}^2 + \phi_{\text{rot}}^2). \tag{6.50}$$

However, to neglect the correction in γ to the expectation value in comparison to the leading term in $(\Delta\phi_{\text{rot}})^2$, now $\gamma^2 \bar{N} n \chi^2 \theta^2 / 8 \ll 1$ is necessary, which in general is a stronger criterion then the limit on γ encountered without the QND readout.

The extra θ_{rest}-dependent term in the expectation value can be compensated by using an estimate for θ_{rest} from the final fluorescence measurement,

$$\hat{\theta}_{\text{rest}} = -\frac{1}{N_J} J_z^{\text{out}} + \frac{1}{N_L} L_z^{\text{out}}, \qquad (6.51)$$

to define a corrected operator for ϕ_{rot}:

$$\hat{\phi}_{\text{rot}}^{\text{Corr}} = \left(\hat{\phi}_{\text{rot}} - \frac{\gamma}{2\sqrt{\bar{N}}} \hat{\theta}_{\text{rest}} \right). \qquad (6.52)$$

This operator takes into account the bias of $\langle \hat{\phi}_{\text{rot}} \rangle$. Such a measurement of θ_{rest} is obviously *not* beyond the quantum limit, as the corresponding operator is not squeezed. Still, for the measurement of $\hat{\phi}_{\text{rot}}^{\text{Corr}}$, the variance has the same leading term, but the γ dependent bias in the expectation value is reduced by a factor $\alpha\gamma/(\bar{N}^{3/2}\theta) \ll 1$:

$$\langle \hat{\phi}_{\text{rot}}^{\text{Corr}} \rangle = \phi_{\text{rot}} + \frac{\alpha\phi_{\text{rot}}}{2\bar{N}} - \frac{\gamma^2\alpha}{2\bar{N}^2} \qquad (6.53)$$

$$\left(\Delta\hat{\phi}_{\text{rot}}^{\text{Corr}} \right)^2 = \frac{2}{n\chi^2\bar{N}^2} + \frac{\alpha\phi_{\text{rot}}^2}{2\bar{N}} + \frac{\gamma^2}{8\bar{N}^2}. \qquad (6.54)$$

Hence the $1/\bar{N}$ term in the variances still has the factor $\alpha\phi_{\text{rot}}^2$. Thus the requirements are comparable to the ones found in the case of separately squeezed ensembles with QND readout, cf. Eq. (6.36), but the variance $(\Delta\hat{\phi}_{\text{Corr}})^2$ is reduced by a factor of 2 in the leading $1/\bar{N}^2$-term, as only two light-atom interactions are necessary here as compared to four in the case of separately squeezed ensembles. The term $\gamma^2/(8\bar{N}^2)$ in Eq. (6.54) however is worse by a factor of $[\alpha(\theta_{\text{rest}}^2 + \phi_{\text{rot}}^2)]^{-1} \gg 1$ then the corresponding term in $(\Delta\hat{\phi}_{\text{rot}})^2$, Eq. (6.50). Its origin is the $1/\bar{N}$ dependence of $(\Delta\hat{\theta}_{\text{rest}})^2$.

6.6 Comparison

We will now analyze the performance of the different schemes discussed up to now by computing and plotting the variances for sets of parameters relevant for experiments. Let us fix the number of photons as $n = 10^{10}$, and the constant χ parameterizing the QND interaction as[7] $\chi = 2 \times 10^{-8}$. A reasonable parameter for the mean atom number per ensemble is $\bar{N} = 10^8$, and we will show how $(\Delta\phi_{\text{rot}})^2$ scales with $\bar{N}$ around this variance. In order to take into account the dependence of the variance on the angles θ_{rest} and ϕ_{rot}, $\theta_{\text{rest}} = \phi_{\text{rot}} = 0.01$ will be fixed in order to operate close to the point of maximal sensitivity of the interferometer.

---

[7]Following the calculation given in [156] the parameters atom number $N = 10^8$, detuning $D = 10\gamma_L$ with the natural linewidth γ_L, cross section of the QND laser beam $A = 0.3$ mm^2 and interaction length $L = 1$ mm give $\chi = 2 \times 10^{-8}$ for the considered ^{87}Rb D$_2$ line [176].
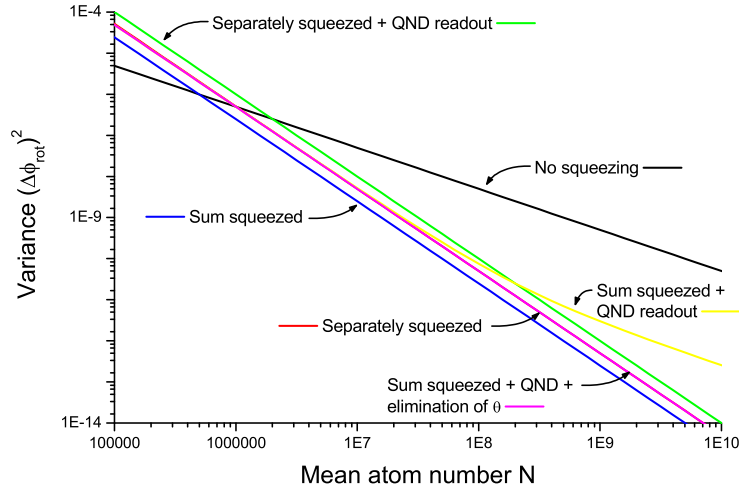
Figure 6.8. *Double-logarithmic plot of the variances $(\Delta\hat{\phi}_{rot})^2$ for (i) no squeezing (black curve), (ii) separate squeezing (red), (iii) separate squeezing and QND readout (green), (iv) squeezing $J_z + L_z$ (blue), (v) squeezing $J_z + L_z$ and performing a QND readout (yellow), and (vi) as (v) but after eliminating the θ_{rest} dependence in $\langle\phi_{rot}\rangle$ (magenta) as a function of $\bar{N}$ for the following set of ideal parameters: $n = 10^{10}$, $\chi = 2 \times 10^{-7}$, $\theta_{rest} = \phi_{rot} = 0.01$, $\alpha = 10^{-7}$ and $\gamma = 10$. The graphs for (ii) and (vi) lie on top of each other.*

To consider an 'ideal' case where noise from the fluorescence measurement can be neglected and where the number difference between the two atomic ensembles can be controlled very well, first assume $\alpha = 10^{-7}$ and $\gamma = 10$. The latter for $\bar{N} = 10^8$ atoms corresponds to $|N_J - N_L|/\bar{N} = 10^{-3}$. As Fig. 6.8 shows, the scaling is identical for all the methods involving squeezing of some observable up to $\bar{N} = 10^8$. The offsets of these curves are given by the numbers of QND measurements involved, *i.e.*, by the factor multiplying the $1/(n\chi^2\bar{N}^2)$ term in the variance. For the measurement of ϕ_{rot} *via* reading out $J_z + L_z$ through a QND interaction, in the graphs the term $\theta_{rest}\gamma/(2\sqrt{\bar{N}})$ shifting the expectation value has been included into the variance, in order to allow for a fair comparison. It is this term which makes the variance scaling only proportional to $1/\bar{N}$ for $\bar{N} \gtrsim 10^9$. Correcting this contribution of θ_{rest} as in Section IV avoids this term, while maintaining the improvement by a factor of 2 compared to the case of squeezing and QND measuring both ensembles separately.

In Fig. 6.9, the variances are plotted for more realistic values of the parameters α and γ. α has been increased to a value of 10^{-2} [168], corresponding to a mean number of $\alpha^{-1} = 100$ fluorescence cycles per atom. γ is set to a value of 100, corresponding to a difference of the number of atoms in the two ensembles of $\sim 1\%$ of the mean number $\bar{N}$ (at $\bar{N} = 10^8$), which is still demanding but should be achievable experimentally [168]. The change of α does influence all the procedures which do not involve a QND read-out. Especially for $\bar{N} \gtrsim 10^8$, the methods of squeezing the individual ensembles or squeezing a joint component deviate

strongly from the $1/\bar{N}^2$ scaling. Furthermore they show the same performance, because the leading term then is proportional to $\alpha/\bar{N}$, with the same pre-factor in both cases. Notice that for $\bar{N} = 10^8$ the variance in these two cases is still around two orders of magnitudes better than in the case without any squeezing. On the other hand, both methods involving a QND readout scale as $1/\bar{N}^2$ up to $\bar{N} = 10^{10}$, with again a factor of two between them. If the sum is squeezed and finally read out *via* a QND measurement without correcting for θ_{rest}, then, as expected, the resolution of the measurement is very poor. Finally, in Fig. 6.10, γ has been increase to $\gamma = 1000$, corresponding to a difference in the number of atoms of 10% at $\bar{N} = 10^8$. Except for the QND measurement of the sum without correction for θ_{rest} in the expectation value, the variances are not affected significantly.

Thus for these sets of experimentally reasonable parameters, both methods involving the preparation of a squeezed state of the atomic ensembles and the read-out via fluorescence measurements improve the performance of the interferometer beyond the limit set by quantum projection noise. As an advantage, the method of squeezing a joint observable of both ensembles only needs a single squeezing operation instead of two, and thus less technical effort.

Performing QND readout measurements further improves the performance, without requiring further experimental setup as compared to the scheme where QND measurements are performed on the incoming atomic ensembles. Squeezing a joint observable gives an advantage of a factor of 2 compared to individual squeezing and read-out. In both cases the QND readout has the additional advantage of canceling non-symmetric contributions in the interaction between light and atoms [175].

The resolution of the interferometer is further limited by decoherence effects during the process of squeezing and the time of free flying of the ensembles in the interferometer. Absorption of photons and related atomic decay rates during the interaction between light and atoms limit the the attainable squeezing. For the case of a continuous squeezing for magnetometry, decoherence has been studied in detail by Madsen *et al.* [174] through a gaussian formalism to describe the atomic and the light ensembles. They identified a dependence of the maximal attainable squeezing depending on the light – atom coupling and on the absorption and decay rates. For Cs atoms, but with parameters similar to the ones used here, they showed that a squeezing parameter $\Delta J_y/J \approx 5 \times 10^{-8}$ can be attained. This corresponds approximately to the degree of squeezing reached here, as for $(\Delta\phi_J)^2 \approx 4 \times 10^{-12}$ we have $\Delta J_y/J = 2N_J\Delta\phi_J/N_J \approx 10^{-6}$.

On the other hand, the decay of the states $|g\rangle$ and $|e\rangle$ has to be taken into account during the interferometer step. Choosing long-lived hyperfine ground-state levels to implement $|g\rangle$ and $|e\rangle$ minimizes this decay. Also, spin squeezed states have been shown to be robust with respect to both, particle loss and dephasing [177], in contrast to, e.g., GHZ states, which are maximally fragile under particle loss. We will leave an in-depth analysis of decoherence in this step to further investigations.

6.7   Macroscopically entangled ensembles

Julsgaard *et al.* demonstrated experimentally in [161] the generation of macroscopic entanglement between two distant atomic ensembles. The scheme, described first in [160], to
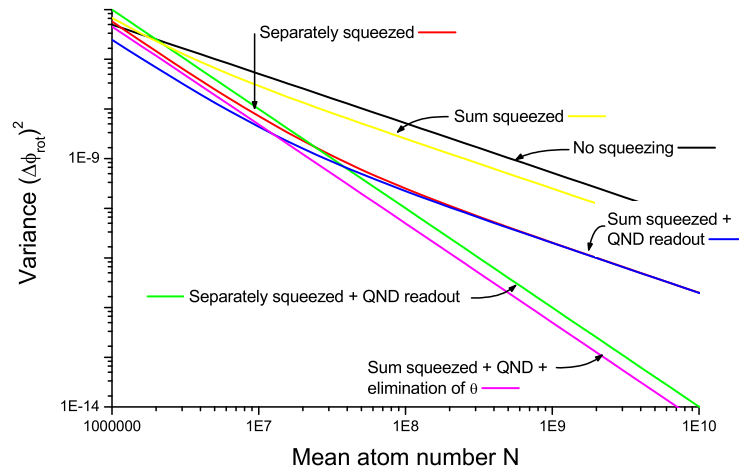
Figure 6.9.   *The variances $(\Delta\phi_{rot})^2$ for the different schemes as a function of $\bar{N}$ for realistic values of the parameters: $\gamma = 100$ and $\alpha = 10^{-2}$; all the other parameters are as in Fig. 6.8. Only two schemes retain the $\bar{N}^{-2}$ scaling for large atom numbers: separately squeezed ensembles with QND readout and jointly squeezed ensembles with QND readout and corrected expectation value.*
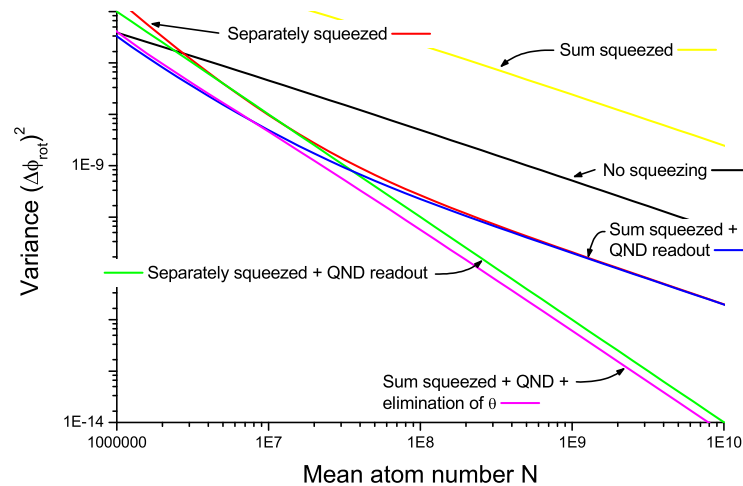

Figure 6.10.   *The variances $(\Delta\phi_{rot})^2$ as a function of $\bar{N}$ for $\gamma = 1000$ and all the other parameters as in Fig. 6.8. Compared to $\gamma = 100$, Fig. 6.9, the variances are nearly unchanged. In the case of squeezing the sum, reading it out via QND measurement, and correcting for θ_{rest}, the offset of the curve is slightly worse, though the scaling remains unchanged.*

generate such a macroscopically entangled state is motivated by the fact that under the ideal condition of $\gamma = 0$ two commuting joint observables can be constructed from $\boldsymbol{J}$ and $\boldsymbol{L}$:

$$\langle [J_y - L_y, J_z + L_z] \rangle \propto (N_J - N_L) = 0, \tag{6.55}$$

i.e., $J_y - L_y$ can be measured without affecting $J_z + L_z$, and vice versa. This can be seen directly from

$$(\mathcal{R}_z(-\chi S_z) \boldsymbol{J}^{\text{in}} - \mathcal{R}_z(-\chi S_z) \boldsymbol{L}^{\text{in}})_y = J_y^{\text{in}} - L_y^{\text{in}}, \tag{6.56}$$

i.e., the first QND interaction leaves the difference of the y components unaffected. Thus after squeezing the sum $J_z + L_z$, also the difference $J_y - L_y$ can be squeezed, without loosing the information gained in the first measurement. To realize this experimentally in the interferometer, after the first squeezing interaction $\boldsymbol{J}$ is rotated by a classical $\pi/2$ pulse around the x axis so that $J_y \to J_z$ while $\boldsymbol{L}$ is rotated by $-\pi/2$ around x giving $-L_y \to L_z$. Then a second laser pulse, again polarized in x direction, interacts consecutively with both ensembles and thus finally carries information about $J_y - L_y$. The outgoing state corresponds to a macroscopically entangled EPR state [160].

In order to make use of both squeezed components and to encode both angles, θ and ϕ, in some way, before and after the interferometer the ensemble vectors $\boldsymbol{J}$ and $\boldsymbol{L}$ are rotated by an angle φ and $-\varphi$, respectively, around the x axis. In this way the plane of rotation of the phase shift is effectively tilted by φ around the x axis. The measurement process now consists of first rotating $\boldsymbol{J}$ and $\boldsymbol{L}$ by $\pm\pi$ and using another QND interaction to measure the sum of the z components. This measurement, scaled correctly by a φ dependent factor, reveals ϕ. To be more explicit, the operator for ϕ_{rot} reads

$$\hat{\phi}_{\text{rot}} = \frac{1}{\cos\varphi} \frac{2}{\bar{N}n\chi^2} \left(S'_y - \widetilde{S}'_y \right). \tag{6.57}$$

We find

$$\langle \hat{\phi}_{\text{rot}} \rangle = \hat{\phi}_{\text{rot}} + \frac{\gamma}{\sqrt{\bar{N}}} \frac{\theta_{\text{rest}}}{2} + \frac{\alpha\,\phi_{\text{rot}}}{2\bar{N}} \tag{6.58}$$

$$(\Delta\hat{\phi}_{\text{rot}})^2 = \frac{1}{\cos^2\varphi} \frac{2}{\bar{N}^2 n\chi^2} + \frac{\alpha\,\theta_{\text{rest}}^2}{2\bar{N}} + \frac{\gamma^2\alpha(\theta_{\text{rest}}^2 - \phi_{\text{rot}}^2)}{8n\bar{N}} + \frac{\gamma^2\,n\chi^2}{8\bar{N}}. \tag{6.59}$$

A measurement of the sum of the y components can be realized after another rotation around x by either a QND or a projection measurement, *i.e.*, we define either

$$\hat{\theta}_{\text{rest}}^{\text{QND}} = \frac{1}{\sin\varphi} \frac{2}{\bar{N}n\chi^2} \left(T'_y - \widetilde{T}'_y \right), \tag{6.60}$$

or

$$\hat{\theta}_{\text{rest}}^{\text{P}} = -\frac{1}{\sin(\varphi)} \left(\frac{1}{N_J} J_y^{\text{out}} - \frac{1}{N_L} L_y^{\text{out}} - \frac{2}{\bar{N}n\chi} T_y \right). \tag{6.61}$$

In the former case, we have

$$\langle \hat{\theta}_{\text{rest}} \rangle = \theta_{\text{rest}} + \frac{\gamma}{\sqrt{\bar{N}}} \frac{\phi_{\text{rot}}}{2} + \frac{\alpha\,\theta_{\text{rest}}}{2\bar{N}} \tag{6.62}$$

$$(\Delta\hat{\theta}_{\text{rest}})^2 = \frac{1}{\sin^2\varphi} \frac{2}{\bar{N}^2 n\chi^2} + \frac{\alpha\,\theta_{\text{rest}}^2}{2\bar{N}} + \frac{\gamma^2\alpha(\theta_{\text{rest}}^2 - \phi_{\text{rot}}^2)}{8n\bar{N}} + \frac{\gamma^2\,n\chi^2}{8\bar{N}}. \tag{6.63}$$

In principle, starting from here the γ-term in the expectation value $\langle\hat{\phi}_{\text{rot}}\rangle$ could again be corrected by combining $\hat{\phi}_{\text{rot}}$ and $\hat{\theta}_{\text{rest}}$, but the last terms in Eqns. (6.59) and (6.63) already point to a difficulty: inferring both angles from macroscopically entangled ensembles is only possible if the difference in the number of atoms can be controlled very well, namely if $\gamma^2/N \ll 1$, because otherwise the term $\propto n\chi^2$ in the variances destroys the advantage obtained from squeezing. Taking into account that $\langle[J_y - L_y, Jz + L_z]\rangle \propto N_J - N_L$, this is a reasonable result, as for large number difference the two non-local operators do not commute, such that squeezing both components independently is not possible.

6.8   Conclusion

It was the aim of this chapter to present and compare several methods to improve the detection of a differential phase shift of two atomic interferometers beyond the standard quantum limit, having in mind especially the application to Sagnac interferometry. For this purpose, we have analyzed the squeezing of individual and joint observables and, in both cases, the read-out of the interferometer via fluorescence detection of the atoms only or by an additional QND interaction. All the methods of squeezing reduce the variance for the differential phase to a $1/\bar{N}^2$ scaling modified by a factor $k/(n\chi^2) \gg 1$, which is determined by the number k of QND interactions involved, by the number of photons n and the parameter χ describing the interaction between atoms and photons. Reaching the Heisenberg limit $1/\bar{N}^2$ is however impossible since $k/(n\chi^2) \gg 1$. In the case of jointly squeezed observables, where k takes the smallest possible value, we found that a Heisenberg-like scaling can only be attained if some constraints on the difference of the number of atoms in both ensembles can be fulfilled. Using fluorescence measurements to read out the atomic spins after the interferometer always produces additional noise scaling as $1/\bar{N}$ due to the photon shot noise.

As an alternative method, a QND measurement can be used to read out the final state of the interferometer, although fluorescence measurements are still necessary to determine the number of atoms in the two ensembles. However, the contribution of the noise introduced by the latter measurements can be reduced to a large extent in this case. As shown, the method with the lowest attainable variance is to perform squeezing and readout via a QND measurement of a joint observable of the two ensembles, provided that the difference between the number of atoms in the two ensembles can be made smaller than approximately $1\% - 10\%$ of the mean number of atoms. Then, this procedure minimizes the number of QND interactions necessary and thus minimizes the factor coming with the $1/\bar{N}^2$ term in the variance. The reduction of the number of squeezing operations furthermore reduces the experimental effort.

Finally we considered the creation of a macroscopically entangled state of the two atomic ensembles *via* squeezing of two non-local, commuting observables. In this case the improvement of the interferometric resolution is limited by the control over the difference of the numbers of atoms in the two atomic ensembles.

Appendix A

Quantum correlations in systems of indistinguishable particles

A.1 Overview

When talking about quantum entanglement of composite systems, it is usually assumed that the various parties are individually accessible and thus especially distinguishable. If each party is represented by a single particle, a spatial separation of the systems by a distance much larger than the size of the wavefunction allows to ignore the indistinguishable nature of the particles for all practical purposes [4]. For this reason, normally the indistinguishability of particles of the same species (*e.g.*, electrons, atoms, photons, . . .) is *not* taken into account.

The situation changes if the particles are brought into close proximity, as it happens for example for two atoms during a gate operation or for two photons overlapping on a beam splitter. As in this case the wavefunctions might significantly overlap, it is impossible to keep track of individual particles, and their inherent indistinguishable nature has to be taken into account. This is the case for the $\sqrt{\textsc{swap}}$ operation for motional state qubits as discussed in Chapter 2. In this chapter we will give an overview over how to characterize *quantum correlations*[1] in such a situation.

Different approches to this problem have been studied in [79–83, 85]. Also, the characteristics of states of indistinguishable particles have been used to manipulate entanglement between distant partices [178] as well as for quantum information tasks as entanglement concentration [179] and quantum state discrimination [180]. Some of the approaches have been reviewed and analyzed by Gittings *et al.* [84]. The objective of this appendix is to give a generalized framework for the study of quantum correlations of indistinguishable particles, and to present and compare different existing measures within this framework.

In Section A.2, after giving a quick overview over the notation which is used in this chapter, a general framework will be introduced to connect properties of states of particles which are indistinguishable and shared between the full single particle space to properties in a space

---

[1] We will use this expression to distinguish this situation from the usual setting of two distinguishable parties where usually the term entanglement is used.

divided between two distant parties. Based on this framework, we will discuss useful properties of measures of quantum correlations in Section A.3 before reviewing and comparing several measures, see Section A.3.3.

A.2   States of distinguishable and indistinguishable particles

A.2.1   Distinguishable particles

In what follows we will mostly concentrate on two particles, system of more particles have, been analyzed in [79, 83, 85]. For two spatially separated particles (or any two subsystems distinguishable in some other way; *e.g.*, a system of proton and a neutron), the total Hilbert space has a tensor product structure $\mathcal{H} = \mathcal{H}_A \otimes \mathcal{H}_C$, where $\mathcal{H}_{A,C}$ are the Hilbert spaces of the two parties A and C, which have dimension K_A and K_C, respectively. If $\{|a_i\rangle, \, i = 1, \ldots, K_A\}$ and $\{|c_i\rangle, \, i = 1 \ldots, K_C\}$ form a basis of $\mathcal{H}_A$ and $\mathcal{H}_C$, respectively, then a basis of the full Hilbert space is given by the product basis

$$\left\{ |a_i, c_j\rangle, \, i = 1 \ldots K_A, \, j = 1 \ldots K_C \right\}. \tag{A.1}$$

A.2.2   Indistinguishable particles: notation

For indistinguishable particles let us take the most general setting of K single particle states. For the moment we will not introduce a partition of these states between two or more parties.

For the case of N fermions sharing this K-dimensional space the Hilbert space is given by the totally antisymmetric subspace of $\mathcal{H}_K^{\otimes N}$, denoted as $\mathcal{A}\left\{\mathcal{H}_K^{\otimes N}\right\}$. A basis of this space is spanned by the vectors

$$|[i_1, \ldots, i_N]\rangle = \frac{1}{\sqrt{N!}} \sum_P (-1)^{|P|} \otimes_{j=1}^N |i_{P(j)}\rangle, \tag{A.2}$$

where P runs through all the permutations of $\{1, \ldots, N\}$ and $|P| = 0$ for an even and $|P| = 1$ for an odd permutation. $[i_1, \ldots, i_N]$ denotes the ordered subset of $\{1, \ldots, K\}$ with N elements [79]. Most of the times it is easier to use *Fock space* notation [4], *i.e.*, we introduce the vacuum state as $|\Omega\rangle$ together with fermionic creation operators $f_i^\dagger$, $i \in \{1, \ldots, K\}$, such that $f_i^\dagger|\Omega\rangle = |i\rangle$. If $f_i^\dagger$ and its adjoint f_i fulfill fermionic anti-commutation relations,

$$\left\{f_i, f_j\right\} = 0, \qquad \left\{f_i^\dagger, f_j^\dagger\right\} = 0, \qquad \left\{f_i, f_j^\dagger\right\} = \delta_{ij}, \tag{A.3}$$

then

$$|[i_1, \ldots, i_N]\rangle = f_{i_1}^\dagger \ldots f_{i_N}^\dagger |\Omega\rangle. \tag{A.4}$$

We will usually identify a general pure state with a totally antisymmetric[2] N-dimensional complex tensor w, by writing

$$|w\rangle = \sum_{i_1, i_2, \ldots, i_N} w_{i_1 i_2 \ldots i_N} f_{i_1}^\dagger f_{i_2}^\dagger \ldots f_{i_N}^\dagger |\Omega\rangle. \tag{A.5}$$

---

[2]This is a redundant assumption as antisymmetry is already implied in the definition of the operators f_i. It however will simplify notation later.

The normalization condition for w reads

$$\sum_{i_1,\dots,i_N=1}^{K} w^*_{i_1\dots i_N} w_{i_1\dots i_N} = \frac{1}{N!}. \tag{A.6}$$

Transformation of the single particle space, *i.e.*, transformations of the annihilation operators

$$f_i \mapsto f'_i = \sum_{j=1}^{K} U_{ij} f_j, \qquad , \forall\, i \in \{1,\dots,K\}, \tag{A.7}$$

where U is a unitary matrix, induce the following transformation on the tensor w:

$$w \mapsto \left(w'_{j_1\dots j_N}\right) = \left(\sum_{i_1\dots i_N=1}^{K} w_{i_1\dots i_N} U_{j_1 i_1} \dots U_{j_N i_N}\right). \tag{A.8}$$

For N bosons in a K-dimensional single particle-space, the Hilbert space is given by the totally symmetric subspace of $\mathcal{H}_K^{\otimes N}$, $\mathcal{S}\{\mathcal{H}_K^{\otimes N}\}$. A basis of this space is spanned by

$$|\{i_1,\dots,i_N\}\rangle = b^\dagger_{i_1} \dots b^\dagger_{i_N}|\Omega\rangle, \qquad i_j \in \{1,\dots,K\} \tag{A.9}$$

where in the set $\{i_1,\dots,i_N\}$ elements may appear more than once. The bosonic creation operators $b^\dagger_i$ and their adjoints fulfill

$$\left[b_i, b_j\right] = 0, \qquad \left[b^\dagger_i, b^\dagger_j\right] = 0, \qquad \left[b_i, b^\dagger_j\right] = \delta_{ij}, \tag{A.10}$$

and a general state can be written as

$$|v\rangle = \sum_{i_1,i_2,\dots,i_N} v_{i_1 i_2\dots i_N} b^\dagger_{i_1} b^\dagger_{i_2} \dots b^\dagger_{i_N}|\Omega\rangle, \tag{A.11}$$

where v now is a totally symmetric tensor. Normalization of v and the transformation of v are the same as in the case of fermions.

A.2.3 Indistinguishable particles shared between distant sites

To set the frame for the further discussion let us replace the situation of two distinguishable particles by a slightly more general setting. Assume two parties A and C separated by a large distance, each owning a set of single particle states (*modes*) described by sets of creation operators

$$C_A = \left\{a^\dagger_i,\, i = 1,\dots,K_A\right\} \quad \text{and} \quad C_C = \left\{c^\dagger_i,\, i = 1,\dots,K_C\right\}, \tag{A.12}$$

respectively. To simplify the situation let us assume that operators within C_A and C_B, respectively, all fullfil bosonic or fermionic commutation relations (although this could be generalized). We will subsequently refer to this setting as the *target space*, meaning that quantum information protocols (as, *e.g.*, distillation, teleportation) are usually described in such a setting of distant parties. If we also limit ourselves to a fixed total number of particles N, then the target Hilbert space has the form

$$\mathcal{H}_T^N = \bigoplus_{n=0,N} \left[\mathcal{S}\left(\mathcal{H}_A^n\right) \otimes \mathcal{S}\left(\mathcal{H}_C^{N-n}\right)\right], \tag{A.13}$$

where $\mathcal{H}_A$ and $\mathcal{H}_C$ are spanned by the single-particle states created from operators from C_A and C_C, respectively, and $\mathcal{S}$ is an appropriate (anti-)symmetrization operation.

On the other hand for many operations (*e.g.*, for the creation of entanglement where an interaction of the particles is indispensable), the two systems have to be brought into close contact, *i.e.*, systems A and C are combined for a certain time. We will describe this combination by a single particle process mapping operators from C_A and C_C to a combined system $C_F = \left\{ f_i^\dagger, i = 1, \ldots, K_A + K_C \right\}$ with (fermionic or bosonic) creation operators $f_i^\dagger$, *i.e.*, we assume *all* particles (of the same type) in C_F to be indistinguishable. We will call the space of combined systems the *operational space*. As we assume a single particle process to map to the operational space, the number of particles is unchanged and we have

$$\mathcal{H}_O^N = \mathcal{S}\left(\mathcal{H}_F^N\right). \tag{A.14}$$

Without loss of generality we assume the mapping to be of the form

$$\mathcal{M}_{T \to O} \; : \quad \begin{cases} \mathcal{H}_T^N & \to & \mathcal{H}_O^N \\ a_i^\dagger & \to & f_i^\dagger & \forall\, i \in \{1, \ldots, K_A\} \\ c_i^\dagger & \to & f_{i+K_A}^\dagger & \forall\, i \in \{1, \ldots, K_B\}. \end{cases} \tag{A.15}$$

Finally we want to go back from the operational space to the target space. For this we again assume a single particle process described by mapping operators from C_{AC} to operators in C_A and C_C. The mapping can be different from the one used initially and in general can have the form[3]

$$\mathcal{M}_{O \to T} \; : \quad \begin{cases} \mathcal{H}_O^N & \to & \mathcal{H}_T^N \\ \left(f_i^\dagger\right) & \to & \left((a_i')^\dagger, (c_j')^\dagger\right) = M\left(f_i^\dagger\right) \end{cases} \;, \tag{A.16}$$

where M is a unitary matrix, $MM^\dagger = \mathbb{1}$. In what follows we want to address methods to qualify and quantify quantum correlations in the operational space by connecting them to properties of states that can be reached via certain mappings to the target space.

A.3   Properties of quantum correlations

A.3.1   Invariance properties of quantum correlations

For distinguishable parties the concept of locality and of local operations is at the heart of entanglement theory. Measures of entanglement have to be invariant under local operations. In this context two types of locality are used: (i) local operations as operations which only involve a certain subset of sites or (ii) operations acting only on an individual particle. For distinguishable particles usually operations on a subset of local sites are identified with operations on only one particle, such that (i) and (ii) are essentially the same and both descriptions are used synonymously. For indistinguishable particles (ii) has no meaning

---

[3]In this case the final Hilbert space again is again $\mathcal{H}_T^N$. A more general procedure which includes tracing out some part of the operational space could be possible, such that the final space would consist of sectors with different total particle numbers.

anymore, as particles are not accessible individually, and every notion of locality, if any, has to be in terms of sites.

Different approaches to measure quantum correlations of indistinguishable particles disagree in which kind of invariance is demanded for the correlation measure. Let us list possible invariance conditions:

Inv 1 ➤ *Invariance with respect to local operations* — The notion of locality present in the target space can be continued to the operational space by grouping the operators $f_i^\dagger$ into the two subsets $\mathcal{M}_{T\to O}(C_A)$ and $\mathcal{M}_{T\to O}(C_B)$. Then if also $\mathcal{M}_{O\to T} = (\mathcal{M}_{T\to O})^{-1}$, local operations in the operational space correspond to local operations in the target space, and it is natural to demand invariance of the correlation measure with respect to local single particle transformations of the form ,assuming $\mathcal{M}_{T\to O}$ as in Eq. (A.15):

$$f_i \to f_i' = \sum_j U_{ij} f_j, \tag{A.17}$$

where $U = U_A \oplus U_B$ and U_A and U_B are K_A and K_B dimensional unitary matrices, respectively.

Inv 2 ➤ *Invariance with respect to all single-particle transformations* — If in general it is allowed to choose $\mathcal{M}_{O\to T}$ freely, such that esepcially $\mathcal{M}_{O\to T} \neq (\mathcal{M}_{T\to O})^{-1}$, then the final mapping from the operation to the target space can partition the operational space in many different ways and thus no explicit locality condition exists. In such a situation it is reasonable to demand invariance with respect to general single particle transformations of the full operational space, *i.e.*, invariance under transformations

$$f_i \to f_i' = \sum_j U_{ij} f_j, \tag{A.18}$$

with U being a general unitary $K_A + K_B$ dimensional matrix.

Inv 3 ➤ *Invariance with respect to creation and annihilation operations* — The list of allowed operations can be enlarged beyond single particle transformations by including (i) two particle transformations, (ii) arbitrary transformations conserving the number of particles, and (iii) arbitrary transformations. In all cases locality in the sense of **Inv 1** might or might not be demanded[4].

A.3.2 Useful vs. useless correlations

Our objective is to quantify quantum correlations in the operational space with respect to their usefulness in the target space. There are essentially two different types of quantum correlations (or, in this case, entanglement) in the target space:

➤ *Spin entanglement* — This is the type of quantum correlations normally referred to when talking about entanglement of distinguishable particles. It corresponds to quantum

---

[4](iii) obviously only is reasonable if a notion of locality in the operational space exists as otherwise any state can be transformed into any other.

correlation between external or internal degrees of freedom (to which we refer as *spin degrees of freedom*, no matter of their actual nature) of particles localized on different sites in space. An example of a spin-entangled state is

$$|\psi_{\text{Spin}}\rangle = \frac{1}{\sqrt{2}}\left(a_1^\dagger c_1^\dagger + a_2^\dagger c_2^\dagger\right)|\Omega\rangle. \tag{A.19}$$

➤ *Space entanglement* — Consider a single particle delocalized between A and C,

$$|\psi_{\text{Single particle}}\rangle = \frac{1}{\sqrt{2}}\left(a_1^\dagger + c_1^\dagger\right)|\Omega\rangle. \tag{A.20}$$

To see that this state, although single-particle, contains quantum correlations, it is best to use an occupation number basis, *i.e.*, a basis spanned by

$$|n_{A_1}\, n_{A_2}\, \ldots\rangle|n_{C_1}\, n_{C_2}\, \ldots\rangle, \quad \text{where } n_{x_i} \in \begin{cases} \{0,1\} & \text{for fermions} \\ \mathbb{N}_0^+ & \text{for bosons} \end{cases}, \tag{A.21}$$

where n_{A_i} (n_{C_i}) is the occupation number of the mode with creation operator $a_i^\dagger$ ($c_i^\dagger$). In this basis $|\psi_{\text{Single particle}}\rangle$ is written as

$$|\psi_{\text{Single particle}}\rangle = \frac{1}{\sqrt{2}}\left(|1\,0\ldots\rangle|0\,0\ldots\rangle + |0\,0\ldots\rangle|1\,0\ldots\rangle\right), \tag{A.22}$$

thus it is indeed an entangled state. It has been shown to violate a Bell inequality and to be useful for quantum teleportation [181].

Also mixtures between spin and space entanglement are possible. An example is provided by

$$|\psi_{\text{Spin-Space}}\rangle = \frac{1}{2}\left(a_1^\dagger + c_1^\dagger\right)\left(a_2^\dagger + c_2^\dagger\right)|\Omega\rangle. \tag{A.23}$$

In [178] a procedure to engineer such a spin-mode entangled state from two maximally spin-entangled states has been given. Talking about distinguishable particles and using the term locality with respect to transformations acting on one particle, *i.e.*, using **Inv 2**, this state is separable as it is a product state of two particles, each in one mode. However, if the notion of locality is with respect to the splitting of single-particle states between A and C, *i.e.*, **Inv 1**, then $|\psi_{\text{Spin-Space}}\rangle$ contains spin entanglement as well as space entanglement, as can be verified by projecting onto the sector with one particle on each site or two particles on either of them, respectively.

Depending on the intended application of quantum correlations in the experiment only one or the other type of quantum correlations might be useful. If for example the internal degree of freedom of some atom should be quantum teleported to a distant site, clearly space entanglement is not useful. Thus, in general there exists a subset USEFUL $\in \mathcal{H}_T$ of states[5] which for a certain application are considered to be interesting.

---

[5]We will concentrate on pure states here. For mixed states USEFUL is a subspace of all density matrices in $\mathcal{H}_T$: USEFUL $\in \mathcal{B}(\mathcal{H}_T)$. Here $\mathcal{B}(\mathcal{H})$ denotes the space of hermitean operators $\rho : \mathcal{H} \to \mathcal{H}$.

From these discussions it is clear, that the assignement of quantum correlations to a given state depends on the definitions of locality as well as of USEFUL. If such notions are given, then we will demand some properties for a *quantum correlation measure*[6] μ:

[M_0] ➤ *Identification of useless states* — $\mu(|\phi\rangle) = 0$ in case $|\phi\rangle \notin$ USEFUL. Otherwise $\mu(|\phi\rangle) \geq 0$. For a *strict measure* we demand that μ detects every state containing quantum correlations, *i.e.*, $\mu(|\phi\rangle) > 0 \Leftrightarrow |\phi\rangle \in$ USEFUL.

[M_1] ➤ *LOCC* — μ must not increase under (a) local operations in the sense of any of the definitions **Inv 1**-**3** given above, (b) POVM measurements, (c) addition of uncorrelated ancillas, and (d) tracing out subspaces. For the purpose of this discussion we will only consider criterion (a).

A.3.3   Measures of quantum correlations

A.3.4   Entanglement in the occupation number basis

We have already introduced the occupation number basis for the target space. It can be generally defined in the operational space as the basis spanned by vectors

$$|n_{F_1} \, n_{F_2} \, \ldots\rangle, \quad \text{where } n_{F_i} \in \left\{ \begin{array}{ll} \{0, 1\} & \text{for fermions} \\ \mathbb{N}_0^+ & \text{for bosons} \end{array} \right. \tag{A.24}$$

and n_{F_i} is the occupation number of modes created by f_i. Considering a partition of the operational space by fixing the transformation $\mathcal{M}_{O \to T} \neq (\mathcal{M}_{T \to O})^{-1}$ readily allows the characterization of quantum correlations of indistinguishable particles in terms of *entanglement between modes*. Such a description has been introduced by Zanardi [79] and has been shown to be a useful description of quantum correlations by Gittings *et al.* [84]. A serious problem of mode entanglement is that the Hilbert space, even though this might be suggested from the notation, does not have a tensor product structure. It is a direct sum of Hilbert space sectors with a fixed total number of particles. Furthermore for massive particles, experimentally accessible operations are those which are direct sums of operators acting in these sectors [182] as changes of the numbers of particles are not realizable without adding a reservoir of particles[7].

The properties of a state in the occupation number basis are, after fixing a partition, well characterized by applying usual entanglement measures, *e.g.*, by the entropy of entanglement, see Eq. (1.14) (or, for mixed states, by the entanglement of formation formation, see Eq. (1.16)). So a suitable (pure state) correlation measure μ_{Mode} can be defined as

$$\mu_{\text{Mode}}(|\psi\rangle\langle\psi|) = E_e(|\psi\rangle\langle\psi|), \tag{A.25}$$

where the evaluation of $E_e(\ldots)$ is done in the occupation number basis and the two subsystems are defined via the partition of the modes. For the following example we assume to

---

[6]This list is not extensive as there are more applicable criteria. For an overview of criteria for entanglement measures in general see, *e.g.*, [42].

[7]Such a reservoir allows to implement operations between sectors of different number of particles, but such operations introduce entanglement between the system and the reservoir.

have for modes f_i $i = 1, \ldots, 4$ and a partition between $\{f_1, f_2\}$ and $\{f_3, f_4\}$ and take

$$\rho_{\text{Spin}} = |\rho_{\text{Spin}}\rangle\langle\rho_{\text{Spin}}| = \frac{1}{2}\left(f_1^\dagger f_3^\dagger + f_2^\dagger f_4^\dagger\right)|\Omega\rangle\langle\Omega|\left(f_3 f_1 + f_4 f_2\right). \tag{A.26}$$

Writing ρ_{Spin} in the basis of $|n_{F_1} n_{F_2}\rangle|n_{F_3} n_{F_4}\rangle$ and tracing out side modes f_1 and f_2 leaves

$$\widetilde{\rho} = \sum_{\substack{n_{F_1}=0,1, n_{F_2}=0,1 \\ n_{F_3}=0,1, n_{F_4}=0,1}} \langle n_{F_3} n_{F_4}|\langle n_{F_3} n_{F_4}|\rho|n_{F_3} n_{F_4}\rangle|n_{F_3} n_{F_4}\rangle|n_{F_1} n_{F_2}\rangle\langle n_{F_1} n_{F_2}| \tag{A.27}$$

$$= \begin{pmatrix} 0 & 0 & 0 & 0 \\ 0 & 1 & 0 & 0 \\ 0 & 0 & 1 & 0 \\ 0 & 0 & 0 & 0 \end{pmatrix}, \tag{A.28}$$

where $\widetilde{\rho}_{\text{Spin}}$ in Eq. (A.28) is given in the basis $\{|n_{F_1}, n_{F_2}\rangle\} = \{|0,0\rangle, |1,0\rangle, |0,1\rangle, |1,1\rangle\}$. Notice that in this basis a physical $\widetilde{\rho}_{\text{Spin}}$ has to have the form of a direct sum:

$$\widetilde{\rho}_{\text{Spin}} = \widetilde{\rho}_{\text{Spin}}^{n_F=0} \oplus \widetilde{\rho}_{\text{Spin}}^{n_F=1} \oplus \widetilde{\rho}_{\text{Spin}}^{n_F=2}, \tag{A.29}$$

where the upper index refers to the number of particles. We can directly calculate

$$\mu_{\text{Mode}}(|\psi_{\text{Spin}}\rangle\langle\psi_{\text{Spin}}|) = S\left(\widetilde{\rho}_{\text{Spin}}\right) = 1, \tag{A.30}$$

which is in direct agreement with the entropy of entanglement of $|\psi_{\text{Spin}}\rangle$ after taking the state back to the target space via $\mathcal{M}_{O\to T} = (\mathcal{M}_{T\to O})^{-1}$, i.e., by considering modes a_i and c_i to be distinguishable. Thus in the occupation number representation, also spin correlations are identified give a non-zero value of the entropy of entanglement. On the other hand for the state containing both, spin and space entanglement, Eq. (A.23), we have

$$\widetilde{\rho}_{\text{Spin-Space}} = \begin{pmatrix} 1 & 0 & 0 & 0 \\ 0 & 1 & 0 & 0 \\ 0 & 0 & 1 & 0 \\ 0 & 0 & 0 & 1 \end{pmatrix} \tag{A.31}$$

and thus

$$\mu_{\text{Mode}}(|\psi_{\text{Spin-Space}}\rangle\langle\psi_{\text{Spin-Space}}|) = 2. \tag{A.32}$$

This suggest that in the target space such a state should be useful for, *e.g.*, teleportation of two qubits from site A to site C (in the target space), and indeed in [84] a protocol to use such a teleportation process has been described. This protocol however directly points to a drawback of mode entanglement: in order for the teleportation to work, *i.e.*, to transfer the content of two (spin) qubits from A to C using $|\psi_{\text{Spin-Space}}\rangle$, a Hamiltonian has to be implemented which does not conserve the number of particles. In [84] this problem is circumvented by introducing a source/sink for particles, *i.e.*, a new subsystem D. Doing this however introduces new correlations between the states of sites A and D, which can only be avoided by putting subsystem D into a coherent state with the number of particles going to infinity (this only works for bosons, for fermions no solution is presented in [84]).

If such operations which are not conserving the number of particles are allowed, or, in other words, if both, spin and space entanglement are considered as useful quantum correlations,

then the correlation measure μ_{Mode} fulfills the requirement [M_0], see also [84, 183]. Requirement [M_1] is obviously fulfilled if invariance is defined via **Inv 1**, as the division of the modes into sets $\{a_i\}$ and $\{c_i\}$ is used for the evaluation E_e. On the other hand, [M_1] is not fulfilled if **Inv 2** is used as the invariance criterion, as via transformations of the full single particle space, for example $a_1^\dagger|\Omega\rangle$ (which has $\mu_{\text{Mode}} = 0$) can be transformed into $(a_1^\dagger + c_1^\dagger)|\Omega\rangle/\sqrt{2}$ (which has $\mu_{\text{mode}} = 1$) [183] under single particle transformations.

A.3.5 Measures invariant under full transformations of the single particle space

A quantum correlation measure invariant under general transformations of the single particle space, *i.e.*, respecting **Inv 2** but not **Inv 1**, has been proposed in [73] for systems of two fermions, and subsequently analyzed in [80, 85] and also it has been modified to be applicable for bosons in [85]. A slightly different version in an otherwise very similar setting has been analyzed in [81].

Let us first consider fermions, where a general state $|w\rangle$ can be described as in Eq. (A.5) by an antisymmetric N dimensional tensor w. Restricting the problem to two fermions in a single particle Hilbert space of even dimension, $K = 2L$, then w is a $2L \times 2L$ complex matrix fulfilling $w_{ij} = -w_{ji}$. Under transformations U of the single particle space, $UU^\dagger = \mathbb{1}$, w is changed according to $w \mapsto w = UwU^\dagger$. As can be shown [183], there especially always exists a U such that $UwU^\dagger = z$, where

$$z = \text{diag}[z_1, \ldots, z_M, z_0], \qquad \text{where} \qquad z_k = \begin{pmatrix} 0 & \zeta_k \\ -\zeta_k & 0 \end{pmatrix}, \qquad (A.33)$$

$M \leq L$, ζ_k real and non-negative and $z_0 = {}_{2L-2M}$ is the $(2L - 2M) \times (2L - 2M)$ dimensional null matrix. This means that there is always a transformation of the single-particle space, such that in the new basis $\{f_i'\}$, $|w\rangle$ can be written

$$|w\rangle = 2 \sum_{k=1}^{M} \zeta_k (f_{2k}')^\dagger (f_{2k-1}')^\dagger|\Omega\rangle. \qquad (A.34)$$

This decomposition in terms of *Slater determinants* $(f_{2k}')^\dagger (f_{2k-1}')^\dagger|\Omega\rangle$ is termed *Slater decomposition*, and (i) it is unique if some order of the coefficients ζ_k is assumed, (ii) it is minimal as rank$\{w\} = 2M$, and (iii) the Slater determinants are pairwise orthogonal [183]. The number M is the *Slater rank* of $|w\rangle$.

These definitions in the operational space can immediately be related to the notions of Schmidt decomposition and Schmidt rank in the target space by choosing the mapping back to the target space as

$$\mathcal{M}_{O \to T} : \quad \begin{cases} \mathcal{H}_O^2 & \to & \mathcal{H}_T^2 \\ (f_{2k}')^\dagger & \to & (a_k')^\dagger & k = 1, \ldots, L \\ (f_{2k-1}')^\dagger & \to & (c_k')^\dagger & k = 1, \ldots, L. \end{cases} \qquad (A.35)$$

Then $|w\rangle = \sum_{k=1}^{M} 2\zeta_k (a_k')^\dagger (c_k')^\dagger|\Omega\rangle \in \mathcal{H}_O^2$ is already in Schmidt decomposed form and has Schmidt rank M. For $|w\rangle \in \mathcal{H}_O^2$ the entropy of entanglement can directly be computed from

the reduced density matrix as

$$E_e(|w\rangle\langle w|) = -\sum_{k=1}^{M}(2\zeta_k)^2 \log_2(4\zeta_k^2), \tag{A.36}$$

and thus this definition can directly be used to quantify the quantum correlations in a state of two fermions in the operational space:

$$\mu_e^F(|w\rangle\langle w|) = -4\sum_{k=1}^{M}\zeta_k^2 \log_2(4\zeta_k^2), \tag{A.37}$$

with the coefficients ζ_k defined by the Slater decomposition, Eq. (A.34). As noted in [81], μ_e^F can also be directly calculated through from the reduced density matrix of $|w\rangle\langle w|$.

The most simple situation to find correlations in a two fermion system is the case of a four dimensional single particle space. In this case another possible correlation measure for the pure two fermion state $|w\rangle = \sum_{i,j=1}^{4} w_{ij}f_i^\dagger f_j^\dagger|\Omega\rangle$ is given by

$$\mu_C^F(|w\rangle\langle w|) = |\langle\widetilde{w}|w\rangle|, \quad \text{where} \quad |\widetilde{w}\rangle = \sum_{i,j=1}^{4}\widetilde{w}_{ij}f_i^\dagger f_j^\dagger|\Omega\rangle \quad \text{with} \quad \widetilde{w}_{ij} = \frac{1}{2}\sum_{k,l=1}^{4}\varepsilon_{ijkl}w_{kl}^*. \tag{A.38}$$

μ_C^F is termed the *fermionic concurrence*, as it is the a fermionic version of the concurrence introduced by Wootters in [184, 185] for a system of two qubits[8]; it is invariant with respect to transformations of the full single particle Hilbert space. The benefit of the fermionic concurrence μ_C^F in contrast to the entropy μ_e^F is that it can be calculated also for mixed states, see [85, 183].

For two bosons, pure in a K-dimensional single-particle Hilbert space $\mathcal{H}_K$ can be written

$$|v\rangle = \sum_{i,j=1}^{K} v_{ij}b_i^\dagger b_j^\dagger|\Omega\rangle \in \mathcal{SH}_K \otimes \mathcal{H}_k, \qquad v_{ij} = v_{ji}, \tag{A.39}$$

where $b_i^\dagger$ are bosonic creation operators. As can be shown, for any $K \times K$ matrix v there always exists a unitary matrix U, such that

$$UvU^\dagger = z \qquad \text{where} \qquad z = \text{diag}[\zeta_1, \ldots, \zeta_M, 0\ldots, 0], \tag{A.40}$$

where $M \le K$ is integer, and the ζ_k are real an non-negative. Thus there always exists a transformation of the single particle space, such that in the new basis $\{b_i'\}$,

$$|v\rangle = \sum_{k=1}^{M} \zeta_k(b')_k^\dagger(b')_k^\dagger|\Omega\rangle, \tag{A.41}$$

Thus every state of two bosons can be written as a combination of pairwise orthogonal *permanents* $(b')_k^\dagger(b')_k^\dagger|\Omega\rangle$; this definition is, analoguos to the case of fermions, called *Slater*

---

[8]Both versions, the two qubit as well as the two fermion concurrence, are intimately connected to the operation of time reversal on both of the qubits or on both of the fermions [183].

decomposition, the number K is the *Slater rank*. As before, from connecting the Slater decomposition to the Schmidt decomposition *via* a suiteable transformation to the target space, a entropy of entanglement can be defined as

$$\mu_e^B(|v\rangle\langle v|) = \sum_{k=1}^{M} \zeta_k^2 \log_2(\zeta_k^2), \tag{A.42}$$

which again is derived in [81] from the reduced density matrix.

States with Slater rank one obviously are non-correlated. For $|\psi_2\rangle = \frac{1}{2}(b_1^\dagger b_1^\dagger + b_2^\dagger b_2^\dagger)|\Omega\rangle$, which has Slater rank 2, the entropy of entanglement is $\mu_e^B(|\psi_2\rangle\langle\psi_2|) = 1$. But a single particle transformation

$$(b')_1^\dagger = -\frac{i}{\sqrt{2}}b_1^\dagger + \frac{i}{\sqrt{2}}b_2^\dagger; \qquad (b')_2^\dagger = \frac{1}{\sqrt{2}}b_1^\dagger + \frac{1}{\sqrt{2}}b_2^\dagger \tag{A.43}$$

allows to write $|\psi_2\rangle$ as the product of two modes: $|\psi_2\rangle = (b')_1^\dagger(b')_2^\dagger|\Omega\rangle$. From this point of view it should not be considered as a quantum correlated state. This problem has been identified by Li *et al.* [82] and corrected through adapting the definition of the entropy as

$$\mu_{e,Li}^B(|v\rangle\langle v|) = -4 \sum_{k=1}^{M/2} \zeta_{2k-1}\zeta_{2k} \log_2(4\zeta_{2k-1}\zeta_{2k}). \tag{A.44}$$

In this context it should be noted that the value of $\mu_e^B(|\psi_2\rangle\langle\psi_2|) = 1$ is not completely arbitrary, as obviously using $\mathcal{M}_{O\rightarrow T}$ from Eq. (A.35) to map from the operational to the target space produces a spatially correlated state which has entropy of entanglement 1. Furthermore, as shown in [183] even a protocol[9] to map $|\psi_2\rangle$ to a maximally spin-entangled state of two qubits exists. Indeed, in the fermionic as well as in the bosonic case, for two particle states the entropy of entanglement calculated from the Slater decomposition specifies the maximum of entanglement which can be obtained *via* optimizing the mapping $\mathcal{M}_{O\rightarrow T}$ and considering *only* spin *or* space entanglement.

Also for bosons a concurrence can be defined in the case of the lowest non-trivial dimension of the particle space $K = 2$ [46]

$$\mu_C^B(|v\rangle\langle v|) = |\langle\widetilde{v}|v\rangle|, \quad \text{where} \quad |\widetilde{v}\rangle = \sum_{i,j=1}^{2} \widetilde{v}_{ij} b_i^\dagger b_j^\dagger|\Omega\rangle \quad \text{with} \quad \widetilde{v}_{ij} = \frac{1}{2}\sum_{k,l=1}^{2} \varepsilon_{ik}\varepsilon_{jl}v_{kl}^*. \tag{A.45}$$

This is expressed much simpler as $\mu_C^B(|\psi\rangle\langle\psi|) = |4\det v|$.

A.4 Conclusion

In this appendix, several concepts for the qualification and the quantification of quantum correlations have been presented and reviewed, which are applicable in situations where the

---

[9]This protocol consists of the repeated application of two steps: an application of a beamsplitter operation and a detection of the occupation number. It has unit success property only asymptotically.

indistinguishable nature of particles has to be taken into account. These concepts basically differ in their notion of locality They either, in the case of the occupation number representation, fix a partition of the full single particle space and pose a locality condition with respect to this partition, or, they avoid any a-priori definition of locality and define invariance with respect to general transformations of the single particle space, as it is the case for all methods based on the Slater decomposition.

With this in mind, it is natural that quantum correlations can be quantified in a different way, and that especially a state might be separable from the point of view of one concept but strongly quantum correlated in th perception of another method. In order to clarify the conditions under which the various concepts can be applied, we have presented a more general framework which could suffer as a building block for a further and more general classification of quantum correlations of indistinguishable particles in the future.

APPENDIX B

THE EXPONENTIAL SPLIT OPERATOR METHOD

To calculate the time evolution of the atomic wavefunction in the optical potentials, the time-dependent Schrödinger equation

$$i\hbar\partial_t|\psi(t)\rangle = H(t)|\psi(t)\rangle \tag{B.1}$$

has to be solved, where the Hamilton operator contains a time-dependent potential term: $H(t) = T + V(t)$. Eq. (B.1) is formally solved by

$$|\psi(t)\rangle = U(t, t_0)|\psi(t_0)\rangle, \tag{B.2}$$

with the *propagator* $U(t, t_0)$ defined as

$$U(t, t_0) = \mathcal{T} \exp\left(-\frac{i}{\hbar} \int_{t_0}^{t} dt' \, H(t')\right), \tag{B.3}$$

where $\mathcal{T}$ is the time-ordering operator. To approximate $U(t, t_0)$, the interval $[t, t_0]$ can be divided into small intervals of lenght $\Delta = (t - t_0)/n$, such that

$$
\begin{aligned}
U(t, t_0) &\approx \mathcal{T} \exp\left(-\frac{i}{\hbar} [H(t_0 + \Delta(n-1))\Delta + \ldots + H(t_0)\Delta]\right) \tag{B.4}\\
&= \exp\left(-\frac{i}{\hbar} H(t_0 + \Delta(n-1))\Delta\right) \cdots \exp\left(-\frac{i}{\hbar} H(t_0)\Delta\right) \tag{B.5}\\
&= U_{n-1} \, U_{n-2} \cdots U_0. \tag{B.6}
\end{aligned}
$$

Each exponential term $U_j = \exp(-i[T + V_j]\Delta/\hbar)$ contains a kinetic term $T = p^2/2m$, which is diagonal in momentum space and a potential term $V_j = V(x, t = t_0 + \Delta j))$, which is diagonal in position space. To evaluate $U_j = \exp(-i[T + V_j]\Delta/\hbar)$ it should be approximated by a product of operators each being diagonal in momentum *or* in position space. Writing $\lambda = -\frac{i\Delta}{\hbar}$, the first approximation is

$$U_j = \exp(\lambda V_j)\exp(\lambda T) + \Delta U_j^{(2)} + O(\lambda^3), \tag{B.7}$$

with the error term given by

$$\Delta U_j^{(2)} = \frac{1}{2}[T, V_j] \, \lambda^2, \tag{B.8}$$

which can readily be obtained from a Taylor expansion. An expression which is exact to the order of λ^2 is given by the symmetric product

$$U_j = \exp\left(\frac{\lambda}{2}T_j\right)\exp\left(\frac{\lambda}{2}V_j\right)\exp\left(\frac{\lambda}{2}T_j\right) + \Delta U_j^{(3)} + O(\lambda^4), \tag{B.9}$$

where now the error term reads

$$\Delta U_j^{(3)} = \frac{1}{24}[T + 2V_j, [T, V_j]]\,\lambda^3. \tag{B.10}$$

More exact expressions can, e.g., be found in [186].

Assuming that $|\psi(t_0)\rangle$ is initially given in position space, $\psi(x)_0 \equiv \langle x|\psi(t_0)\rangle$, first a Fourier transform is performed:

$$\widetilde{\psi}(k) = \frac{1}{\sqrt{2\pi}}\int\limits_{-\infty}^{\infty} dx\, e^{-ikx}\psi(x). \tag{B.11}$$

Now the application of $\exp(-\lambda T/2)$ simply corresponds to multiplying $\widetilde{\psi}(k)$ with a factor,

$$\widetilde{\psi}'(k) = \exp\left(\frac{\hbar^2\lambda}{4m}k^2\right)\widetilde{\psi}(k). \tag{B.12}$$

Transforming $\widetilde{\psi}'(k)$ back to position space,

$$\psi'(x) = \frac{1}{\sqrt{2\pi}}\int\limits_{-\infty}^{\infty} dk\, e^{ikx}\widetilde{\psi}'(k), \tag{B.13}$$

allows to apply the potential term:

$$\psi''(x) = \exp\left(\lambda V_0(x)\right)\psi'(x). \tag{B.14}$$

After another Fourier transformation, thus obtaining $\widetilde{\psi}''(k)$ also the final propagator in momentum space can be applied,

$$\widetilde{\psi}'''(k) = \exp\left(\frac{\hbar^2\lambda}{4m}k^2\right)\widetilde{\psi}''(k). \tag{B.15}$$

Repeating the steps of Eqns. (B.12) – (B.15) N times (where indeed except for the first and for the last step, (B.12) and (B.15) can be combined into one operation), gives an approximation to $\psi(x, t = N\Delta)$ after a final Fourier transformation to position space.

The power of the split operator method relies (i) on the fact that it is unconditionally stable and more accurate than finite difference methods [187] and (ii) on the existence of fast methods for performing the Fourier transform of discretized data, known as *Fast Fourier Transformation* (FFT, [187]).

BIBLIOGRAPHY

[1] R. Feynman. *The Feynman lectures on computation*. Addison-Wesley 1996.

[2] E. Schrödinger. *Die gegenwärtige Situation in der Quantenmechanik*. Naturwissenschaften **23**, 807 (1935).

[3] J.S. Bell. *On the Einstein-Podolsky-Rosen paradox*. Physics **1**, 195 (1964).

[4] A. Peres. *Quantum theory: Concepts and Methods*. Kluwer Academic 1995.

[5] G.E. Moore. *Cramming More Components Onto Integrated Circuits*. Electronics **38**, 114 (1965).

[6] R. Laflamme, D.G. Cory, C. Negrevergne, and L. Viola. *NMR Quantum Information Processing and Entanglement*. Qu. Inf. Comp. **2**, 166 (2003).

[7] B.E. Kane. *A silicon-based nuclear spin quantum computer*. Nature (London) **393**, 133 (1998).

[8] D. Loss and D.P. DiVincenzo. *Quantum computation with quantum dots*. Phys. Rev. A **57**, 120 (1998).

[9] Y. Makhlin, G. Schön, and A. Shnirman. *Quantum-state engineering with Josephson-junction devices*. Rep. Mat. Phys. **73**, 357 (2001).

[10] C. Monroe, D.M. Meekhof, B.E. King, W.M. Itano, and D.J. Wineland. *Demonstration of a fundamental quantum logic gate*. Phys. Rev. Lett. **75**, 4714 (1995).

[11] F. Schmidt-Kaler, H. Häffner, M. Riebe, S. Gulde, G.P.T. Lancaster, T. Deuschle, C. Becher, C.F. Roos, J. Eschner, and R. Blatt. *Realization of the Cirac-Zoller controlled-NOT quantum gate*. Nature (London) **422**, 408 (2003).

[12] D. Leibfried, D.B. DeMarco, V. Meyer, D. Lucas, M. Barrett, J. Britton, W.M. Itano, B. Jelenkovic, C. Langer, T. Rosenband, and D.J. Wineland. *Experimental demonstration of a robust, high-fidelity geometric two ion-qubit phase gate*. Phys. Rev. Lett. **422**, 412 (2003).

[13] J. Denschlag, D. Cassettari, and J. Schmiedmayer. *Guiding Neutral Atoms with a Wire*. Phys. Rev. Lett. **82**, 2014 (1999).

[14] L. Guidoni and P. Verkerk. *Optical lattices: cold atoms ordered by light*. J. Opt. B **1**, R23 (1999).

[15] M. Greiner, O. Mandel, T. Esslinger, T.W. Hänsch, and I. Bloch. *Quantum phase transition from a superfluid to a Mott insulator in a gas of ultracold atoms*. Nature (London) **415**, 39 (2002).

[16] D. Jaksch, H.-J. Briegel, J.I. Cirac, C.W. Gardiner, and P. Zoller. *Entanglement of atoms via controlled collisions*. Phys. Rev. Lett. **82**, 1975 (1999).

[17] T. Calarco, E.A. Hinds, D. Jaksch, J. Schmiedmayer, J.I. Cirac, and P. Zoller. *Quantum gates with neutral atoms: controlling collisional interactions in time-dependent traps*. Phys. Rev. A **61**, 022304 (2000).

[18] G.K. Brennen, C.M. Caves, P.S. Jessen, and I.H. Deutsch. *Quantum logic gates in optical lattices*. Phys. Rev. Lett. **82**, 1060 (1999).

[21] D. Jaksch, J.I. cirac, P. Zoller, S.L. Rolston, R. Cote, and M.D. Lukin. *Fast quantum gates for neutral atoms*. Phys. Rev. Lett. **85**, 2208 (2000).

[19] G.K. Brennen, I.H. Deutsch, and P.S. Jessen. *Entangling dipole-dipole interactions for quantum logic with neutral atoms*. Phys. Rev. A **61**, 062309 (2000).

[20] G.K. Brennen, I.H. Deutsch, and C.J. Williams. *Quantum logic for trapped atoms via molecular hyperfine interactions*. Phys. Rev. A **65**, 2208 (2002).

[22] J. Dalibard and C. Cohen-Tannoudji. *Laser cooling below the Doppler limit by polarization gradients: simple theoretical models*. J. Opt. Soc. Am. B **6**, 2023 (1989).

[23] O. Mandel, M. Greiner, A. Widera, T. Rom, T.W. Hänsch, and I. Bloch. *Coherent transport of neutral atoms spin-dependent optical lattice potentials*. Phys. Rev. Lett. **91**, 010407 (2003).

[24] O. Mandel, M. Greiner, A. Widera, T. Rom, T.W. Hänsch, and I. Bloch. *Controlled collisions for multi-particle entanglement of optically trapped atoms*. Nature (London) **425**, 937 (2003).

[25] R. Raussendorf and H.J. Briegel. *A one-way quantum computer*. Phys. Rev. Lett. **86**, 5188 (2001).

[26] T. Calarco, U. Dorner, P. Julienne, C. Williams, and P. Zoller. *Quantum computations with atoms in optical lattices: marker qubits and molecular interactions*. quant-ph page 0403197 (2004).

[27] G. Birkl, F.B.J. Buchkremer, R. Dumke, and W. Ertmer. *Atom Optics with Microfabricated Optical Elements*. Opt. Comm. **191**, 67 (2001).

[29] R. Dumke, M. Volk, T. Muether, F.B.J. Buchkremer, G. Birkl, and W. Ertmer. *Microoptical Realization of Arrays of Selectively Addressable Dipole Traps: A Scalable Configuration for Quantum Computation with Atomic Qubits*. Phys. Rev. Lett. **89**, 097903 (2002).

[28] F.B.J. Buchkremer, R. Dumke, M. Volk, T. Muether, G. Birkl, and W. Ertmer. *Quantum Information Processing with Microfabricated Optical Elements*. Las. Phys. **12**, 736 (2002).

[31] D. Frese, B. Ueberholz, S. Kuhr, W. Alt, D. Schrader, V. Gomer, and D. Meschede. *Single atoms in an optical dipole trap: Towards a deterministic source of cold atoms*. Phys. Rev. Lett. **85**, 3777 (2000).

[32] N. Schlosser, G. Reymond, I. Protsenko, and P. Grangier. *Sub-poissonian loading of single atoms in a microscopic dipole trap*. Nature (London) **411**, 1024 (2001).

[30] S. Bergamini, D. Darquié, M. Jones, L. Jacubowiez, A. Browaeys, and P. Grangier. *Holographic generation of micro-trap array for single atoms*. J. Opt. Soc. Am. B **21**, 1889 (2004).

[33] M. Kitagawa and M. Ueda. *Squeezed spin states*. Phys. Rev. A **47**, 5138 (1993).

[34] A. Sørensen and K. Mølmer. *Entanglement and Extreme Spin Squeezing*. Phys. Rev. Lett. **86**, 4431 (2001).

[35] B. Yurke, S.L. McCall, and J.R. Clauder. *SU(2) and SU(1,1) interferometers*. Phys. Rev. A **33**, 4033 (1986).

[36] D.J. Wineland, J.J. Bollinger, W.M. Itano, F.L. Moore, and D.J. Heinzen. *Spin squeezing and reduced quantum noise in spectroscopy*. Phys. Rev. A **46**, R6797 (1992).

[37] M.D. Lukin. *Colloquium: Trapping and manipulating photon states in atomic ensembles*. Rep. Mat. Phys. **75**, 457 (2003).

[38] B. Julsgaard, J. Sherson, J.I. Cirac, J. Fiurasek, and E.S. Polzik. *Experimental demonstration of quantum memory for light*. Nature (London) (2004). accepted.

[39] M.A. Nielsen and I.L.Chuang. *Quantum Computation and Quantum Information*. Cambridge University Press 2000.

[40] D. Bouwmeester, A. Ekert, and A. Zeilinger. *The Physics of Quantum Information: Quantum Cryptography, Quantum Teleportation, Quantum Computation*. Springer 2000.

[41] M. Lewenstein, H. Kreutzmann, and K. Eckert. *Quanteninformationstheorie 2* 2001. available online from http://fs-maphy.uni-hannover.de.

[42] F. Hulpke. *Verschränkungsmaße für Zustände von zwei und drei Quantensystemen*. Diploma thesis Universität Marburg 2000.

[43] C. Bennet, D. DiVincenzi, J. Smolin, and W. Wootters. *Mixed state entanglementand quantum error correction*. Phys. Rev. A **54**, 2046 (1996).

[44] Wikipedia. *Sheffer Stroke*. http://en.wikipedia.org/wiki/Sheffer_stroke.

[45] A. Barenco, C.H. Bennet, R. Cleve, D.P. Divincenzo, N. Margolus, P. Shor, T. Sleator, J.A. Smolin, and H. Weinfurter. *Elementary gates for quantum computation*. Phys. Rev. A **52**, 3457 (52).

[46] K. Eckert, J. Mompart, X.X. Yi, J. Schliemann, D. Bruß, G. Birkl, and M. Lewenstein. *Quantum computing in optical microtraps based on the motional states of neutral atoms*. Phys. Rev. A **66**, 042317 (2002).

[47] J. Gruska. *Quantum Computing*. Mc Graw Hill 1999.

[48] Fraunhofer FIRST Berlin. *Fraunhofer Quantum Computing Simulator*. http://www.qc.fraunhofer.de/.

[49] Los Alamos National Laboratory. *The quantum information roadmapping project*. http://qist.lanl.gov.

[50] D.P. DiVincenzo. *Topic in Quantum Computer*. Mesoscopic electron transport (1996). PrePrint: cond-mat/9612126.

[51] S.E. Hamann, D.L. Haycock, G. Klose, P.H. Pax, I.H. Deutsch, and P.S. Jessen. *Resolved-sideband Raman cooling to the ground state of an optical lattice*. Phys. Rev. Lett. **80**, 4149 (1998).

[52] H. Perrin, A. Kuhn, I. Bouchoule, and C. Salomon. *Sideband cooling of neutral atoms in a far-detuned optical lattice*. Europhys. Lett. **42**, 395 (1998).

[53] V. Vuletic, C. Chin, A.J. Kerman, and S. Chu. *Degenerate Raman sideband cooling of trapped caesium atoms at very high densities*. Phys. Rev. Lett. **81**, 5768 (1998).

[54] D.J. Han, S. Wolf, S. Oliver, C. McCormick, M.T. Depue, and D.S. Weiss. *3D Raman sideband cooling of caesium atoms at high density*. Phys. Rev. Lett. **85**, 724 (2000).

[55] H.D. Dehmelt. *Mono-ion osciallator as potential ultimate laser frequency standard*. IEEE Trans. Instr. Meas. **31**, 83 (1982).

[56] V.I. Balykin, V.G. Minogin, and V.S. Letokhov. *Electromagnetic trapping of cold atoms*. Reports on Progress in Physics **63**, 1429 (2000).

[57] R. Grimm, M. Weidemüller, and Y.B. Ovchinnikov. *Optical dipole traps for neutral atoms*. Adv. At. Mol. Opt. Phys. **42**, 95 (2000).

[58] S. Chu, J.E. Bjorkholm, A. Ashkin, and A. Cable. *Experimental observation of optically trapped atoms*. Phys. Rev. Lett. **57**, 314 (19986).

[59] J. Reichel, W. Hänsel, P. Hommelhoff, and T.W. Hänsch. *Applications of integrated magnetic microtraps*. Appl. Phys. B **72**, 81 (2001).

[60] R. Folman, P. Krüger, D. Cassettari, B. Hessmo, T. Maier, and J. Schmiedmayer. *Controlling cold atoms unsing nanofabricated surfaces: Atom chips*. Phys. Rev. Lett. **72**, 81 (2000).

[61] P.S. Jessen and I.H. Deutsch. *Optical lattices*. In B. Bederson and H. Walther, editors, *Advances in Atomic, Molecular, and Optical Physics* volume 37 page 95. Academic, San Diego 1996.

[62] E. Charron, E. Tiesinga, F. Mies, and C. Williams. *Optimizing a phase gate using quantum interference*. Phys. Rev. A **88**, 077901 (2002).

[63] T. Takekoshi, J.R. Yeh, and R.J. Knize. *Quasi-electrostatic trap for neutral atoms*. Phys. Rev. A **114**, 421 (1995).

[64] CO_2 laser optical lattice with cold rubidium atoms. *S. Friebel and C. D'Andrea and J. Walz and M. Weitz and T.W.Hänsch*. Phys. Rev. A **57** (1), R20 (1998).

[65] R. Dumke, T. Muether, M. Volk, W. Ertmer, and G. Birkl. *Interferometer-Type Structures for Guided Atoms*. Phys. Rev. Lett. **89**, 220402 (2002).

[66] D. Jaksch. *Optical Lattices, Ultracold Atoms and Quantum Information Processing*. Cont. Phys **45**, 367 (2004).

[67] D. Jaksch, C. Bruder, J.I. Cirac, C.W. Gardiner, and P. Zoller. *Cold bosonic atoms in optical lattices*. Phys. Rev. Lett. **81**, 3108 (1998).

[68] F.B.J. Buchkremer, R. Dumke, H. Levsen, G. Birkl, and W. Ertmer. *Wave Packet Echoes in the Motion of Trapped Atoms*. Phys. Rev. Lett. **85**, 3121 (2000).

[69] S. Peil, J. V. Porto, B. Laburthe Tolra, J. M. Obrecht, B. E. King, M. Subbotin, S. L. Rolston, and W. D. Phillips. *Patterned loading of a Bose-Einstein condensate into an optical lattice*. Phys. Rev. A **67**, 051603(R) (2003).

[70] R. Scheunemann, F. S. Cataliotti, T. W. Hänsch, and M. Weitz. *Resolving and addressing atoms in individual sites of a CO2-laser optical lattice*. Phys. Rev. A **62**, 051801 (2000).

[71] A. Recati, T. Calarco, P. Zanardi, J.I. Cirac, and P. Zoller. *Holonomic quantum computation with neutral atoms*. Phys. Rev. A **66**, 032309 (2002).

[72] M. Morinaga, I. Bouchoule, J.-C. Karam, and C. Salomon. *Manipulation of Motional Quantum States of Neutral Atoms*. Phys. Rev. Lett. **83**, 4037 (1999).

[73] J. Schliemann, D. Loss, and A.H. MacDonald. *Double-occupancy errors, adiabaticity, and entanglement of spin qubits in quantum dots*. Phys. Rev. B **63**, 85311 (2001).

[74] Patrik Öhberg and Stig Stenholm. *Hartree-Fock treatment of the two-component Bose-Einstein condensate*. Phys. Rev. A **57**, 1272 (1998).

[75] Eric W. Weisstein. *MathWorld – Gram-Schmidt Orthonormalization*. http://mathworld.wolfram.com/Gram-SchmidtOrthonormalization.html.

[76] I. Bouchoule, H. Perrin, A. Kuhn, M. Morinaga, and C. Salomon. *Neutral atoms prepared in Fock states of a one-dimensional harmonic potential*. Phys. Rev. A **59**, R8 (1999).

[77] S.L. Cornish, N.R. Clausen, J.L. Roberts, E.A. Cornell, and C.E. Wieman. *Stable ^{85}Rb Bose-Einstein Condensates with Widely Tunable Interactions*. Phys. Rev. Lett. **85**, 1795 (2000).

[78] W. Hänsel, J. Reichel, P. Hommelhoff, and T. W. Hänsch. *Trapped-atom interferometer in a magnetic microtrap*. Phys. Rev. A **64**, 063607 (2001).

[79] P. Zanardi. *Quantum Entanglement in Fermionic Lattices*. Phys. Rev. A **65**, 042101 (2002).

[80] J. Schliemann, J.I. Cirac, M. Kus, M. Lewenstein, and D. Loss. *Quantum Correlations in Two-Fermion Systems*. Phys. Rev. A **64**, 022303 (2001).

[85] K. Eckert, J. Schliemann, D. Bruß, and M. Lewenstein. *Quantum Correlations in Systems of Indistinguishable Particles*. Ann. Phys. **299**, 88 (2002).

[81] R. Paškauskas and L. You. *Quantum Correlations in Two-Boson Wavefunctions*. Phys. Rev. A **64**, 042310 (2001).

[82] Y.S. Li, B. Zeng, X.S. Liu, and G.L. Long. *Entanglement in a two-identical-particle system*. Phys. Rev. A **64**, 054302 (2001).

[83] V. Vedral. *Entanglement in The Second Quantization Formalism*. Central Eur.J.Phys. **1**, 289 (2003).

[84] J.R. Gittings and A.J. Fisher. *Describing mixed spin-space entanglement of pure states of indistinguishable particles using an occupation number basis*. Phys. Rev. A **66**, 032305 (2002).

[86] J.Y. Courtois ang G. Grynberg. *Probe transmission in one-dimensional optical molasses: Theory for linearly cross-polarized cooling beams*. Phys. Rev. A **46**, 7060 (1992).

[87] F. Renzoni and T. Brandes. *Charge transport through quantum dots via time-varying tunnel coupling*. Phys. Rev. B **64**, 245301 (2001).

[88] T. Brandes and T. Vorrath. *Adiabatic transfer of electrons in coupled quantum dots*. Phys. Rev. B **66**, 075341 (2002).

[89] D.G. Angelakis, M.F. Santos, V. Yannopapas, and A. Ekert. *Quantum computation in photonic crystals*. quant-ph page 040189 (2004).

[90] J.D. Joannopoulos, R.D. Meade, and J.N. Winn. *Photonic Crystals: Molding the Flow of Light*. Princeton Univ. Press 1995.

[91] J. Simon. *Numerical studies with quantum gates on neutral atoms*. Diploma thesis Universität Heidelberg 2001.

[92] H.J. Briegel R. Raussendorf, D.E. Browne. *Measurement-based quantum computation on cluster states*. Phys. Rev. A **68**, 022312 (2003).

[93] R. Motwani and P. Raghavan. *Randomized algorithms*. Cambridge University Press 1995.

[94] A. Childs, E. Farhi, and S. Gutmann. *An example of the difference between quantum and classical random walks*. Quantum Information processing **1**, 35 (2002).

[95] J. Kempe. *Quantum random walks: an introductory overview*. Cont. Phys. **44**, 307 (2003).

[96] D. Aharonov, A. Ambainis, J. Kempe, and U. Vazirani. *Quantum Walks On Graphs*. Proc. ACM Symp. Th. of Comp. (STOC'01) page 50 (2001).

[97] A. Nayak and A. Vishwanath. *Quantum Walk on the Line*. quant-ph page 0010117 (2000).

[98] T.D. Mackay, S.D. Bartlett, L.T. Stephenson, and B.C. Sanders. *Quantum walks in higher dimensions*. J. Phys. A **35**, 2745 (2002).

[99] J. Kempe. *Quantum Random Walks Hit Exponentially Faster*. In *Proc. of 7th Intern. Workshop on Randomization and Approximation Techniques in Comp. Sc.* page 354. RANDOM'03 2003.

[100] A.M. Childs, R. Cleve, E. Deotto, E. Farhi, S. Gutmann, and D.A. Spielman. *Exponential algorithmic speedup by quantum walks*. In *Proc. 35th ACM Symposium on Theory of Computing* page 59. STOC 2003 2003.

[101] N. Shenvi, J. Kempe, and K.B. Whaley. *Quantum random-walk search algorithm*. Phys. Rev. A **67**, 052307 (2003).

[102] A.M. Childs and J. Goldstone. *Spatial search by quantum walk*. Phys. Rev. A **70**, 022314 (2004).

[103] A. Ambainis, J. Kempe, and A. Rivosh. *Coins Make Quantum Walks Faster*. quant-ph page 0402107 (2004).

[104] W. Dür, R. Raussendorf, V.M. Kendon, and H.J. Briegel. *Quantum walks in optical lattices*. Phys. Rev. A **66**, 052319 (2002).

[105] P.L. Knight, E. Roldan, and J.E. Sipe. *Quantum walk on the line as an interference phenomenon*. Phys. Rev. A **68**, 020301 (2003).

[106] H. Jeong, M. Paternostro, and M.S. Kim. *Simulation of quantum random walks using the interference of a classical field*. Phys. Rev. A **69**, 012310 (2003).

[107] Y. Omar, N. Paunkovic, L. Sheridan, and S. Bose. *Quantum Walk on a Line with Two Entangled Particles*. quant-ph page 0411065 (2004).

[108] B.C. Travaglione and G.J. Milburn. *Implementing the quantum random walk*. Phys. Rev. A **65**, 032310 (2002).

[109] Z. Zan, J. Du, H. Li, T. Yang, Z. Chen, and J. Pan. *Implement Quantum Random Walks with Linear Optics Elements*. quant-ph page 0212149 (2002).

[110] Eric W. Weisstein *et al.* *MathWorld – Galton Board*. http://mathworld.wolfram.com/GaltonBoard.html.

[111] D. Bouwmeester, I. Marzoli, G.P. Karman, W. Schleich, and J.P. Woerdman. *Optical Galton board*. Phys. Rev. A **61**, 013410 (2000).

[112] P.L. Knight, E. Roldan, and J.E. Sipe. *Optical Cavity Implementations of the Quantum Walk*. Opt. Comm. **227**, 147 (2003).

[113] P.L. Knight, E. Roldan, and J.E. Sipe. *Propagating Quantum Walks: the origin of interference structures*. J. Mod. Opt. **51**, 1761 (2004).

[114] D. Meyer. *From quantum cellular automata to quantum lattice gases*. J. Stat. Phys. **85**, 551 (11996).

[115] B. Tregenna, W. Flanagan, R. Maile, and V. Kendon. *Controlling discrete quantum walks: coins and initial states*. New J. Phys **5**, 83 (2003).

[116] V. Kendon and B. Tregenna. *Decoherence can be useful in quantum walks*. Phys. Rev. A **67**, 042315 (2003).

[117] V. Kendon and B. Tregenna. *One dimensional quantum walk with unitary noise*. Lecture Notes Phys. **633**, 253 (2003).

[118] V. Kendon and B. Tregenna. *Decoherence in Discrete Quantum Walks*. In *Quantum Communication, Measurement & Computing*. Rinton Press 2003.

[119] H. Kreutzmann, U. V. Poulsen, M. Lewenstein, R. Dumke, W. Ertmer, G. Birkl, and A. Sanpera. *Coherence Properties of Guided-Atom Interferometers*. Phys. Rev. Lett. **92**, 163201 (2004).

[120] E. Arimondo. In E. Wolf, editor, *Progress in Optics* volume 35 page 257. Elsevier Science 1996.

[121] K. Bergmann, H. Theuer, and B. Shore. *Coherent population transfer among quantum states of atoms and molecules*. Rep. Mat. Phys. **70**, 1003 (1998).

[122] S.E. Harris. *Electromagnetically induced transparency*. Phys. Today **50**, 36 (1997).

[123] J.P. Marangos. *Topical review electromagnetically induced transparency*. J. Mod. Opt. **45**, 471 (1998).

[124] P. Marte, P. Zoller, and J.L. Hall. *Coherent atomic mirrors and beam splitters by adiabatic passage in multilevel systems*. Phys. Rev. A **44**, R4118 (1991).

[125] A. Aspect, E. Arimondo, R. Kaiser, N. Vansteenkist, and C. Cohen-Tannoudji. *Laser Cooling below the One-Photon Recoil Energy by Velocity-Selective Coherent Population Trapping*. Phys. Rev. Lett. **61**, 826 (1988).

[126] G. Morigi, J. Eschner, and C.H. Keitel. *Ground State Laser Cooling Using Electromagnetically Induced Transparency*. Phys. Rev. Lett. **85**, 4458 (2000).

[127] C.F. Roos, D. Leibfried, A. Mundt, F. Schmidt-Kaler, J. Eschner, and R. Blatt. *Experimental Demonstration of Ground State Laser Cooling with Electromagnetically Induced Transparency*. Phys. Rev. Lett. **85**, 5547 (2000).

[128] L.V. Hau, S.E. Harris, Z. Dutton, and C.H. Behroozi. *Light speed reduction to 17 metres per second in an ultracold atomic gas*. Nature (London) **397**, 594 (1999).

[129] M.D. Lukin and A. Imamoglu. *Controlling photons using electromagnetically induced transparency*. Nature (London) **413**, 273 (2001).

[130] P.R. Hemmer and M.G. Prentiss. *Coupled-pendulum model of the stimulated resonance Raman effect*. J. Opt. Soc. Am. B **5**, 1613 (1998).

[131] C.L.G. Alzar, M.A.G. Martinez, and P. Nussenzveig. *Classical analog of electromagnetically induced transparency*. Am. J. Phys. **70**, 37 (2002).

[132] S. Guérin, S. Thomas, and H. R. Jauslin. *Optimization of population transfer by adiabatic passage*. Phys. Rev. A **65**, 023409 (2002).

[133] A.D. Greentree, J.H. Cole, A.R. Hamilton, and Lloyd C.L. Hollenberg. *Coherent electronic transfer in quantum dot systems using adiabatic passage*. quant-ph page 0407008 (2004).

[134] L. Allen and J.H. Eberly. *Optical Resonance and Two-Level Atoms*. Wiley, New York 1975.

[135] M.P. Fewell, B.W. Shore, and K. Bergmann. *Coherent Population Transfer among Three States: Full Algebraic Solutions and the Relevance of Non Adiabatic Processes to Transfer by Delayed Pulses*. Aust. J. Phys. **50**, 281 (1997).

[136] M. Weitz, B.C. Young, and S. Chu. *Atomic Interferometer Based on Adiabatic Population Transfer*. Phys. Rev. Lett. **73**, 2563 (1994).

[137] M. Hennrich, A. Kuhn T. Legero, and G. Rempe. *Counter-intuitive vacuum-stimulated Raman scattering*. J. Mod. Opt. **50**, 935 (2003).

[138] M. Mackie, R. Kowalski, and J. Javanainen. *Bose-Stimulated Raman Adiabatic Passage in Photoassociation*. Phys. Rev. Lett. **84**, 3803 (2000).

[139] A. André and M.D. Lukin. *Manipulating Light Pulses via Dynamically Controlled Photonic Band gap*. Phys. Rev. Lett. **89**, 143602 (2002).

[140] M. Fleischhauer and M.D. Lukin. *Quantum memory for photons: Dark-state polaritons*. Phys. Rev. A **65**, 022314 (2002).

[141] T.G. Tiecke, M. Kemmann, Ch. Buggle, I. Shvarchick, W. von Klizing, and J.T.M. Walraven. *Bose-Einstein condensation in a magnetic double-well potential*. J. Opt. B: Quant. Semiclass. Opt. **5**, S119 (2003).

[142] F. Scharnberg. Private communication.

[143] V.S. Malinovsky and D.J. Tannor. *Simple and robust extension of the stimulated Raman adiabatic passage technique to N-level systems*. Phys. Rev. A **56**, 4929 (1997).

[144] R. Unanyan, M. Fleischhauer, B.W. Shore, and K. Bergmann. *Robust creation and phase-sensitive probing of superposition states via stimulated Raman adiabatic passage (STIRAP) with degenerate dark states*. Optics Communications **155**, 144 (1998).

[145] R. Unanyan, B.W. Shore, and K. Bergmann. *Laser-driven population transfer in four-level atoms: Consequences of non-Abelian geometrical adiabatic phase factors*. Phys. Rev. A **59**, 2910 (1999).

[146] J. Mompart R. Corbalan and L. Roso. *Coherent Population Trapping in Two-Electron Three-Level Systems with Aligned Spins*. Phys. Rev. A **88**, 023603 (2001).

[147] D. Cassettari, B. Hessmo, R. Folman, T. Maier, and J. Schmiedmayer. *A Beam Splitter for Guided Atoms on an Atom Chi*. Phys. Rev. Lett. **85**, 5483 (2000).

[148] M.J. Snadden, J.M. McGuirk, P. Bouyer, K.G. Haritos, and M.A. Kasevich. *Measurement of the Earth's gravity gradient with an atom interferometer-based gravity gradiometer*. Phys. Rev. Lett. **81**, 971 (1998).

[149] J.M. McGuirk, G.T. Foster, J.B. Fixler, M.J. Snadden, and M.A. Kasevich. *Sensitive absolute-gravity gradiometry using atom interferometry*. Phys. Rev. A **65**, 033608 (2002).

[151] G. Sagnac. *Theorie de l'experience de Sagnac*. Comptes Rendus **157**, 708 (1913).

[150] E.J. Post. *Sagnac Effect*. Rep. Mat. Phys. **39**, 475 (1967).

[152] P.R. Berman. *Atom Interferometry*. Academic Press 1996.

[153] P. Kok, S.L. Braunstein, and J.P. Dowling. *Quantum lithography, entanglement and Heisenberg-limited parameter estimation*. quant-ph page 0402083 (2004).

[154] S.F. Huelga, C. Macchiavello, T. Pellizzari, A.K. Ekert, M.B. Plenio, and J.I. Cirac. *On the Improvement of Frequency Stardards with Quantum Entanglement*. Phys. Rev. Lett. **79**, 3865 (1997).

[155] D.M. Greenberger, M. Horne, and A. Zeilinger. *Bell's theorem, quantum theory, and conceptions of the universe*. page 69. Kluwer 1989.

[156] A. Kuzmich, N.P. Bigelow, and L. Mandel. *Atomic quantum nondemolition measurementsand squeezing*. Europhys. Lett. **42**, 481 (1998).

[157] A. Kuzmich, L. Mandel, and N.P. Bigelow. *Generation of spin squeezing via continuous quantum nondemolition measurement*. Phys. Rev. Lett. **85**, 1594 (2000).

[158] A. Kuzmich, Klaus Mølmer, and E.S. Polzik. *Spin Squeezing in an Ensemble of Atoms Illuminated with Squeezed Light*. Phys. Rev. Lett. **79**, 4782 (1997).

[159] J. Hald, J.L. Sørensen, C. Schori, and E.S. Polzik. *Spin Squeezed Atoms: A Macroscopic Entangled Ensemble Created by Light.* Phys. Rev. Lett. **83**, 1319 (1999).

[160] L.-M. Duan, J.I. Cirac, P. Zoller, and E.S. Polzik. *Quantum Communication between Atomic Ensembles Using Coherent Light.* Phys. Rev. Lett. **85**, 5643 (2000).

[161] B. Julsgaard, A. Kozhekin, and E.S. Polzik. *Experimental long-lived entanglement of two macroscopic objects.* Nature (London) **413**, 400 (2001).

[162] M.D. Lukin, S.F. Yelin, and M. Fleischhauer. *Entanglement of Atomic Ensembles by Trapping Correlated Photon States.* Phys. Rev. Lett. **84**, 4232 (2000).

[163] C. Jentsch, T. Müller, E. Rasel, and W. Ertmer. *HYPER: A Satellite Mission in Fundamental Physics Based on High Precision Atom Interferometry.* Gen. Rel. Grav. **36**, 2197 (2004).

[164] V. Petersen, L.B. Madsen, and K. Mølmer. *Magnetometry with entangled atomic samples.* quant-ph page 0409202 (2004).

[165] K.P. Zetie, S.F. Adams, and R.M. Tocknell. *How does a Mach-Zehnder interferometer work?* Phys. Educ. **35**, 46 (2000).

[166] G.B. Malykin. *The Sagnac effect: correct and incorrect explanation.* Physics-Uspekhi **43**, 1229 (2000).

[167] E. Rasel. Private communication.

[168] G. Santarelli, Ph. Laurent, P. Lemonde, A. Clairon, A.G. Mann, S. Chang, A.N. Luiten, and C. Salomon. *Quantum Projection Noise in an Atomic Fountain: A High Stability Cesium Frequency Standard.* Phys. Rev. Lett. **82**, 4619 (1999).

[169] L.-M. Duan, J.I. Cirac, and P. Zoller. *Quantum entanglement in spinor Bose-Einstein condensates.* Phys. Rev. A **65**, 033619 (2002).

[170] A. Sørensen and K. Mølmer. *Spin-Spin Interaction and Spin Squeezing in an Optical Lattice.* Phys. Rev. Lett. **83**, 2274 (1999).

[171] M. Takeuchi, S.Ichihara, T. Takano, M. Kumakura, T. Yabuzaki, and Y. Takahashi. *Spin Squeezing via One-Axis Twisting with Coherent Light.* quant-ph page 0410132 (2004).

[172] Y. Takahashi, K. Honda, N. Tanaka, K. Toyoda, K. Ishikawa, and T. Yabuzaki. *Quantum nondemolition measurement of spin via the paramagnetic Faraday rotation.* Phys. Rev. A **60**, 4974 (1999).

[173] C. Cohen-Tannoudji and J. Dupont-Roc. *Experimental Study of Zeeman Light Shifts in Weak Magnetic Fields.* Phys. Rev. A **5**, 968 (1972).

[174] L.B. Madsen and K. Mølmer. *Spin squeezing and precision probing with light and samples of atoms in the gaussian approximation.* quant-ph page 0406146 (2004).

[175] T.A.B. Kennedy A. Kuzmich. *Non-symmetric entanglement of atomic ensembles*. Phys. Rev. Lett. **92**, 030407–2 (2004).

[176] T. Müller and C. Jentsch. Private communication 2004.

[177] J.K. Stockton, J.M. Geremia, A.C. Doherty, and H. Mabuchi. *Characterizing the entanglement of symmetric many-particle spin-(1/2) systems*. Phys. Rev. A **67**, 022112 (2003).

[178] Y. Omar, N. Paunkovic, S. Bose, and V. Vedral. *Spin-Space Entanglement Transfer and Quantum Statistics*. Phys. Rev. A **65**, 062305 (2002).

[179] N. Paunkovic, Y. Omar, S. Bose, and V. Vedral. *Entanglement Concentration Using Quantum Statistics*. Phys. Rev. Lett. **88**, 187903 (2002).

[180] S. Bose, A. Ekert, Y. Omar, N. Paunkovic, and V. Vedral. *Optimal State Discrimination Using Particle Statistics*. Phys. Rev. A **68**, 052309 (2003).

[181] H.W. Lee and J. Kim. *Quantum teleportation and Bell's inequality using single particle entanglement*. Phys. Rev. A **63**, 12305 (2000).

[182] P. Zanardi, J. Schliemann, and J.I. Cirac. Private communication.

[183] K. Eckert. *Quantum Correlations in Fermionic and Bosonic Systems*. Diploma thesis Universität Hannover 2001.

[184] S. Hill and W.K. Wootters. *Entanglement of a pair of quantum bits*. Phys. Rev. Lett. **78**, 5022 (1997).

[185] W.K. Wootters. *Quantum entanglement as a quantifiable resource*. Phys. Rev. A **356**, 1717 (1998).

[186] A.D. Bandrauk and H. Shen. *Exponential split operator methods for solving the time dependent Schrödinger equation*. J. Chem. Phys. **99**, 1185 (1993).

[187] W.H. Press, W.A. Teukolsky, W.T. Vetterling, and B.P. Flannery. *Numerical Recipes in C*. Cambridge University Press 1992.

LIST OF CO-AUTHORED PUBLICATIONS

[I] *Quantum correlations of indistinguishable particles*

We discuss quantum correlations in systems of indistinguishable particles in relation to entanglement in composite quantum systems consisting of well separated subsystems. Our studies are motivated by recent experiments and theoretical investigations on quantum dots and neutral atoms in microtraps as tools for quantum information processing. We present analogies between distinguishable particles, bosons, and fermions in low-dimensional Hilbert spaces. We introduce the notion of Slater rank for pure states of pairs of fermions and bosons in analogy to the Schmidt rank for pairs of distinguishable particles. This concept is generalized to mixed states and provides a correlation measure for indistinguishable particles. Then we generalize these notions to pure fermionic and bosonic states in higher-dimensional Hilbert spaces and also to the multi-particle case. We review the results on quantum correlations in mixed fermionic states and discuss the concept of fermionic Slater witnesses. Then the theory of quantum correlations in mixed bosonic states and of bosonic Slater witnesses is formulated. In both cases we provide methods of constructing optimal Slater witnesses that detect the degree of quantum correlations in mixed fermionic and bosonic states.

K. Eckert, J. Schliemann, D. Bruß, and M. Lewenstein, Annals of Physics **299**, 88 – 127 (2002).

[II] *Quantum computing in optical microtraps based on the motional states of neutral atoms*

We investigate quantum computation with neutral atoms in optical microtraps where the qubit is implemented in the motional states of the atoms, i.e., in the two lowest vibrational states of each trap. The quantum gate operation is performed by adiabatically approaching two traps and allowing tunneling and cold collisions to take place. We demonstrate the capability of this scheme to realize a square root of swap gate, and address the problem of double occupation and excitation to other unwanted states. We expand the two-particle wave function in an orthonormal basis and analyze quantum correlations throughout the whole gate process. Fidelity of the gate operation is evaluated as a function of the degree of adiabaticity in moving the traps. Simulations are based on rubidium atoms in state-of-the-art optical microtraps with quantum gate realizations in the few tens of milliseconds duration range.

K. Eckert, J. Mompar, X.X. Yi, J. Schliemann, D. Bruß, G. Birkl and M. Lewenstein, Pysical Review A **66** 042317-1 – 042317-11 (2002).

[III] *Entanglement properties of composite quantum systems*

We present here an overview of our work concerning entanglement properties of composite quantum systems. The characterization of entanglement, i.e. the possibility to assert if a given quantum state is entangled with others and how much entangled it is, remains one of the most fundamental open questions in quantum information theory. We discuss our recent results related to the problem of separability and distillability for distinguishable particles, employing the tool of witness operators. Finally, we also state our results concerning quantum correlations for indistinguishable particles.

K. Eckert, O. Gühne, F. Hulpke, P. Hyllus, J. Korbicz, J. Mompart, D. Bruß, M. Lewenstein, and A. Sanpera, in: *Quantum Information Processing*, Gerd Leuchs, Thomas Beth (Eds), Wiley-VCH (2003).

[IV] *Quantum Computing with Spatially Delocalized Qubits*

We analyze the operation of quantum gates for neutral atoms with qubits that are delocalized in space, i.e., the computational basis states are defined by the presence of a neutral atom in the ground state of one out of two trapping potentials. The implementation of single-qubit gates as well as a controlled phase gate between two qubits is discussed and explicit calculations are presented for rubidium atoms in optical microtraps. Furthermore, we show how multiqubit highly entangled states can be created in this scheme.

J. Mompart, K. Eckert, W. Ertmer, G. Birkl, and M. Lewenstein, Physical Review Letters **90**, 147901-1 – 147901-4 (2003).

[V] *Finite size effects in entangled rings of qubits*

We study translationally invariant rings of qubits with a finite number of sites N, and find the maximal nearest-neighbor entanglement for a fixed z component of the total spin. For small numbers of sites our results are analytical. The use of a linearized version of the concurrence allows us to relate the maximal concurrence to the ground state energy of an XXZ spin model, and to calculate it numerically for N¡25. We point out some interesting finite-size effects. Finally, we generalize our results beyond nearest neighbors.

T. Meyer, U.V. Poulsen, K. Eckert, M. Lewenstein, and D. Bruß, International Journal of Quantum Information **2**, 149 – 169 (2004).

[VI] *Three-level atom optics via the tunneling interaction*

Three-level atom optics is introduced as a simple, efficient, and robust method to coherently manipulate and transport neutral atoms. The tunneling interaction among three trapped states allows us to realize the spatial analog of the stimulated Raman adiabatic passage, coherent population trapping, and electromagnetically induced transparency techniques and offers a wide range of possible applications. We investigate an implementation in optical microtrap arrays and show that under realistic parameters the coherent manipulation and transfer of neutral atoms among dipole traps could be realized in the millisecond range.

K. Eckert, M. Lewenstein, R. Corbalán, G. Birkl, W. Ertmer, and J. Mompart, Physical Review A **70**, 023606-1 – 023606-5 (2004).

[VII] *Cavity QED quantum phase gates for a single longitudinal mode of the intracavity field*

A single three-level atom driven by a longitudinal mode of a high-Q cavity is used to implement two-qubit quantum phase gates for the intracavity field. The two qubits are associated to the zero-and one-photon Fock states of each of the two opposite circular polarization states of the field. The three-level atom yields the conditional phase gate provided the two polarization states and the atom interact in a V-type configuration and the two photon resonance condition is fulfilled. Microwave and optical implementations are discussed with gate fidelities being evaluated against several decoherence mechanisms such as atomic velocity fluctuations or the presence of a weak magnetic field. The use of coherent states for both polarization states is investigated to assess the entanglement capability of the proposed quantum gates.

R. García-Maraver, R. Corbalán, K. Eckert, S. Rebic, M. Artoni, and J. Mompart, Physical Review A (accepted) and quant-ph/0407250 (2004).

ACKNOWLEDGMENTS

Curriculum Vitae

30. November 1975	Geboren in Großburgwedel
1982 bis 1986	Besuch der Grundschule IV in Burgdorf
1986 bis 1988	Besuch der Orientierungsstufe II in Burgdorf
1988 bis 1995	Besuch des Gymnasiums Burgdorf
Juni 1995	Abitur am Gymnsium Burgdorf
Aug. 1995 bis Sept. 1996	Zivildienst in einer Wohnstätte für geistig Behinderte der Behindertenhilfe Berkhöpen-Burgdorf GmbH
Okt. 1996 bis Nov. 2001	Beginn des Studiums der Physik an der Universität Hannover
September 1998	Vordiplom in Physik
Dezember 2001	Diplom in Physik
seit Januar 2002	Wissenschaftlicher Mitarbeiter in der Arbeitsgrupper von Prof. Dr. Maciej Lewenstein an der Universität Hannover. Arbeitsgebiet: Quanteninformationsverarbeitung.